LBL-29710
CONF-9009228

Lawrence Berkeley Laboratory
UNIVERSITY OF CALIFORNIA

EARTH SCIENCES DIVISION

Proceedings of the TOUGH Workshop

Lawrence Berkeley Laboratory
Berkeley, California

September 13–14, 1990

Karsten Pruess, Editor

September 1990

LBL-29710
Copy 2
Bldg. 50 Library.
LOAN COPY
Circulates
for 2 weeks

Prepared for the U.S. Department of Energy under Contract Number DE-AC03-76SF00098.

DISCLAIMER

This document was prepared as an account of work sponsored by the United States Government. While this document is believed to contain correct information, neither the United States Government nor any agency thereof, nor the Regents of the University of California, nor any of their employees, makes any warranty, express or implied, or assumes any legal responsibility for the accuracy, completeness, or usefulness of any information, apparatus, product, or process disclosed, or represents that its use would not infringe privately owned rights. Reference herein to any specific commercial product, process, or service by its trade name, trademark, manufacturer, or otherwise, does not necessarily constitute or imply its endorsement, recommendation, or favoring by the United States Government or any agency thereof, or the Regents of the University of California. The views and opinions of authors expressed herein do not necessarily state or reflect those of the United States Government or any agency thereof or the Regents of the University of California.

LBL-29710
September 1990

Proceedings of the TOUGH Workshop

Lawrence Berkeley Laboratory
Berkeley, California

September 13–14, 1990

Karsten Pruess, Editor

Earth Sciences Division
Lawrence Berkeley Laboratory
University of California
Berkeley, California 94720

This work was supported by the U.S. Department of Energy under Contract No. DE-AC03-76SF00098.

Table of Contents

Preface v

Welcome and Introduction vii

Workshop Program ix

List of Attendees xiii

Unsaturated Zone Hydrology

Two-Phase Nonisothermal Hydrologic Transport Simulations at the Apache Leap Tuff Field Site 1
M. Shaikh, T.-C. J. Yeh and T. C. Rasmussen

Modeling Hydrothermal Flow in Variably Saturated, Fractured, Welded Tuff During the Prototype Engineered Barrier System Field Test of the Yucca Mountain Project 9
T. Buscheck and J. J. Nitao

Unsaturated Zone Moisture and Vapor Movement induced by Temperature Variations in Asphalt Barrier Field Lysimeters 15
D. J. Holford and M. J. Fayer

Environmental Issues

Gaseous Transport of Volatile Organics in Porous Media: Comparison of Mathematical Models 21
J. M. Farr

STMVOC: A Numerical simulator for Three Phase Contaminant Transport in Nonisothermal System 29
R. W. Falta and K. Pruess

Geothermal Reservoir Studies

A Simple Model of A Vapour-dominated Geothermal Reservoir 37
M. J. O'Sullivan

Injection of Cold Water and Air into a Two-phase Volcanic Hydrothermal System 45
M. C. Suárez and A. Manon

Water-CO_2 Version of MULKOM Code: A Tool for Studying the Origin and Trends of CO_2 in Geothermal Reservoirs 53
C. Calore, G. Gianelli and K. Pruess

Case Study Using Faster TOUGH 61
T. Okabe, K. Osato and S. Takasugi

Code Enhancements I

Incorporation into TOUGH of an Analytical Source/Sink Term for Fracture/Matrix Flow 67
R. W. Zimmerman and G. S. Bodvarsson

On Verification, Use and Treatment of Non-Newtonian Behavior of the Numerical Simulator MULKOM-GWF 73
Y.-S. Wu and K. Pruess

Overview of TOUGH2, A General-Purpose Numerical Simulator for Multiphase Nonisothermal Flows 89
K. Pruess

Performance Assessment

Modeling Studies of Gas Movement and Moisture Migration at Yucca Mountain, Nevada 99
Y. W. Tsang and K. Pruess

Phasic Pressure Difference Effects in Two-Phase Flow for Dissolved Gas Exsolution 107
S. W. Webb and J. C. Chen

Verification of TOUGH2 Against a Semianalytical Solution for Transient Two-phase Fluid and Heat Flow in Porous Media 113
C. Doughty and K. Pruess

Two-Phase Flow Experiments

Use of TOUGH Computer Code to Simulate a Laboratory-Scale Experiment 121
R. T. Green, R. H. Martin and S. Svedeman

Two-phase Flow and Solute Transport Simulations in a Tuff Drillcore 127
T. McCartin, R. Codell and T. Nicholson

Interpretation of Hydraulic Tests in a Two-phase Flow System Using TOUGH 133
S. Finsterle and S. Mishra

Code Enhancements II

Making MULKOM/TOUGH Faster and Easier to Use 139
D. Bullivant

Increasing the Efficiency of the TOUGH Code for Running Large-scale Problems in Nuclear Waste Isolation 143
J. J. Nitao

Speeding-up TOUGH 149
S. White

Appendix: TOUGH Questions 157

Preface

A workshop on applications and enhancements of the TOUGH/MULKOM family of multiphase fluid and heat flow simulation programs was held at Lawrence Berkeley Laboratory on September 13–14, 1990. The workshop was attended by 62 scientists from seven countries with interests in geothermal reservoir engineering, nuclear waste isolation, unsaturated zone hydrology, environmental problems, and laboratory and field experimentation.

The meeting featured 21 technical presentations, extended abstracts of which are reproduced in the present volume in unedited form. Simulator applications included processes on a broad range of space scales, from centimeters to kilometers, with transient times from seconds to geologic time scales. A number of code enhancements were reported that increased execution speeds for large 3-D problems by factors of order 20, reduced memory requirements, and improved user-friendliness.

The workshop closed with an open discussion session that focussed on future needs and means for interaction in the TOUGH user community. Input from participants was gathered by means of a questionnaire that is reproduced in the appendix. There appeared to be agreement among participants that this kind of a meeting is useful, and that another TOUGH workshop should be held in 1 1/2 to 2 years. Strong interest was also expressed in printing some kind of newsletter, that would help to distribute information about current TOUGH/MULKOM applications, including new technical reports and papers, and code enhancements. Many participants volunteered to provide items and articles for the newsletter. It was agreed that contributions would be mailed to LBL, which would begin to produce and distribute such a newsletter in an informal way.*

September 1990

Karsten Pruess

---

*To receive the TOUGH Newsletter, or to submit contributions, write to: Karsten Pruess, Lawrence Berkeley Laboratory, MS 50E, One Cyclotron Rd., Berkeley, CA 94720.

Welcome and Introduction
TOUGH Workshop

September 13–14, 1990
Lawrence Berkeley Laboratory
Berkeley, California, USA

Welcome to the TOUGH Workshop! We are pleased to host a meeting that is devoted to applications and enhancements of the TOUGH numerical simulation program. TOUGH has been available for 3+ years, and the workshop was organized in response to a growing interest for more interaction and support among TOUGH users. This workshop gathers people with different backgrounds around a shared focus on numerical simulation, and provides an opportunity to exchange experiences and advances from different fields. This folder contains the technical program, a preliminary list of attendees, and extended abstracts of the papers that will be presented.

Numerical simulations discussed in these papers address a broad range of topics in the areas of geothermal reservoir engineering, geologic disposal of nuclear waste, unsaturated zone hydrology, environmental problems, and design and analysis of two-phase flow experiments. Several authors report on code enhancements to achieve a more comprehensive description of multiphase flow processes, improve speed and efficiency of computation, and facilitate applications to complex problems.

Multiphase fluid and heat flows in the subsurface are of interest in a number of engineering disciplines that deal with the development of energy resources and with environmental protection. Numerical modeling has emerged as a powerful tool for increasing our understanding of complex flow systems.

A number of people have expressed an interest in code demonstrations, and in exchanging enhancements to the TOUGH code. In planning the workshop, we had expected that two days would provide sufficient time to have some code demonstration sessions, in addition to sessions with technical papers. However, the number of papers submitted easily filled the two-day program so that, unfortunately, it was not possible to include code demonstration sessions. We strongly believe that an open and interactive approach to development and sharing of software can offer large benefits to all participants, and we encourage workshop participants to seek out appropriate contacts and exchanges on a personal basis. The discussion session at the end of the workshop will give an opportunity to examine needs and possible means for furthering contacts and communication in the TOUGH user community.

Karsten Pruess

Earth Sciences Division
Lawrence Berkeley Laboratory

PROGRAM

TOUGH Workshop
September 13–14, 1990

Thursday, September 13, 1990

A.M.

7:30 Registration: Building 70A, Room 3377

8:30 Welcome and Introduction (Karsten Pruess, LBL)

9:00 **Session 1: Unsaturated Zone Hydrology**
(chairman: Chin-Fu Tsang, LBL)

Two-Phase Nonisothermal Hydrologic Transport Simulations at the Apache Leap Tuff Site
M. Shaikh, T.-C. J. Yeh and T. C. Rasmussen, University of Arizona, Tucson, AZ

Modeling Hydrothermal Flow in Variably Saturated, Fractured,Welded Tuff During the Prototype Engineered Barrier System Field Test of the Yucca Mountain Project
T. A. Buscheck and J. J. Nitao, Lawrence Livermore National Laboratory, Livermore, CA

Unsaturated Zone Moisture and Vapor Movement Induced by Temperature Variations in Asphalt Barrier Field Lysimeters
D. J. Holford and M. J. Fayer, Pacific Northwest Laboratory, Richland, WA

10:30 Coffee Break

11:00 **Session 2: Environmental Issues**
(chairman: Keshav Goyal, Calpine Corp.)

Gaseous Transport of Volatile Organics in Porous Media: Comparison of Mathematical Models
J. M. Farr, Levine-Fricke, Inc., Emeryville, CA

STMVOC: A Numerical Simulator for Three Phase Contaminant Transport in Nonisothermal Systems
R. W. Falta and K. Pruess, Lawrence Berkeley Laboratory, Berkeley, CA

P.M.

12:00 Lunch Break

1:30 **Session 3: Geothermal Reservoir Studies**
(chairman: Mark McGuinness, DSIR)

A Simple Model of a Vapour-Dominated Geothermal Reservoir
M. J. O'Sullivan, The University of Auckland, New Zealand

Injection of Cold Water and Air into a Two-Phase Volcanic Hydrothermal System
M. C. Suarez and A. M. Manon, Comision Federal de Electricidad, Morelia, Mexico

Water-CO_2 Version of MULKOM: A Tool for Studying the Origin and Trends of CO_2 in Geothermal Reservoirs
C. Calore and G. Gianelli, Istituto Internazionale per le Ricerche Geotermiche, Pisa, Italy and K. Pruess, Lawrence Berkeley Laboratory, Berkeley, CA

Case Study Using Faster TOUGH
T. Okabe, K. Osato and S. Takasugi, Geothermal Energy Research and Development Co., Tokyo, Japan

3:30 Coffee Break

4:00 **Session 4: Code Enhancements I**
(chairman: Todd Rasmussen, University of Arizona)

Incorporation into TOUGH of an Analytical Source/Sink Term for Fracture/Matrix Flow
R. W. Zimmerman and G. S. Bodvarsson, Lawrence Berkeley Laboratory, Berkeley, CA

On Verification, Use, and Treatment of Non-Newtonian Behavior of the Numerical Simulator MULKOM-GWF
Y. S. Wu, HydroGeoLogic, Inc., Herndon, VA and K. Pruess, Lawrence Berkeley Laboratory, Berkeley, CA

Overview of TOUGH2, A General-Purpose Numerical Simulator for Multiphase Nonisothermal Flows
K. Pruess, Lawrence Berkeley Laboratory, Berkeley, CA

5:30 Adjourn

7:00 Banquet (Speaker: T. N. Narasimhan, LBL and University of California, "The Lure of the Computer")

Friday, September 14, 1990

A.M.

8:30 **Session 5: Performance Assessment**
(chairman: Mert Fewell, Sandia)

Modeling Studies of Gas Movement and Moisture Migration at Yucca Mountain, Nevada
Y. W. Tsang and K. Pruess, Lawrence Berkeley Laboratory, Berkeley, CA

Phasic Pressure Difference Effects in Two-Phase Flow for Dissolved Gas Exsolution
S. W. Webb, Sandia National Laboratories, Albuquerque, NM, and J. C. Chen, Lehigh University, Bethlehem, PA

Verification of TOUGH2 Against a Semianalytical Solution for Transient Two-Phase Fluid and Heat Flow in Porous Media
C. Doughty and K. Pruess, Lawrence Berkeley Laboratory, Berkeley, CA

10:00 Coffee Break

10:30 **Session 6: Two-Phase Flow Experiments**
(chairman: Marcelo Lippmann, LBL)

Use of TOUGH Computer Code to Simulate a Laboratory-Scale Experiment
R. T. Green and R. H. Martin, Southwest Research Institute,San Antonio, TX

Two-Phase Flow and Solute Transport Simulations in a Tuff Drillcore
T. McCartin, R. Codell, T. Nicholson, Nuclear Regulatory Commission, Washington, DC, and T. Rasmussen, University of Arizona, Tucson, AZ

Interpretation of Hydraulic Tests in a Two-Phase Flow System Using TOUGH
S. Finsterle, Swiss Federal Institute of Technology, Zurich, Switzerland, and S. Mishra, Intera, Inc., Austin, TX

P.M.

12:00 Lunch Break

1:30 **Session 7: Code Enhancements II**
(chairman: Tom Nicholson, NRC)

Making MULKOM/TOUGH Faster and Easier to Use
D. Bullivant, The University of Auckland, New Zealand

Increasing the Efficiency of the TOUGH Code for Running Large-Scale Problems in Nuclear Waste Isolation
J. J. Nitao, Lawrence Livermore National Laboratory, Livermore, CA

Speeding up TOUGH
S. White, Department of Scientific and Industrial Research, Wellington, New Zealand

3:00 Coffee Break

3:30 **Session 8: Open Discussion: Whither TOUGH?**
(chairman and moderator: Mike O'Sullivan, University of Auckland)

5:30 Adjourn

List of Attendees
TOUGH Workshop

Ian Acworth
University of New South Wales
Kensington, NSW 2033
Australia

Adeyinka Adenekan
Lawrence Berkeley Laboratory
Earth Sciences Division, MS 50E
One Cyclotron Road
Berkeley, CA 94720

Moshen Alavi
Lawrence Berkeley Laboratory
Earth Sciences Division, MS 50E
One Cyclotron Road
Berkeley, CA 94720
415-486-4381

Emilio U. Antunez
Geothermex, Inc.
5221 Central Ave., Ste. 201
Richmond, CA 94804
415-527-9876

Ralston W. Barnard
Sandia National Laboratories
Division 6313
P.O. Box 5800
Albuquerque, NM 87185
505-845-8403
rwbarna@sandia.gov

Dr. Gudmundur S. Bodvarsson
Lawrence Berkeley Laboratory
Earth Sciences Division, MS 50E
One Cyclotron Road
Berkeley, CA 94720
415-486-4789

Albin Brandstetter
Science Apps. Internal. Corp.
101 Convention Center Dr.
Las Vegas, NV 89109
702-794-7279

Dr. David Bullivant
Dept. of Theor. and Appl. Mech.
University of Auckland
Private Bag
Auckland,
New Zealand
(649) 737 999
etm_dpb@aukuni.ac.nz@relay.cs.net

Dr. T. A. Buscheck
Earth Sciences Division, MS L-206
Lawrence Livermore National Lab.
Livermore, CA 94550
busch@S53.es.llnl.gov

George Butler
Intera Inc.
6850 Austin Center Blvd, Ste. 300
Austin, TX 78723
512-346-2000

Dr. Claudio Calore
Istituto Internazionale
per le Ricerche Geotermiche
Piazza Solferino, 2
56126 Pisa,
Italy
(50) 41503
model@icnucevm.bitnet

Dr. John C. Chen
Lehigh University
111 Research Dr., Bldg. A
Bethlehem, PA 18015
215-758-4091

Dr. John R. Counsil
1148 Shadyoak Place
Santa Rosa, CA 95404
707-538-2288

Peter B. Davies
Sandia National Laboratories
Division 6344
P.O. Box 5800
Albuquerque, NM 87185
505-846-6211

Jerry D. Davis
Westinghouse Hanford Co.
P.O. Box 1970
Richland, WA 99352
509-376-8919

Christine Doughty
Lawrence Berkeley Laboratory
Earth Sciences Division, MS 50E
One Cyclotron Road
Berkeley, CA 94720
415-486-6453
chrissy@lbl.gov

Colin Dugeon
University of New South Wales
Kensington, NSW 2033
Australia

Dr. Ron Falta
Lawrence Berkeley Laboratory
Earth Sciences Division, MS 50E
One Cyclotron Road
Berkeley, CA 94720
415-486-4160
falta@lbl.gov

John M. Farr
Levine-Fricke, Inc.
1900 Powell St., 12th Fl.
Emeryville, CA 94608
415-652-4500

Merton E. Fewell
Org. 6313
Sandia National Labs.
P.O. Box 5800
Albuquerque, NM 87185
505-844-7120
mefewel@sandia.gov

Stefan Finsterle
Versuchsanstalt für Wasserbau
VAW DOL C13
ETH-Zentrum
CH-8092 Zürich,
Switzerland
(01) 256 51 03
jtroesch@czeth5a

Dr. Keshav Goyal
Calpine Corporation
1160 N. Dutton, Ste. 200
Santa Rosa, CA 95401
707-578-2739

Dr. Ronald T. Green
CNWRA, Southwest Res. Inst.
6220 Culebra Rd.
San Antonio, TX 78228
512-522-5305
rgreen@ccfvax.ccf.swri.edu

Dr. Diana J. Holford
Pacific Northwest Laboratory
MS K6-77
P.O. Box 999
Richland, WA 99352
509-376-8318
diana@phoebus.hydro.pnl.gov

Polly L. Hopkins
Sandia National Laboratories
Org. 1511
P.O. Box 5800
Albuquerque, NM 87185
505-846-1739

Michael Knight
University of New South Wales
Kensington, NSW 2033
Australia

Cheng-Hsien Lai
Lawrence Berkeley Laboratory
Earth Sciences Division, MS 50E
One Cyclotron Road
Berkeley, CA 94720
415-486-6110

Kay Lie
Maxwell Lab/S-Cubed
San Diego, CA 92123
619-453-0060

William Light
Lawrence Berkeley Laboratory
Earth Sciences Division, MS 50E
One Cyclotron Road
Berkeley, CA 94720
415-642-2130
ucblight@lbl.gov

Ning Lu
Disposal Safety, Inc.
1660 L Street, Ste. 314
Washington, DC 20036
202-293-3993
ins_anl@jhuums

Dr. Ronald H. Martin
CNWRA
Southwest Research Inst.
6220 Culebra Rd.
San Antonio, TX 78228
512-522-5541

Dr. Tim J. McCartin
U.S. NRC
MS NLS/260
Washington, DC 20555
301-492-3847

Jim McCord
Sandia National Laboratories
Division 6416
P.O. Box 5800
Albuquerque, NM 87185
505-844-5157

Dr. Thomas V. McEvilly
Lawrence Berkeley Laboratory
Earth Sciences Division, MS 50E
One Cyclotron Road
Berkeley, CA 94720
415-486-7347

Dr. Mark McGuinness
Appl. Math. Div.
DSIR
P.O. Box 1335
Wellington,
New Zealand
(64 4) 727 855
srwmmjm@windy.dsir.govt.nz

Dr. Anthony J. Menzies
Geothermex, Inc.
5221 Central Ave., Ste. 201
Richmond, CA 94804
415-527-9876

Tom E. Michener
Battelle Pac. Northwest Laboratory
P.O. Box 999
Richland, WA 99352
509-375-2162

William Milne-Home
University of New South Wales
Kensington, NSW 2033
Australia

Mohammed G. Mustafa
Lawrence Livermore National Lab
Nuclear Chemistry Division
Livermore, CA 94550
415-422-5523
mustafa@deneb.llnl.gov

Dr. T. N. Narasimhan
Lawrence Berkeley Laboratory
Earth Sciences Division, MS 50E
One Cyclotron Road
Berkeley, CA 94720
415-486-5665
vijaya@lbl.gov

Thomas J. Nicholson
U.S. Nuc. Reg. Commission
RES/WMB NL/S-260
Washington, DC 20555
301-492-3856

Dr. John J. Nitao
Earth Sciences Division, MS L-206
Lawrence Livermore National Lab.
Livermore, CA 94550
415-423-0297
nitao@s13.es.llnl.gov

Dr. Takashi Okabe
GERD Ltd.
Kyodo Bldg.,11-7 Kabuto-cho
Nihonbashi, Chuo-ku
Tokyo, 103
Japan
(03) 666-5822

Dr. Michael O'Sullivan
Dept. of Theor. and Appl. Mech.
University of Auckland
Private Bag
Auckland,
New Zealand
(469) 737 999
etm_osulliva@aukuni.ac.nz

Melvin G. Piepho
Westinghouse Hanford Co.
3200 George Washington Way
Richland, WA 99352
509-376-2726

Dr. Karsten Pruess
Lawrence Berkeley Laboratory
Earth Sciences Division, MS 50E
One Cyclotron Road
Berkeley, CA 94720
415-486-6732
pruess@lbl.gov

Peter M. Pyle
BGI
27 San Francisco Blvd.
San Anselmo, CA 94960
415-465-1744

Todd C. Rasmussen
University of Arizona
Dept. Hydrology & Water Resources
Tucson, AZ 85721

Erika Schlueter
Lawrence Berkeley Laboratory
Earth Sciences Division, MS 50E
One Cyclotron Road
Berkeley, CA 94720
415-486-5875

Mike Shook
Idaho National Engineering Lab
P.O. Box 1625, MS 2107
Idaho Falls, ID 83415
208-526-6945

Dr. Allan Spivak
Intera West
11444 West Olympic Blvd., 10th Fl.
Los Angeles, CA 90064
213-312-9574

Dr. Cesar Suarez
CFE
A.P. 31-C
A. Volta 655
58290 Morelia, Michoacan
Mexico
(451) 48050-135

Alex H. Treadway
Sandia National Laboratories
Org. 6313
P.O. Box 5800
Albuquerque, NM 87185
505-844-6850
ahtread@sandia.gov

Dr. Yvonne Tsang
Lawrence Berkeley Laboratory
Earth Sciences Division, MS 50E
One Cyclotron Road
Berkeley, CA 94720
415-486-7047
ytsang@lbl.gov

Dr. Chin-Fu Tsang
Lawrence Berkeley Laboratory
Earth Sciences Division, MS 50E
One Cyclotron Road
Berkeley, CA 94720
415-486-5782
chinfu@lbl.gov

Marina Voskanian
State Lands Commission
245 W. Broadway, Ste. 425
Long Beach, CA 90802

Dr. Joseph Wang
Lawrence Berkeley Laboratory
Earth Sciences Division, MS 50E
One Cyclotron Road
Berkeley, CA 94720
415-486-6753
jwang@lbl.gov

Dr. Stephen W. Webb
Division 6344
Sandia National Laboratories
Albuquerque, NM 87185
505-844-7037

Rex G. Wescott
U.S. Nuc. Reg. Commission
Washington, DC 20555
301-492-0167

Dr. Mark D. White
Battelle–PNL
P.O. Box 999
Richland, WA 99352
509-375-2183

Dr. Stephen P. White
Applied Mathematics Division
DSIR
P.O. Box 1335
Wellington,
New Zealand
(64 4) 727 855
srwmspw@wnv.dsir.govt.nz

Dr. Yu-Shu Wu
HydroGeoLogic, Inc.
503 Carlisle Drive, Ste. 250
Herndon, VA 22070
703-478-5186

Two-Phase Nonisothermal Hydrologic Transport Simulations at the Apache Leap Tuff Field Site

M. Shaikh, T.-C.J. Yeh, and T.C. Rasmussen
Department of Hydrology and Water Resources
University of Arizona, Tucson AZ 85721

INTRODUCTION

A field-scale heater test is proposed for investigating hydrothermologic processes in unsaturated fractured rock related to the disposal of high-level radioactive waste in an underground repository. The test will be conducted in moderately welded tuff at the Apache Leap Tuff Site in Central Arizona (Figure 1). The data collected from the experiment will be provided to the INTRAVAL program which is an internationally sponsored effort to validate hydrologic transport models.

An earlier heater test by Davies (1987) was conducted near the proposed heater site in densely welded tuff and provides initial data sets which are being used to design the field-scale experiment (Figures 2 and 3). Davies also conducted laboratory hydrothermologic experiments on unfractured drillcores which are interpreted by McCartin et al. (this meeting). Additional laboratory nonisothermal experiments are currently being conducted to provide supplemental data sets.

TOUGH (a multi-phase, nonisothermal computer simulation program) is used as part of the experimental design phase for the purpose of determining the optimal heater size and heating duration, as well as the location and number of monitoring intervals surrounding the heater. The monitoring equipment will be employed to obtain temperature, water saturation, matric potentials, solute concentrations and other variables critical to the understanding of thermally induced hydrologic transport on field scales.

Described in this presentation are the salient features of thermally induced flow and transport as determined from experimental experience with previous laboratory and field nonisothermal tests. Also presented is a discussion of ongoing simulation efforts used to guide the experimental design. Due to the paucity of experience related to thermal disturbances at depth in unsaturated, fractured media, the experimental design has evolved as more data and monitoring tools have become available.

IMPORTANT PROCESSES

The processes which may affect non-isothermal flow and transport include thermal, liquid, solute, vapor, and gas movement, which can be described by five coupled nonlinear partial differential equations (PDE's). Of special interest is the coupling between processes which causes complex interactions. The five PDE's must be solved using theoretical or observed phenomenological coefficients. Some of the coefficients are highly nonlinear and hysteretic functions of fluid potential and water content.

Predictions based on the solution of the equations described above must be tempered by observations. Experience from laboratory experiments indicate

a number of important phenomena which substantially affect fluid flow and solute transport. Laboratory experimental results indicate:

- Latent heat transport in the vapor phase, with sensible heat transport in the solid, liquid, and gas phases;
- A strong heat-pipe effect arising from countercurrent liquid-vapor flows which causes desiccation near the heat source and a concomitant accumulation of water away from the source;
- The possibility for osmotic potential to reduce the magnitude of the heat-pipe effect due to solute concentration effects on vapor pressure reduction and osmotic potential near the heater; and
- The dissolution and precipitation of silica in fractures which can alter the physical properties of the bulk rock.

These laboratory findings must be balanced by experimental evidence conducted over field scales using less artificial boundary conditions. The field scale findings include:

- Heat transport occurs from the source as sensible and latent heat, causing a desiccation of the rock near the source which expands over time.
- Liquid water accumulates in boreholes and openings near the heat source, with little water accumulation in the rock matrix (Figure 4).
- Substantial air movement occurs through fracture networks due to orographic and barometric gradients.

The nonwaste portion of the waste-repository structure will undoubtedly affect the hydrothermologic regime as well. The placement of shafts, seals, drifts, boreholes, ventilation ducts, and drains will have an impact on fluid flow and solute transport. In particular, the operation of the ventilation system will affect the transport in the vapor phase by:

- The injection of dry, cooler exterior air which will be circulated through the open repository;
- The resultant transport of water through the repository as vapor;
- The discharge of warm, humid air to the atmosphere; and
- The alteration of the existing orographic and barometric circulation within the subsurface.

By circulating air through the repository, substantial quantities of water will be removed and discharged to the atmosphere, thus causing the desiccation and cooling of interior repository surfaces. For isolated chambers within the repository, substantial condensation may or may not occur depending upon the moisture and thermal gradients across the chamber.

SIMULATION OBJECTIVES

The proposed field-scale experiment is being designed with the above-described hydrothermologic features in mind so that important aspects of coupled heat, liquid, gas and solute transport can be observed. Knowing what kind of monitoring equipment to install, where to place the monitoring equipment, and where and how the heater should be placed and operated requires that a simulation model be employed which incorporates as many of the processes as possible.

Simulations will be used to identify the important features of the heater experiment including zones of saturation, regions where fracture flows are expected, and accumulation of high salinity waters near the evaporation

front. Once the size and location of these zones have been identified, various monitoring and sampling strategies will be examined and tested prior to conducting the field-scale heater experiment. The effects of gravity, fracture properties, initial water saturation, initial solute concentration, and material heterogeneities will be examined using sensitivity analyses. The types and locations of sensors to be installed will also be simulated to determine the required sensor sensitivities and the regions where the greatest changes are expected.

SIMULATION INPUTS

Inputs to the simulation model include physical properties of the rock matrix as well as fracture properties. To obtain the physical properties, laboratory tests of rock cores obtained near the proposed heater site are used to provide preliminary estimates of rock matrix parameters, such as the rock thermal, hydraulic, pneumatic, and solute transport properties (Rasmussen et al., 1990). Coupling between processes are also estimated using laboratory experiments conducted under nonisothermal conditions in a closed system, and monitored using a dual-source gamma ray attenuation device. The fracture network at the field site has been inventoried by Thornburg (1990) and is presented as Figure 5. The location of the heater with respect to the fracture network is an essential component of the experimental design.

Other necessary simulation inputs are the boundary conditions. An important requirement for boundary conditions in the unsaturated zone is the ability to impose constant gradient, as opposed to constant flux, boundary conditions. For saturated media both conditions are interchangeable, but for this application the coefficient relating the gradient to the flux is a nonlinear function of water content. The proposed modification consists of allowing a constant gradient boundary condition to be prescribed, which is equivalent to a constant flux boundary condition only when the hydraulic, pneumatic or thermal conductivities remain constant as a function of matric suction. Additionally, model inputs of borehole surfaces must be considered. Rather than treating the borehole walls as no flow boundaries, transport into and along boreholes must be considered.

SIMULATION RESULTS

The proposed field heater experiment is simulated by TOUGH using two-dimensional cylindrical space coordinates (Figure 6). The heater is initially placed at a depth of three meters. As an example of the use of TOUGH for experimental design purposes, Figure 6 also presents simulation output at 127 days following the initiation of the heat pulse. The simulation assumes uniform material properties (no fractures or boreholes). Drying around the heat source is evident, and a zone of near-saturation is appearing above and away from the heat source. The fact that the zone is not directly above the source is most likely due to the shallow position of the heat source and the resultant affect of the surface boundary condition. Thus, the depth of the heat source will probably affect where saturation zones will appear. Additional simulation results will be presented at the meeting to demonstrate other examples of the use of TOUGH for experimental design purposes.

REFERENCES

Davies, B.E., 1987, Measurement of Thermal Conductivity and Diffusivity in an Unsaturated, Welded Tuff, M.S. Thesis, University of Arizona.

Nitao, J.J., 1990, Near-Field Thermal Fluid Effects, Presentation to The Nuclear Waste Technical Review Board, March 19-20.

Rasmussen, T.C., D.D. Evans, P.J. Sheets, and J.H. Blanford, 1990, Unsaturated Fractured Rock Characterization Methods and Data Sets at the Apache Leap Tuff Site, NUREG/CR-5596.

Thornburg, T.M., 1990, Electrical Resistivity of Unsaturated, Fractured Tuff: Influence of Moisture Content and Geologic Structure, M.S. Thesis, University of Arizona.

FIGURES

1 Proposed location of field heater test at the Apache Leap Tuff Site.

2 Diagram of heating element and thermocouple located behind packer (right borehole) and packers isolating psychrometers (left borehole) at Queen Creek road tunnel site.

3 Observed water content in tuff around the heater borehole as a function of time for heating experiment in the Queen Creek road tunnel.

4 Simulated and observed rock matrix water content in prototype field heater test at G-Tunnel, Nevada Test Site. (From Nitao, 1990)

5 Structural lineaments interpreted from aerial photographs of fracture planes exposed in outcrop at heater site.

6 View of simulated heat source located three meters below ground surface (above) and simulated liquid saturation distribution around heat source at 127 days (below).

REFERENCES

Davies, B.E., 1987, Measurement of Thermal Conductivity and Diffusivity in an Unsaturated, Welded Tuff, M.S. Thesis, University of Arizona.

Nitao, J.J., 1990, Near-Field Thermal Fluid Effects, Presentation to The Nuclear Waste Technical Review Board, March 19-20.

Rasmussen, T.C., D.D. Evans, P.J. Sheets, and J.H. Blanford, 1990, Unsaturated Fractured Rock Characterization Methods and Data Sets at the Apache Leap Tuff Site, NUREG/CR-5596.

Thornburg, T.M., 1990, Electrical Resistivity of Unsaturated, Fractured Tuff: Influence of Moisture Content and Geologic Structure, M.S. Thesis, University of Arizona.

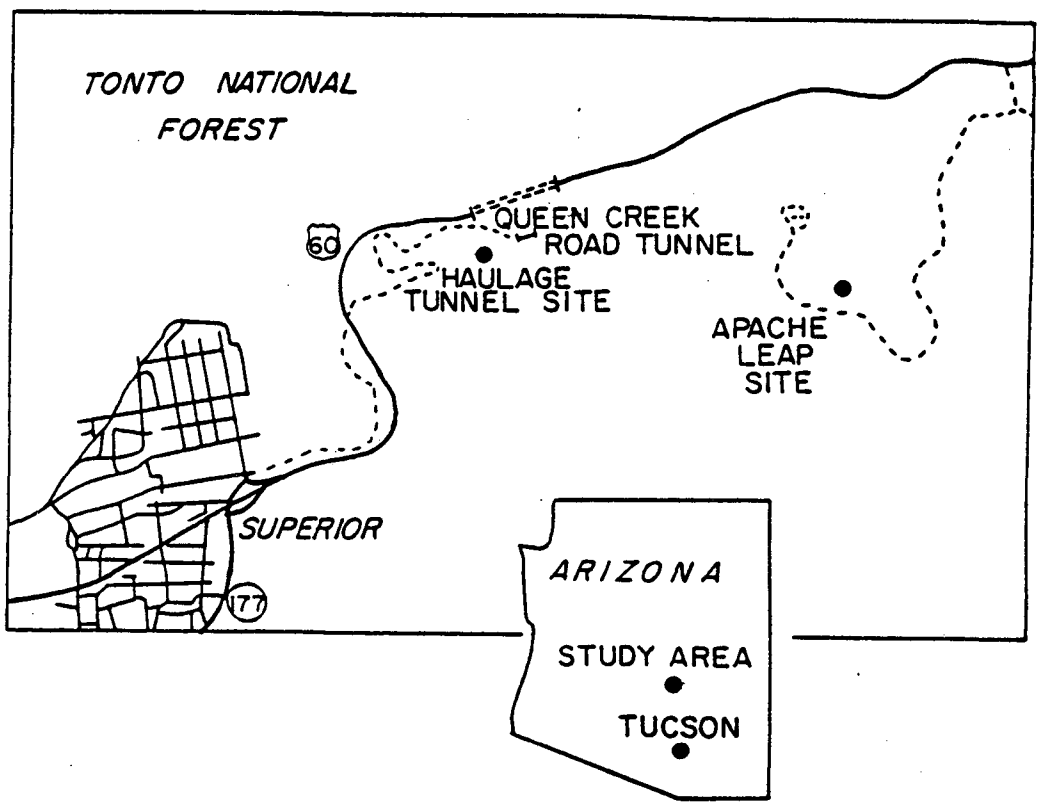

Figure 1 Proposed location of field heater test at the Apache Leap Tuff Site.

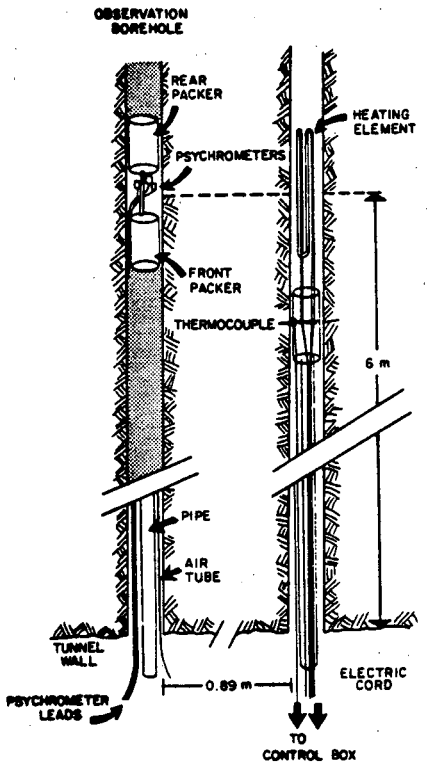

Figure 2 Diagram of heating element and thermocouple located behind packer (right borehole) and packers isolating psychrometers (left borehole) at Queen Creek road tunnel site.

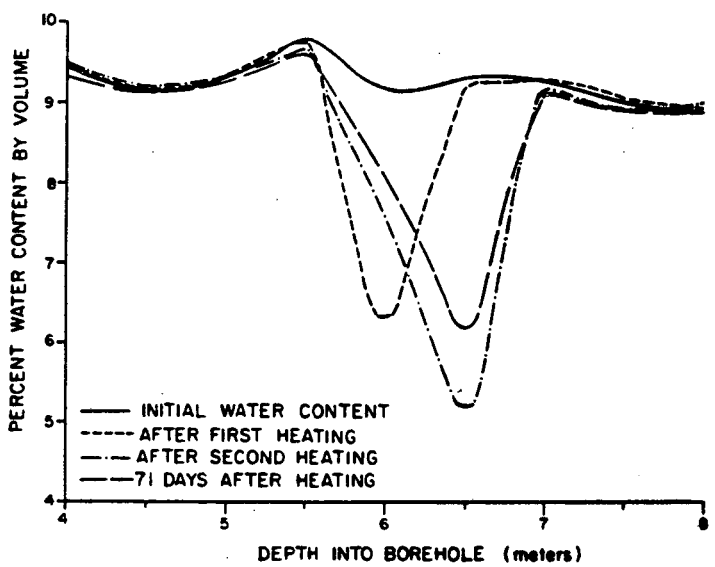

Figure 3 Observed water content in tuff around the heater borehole as a function of time for heating experiment in the Queen Creek road tunnel.

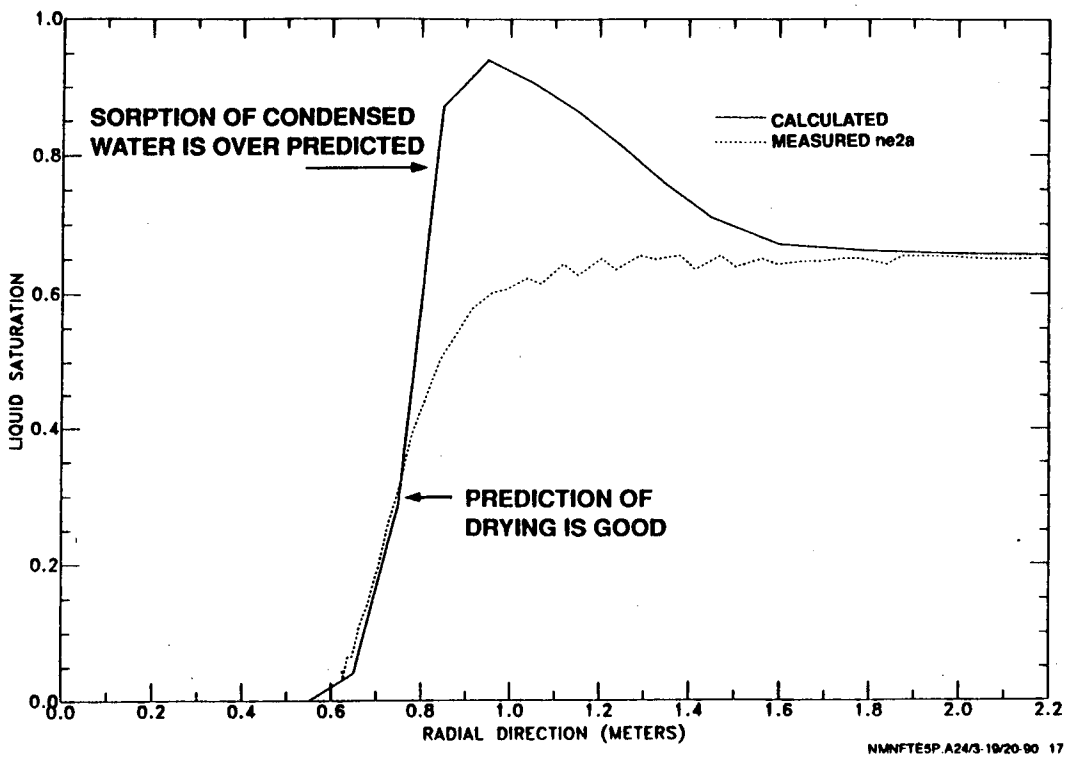

Figure 4 Simulated and observed rock matrix water content in prototype field heater test at G-Tunnel, Nevada Test Site. (From Nitao, 1990)

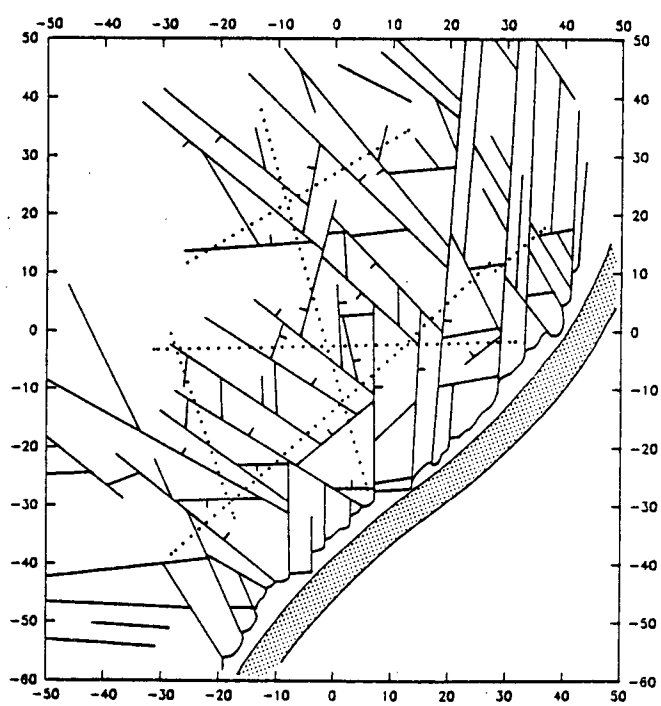

Figure 5 Structural lineaments interpreted from aerial photographs of fracture planes exposed in outcrop at heater site.

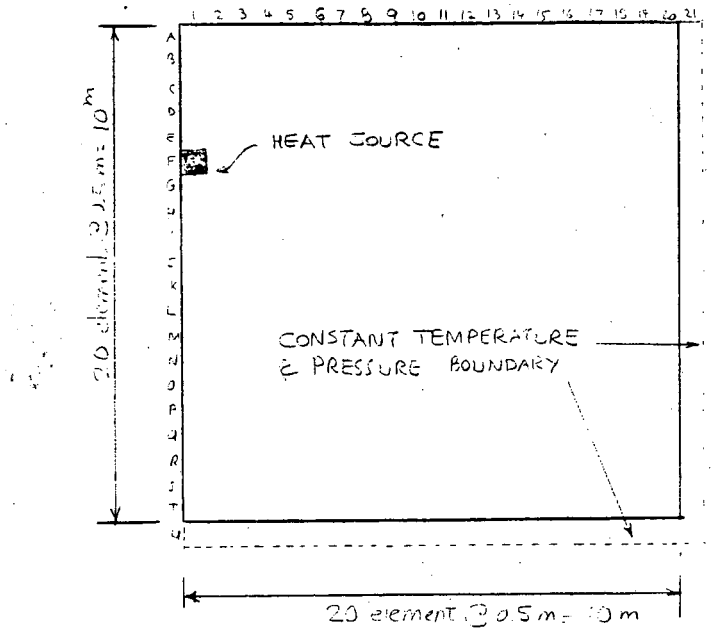

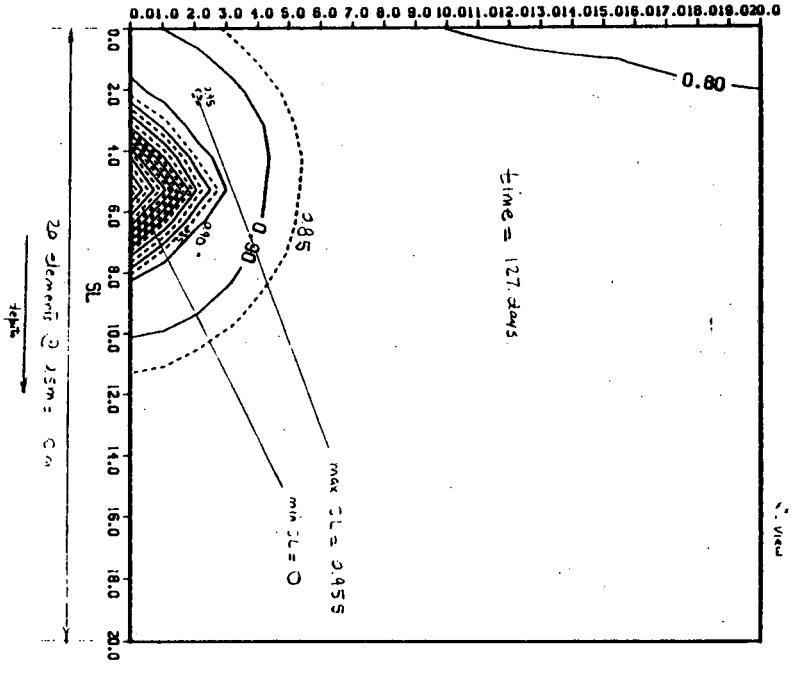

Figure 6 View of simulated heat source located three meters below ground surface (above) and simulated liquid saturation distribution around heat source at 127 days (below).

Modeling Hydrothermal Flow in Variably Saturated, Fractured, Welded Tuff During the Prototype Engineered Barrier System Field Test of the Yucca Mountain Project

Thomas A. Buscheck and John J. Nitao

Earth Science Department

Lawrence Livermore National Laboratory

1. Introduction

The Yucca Mountain Project (YMP) of the U.S. Department of Energy (DOE) is investigating the suitability of the tuffaceous rocks occurring in the unsaturated zone at Yucca Mountain, Nevada for nuclear waste storage. The Engineered Barrier System Field Tests (EBSFT) will be conducted within the Topopah Spring member of the Paintbrush Tuff at Yucca Mountain, primarily to examine the thermohydrological response of the repository environment to thermal loading from waste packages (Yow, 1985). The Prototype Engineered Barrier System Field Test (PEBSFT) was carried out by Ramirez and others (1989, 1990) in G-Tunnel complex of the Nevada Test Site to test and evaluate components of the geophysical instrumentation network and to support the validation of thermohydrological models. This report describes the modeling of the PEBSFT carried out by Buscheck and Nitao (1990) with the V-TOUGH code (Nitao, 1989) which is a modified version of the TOUGH code (Pruess, 1987).

2. Discussion of Numerical Models, Physical Data and Assumptions

The Grouse Canyon member of the Belted Range tuff found in G-Tunnel consists of a highly fractured, densely welded tuff. In situ permeability testing found fractures to be major conduits for fluid flow (Ramirez and others, 1990) which are discretely accounted for in our fracture/matrix (F/M) model. As such, we utilize distinct fracture and matrix properties considered to be applicable to Grouse Canyon tuff, including data obtained by Peters and others (1984) for Topopah Springs sample G4-6. Based on Zimmerman and Blanford (1986) we assumed an initial matrix saturation, S_{mi} of 65 percent and a matrix porosity, ϕ_m of 20 percent. Based on permeability measurements and fracture surveys conducted by Ramirez and others (1989 and 1990), we assumed a fracture aperture, b of 100 μm and a fracture spacing, B of 0.3 m and determined the fracture permeability on the basis of the cubic law.

The F/M model assumes an infinitely long, horizontal heater, orthogonally intersected by uniformly spaced fractures, with periodic boundaries along the symmetry planes down the center of the fracture and matrix, respectively, (Figure 1). With gravity neglected, the model is radially symmetric about the heater axis. Table 1 lists the numerical grid spacing. The heater is a 0.25-m-diameter heat generation cell with a three-stage heating schedule: (1) full-power at 1 kw/m ($0 < t < 4$ months), (2) a linear "rampdown" from full power to zero ($4 < t < 6$ months), and (3) no heating ($6 < t < 12$ months).

A comparison with the temperatures measured during the PEBSFT found the infinite heater assumption results in the F/M model overpredicting temperatures. It is necessary to account for the finite heater length because heat flow around the heater is spherical (rather than radial as is assumed in the F/M model). Due to the impracticality of discretely accounting for all of the fractures along the entire heater length, it was necessary to account for fractures with an equivalent continuum model (ECM). For situations in which the matrix and fractures are effectively in equilibrium, fracture and matrix properties may be volume-averaged with the bulk porosity, ϕ_b, bulk saturation, S_b, and bulk conductivity, K_b (either thermal or hydraulic) of the equivalent medium given by:

$$\phi_b = \phi_f + (1-\phi_f)\phi_m$$

$$S_b = \frac{S_f\phi_f + S_m(1-\phi_f)\phi_m}{\phi_f + (1-\phi_f)\phi_m}$$

$$K_b = K_m(1-\phi_f) + K_f\phi_f$$

where ϕ_m, S_m, ϕ_f, and S_f are the porosity and saturation of the matrix and fractures, respectively. In general, the ECM is appropriate for situations where the fracture spacing is small enough to result in a

negligible lag in the hydrothermal response in the matrix relative to that of the fractures. For the ECM we applied the actual PEBSFT heating schedule: (1) full-power at 1.12 kw/m ($0 < t < 128$ days), (2) a linear "rampdown" to zero power ($128 < t < 195$ days), and no heating ($t > 195$ days). Note that this only deviates slightly from the schedule used in the F/M model. With gravity neglected, the model is radially symmetric about the heater axis and, due to the remoteness of the constant property boundaries, is axially symmetric about the midpoint of the heater. Table 2 lists the numerical grid spacing.

3. Discussion of Results

3.1 Fracture/Matrix Model

In addition to simulating the reference case, a parameter sensitivity study was carried out, investigating the following matrix properties: porosity, permeability, and initial saturation; and fracture properties: aperture, permeability, and spacing. The impact of vapor venting through the heater borehole to the access drift was investigated as well as the functional dependency of the rate of drying-out of the rock on the heating rate. For all cases, heat flow was found to be conduction-dominated, accounting for 88.5 percent of the total heat flow during the full-power stage in the reference case.

Drying of the matrix is seen to preferentially occur along the heater borehole wall and the fracture face (Figure 2). As in Figure 1, axial distance is with respect to the fracture midplane and radial distance is with respect to the heater axis. Due to the low matrix permeability, high gas-phase pressures are required to drive water vapor to the free faces (Figure 3). Upon reaching the fractures, most of the vapor is driven radially away from the boiling zone to the condensation zone where, due to the high suction potential, it is imbibed by the matrix. In cases where borehole venting was allowed, some vapor flows radially towards the heater and out to the access drift. During the full-power stage of the reference case, venting removed 35 percent of the moisture driven from the dried-out zone, thereby removing 4.4 percent of the cumulative thermal input. The volume of the dried-out zone was found to be proportional to $\sqrt{k_m}/B$ and $Q_h^{5/2}$ where Q_h is the heat generation rate per unit length of heater. For $b > 10\ \mu m$ the volume of the dried-out zone is insensitive to b. Therefore, for most of the fractures observed in G-Tunnel, flow resistance in the fractures is unlikely to throttle the rate of drying.

As the rock cools below boiling conditions, vapor flow, particularly along fractures, dominates re-wetting of the dried-out zone. Due to the large increase in vapor pressure, nearly all of the air has been driven away from the boiling zone. Condensation results in gas-phase pressures dropping below atmospheric, pulling vapor in towards the dried-out zone. In addition to the bulk flow of vapor, saturation gradients and the corresponding relative humidity gradients result in binary diffusion-driven vapor flow from wetter to drier regions, particularly along fractures. Upon reaching drier rock, this vapor condenses along fracture faces and is imbibed by the matrix. Because re-wetting is dominated by binary gas diffusion and capillary condensation along fractures, re-wetting is strongly dependent on the fracture distribution and connectivity, and is much less sensitive to fracture aperture and permeability.

3.2 Equivalent Continuum Model

In the rock the agreement between the ECM-predicted and the measured temperatures is outstanding (Figure 4). At the borehole wall, the ECM overpredicts temperatures (with a 7^oC discrepancy at the end of full-power heating). This discrepancy is at least partly due to heat source itself. Both during the PEBSFT and benchtop testing of the heater, the top of the heater was observed to be approximately 40^oC hotter than the bottom of the heater. The borehole temperatures in Figure 4 were measured at the bottom of the heater borehole. Had temperatures been measured on the upper borehole wall, it is likely that the predicted temperatures would be bracketed by the measured temperatures. The outstanding agreement between the predicted and measured temperatures is at least partly attributed to heat flow around the PEBSFT being dominated by conduction. Consequently, even though certain aspects (notably wetting behavior) of the fluid flow field are not well represented by the ECM, the temperature field is relatively insensitive to discrepancies between the predicted and actual heat convection behavior.

Figure 5 is a comparison of the predicted and measured radial saturation profile at the midpoint of the heater at the end of full-power heating. The measured profiles were obtained by neutron logging along two observation boreholes, ne2a (located above the heater) and ne6 (located below the heater).

For the dried-out zone, the agreement between the ECM and the measured data is quite good. Apparently, the assumption that flow resistance in the matrix is negligible holds reasonably well for drying. Conversely, this assumption (along with the assumption that gravity is negligible) results in a significant discrepancy between the predicted and observed wetting behavior. Because matrix imbibition is very slow relative to the time-scale of the PEBSFT, neglecting the time it takes for the matrix to imbibe the condensate, results in the ECM confining the saturation "halo" to a very tight interval. Saturation measurements showed a negligible increase in saturation beyond the boiling front. Moreover, temperatures measured along one side of the boiling zone indicated a region where two-phase conditions persisted, probably caused by gravity drainage of condensate from above. Figure 5 also indicates the impact of gravity drainage on drying behavior. Although temperatures above the heater were hotter than below, drying above the heater lagged behind drying below the heater. Above the heater, condensate drainage causes refluxing, thereby retarding the drying rate, while below the heater, condensate constantly drains away from the boiling front.

4. Conclusions

Using the V-TOUGH code the PEBSFT was modeled using two different conceptual models: (1) discretely representing the fracture and matrix properties (F/M model) and (2) volume-averaging their properties through the use of an equivalent continuum model (ECM). Using the F/M model, the distinct hydrothermal response of the fracture and matrix could be observed, along with some of the functional dependencies of drying and wetting behavior to various parameters, including heating rate. Heat flow was found to be dominated by conduction, with the explicit representation of the finite heater length (in the ECM) being crucial to obtaining a good match with the observed temperatures. While the ECM was found to adequately represent drying behavior, neglecting flow resistance in the matrix to imbibition and the effect of gravity on condensate drainage, were found to result in significant discrepancies between predicted and observed wetting behavior.

Acknowledgements

The authors acknowledge the helpful review comments of D. Chesnut and R. Knapp. Work performed under the auspices of the U.S. Department of Energy by Lawrence Livermore National Laboratory under Contract W-7405-Eng-48.

References

Buscheck, T. A. and J. J. Nitao, "Modeling Hydrothermal Flow in Variably Saturated, Fractured, Welded Tuff During the Prototype Engineered Barrier System Field Test in G-Tunnel Complex", UCID- , Lawrence Livermore National Laboratory, Livermore, CA, 1990 (in preparation).

Nitao, J. J., "V-TOUGH - An Enhanced Version of the TOUGH Code for the Thermal and Hydrologic Simulation of Large-Scale Problems in Nuclear Waste Isolation", UCID-21954, Lawrence Livermore National Laboratory, Livermore, CA, September, 1989.

Peters, R. R., E. A. Klavetter, I. J. Hall, S. C. Blair, P. R. Hellers, and G. W. Gee, "Fracture and Matrix Hydrologic Characteristics of Tuffaceous Materials from Yucca Mountain, Nye County, Nevada", SAND84-1471, Sandia National Laboratories, Albuquerque, N. M., December 1984.

Pruess, K. "Tough User's Guide", Nucl. Regul. Comm. Rep. NUREG/CR-4645, Washington,D.C.,1987.

Ramirez, A. L., J. Beatty, T. A. Buscheck, R. Carlson, W. Daily, V. R. Latorre, K. Lee, W. Lin, N. Mao, J. J. Nitao, D. Towse, T. S. Ueng, D. Watwood, and D. G. Wilder, "Prototype Engineered Barrier System Field Test (PEBSFT): Progress Report through November 1, 1988", UCID-21640, Lawrence Livermore National Laboratory, Livermore, CA, 1989.

Ramirez, A. L., T. A. Buscheck, R. Carlson, W. Daily, K. Lee, W. Lin, N. Mao, T. S. Ueng, H. Wang, and D. Watwood, "Prototype Engineered Barrier System Field Test (PEBSFT) - Final Report", UCID- , Lawrence Livermore National Laboratory, Livermore, CA, 1990.

Yow, J., Jr., "Concept for Waste Package Environment Tests in the Yucca Mountain Exploratory Shaft", UCID-20450, Lawrence Livermore National Laboratory, Livermore, CA, 1985.

Zimmerman, R. M., and M. B. Blanford, "Expected Thermal and Hydrological Environments for Waste Emplacement Holes Based on G-Tunnel Heater Experiments", Proc. 27th Symposium on Rock Mechanics, Chapter 125, pp. 874-882, 1986.

Table 1
Numerical Grid Spacing for the
45x26 R-Z Fracture/Matrix Model Mesh

Radial Direction, ΔR (m)							
0.125	0.025	0.05	18*0.1	10*0.2	2*0.3	0.4	4*0.5
1.0	2*2.0	2*4.0	10.	1.0×10^{-30}			
Vertical Direction, ΔZ (m)							
0.00005	0.0001	0.00015	0.00023	0.00034	0.00051	0.00076	0.00114
0.00171	0.00257	0.00386	0.00578	0.00867	12*0.01	0.00413	

Table 2
Numerical Grid Spacing for the
34x17 R-Z Equivalent Continuum Model Mesh

Radial Direction, ΔR (m)							
0.125	0.025	0.05	13*0.1	5*0.2	6*0.3	0.4	0.8
1.6	3.2	6.4	12.8	1.0×10^{-30}			
Vertical Direction, ΔZ (m)							
0.02	4*0.325	0.18	0.20	4*0.325	0.65	1.3	2.6
5.2	10.4	1.0×10^{-30}					

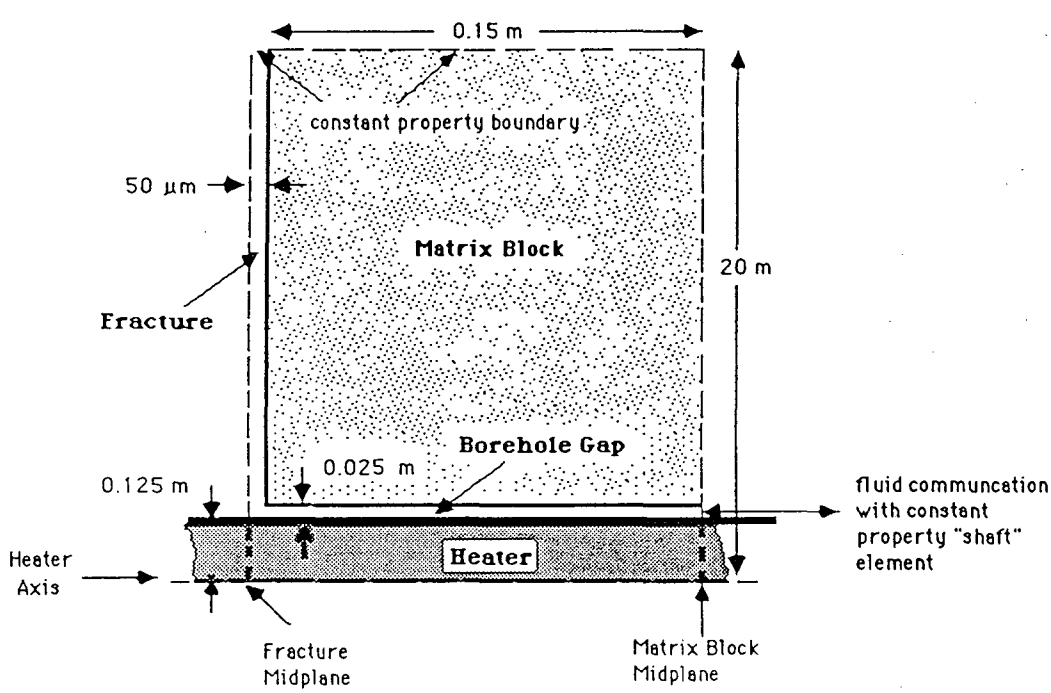

Figure 1. Schematic of the conceptual model used in the F/M model. Figure is not to scale.

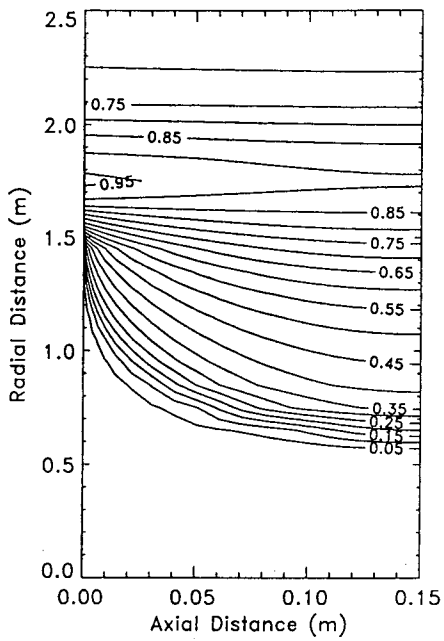

Figure 2. Contour plot of saturation at the end of full-power heating (t = 4 months) for the F/M model. Axial distances are exaggerated by a factor of 10.

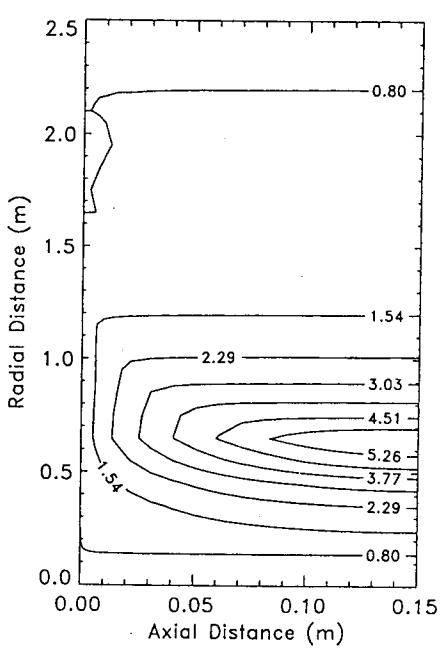

Figure 3. Contour plot of gas-phase pressure (*atm*) at the end of full-power heating (t = 4 months) for the F/M model. Axial distances are exaggerated by a factor of 10.

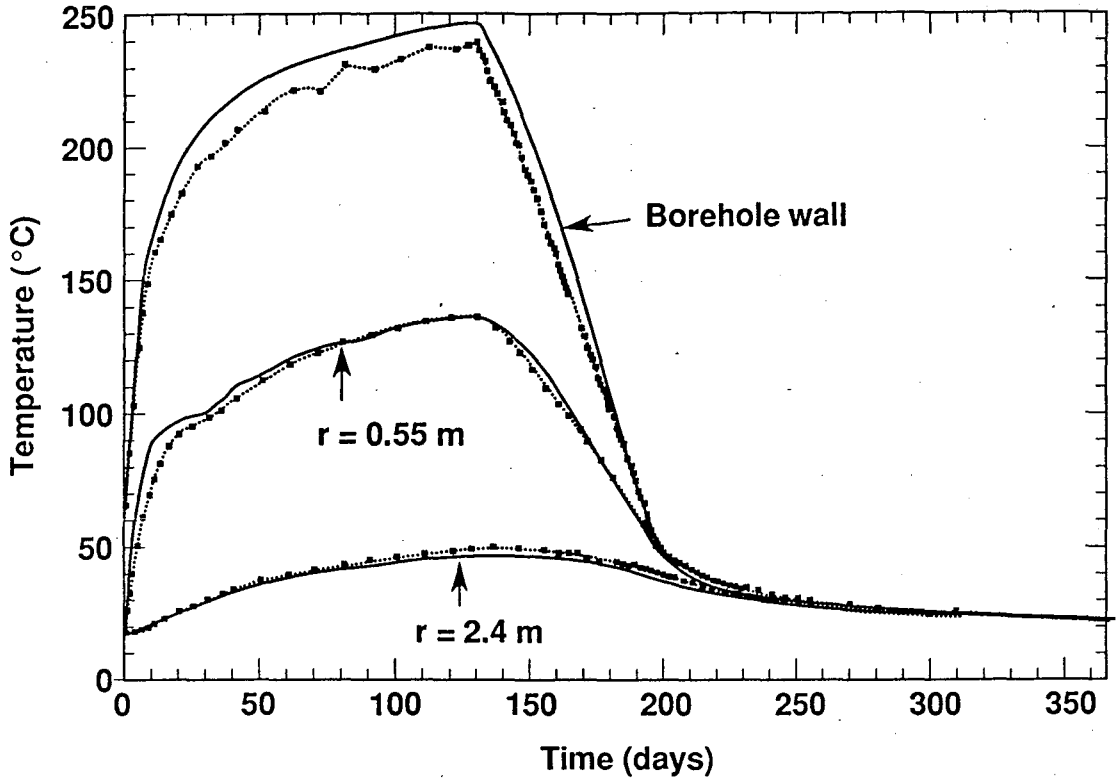

Figure 4. A comparison of the ECM-predicted (solid lines) and measured temperature history at three radial distances, located at the midpoint of the heater.

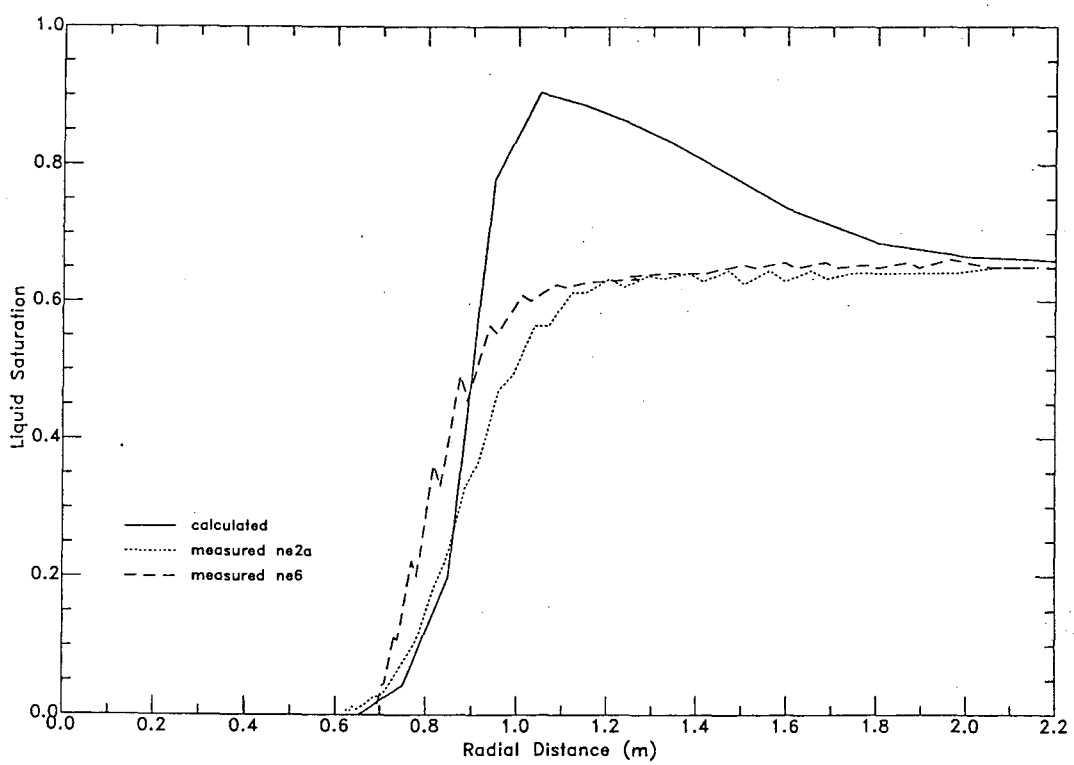

Figure 5. A comparison of the ECM-predicted and measured radial saturation profiles at the end of full-power heating (t = 128 days) at the midpoint of the heater.

UNSATURATED ZONE MOISTURE AND VAPOR MOVEMENT INDUCED BY TEMPERATURE VARIATIONS IN ASPHALT BARRIER FIELD LYSIMETERS

Diana J. Holford and Michael J. Fayer
Pacific Northwest Laboratory
P.O. Box 999, MSIN K6-77
Richland, Washington 99352
509-376-8318, FTS 444-8318, FAX 509-376-4428

Protective barriers are being considered for use at the Hanford Site to enhance the isolation of radioactive wastes from water, plant, and animal intrusion. Lysimeters were constructed to evaluate the performance of asphalt barrier formulations under natural environmental conditions. These lysimeters (Figure 1) were constructed of 1.7-m lengths of PVC pipe that have a diameter of 30 cm. The lysimeters were filled with layers of gravel, coarse sand, and asphalt (Freeman and Gee 1989a). The sand and gravel placed under the asphalt barrier were wet when installed (Freeman and Gee 1989b). TOUGH was used to conduct simulations to assess the effect of temperature variations on moisture and vapor movement beneath the asphalt layer in field test lysimeters. All variables in TOUGH were converted to double precision so that simulations could be run on a Sun-4 UNIX workstation. A radially symmetric grid (Figure 2) was used to simulate the lysimeter.

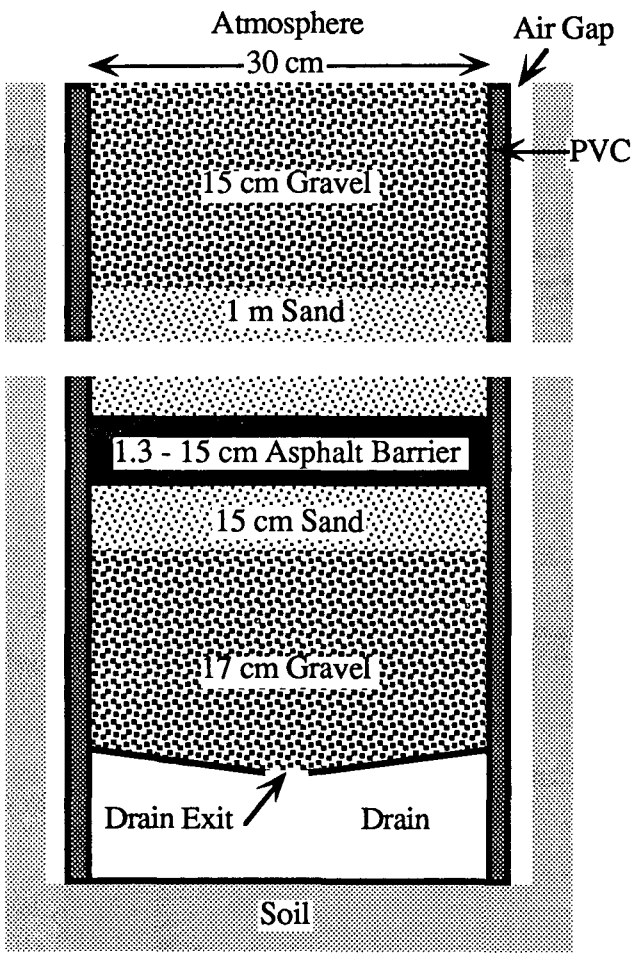

Figure 1: Cross Section of Lysimeter.

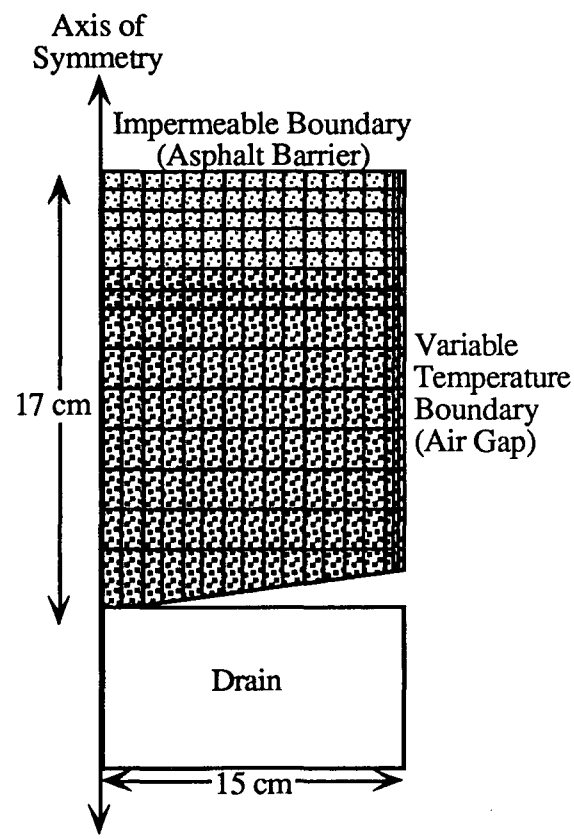

Figure 2: Cross Section of radial grid (Scale 2x that of Figure 1).

Figure 3 shows measured monthly water drainage from a control lysimeter (with no asphalt layer) for the 2-year period since the lysimeter was installed in July 1988. Also shown is the average monthly rainfall and soil temperature measured at a nearby site (Stone et al. 1983). Because there is no barrier to impede infiltration, drainage correlates to rainfall with a lag time of one month.

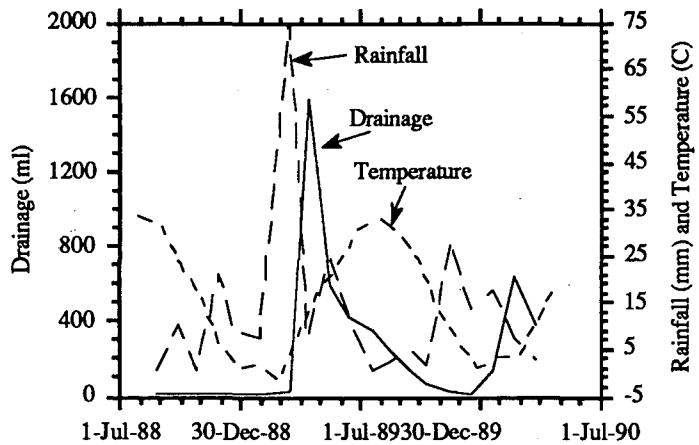

Figure 3: Drainage from lysimeter #9 (control) compared with average monthly rainfall and soil temperature at 1.3 cm depth.

Figure 4 shows drainage from a lysimeter with a rubberized asphalt layer compared with the same rainfall and temperature data shown in Figure 3. Unlike the control lysimeter, drainage correlates to temperature. Also, the amount of drainage is small compared with the control lysimeter and shows no correlation with rainfall. For these reasons, we hypothesize that the drainage water is not from leakage through the barrier, but is residual water from the installation of the barriers. This hypothesis is further borne out by the fact that salt placed above the asphalt barrier has not been found in the drainage water.

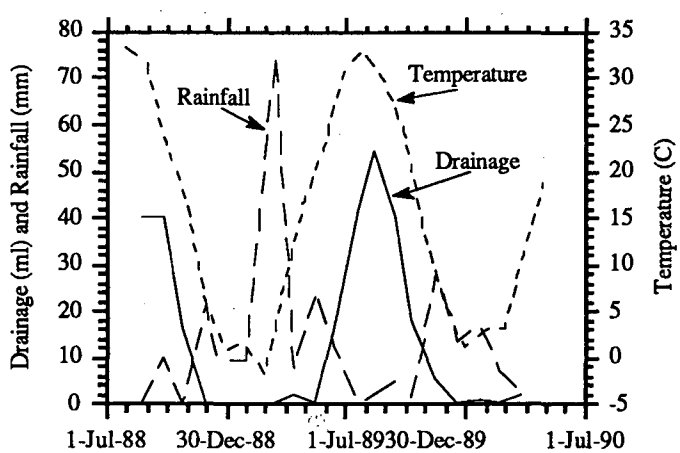

Figure 4: Drainage from lysimeter #2 (rubberized asphalt barrier) compared with average monthly rainfall and soil temperature at 1.3 cm depth.

TOUGH was used to conduct two axi-symmetric simulations of the lysimeter to assess the effect of temperature variations on water movement in the liquid and vapor phase beneath the asphalt layer. In the first simulation, the lysimeter temperature was maintained at a constant temperature of 15.3 °C (the yearly average soil temperature). For the variable temperature simulation, the average monthly temperature at 1.3 cm depth (Figure 5) was applied along the side boundary of the model (Figure 1). The drain was held at a constant temperature of 15.3 °C. The initial temperature throughout the entire system was 32.9 °C (the average July soil temperature). The initial water saturation for the sand layer was 90% and the gravel layer was 10%.

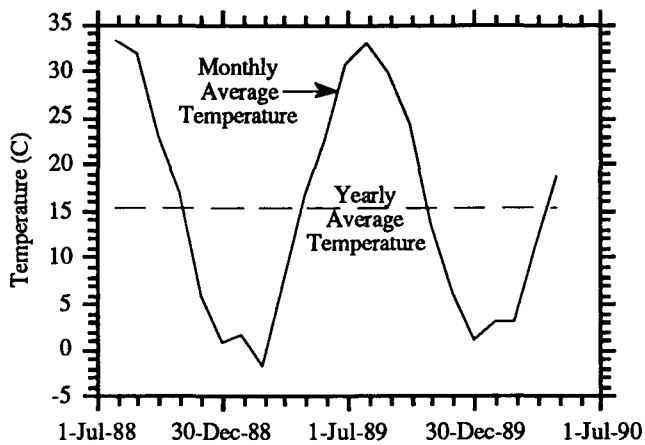

Figure 5: Monthly and yearly average temperatures at 1.3 cm depth in soil at the Hanford Meteorological Station.

Thermal conductivities at saturated and dry conditions (0.29 and 2.2 W/m°C) were estimated from properties for average soils (Hillel 1980). Specific heat of quartz (Hillel 1980) was used for the sand, and specific heat of granite (Weast 1982) was used for gravel. Nodes next to the variable temperature boundary were given a large (10^8) specific heat so that they would remain at the specified temperature.

The parameters used for the hydraulic properties of the soils (Table 1) are for van Genuchten moisture retention and Burdine hydraulic conductivity functions (van Genuchten 1980). The coarse sand parameters were fit to data for coarse sand from the literature (Mualem 1976), and the gravel parameters were fit to estimated gravel properties from (Fayer et al. 1985).

Table 1. Parameters for Describing Hydraulic Properties with the van Genuchten Functions

Material	S_{lr}	S_{ls}	α (1/Pa)	λ	K_s (m/yr)
Coarse Sand	0.02247	1.00	0.000741	0.64331	1.09×10^{-10}
Pea Gravel	0.01193	1.00	0.050365	0.54260	3.57×10^{-10}

Figure 6 shows a comparison of drainage predicted by constant temperature and variable temperature simulations.

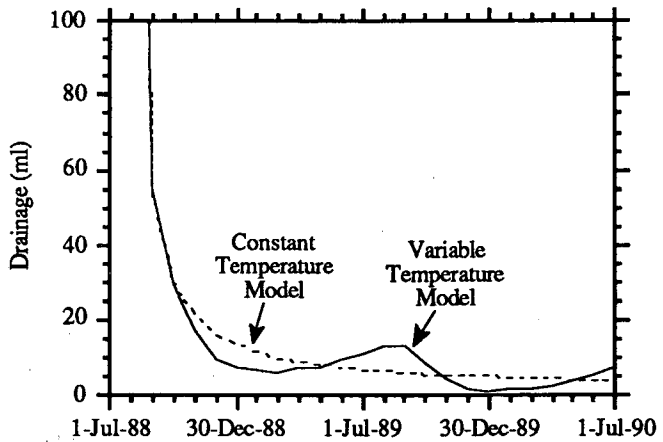

Figure 6: Comparison of drainage predicted by constant temperature and variable temperature simulations.

The variable temperature shows a decrease in drainage relative to the constant temperature simulation when temperatures are below the yearly average and an increase in drainage when temperatures are above the yearly average. However, the increase in drainage in summer is not as great as actually observed in many of the lysimeters (Figure 7). Drainage from an asphalt barrier lysimeter reached a maximum of 54 ml in August 1989, whereas the simulated drainage for that month was 13 ml.

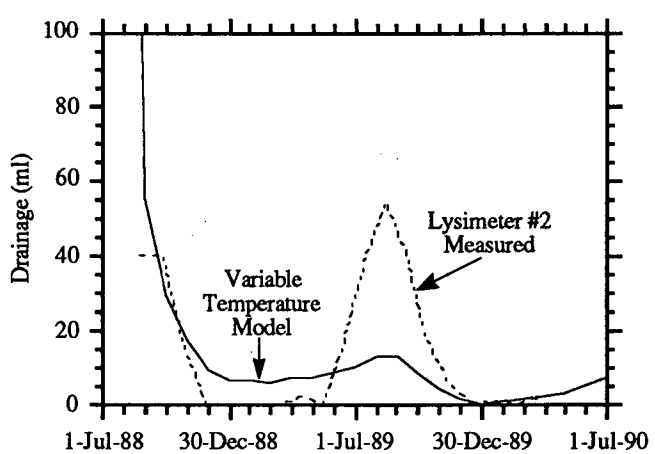

Figure 7: Comparison of drainage predicted by variable temperature model and measured from an asphalt barrier lysimeter.

The difference between the drainage rates in winter and summer is illustrated by the simulated flow fields for February and August 1989 in Figures 8 and 9. Overall, flow velocities are much higher in August than in February, delivering more liquid mass to the drain in the lower left-hand corner. The absolute temperature is much higher in August, with the highest temperature (32.8 °C) along the right-hand side and the lowest (29.4 °C) at the lower left-hand corner. The saturated vapor pressures are much higher in August, and the vapor pressure gradient is an order

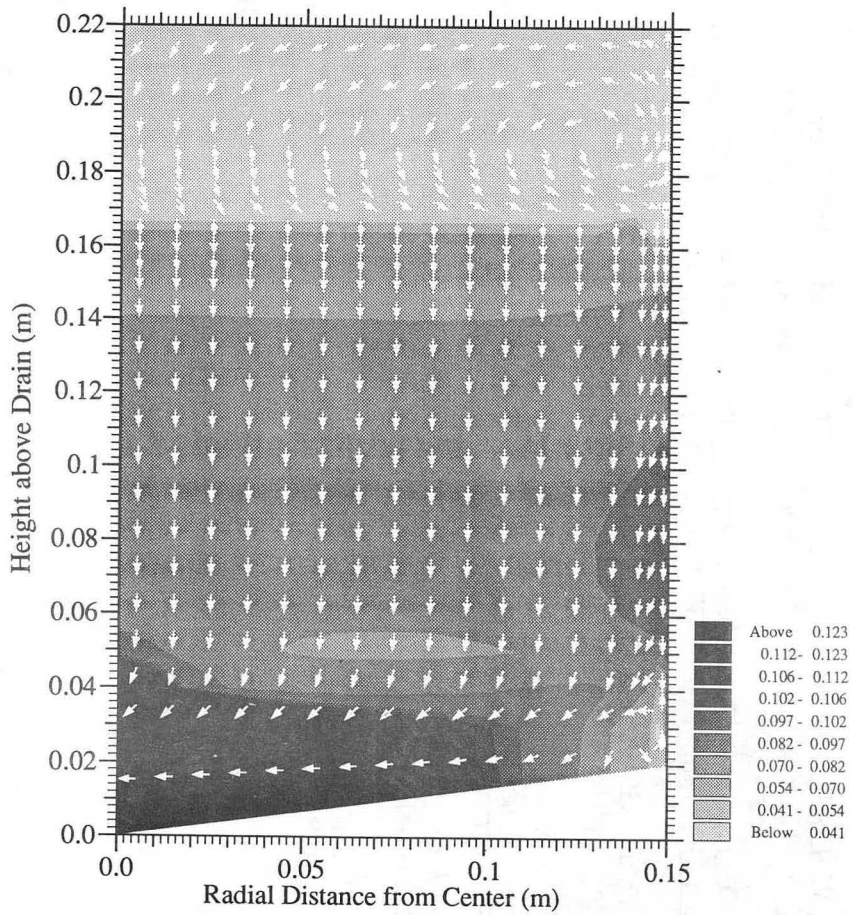

Figure 8: Simulated liquid velocities for February 1989 (minimum = 6.0×10^{-4}, maximum = 2.8 m/yr)

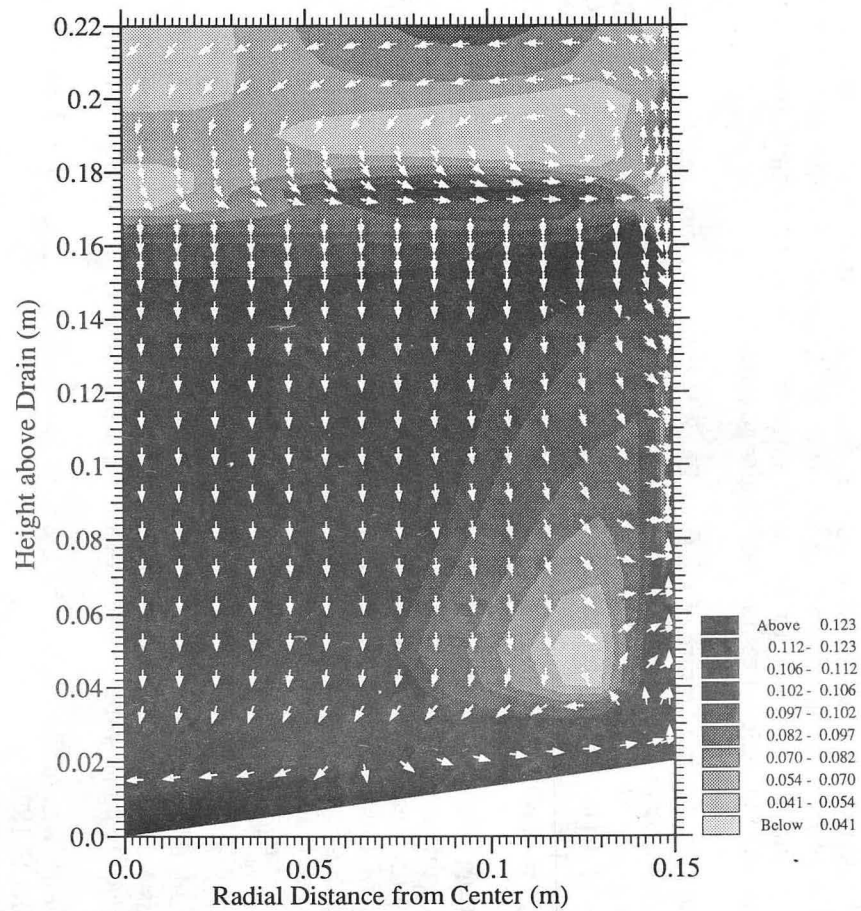

Figure 9: Simulated liquid velocities for August 1989 (minimum = 9.2×10^{-3}, maximum = 6.6 m/yr)

of magnitude higher. The vapor pressure gradient in August follows the temperature gradient from the right-hand side to the lower left-hand corner, driving water in the vapor phase to the drain, where it condenses at the cooler drain temperatures. In August, the higher temperature along the right-hand side caused the column to dry out slightly, causing some upward flow along that side. This effect may have impeded the simulated drainage slightly.

The most interesting feature of the flow fields is the convection cell that formed in the wet, sandy layer. Because the dry, gravel layer acts as a barrier to downward flow of water, the water in the wet layer circulates because of liquid density differences caused by the temperature gradient across the system. The convection cell flows counterclockwise in the summer and clockwise in the winter; however, the convection cell flows counterclockwise during January and February because temperatures in the column are between 1.5 and 4 °C, and the density of water is highest at 4 °C.

The effect of temperature on the hydraulic conductivity of the soils was not included in this simulation, and this would enhance the differences in drainage simulated in winter and summer. Also, diurnal temperature variations could cause greater drainage to occur in the summer months, while freezing of soil moisture during the winter months would stop drainage from the column. Future simulations could include the effect of a temperature gradient in the air gap around the lysimeters, rather than imposing a uniform temperature. Also, simulations for individual months could be rerun using diurnal temperature variations rather than just the monthly average temperature.

Although the simulated drainage does not match the observed drainage in magnitude, the seasonal trends are the same. This provides supporting evidence that temperature variations can affect drainage of residual water from beneath the asphalt barrier in the lysimeters.

This work was funded in part by the U.S. Department of Energy under Contract DE-AC06-76RLO 1830.

REFERENCES

Fayer, M. J., W. Conbere, R. R. Heller and G. W. Gee. (1985). Model Assessment of Protective Barrier Designs. PNL-5604. Pacific Northwest Laboratory, Richland, Washington.

Freeman, H. D. and G. W. Gee. (1989a). Hanford Protective Barriers Program: Status of Asphalt Barrier Studies - FY 1988. PNL-7153. Pacific Northwest Laboratory, Richland, Washington.

Freeman, H. D. and G. W. Gee. (1989b). Hanford Protective Barriers Program: Status of Asphalt Barrier Studies - FY 1989. PNL-7153. Pacific Northwest Laboratory, Richland, Washington.

Hillel, D. (1980). Fundamentals of Soil Physics. Academic Press, New York, New York.

Mualem, Y. (1976). A Catalogue of the Hydraulic Properties of Soils. Research Progress Report 442. Technion, Israel Institute of Technology, Haifa, Israel.

Stone, W. A., J. M. Thorp, O. P. Gifford and D. J. Hoitink. (1983). Climatological Summary for the Hanford Area. PNL-4622. Pacific Northwest Laboratory, Richland, Washington.

van Genuchten, M. T. (1980). "A Closed-Form Equation for Predicting the Hydraulic Conductivity of Unsaturated Soils." Soil Sci. Soc. Am. J. 44: 892-898.

Weast, R. C. (1982). CRC Handbook of Chemistry and Physics. CRC Press, Inc., Boca Raton, Florida.

GASEOUS TRANSPORT OF VOLATILE ORGANICS IN POROUS MEDIA: COMPARISON OF MATHEMATICAL MODELS

John M. Farr
Levine•Fricke, Inc., 1900 Powell St., Emeryville, CA 94608

ABSTRACT

In diffusion dominated transport, traditional mathematical formulations, such as used in TOUGH, do not rigorously handle cases where the phase mass density is significantly dependent on phase composition. Such is the case for near-static transport volatile organic compounds in subsurface gas, a case currently of great interest in the study of environmental problems. The "Dusty-Gas" Model (Mason, et al., 1967) is a set of complex constitutive equations that simulate observed transport behavior more accurately than the traditional models. However, for workers accustomed to the modeling framework described in the transport phenomena literature, the dusty gas model is difficult to understand and implement for general transient simulations. Rigorous numerical simulators, such as TOUGH, have yet to be developed around the Dusty-Gas Model. Thus, there is a need to update the mathematical formulations used in traditional transport models to enhance the generality and accuracy of existing numerical simulators.

As an alternative to the dusty gas model, a simple new transport formulation was developed using the traditional modeling framework of the transport phenomena literature. Identification of the reference advective velocity given by Darcy's Law, as a function of the species drift velocities in a mixture, allowed for derivation of new molecular diffusion equations. These new constitutive relations were coded into a modified version of TOUGH, where the representation of water was replaced with that of a volatile organic compound, and Klinkenberg and Knudsen effects were added. The new formulation was compared to that used in TOUGH, where the Darcy seepage velocity is taken as a mass-average velocity, and to the formulation commonly used in chemical engineering, where the Darcy seepage velocity is taken as a mole-average velocity. Significant differences in transport behavior is shown by each of these three models. The new transport formulation is found to reproduce experimental results and represent the Dusty-Gas Model behavior quite well.

INTRODUCTION

Existing transport models in the hydrologic community fail to adequately describe cases where phase mass densities depend significantly on composition. Diffusive fluxes (or more generally, non-advective fluxes) must be referenced to an advective reference velocity, and existing models are inadequate because the advective reference velocity represented by Darcy's law has been misinterpreted.

There are two common forms of the binary molecular diffusion equation that, while quite general, describe fluxes in different ways. The first,

$$J_i^{NN} = -cD_{ij}^{*}\nabla\chi_i \tag{1}$$

describes the molar flux relative to a mole-average velocity, which is given by:

$$\nu^N = \frac{\Sigma c_i \nu_i}{\Sigma c_i} \tag{2}$$

The second diffusion flux equation,

$$J_i^{MM} = -\rho D_{ij}^{*}\nabla\omega_i \tag{3}$$

describes the mass flux relative to a mass-average velocity, which is given by (see list of symbols for definition of terms):

$$\nu^M = \frac{\Sigma \rho_i \nu_i}{\Sigma \rho_i} \tag{4}$$

Textbooks in chemical engineering recommend the use of equation (1) for modeling gaseous transport in tubes or porous catalysts (eg., Bird et al., 1960; Cussler, 1984). The use of equation (1) in a molar continuity equation for porous media transport modeling assumes that Darcy's law yields a macroscopic mole-average velocity. In contrast, most subsurface transport models use equation (3) to describe diffusion fluxes, thereby taking the Darcy seepage velocity as a macroscopic mass-average velocity (eg., Abriola and Pinder, 1985; Pollock, 1986; Pruess, 1987). Equation (1) is generally incorporated into a molar continuity equation, along with the required state equations, to form what is referred to here as the "Mole Model" for transport simulation. Equation (3) is generally incorporated into a mass continuity equation, along with required state equations, to form the "Mass Model".

It was suggested by Farr and McWhorter (1988) that the Darcy seepage velocity gives a macroscopic mole-average velocity (in keeping with the chemical engineering literature) and that the Mole Model, with equation (1) should be used to describe the diffusion flux relative to the Darcy advection. (Using the Mole Model does linearize many subsurface transport problems that are otherwise non-linear because the total molar density, c , in equation (1) is a function of only pressure and temperature for an ideal gas, whereas the mass density in equation (3) is a function of composition as well.) However, use of the Mole Model is incorrect in light of confirmed experimental observations supporting Graham's law of diffusion (Graham, 1833; Hoogschagen, 1953; Wicke and Hugo, 1961; Wakao and Smith, 1962; Rothfeld, 1963; Remick and Geankopplis, 1973). These observations show that the ratio of molar fluxes (relative to coordinates fixed on the porous medium)

under isobaric conditions is given by Graham's law of diffusion:

$$\frac{N_A}{N_B} = -\left[\frac{M_B}{M_A}\right]^{1/2} \tag{5}$$

and this holds for all pressures and pore sizes (not just in the Knudsen regime). This is in contrast to the equimolar and equimass counter diffusion predicted by the "Mole" and "Mass" Models, respectively. Thus, the Darcy seepage velocity represents neither a macroscopic mass-average velocity nor a mole-average velocity.

The Dusty-Gas Model was developed (Mason, et al., 1967) to address the shortcomings of the Mass and Mole Models. The Dusty-Gas Model, recently reviewed by Thorstenson and Pollock (1989), rigorously represents multicomponent diffusion effects, but it provides only constitutive equations, and no transient simulators incorporating the Dusty-Gas Model are currently available. In contrast, several rigorous transient simulators, such as TOUGH, are available which are based on the traditional modeling framework of the transport phenomena literature (eg., Bird, et al., 1960). In order to correctly utilize the transport phenomena modeling framework, the meaning of the Darcy seepage velocity must be known in terms of a weighted average of species drift velocities (analogous to equations (2) and (4)), and this is identified below.

The Graham-Average Velocity

Using equation (5) and the general modeling framework of the transport-phenomena literature (Bird, et al., 1960; Clazie, et al., 1967), the weighted average of species drift velocities given by the Darcy seepage velocity can be shown to be:

$$\nu^G = \frac{\Sigma M_i^{1/2} c_i \nu_i}{\Sigma M_i^{1/2} c_i} \tag{6}$$

or in terms of mass densities,

$$\nu^G = \frac{\Sigma M_i^{-1/2} \rho_i \nu_i}{\Sigma M_i^{-1/2} \rho_i} \tag{7}$$

The reference velocity given by equations (6) and (7) will be referred to here as the Graham-average velocity, in recognition of the much overlooked work of Thomas Graham during the mid-1800s, and the superscript G will denote this reference velocity. Equations (6) and (7) represent the macroscopic velocity that is directly related to the viscous flux given by Darcy's law.

Derivation of New Molecular Diffusion-Flux Equations

Now that the required reference velocity has been defined, new diffusion-flux equations can be derived. Clazie's equation (3-15)

(Clazie, et al., 1967) allows for general transformations in diffusion flux equations given the diffusion flux equation relative to one reference velocity, and provided that the required reference velocities have been defined as weighted averages of species drift velocities, as in equations (2), (4), (6), and (7). Using equation (6), the transformation of equation (1) results in the following equation for molar diffusion flux of species A relative to the Graham-average velocity in a binary mixture:

$$J_A^{NG} = - \left[1 + \frac{c_A M_B^{1/2} - c_A M_A^{1/2}}{c_A M_A^{1/2} + c_B M_B^{1/2}} \right] c D_{AB}^{*} \nabla \chi_A \tag{8}$$

The second term in equation (8) represents the difference between this new diffusion flux equation and the traditional equation (1). Equation (8) can be further reduced to give

$$J_A^{NG} = - \left[\frac{M_B^{1/2}}{\chi_A M_A^{1/2} + \chi_B M_B^{1/2}} \right] c D_{AB}^{*} \nabla \chi_A \tag{9}$$

The corresponding equations for binary <u>mass</u> diffusion flux relative to the Graham-average velocity are

$$J_A^{MG} = - \left[\frac{M_B^{-1/2}}{\omega_A M_A^{-1/2} + \omega_B M_B^{-1/2}} \right] \rho D_{AB}^{*} \nabla \omega_A \tag{10}$$

and

$$J_B^{MG} = - \left[\frac{M_A^{-1/2}}{\omega_A M_A^{-1/2} + \omega_B M_B^{-1/2}} \right] \rho D_{BA}^{*} \nabla \omega_B \tag{11}$$

Code modifications were made to incorporate these new diffusion equations into TOUGH's general mass continuity equations. The resulting modified mathematical model, refferred to here as the "Graham Model", can be shown to be equivalent to the Dusty-Gas Model for the molecular diffusion regime when thermal and pressure diffusion are neglected. To better handle transport in lower-permeability media, representation for Knudsen and Klinkenberg effects were added to a second modified version of TOUGH, and the simulation results from both these modified versions of TOUGH were compared to results from two less-modified versions of TOUGH. The least modified version leaves the transport equations of TOUGH intact (with the properties of water replaced by those of a volatile organic compound) to represent the "Mass Model". The other modified version replaces the existing TOUGH diffusion-flux equations (binary equations (3)) with equations (1) to represent the "Mole Model".

Knudsen and Klinkenberg effects represent the portions of the diffusive and advective transport, respectively, that are not accounted for in the constitutive equations discussed above.

Darcy's law and the molecular diffusion equations discussed above are not applicable in the Knudsen regime, where molecule-wall collisions dominate over molecule-molecule collisions, such as occurs in very low-permeability media and/or at low gas-phase pressures. Under environmental conditions, the transition from the molecular diffusion regime in gases begins at about $k=5 \times 10^{-13}$ m^2, and the importance of Knudsen and Klinkenberg effects increases with decreasing permeability. To handle the transitional and Knudsen regimes, modifications to TOUGH's MULTI Subroutine were made to add Knudsen diffusion to the molecular diffusion, and modify the permeability used in Darcy's law, using Thorstenson and Pollock's equations (60) - (69) (Thorstenson and Pollock, 1989).

The differences in simulation results between the three models presented here are most pronounced in near-static conditions, where diffusion fluxes dominate over advective fluxes. Comparisons of simple steady-state results are described below, followed by comparisons of transient simulation results using the modified versions of TOUGH.

Comparison of Steady-State Diffusion Fluxes

To evaluate the maximum difference in fluxes given by the models presented here, comparisons are made of the predicted steady-state diffusion fluxes under isobaric, isothermal conditions in coarse-grained media (molecular-diffusion regime). Equations (1), (3), and (10) are used to represent the "Mole", "Mass", and "Graham" Models, repectively, with the flux units of equation (1) converted from moles to mass. For horizontal counter diffusion of 1,1 DCE in moist air, where the mass concentration of DCE varies linearly along a 50 cm column from zero at one end to saturation at the other (1 atm and 20°C), the Mole Model gives 5.25×10^{-4} mg/cm^2s, the Mass Model gives 2.07×10^{-4} mg/cm^2s, and the Graham Model gives 3.40×10^{-4} mg/cm^2s. Taking the results from the Graham Model as the correct flux, the Mole Model over predicts by 1.85×10^{-4} mg/cm^2s (54% relative error), and the Mass Model under predicts by 1.33×10^{-4} mg/cm^2s (-39% relative error). It is also worth noting that significant errors can arise when using the Mass or Mole Models for water-vapor transport at elevated temperatures, such as in geothermal modeling applications.

Comparison of Transient Behavior

Comparing the transient behavior of the various models is important because during transient simulations, diffusion-induced pressure gradients develop unless the system is completely open (eg., in a thin slab of porous medium bounded on both sides by constant-pressure chambers). This type of behavior is predicted using the Mass Model, although the process details are incorrectly simulated. Under the equimass counter diffusion simulated by the Mass Model, a diffusion-induced pressure gradient (that is larger than that actually observed) develops, modifying the behavior from that given by the isobaric steady-state flux equations. This behavior has generally gone unnoticed in the hydrologic community

due to the fact that in prominently published works, the gas-phase has been taken as static and the equation of motion has not been explicitly solved. In the Mole Model, where equimolar diffusion is predicted under static conditions, no pressure gradients develop. This is also incorrect, as discussed below.

TOUGH Simulation Results

Using the modified TOUGH codes, modeling simulations were run to compare the behavior of the three mathematical models for gaseous transport. As a reference, all of the modeling results will be compared to the experimentally observed behavior that is well described by the Dusty Gas Model (DGM); this will be referred to as the DGM behavior. It should be understood that the DGM contains only constitutive relations, and that the DGM behavior referred to here is is either steady-state or transient behavior deduced from DGM theory (Mason, et al., 1967; Cunningham and Williams, 1980).

A set of simulations were run for horizontal counter-diffusion of chloroform and air in a closed 10-cm column with small (closed) reserviors at each end. At time zero, the column and one of the end reserviors contain pure air, while the other end reservoir contains air with a known concentration of chloroform vapors. For counter-diffusion in this type of closed system, the DGM predicts that the initial non-equimolar inter-diffusion of differing molecular-mass species creates a pressure gradient that produces a viscous flux. A quasi steady-state then rapidly develops, wherein the <u>total</u> molar fluxes of the two species are equal and opposite. The diffusion-induced viscous flux then exactly counterbalances the non-equimolar inter-diffusion flux, and this balance is maintained until large concentration differences have occurred in the end reservoirs. Simulations were performed for a wide range of media conductivities, from $k=10^{-5}$ to $k=10^{-20}$ m^2.

Horizontal, closed-system simulations using the Mass Model showed unrealistically large viscous fluxes caused by the large diffusion-induced pressure gradients that develop. Despite this lack of proper representation of the process details, the Mass Model shows the expected quasi steady-state equimolar counter-diffusion down to $k=10^{-13}$ m^2. Below this conductivity, the model results rapidly deviate from the DGM behavior, and the expected quasi steady-state does not developed.

As expected, closed-system simulations using the Mole Model show that equimolar counter-diffusion is maintained over all conductivities, although in this case the process details are incorrectly simulated, because no pressure gradient or viscous flux develops as a result of the inter-diffusion. (Note, as an aside, that due to the more linear nature of the Mole Model, solution convergence times were found to be significantly less than those required for either the Mass Model or the Graham Model.)

The simple Graham Model produces quasi steady-state equimolar counter-diffusion down to $k=10^{-14}$ m^2, and by virtue of the equations used, properly represents the viscous flux and the purely diffusional fluxes. By adding Knudsen and Klinkenberg effects, the Graham Model maintains the DGM behavior down to $k=10^{-16}$ m^2. Pressure diffusion effects were found to be insignificant for the cases studied, and due to the additional computational time required to represent it, pressure diffusion was neglected in most simulations.

A second set of simulations was performed for open horizontal systems, where significant pressure gradients develop only in low-conductivity media. The Mass Model fails to match DGM behavior for all media; it predicts equimass diffusion. The Mole Model also fails for all media; it predicts equimolar diffusion. For an open system such as this, the DGM predicts that the counter-diffusion will follow Graham's Law of diffusion (equation (3)), which the Graham Model shows down to $k=10^{-17}$. When Knudsen and Klinkenberg effects are added, the Graham Model simulates the DGM behavior down to $k=10^{-20}$ m^2.

Finally, vertical open systems (otherwise identical to the horizontal cases) were simulated, and the magnitude of differences between the chloroform fluxes predicted by the three models was found to be greater than the density-driven advective fluxes created by saturated vapors in air at 20°C for media with $k < 10^{-11}$ m^2.

LIST OF SYMBOLS

c = total molar phase density = P/RT (for ideal gases)

ρ = total mass density of gas phase

c_i, ρ_i = molar and mass concentrations, respectively, of species i

χ_i, ω_i = mole and mass fractions = ρ_i/ρ and c_i/c, respectively

ν_i = species drift velocity (relative to fixed coordinates)

D_{ij}^{*} = effective diffusion coefficient (for i in j), accounting for porosity and tortuosity of media

J_i^{FR} = diffusion flux of i in units of "F", relative to the "R^{th}" advective reference velocity

$\mathbf{N}_i$ = molar flux of i relative to fixed coordinates

M_i = molecular mass of species i

M = superscript for mass diffusion flux and mass-ave ref. vel.

N = superscript for molar diffusion flux and mole-ave ref. vel.

REFERENCES

Abriola, L. M., and G. F. Pinder, A multiphase approach to the modeling of porous media contamination by organic compounds, 1. Equation development, Water Resour. Res., 21(1), 11-18, 1985a.

Bird, R. B., W. E. Stewart, and E. N. Lightfoot, Transport Phenomena, John Wiley and Sons, New York, 1960

Clazie, R.N., G. Klein, and T. Vermeulen, Multicomponent Diffusion: Generalized Theory With Ion-Exchange Applications, Sea Water Conversion Laboratory Report No. 67-4 and Water Resources Center Desalination Report No. 19, Univ. of Calif., Berkeley, 1967.

Cunningham, R. E., and R. J. J. Williams, Diffusion in Gases and Porous Media, Plenum Press, New York, 1980.

Cussler, E. L., Diffusion: Mass Transfer in Fluid Systems, Cambridge Univ. Press, 1984.

Farr, J.M. and D.B. McWhorter, Advective reference velocities and gas-phase diffusion in porous media, Fall Meeting '88, Abst. in EOS Trans. Am. Geophys. Union, 69(44), 1216, 1988.

Graham, T., Phil. Mag., 2, 175, 269, 351, 1833.

Hoogschagen, J., J. Chem. Phys., 21(2096), 1953.

Mason, E. A., A. P. Malinauskas, and R. B. Evens III, Flow and Diffusion of Gases in Porous Media, J. Chem. Phys., 46(8), 3199-3216, 1967.

Pollock, D. W., Simulation of Fluid Flow and Energy Transport Processes Associated With High-Level Radioactive Waste Disposal in Unsaturated Alluvium, Water Res. Resear., 22(5), 765-775, 1986.

Pruess, K., TOUGH User's Guide, Earth Science Division, Lawrence Berkeley Laboratory, LBL-20700, NUREG/CR-4645, 1987.

Remick, R. R., and C. J. Geankoplis, Ind. Eng. Chem. (Fund.), 12(214), 1973.

Rothfeld, L. B., AIChE Jl., 9(19), 1963.

Thorstenson, D.C., and D.W. Pollock, Gas Transport in Unsaturated Zones: Multicomponent Systems and the Adequacy of Fick's Laws, Water Res. Resear., 25(3), 477-507, 1989.

Wakao, N., and J. M. Smith, Chem. Eng. Sci., 17(825), 1962.

Wicke, E., and P. Hugo, Z. Phys. Chem., 29(401), 1961.

STMVOC: A NUMERICAL SIMULATOR FOR THREE PHASE CONTAMINANT TRANSPORT IN NONISOTHERMAL SYSTEMS

R.W. Falta and K. Pruess

Earth Sciences Division, Lawrence Berkeley Laboratory

Subsurface contamination by nonaqueous-phase liquids (NAPLs), such as organic solvents and hydrocarbon fuels, is a serious problem in the United States and other industrialized countries. The complete removal of these chemicals by conventional technologies is difficult, time-consuming, and expensive. Recently, the sweeping of contaminated areas with steam has been examined as an alternative remediation method. Several laboratory-scale experiments (Hunt et al., 1988; Basel and Udell, 1989; Udell, personal communication, 1989) and a field experiment (Udell and Stewart, 1989) have demonstrated that steam treatment may be an effective cleanup method. A schematic illustration of a possible steam-injection remediation system is shown in Figure 1. To gain a better quantitative understanding of the steam-injection process, and to aid in the design of future experiments and remedial efforts, we have developed a numerical simulator that can model the complex fluid- and heat-flow processes arising in a steam-sweep operation. This paper presents a brief description of the simulator along with some numerical results obtained using the simulator. Full details of the numerical formulation along with several examples of the code's application may be found in Falta (1990).

NUMERICAL FORMULATION

The numerical simulator, which will be referred to as STMVOC, has been developed for the purpose of modeling true three-phase flow in systems undergoing rapid changes in temperature. The simulator is based on a general integral-finite-difference multiphase formulation known as MULKOM (Pruess, 1983, 1988). Several versions of MULKOM have been developed for solving various multiphase flow problems. The features and capabilities of these different versions have been summarized by Pruess (1988). The STMVOC code is a direct descendent of the TOUGH simulator (Pruess, 1987) with appropriate modifications to account for the NAPL/organic chemical.

In the present formulation, the multiphase system is assumed to be composed of three mass components: air (or some other noncondensible gas), water, and a slightly miscible organic chemical. These three components may be present in different proportions in any of the three phases, gas, water, and NAPL. Each phase flows in response to pressure and gravitational forces according to the multiphase extension of Darcy's law, including effects of relative permeability and capillary pressure between the phases.

Transport of the three mass components occurs by advection in all three phases and by multicomponent diffusion in the gas phase. It is assumed that the three phases are in local chemical and thermal equilibrium and that no chemical reactions are taking place other than interphase mass transfer. Mechanisms of interphase mass transfer for the organic chemical component include evaporation and boiling of the NAPL, dissolution of the NAPL into the liquid-water phase, condensation of the organic chemical from the gas phase into the NAPL, and equilibrium phase partitioning of the organic chemical between the gas, water, and solid phases. Interphase mass transfer of the water component includes the effects of evaporation and boiling of the water phase, dissolution of water in the NAPL (not usually important), and condensation of water vapor from the gas phase. The interphase mass transfer of the air component consists of equilibrium phase partitioning of the air between the gas, liquid-water, and

NAPL phases.

Heat transfer occurs due to conduction, multiphase convection, and gaseous diffusion. The heat-transfer effects of phase transitions between the NAPL, water, and gas phases are fully accounted for by considering the transport of both latent and sensible heat. The overall porous-media thermal conductivity is calculated as a function of water and NAPL saturation and depends on the chemical characteristics of the NAPL.

Secondary water and NAPL phase parameters such as saturated vapor pressure and viscosity are calculated as a function of temperature, whereas parameters such as specific enthalpy and density are computed as functions of both temperature and pressure. The gas-phase properties, such as specific enthalpy, viscosity, density, and component molecular diffusivities, are considered to be functions of temperature, pressure, and gas-phase composition. The solubility of the organic chemical in water may be specified as a function of temperature, and the gas-water Henry's constant for the organic chemical is calculated as a function of temperature. The gas-water and gas-NAPL Henry's constant for air is assumed to be constant, as is the water solubility in the NAPL phase.

The necessary NAPL/organic chemical thermophysical and transport properties are computed by means of a general equation of state package. This equation of state package is largely based on semi-empirical corresponding states methods in which chemical parameters are calculated as functions of the critical properties of the chemical such as the critical temperature and pressure. Because these data are available for hundreds of organic compounds, the NAPL/organic chemical equation of state package is flexible in its application.

The STMVOC simulator may be used for one-, two-, or three-dimensional anisotropic, heterogeneous porous or fractured systems having complex geometries. The porous-media porosity may be specified to be a function of pore pressure and temperature, but no stress calculations are made. The simulator has been verified by comparisons with analytical solutions for one-dimensional two-phase flow (Buckley and Leverett, 1942) and with a semianalytical solution for a two-phase heat pipe with a noncondensible gas (Udell and Fitch, 1985).

VALIDATION WITH A ONE-DIMENSIONAL LABORATORY EXPERIMENT

The results of a series of laboratory-scale column experiments were recently reported by Hunt et al. (1988). The experiments were designed to evaluate the mobilization and transport of a NAPL during water- and steam-flooding. These experiments were conducted in a sand-packed glass column with a length of 91 cm and diameter of 5.1 cm. The sand in the column had a porosity of 0.385 and a permeability of about $1.6 \times 10^{-11} m^2$ and was initially water saturated. The column was fully instrumented with pressure transducers and thermocouples providing detailed pressure and temperature measurements during the experiments. A diagram of the experimental geometry is shown in Figure 2. Further details of the experimental apparatus and methodology are given by Hunt et al. (1988).

Three experiments were performed, each using a different NAPL: trichloroethylene (TCE), a mixture of benzene and toluene, and gasoline. In each experiment, 18 ml of the NAPL was injected into the column centerline 27.0 cm from the inlet. This was followed by cold-water injection at a Darcy velocity of 15 m/d for several pore volumes. The flow rate was then lowered to about 1.5 m/d prior to steam injection. During the TCE experiment, cold water was injected at a rate of 15 m/d for 9.5 pore volumes, and at a rate of 1.5 m/d for 3 pore volumes. Following the cold-water injection, steam with a quality of about 0.5 (a specific enthalpy of about 1560 kJ/kg) was injected at a rate of 0.127 kg/h until some time after steam breakthrough at the outlet. The water mass flow rate used during the steam injection is equivalent to that used during the 1.5 m/d waterflood.

For the purpose of validating the STMVOC simulator, the TCE experiment was modeled. The one-dimensional mesh consisted of 50 elements with a uniform mesh spacing of 1.82 cm. During the course of the simulation, several boundary conditions were required to model the different experimental conditions (i.e., NAPL injection, water injection, steam injection). The three-phase capillary pressure curves were calculated by using functions given by Parker et al. (1987). The values of the empirical constants used in the calculation of the capillary pressures are those suggested by Parker et al. (1987) for use in sandy systems. The three-phase NAPL relative permeability was computed by Stone's first

method (Stone, 1970) with the normalization of Aziz and Settari (1979). The water- and gas-phase relative permeabilities were taken to be the respective scaled saturations cubed (see, for example, Stewart and Udell, 1988). The residual TCE phase saturation (below which separate-phase TCE flow cannot occur) was assumed to be 0.05. Most of the TCE thermophysical constants required by the STMVOC code are given by Reid et al. (1987).

Figure 3 shows the simulated TCE phase saturation after the waterflood and the temperature profile and TCE phase saturation during the steamflood. In the simulation, the TCE becomes distributed over a large portion of the column at a saturation of slightly more than 0.05 during the high-flow-rate waterflood. At this point, the separate-phase TCE is nearly immobile and the transport of TCE in the column is dominated by dissolution of the upstream edge of the TCE and advection in the flowing water phase. When steam is injected into the column and the steam-condensation front reaches the zone containing the TCE, the TCE is very effectively mobilized. As the steam front propagates through the column, the TCE (which has a normal boiling point of 87 $^{\circ}C$) forms a sharp NAPL bank just ahead of the steam-condensation front. In the narrow zone occupied by the TCE, transport of the TCE occurs primarily due to advection in the gas-phase and separate-phase TCE flow. As the trailing edge of the TCE boils and evaporates, it is carried ahead by the gas phase to a cooler part of the column, where it condenses. Due to the rapid drop in temperature ahead of the steam-condensation front, and the strong dependence of TCE vapor pressure on temperature, the region in which TCE boiling, evaporation, and condensation occur tends to be very small. This results in an increase in the TCE phase saturation in this area to a value greater than the residual saturation. As a result of this increased TCE saturation and the decreased TCE liquid viscosity at the higher temperatures, separate-phase TCE flow is facilitated.

Stewart and Udell (1988) present a theoretical evaluation of the mechanisms of NAPL displacement by steam injection and conclude that the maximum possible NAPL saturation ahead of the steam-condensation front is determined mainly by the ratio of NAPL and water viscosities. The maximum NAPL saturation shown in Figure 3 of about 0.3 is in approximate agreement with their theoretical results.

Figure 4 shows a comparison of the experimental data with the numerical simulation results for the pressure gradient between the first two pressure transducers. As explained by Hunt et al. (1988), the pressure-gradient data reflect three distinct multiphase-flow conditions. The early part of the curve, from about 12.5 to about 12.65 displaced pore volumes is indicative of single-phase liquid-water flow between the pressure ports. The center part of the curve, from about 12.65 to about 13.0 displaced pore volumes, reflects multiphase flow between the pressure ports. The large rise in the pressure gradient from about 12.65 to about 12.7 displaced pore volumes occurs as the steam front passes the first pressure transducer and is a result of the rapid change in capillary pressure at this location.

From about 12.7 to about 12.9 displaced pore volumes, the pressure gradient continues to increase as a high-velocity steam zone develops between the pressure ports. At about 12.9 displaced pore volumes, the steam front passes by the second pressure transducer, and the capillary pressure gradient between the transducers diminishes. In the final part of the curve, from about 13.0 to 13.5 displaced pore volumes, the pressure gradient becomes nearly constant at a value of about 25 kPa/m and is representative of single-phase high-velocity steam flow between the transducers. The calculated pressure gradient shown in Figure 4 reflects the different flow conditions discussed above and approximately matches the experimental data.

Figure 5 shows the measured and calculated cumulative volume of TCE removed from the column during the experiment. Prior to steam injection at 12.5 displaced pore volumes, TCE was removed from the column by dissolution and advection in the water phase only. Hunt et al. (1988) report that the concentration of TCE in water leaving the column was at the TCE solubility limit. After about one pore volume of fluid was displaced by the steam injection, and just before steam breakthrough at the outlet, separate-phase TCE was produced. The numerically calculated result is in good quantitative agreement with the experimental data. The experimentally measured and numerically calculated locations of the steam-condensation front are compared in Figure 6. Again, the numerical simulation closely matches the experimental data.

SUMMARY

A numerical simulator has been developed for modeling three-phase flow in nonisothermal systems. The code has been successfully verified with analytical solutions for multiphase flow and heat transfer. The simulator has been validated in part by the simulation of a laboratory-column steamflood experiment involving TCE. In addition to the validation effort summarized here, we have been able to successfully simulate a series of two-dimensional steamflood experiments performed by Basel and Udell (1989) and by Udell (personal communication, 1989). These two-dimensional experiments included the effects of gravity, variable initial water saturation, and heterogeneity. The two-dimensional simulation results are presented in Falta (1990).

With validation of the code nearly complete, our future efforts in this area will largely be directed toward the simulation of field-scale experiments and the effective design of remedial systems.

REFERENCES

Aziz, K., and Settari, A., 1979. Petroleum Reservoir Simulation. Applied Science Publishers, London.

Basel, M.D., and Udell, K.S., 1989. Two dimensional study of steam injection into porous media. Presented at the 1989 ASME Winter Annual Meeting, Multiphase Transport in Porous Media, San Francisco, California.

Buckley, S.E., and Leverett, M.C., 1942. Mechanism of fluid displacement in sands. AIME Trans., v. 146, p. 107-116.

Falta, R.W., 1990. Multiphase Transport of Organic Chemical Contaminants in the Subsurface. Ph.D. thesis. University of California at Berkeley.

Hunt, J.R., Sitar, N., and Udell, K.S., 1988. Nonaqueous phase liquid transport and cleanup, 2. Experimental studies. Water Resour. Res., v. 24, no. 8, p. 1259-1269.

Parker, J.C., Lenhard, R.J., and Kuppusamy, T., 1987. A parametric model for constitutive properties governing multiphase flow in porous media. Water Resour. Res., v. 23, no. 4, p. 618-624.

Pruess, K., 1983. Development of the general purpose simulator MULKOM. Earth Sciences Division Annual Report 1982. Lawrence Berkeley Laboratory Report LBL-15500.

Pruess, K., 1987. TOUGH user's guide. Nucl. Regul. Comm. Rep. NUREG/CR-4645, Washington, D. C.

Pruess, K., 1988. SHAFT, MULKOM, TOUGH: A set of numerical simulators for multiphase fluid and heat flow. Lawrence Berkeley Laboratory Report LBL-24430.

Reid, R.C., Prausnitz, J.M., and Poling, B.E., 1987. The Properties of Gases and Liquids. McGraw-Hill, New York.

Stewart, L.D., and Udell, K.S., 1988. Mechanism of residual oil displacement by steam injection. SPE Res. Eng., November, p. 1233-1242.

Stone, H.L., 1970. Probability model for estimating three-phase relative permeability. J. Pet. Technol., v. 22, no. 1, p. 214-218.

Udell, K.S., and Fitch, J.S., 1985. Heat and mass transfer in capillary porous media considering evaporation, condensation and non-condensible gas effects. Heat Transfer in Porous Media and Particulate Flows, ASME HTD Vol. 46.

Udell, K.S., and Stewart, L.D., 1989. Field study of in situ steam injection and vacuum extraction for recovery of volatile organic solvents. University of California, UCB-SEEHRL Report No. 89-2.

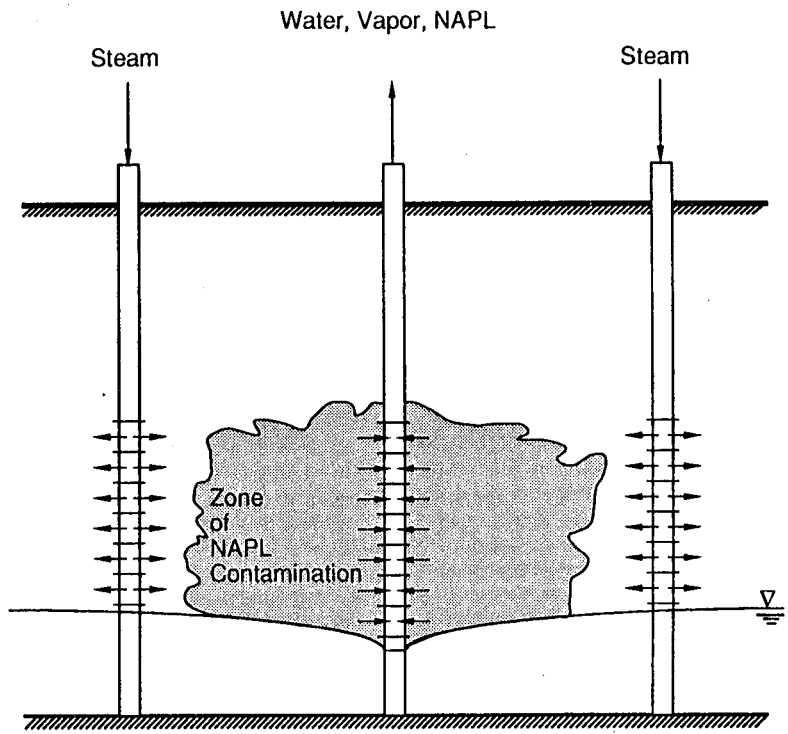

Figure 1. Diagram of a possible steam-injection remediation system.

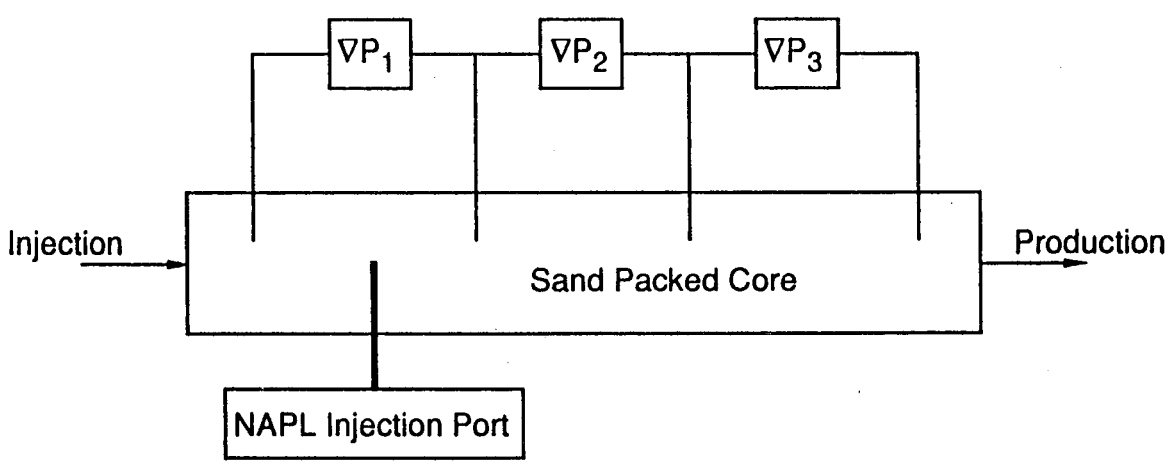

Figure 2. Experimental geometry used by Hunt *et al.* (1988).

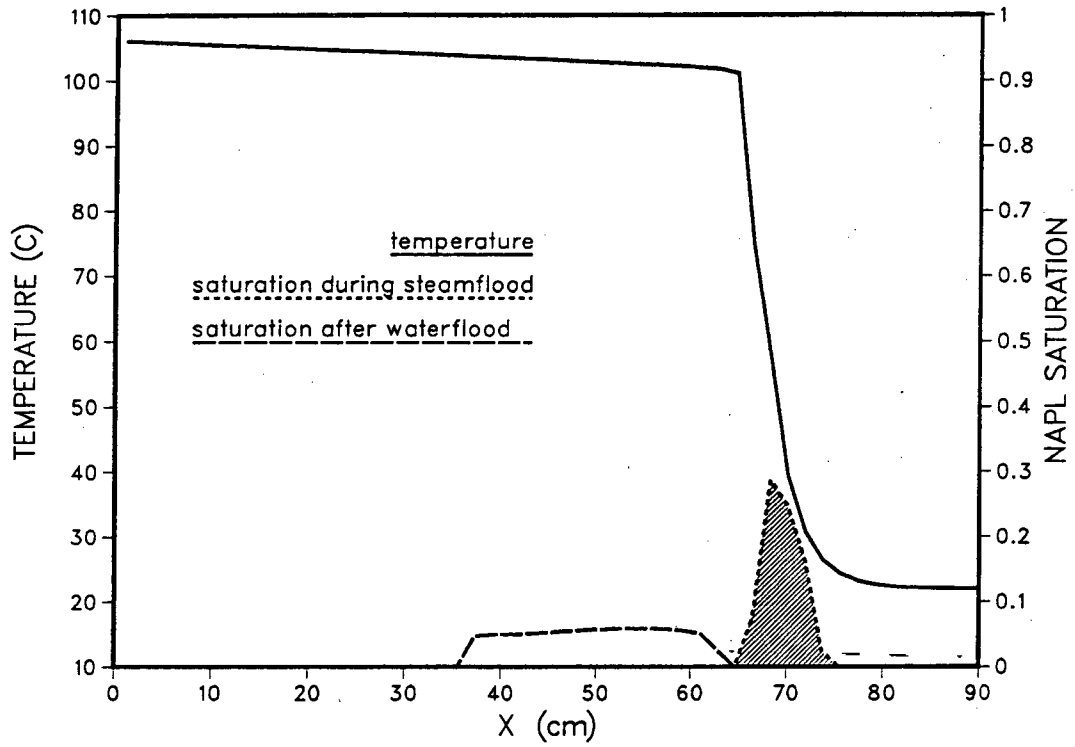

Figure 3. Calculated NAPL saturation after waterflood and calculated temperature profile and NAPL saturation during steamflood.

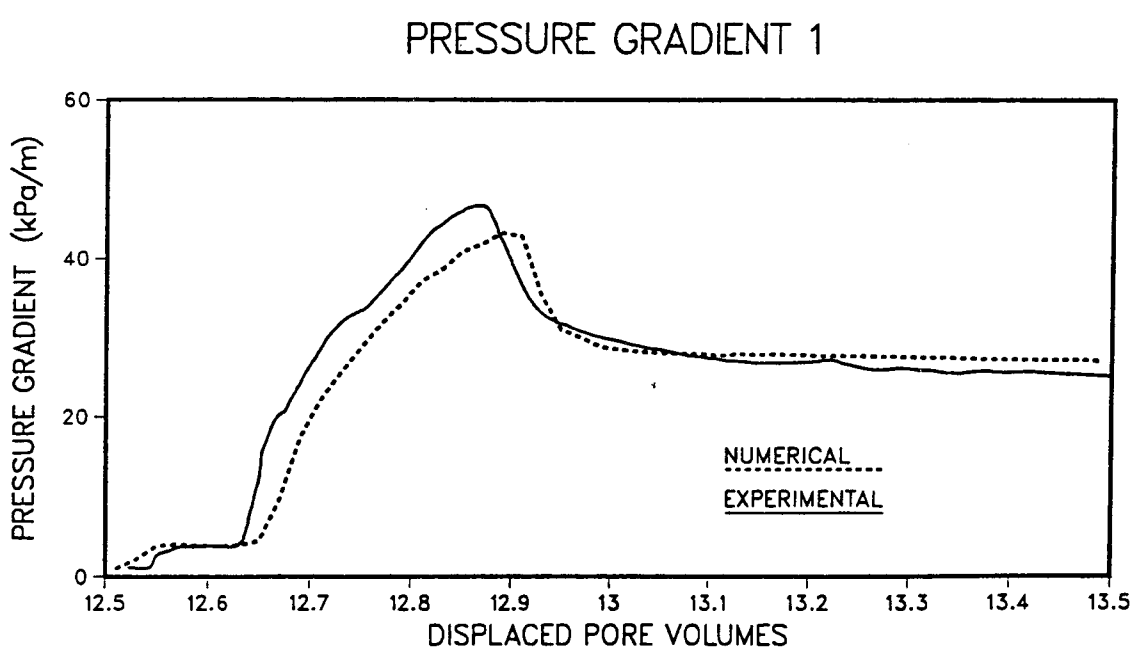

Figure 4. Comparison of numerical solution with the experimental data of Hunt *et al.* (1988) for the pressure gradient between the first two pressure transducers.

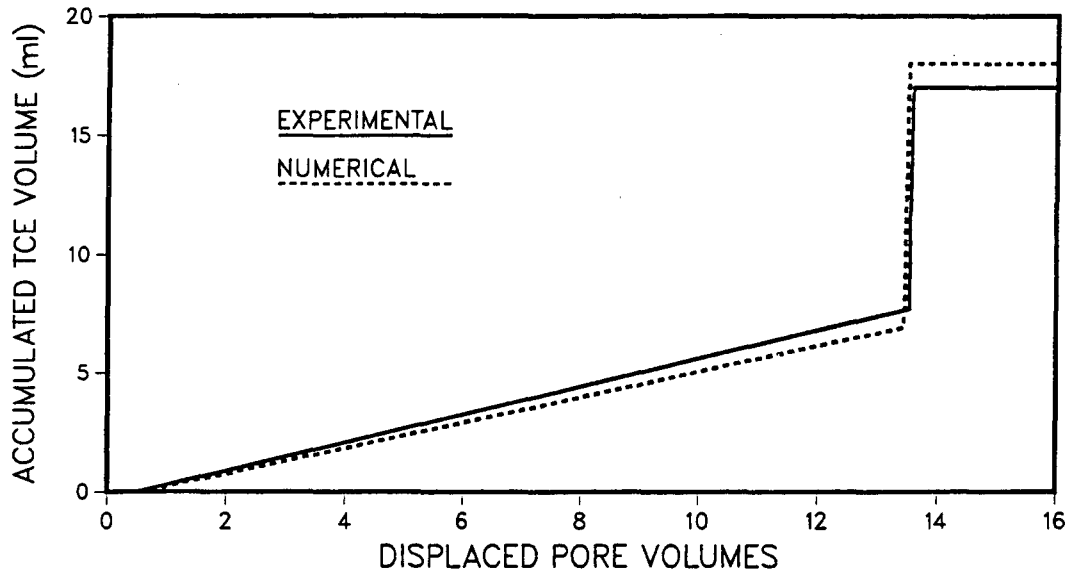

Figure 5. Comparison of numerical solution with the experimental data of Hunt *et al.* (1988) for the cumulative volume of TCE removed from the column.

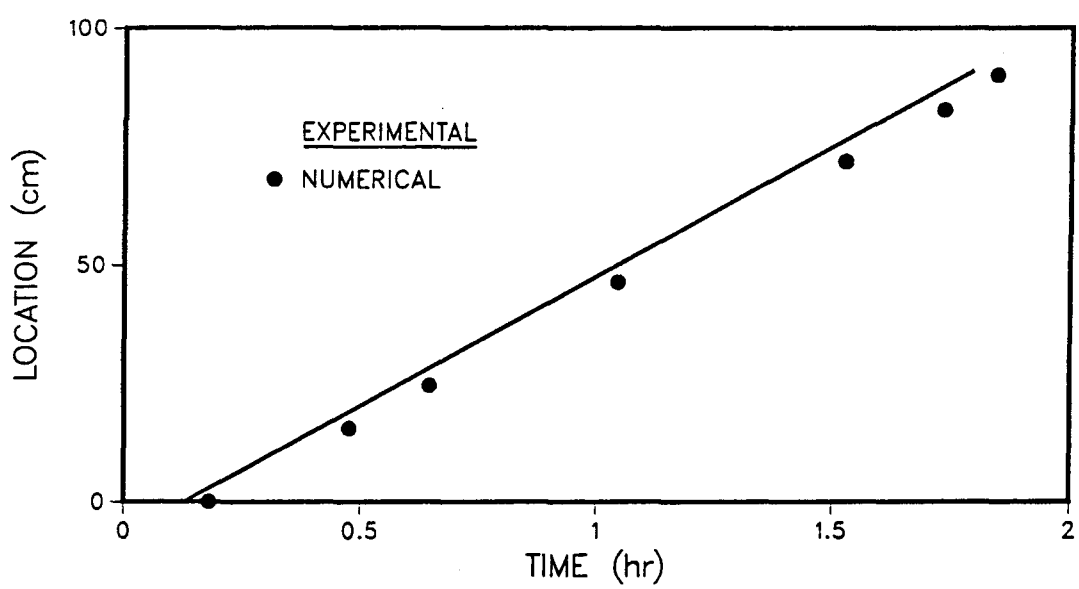

Figure 6. Comparison of numerical solution with the experimental data of Hunt *et al.* (1988) for the location of the steam-condensation front in the column.

A Simple Model of a Vapour-Dominated Geothermal Reservoir

by

M. J. O'Sullivan

Engineering Science Department
University of Auckland

ABSTRACT

Numerical experiments with a simple model of a vapour-dominated geothermal system are described. The model, representing a typical vertical slice through the field, is used to investigate the effect of the bottom boundary conditions on the behaviour of the model. It is found that the pressure and vapour saturation must be fixed at the base of the model in order to obtain a stable vapour-dominated state. The simulations described were carried out with a modified version of the MULKOM reservoir simulation package.

INTRODUCTION

The models discussed here were set up by the author and co-workers (GENZL, 1986, Saptadji, 1987) as the preliminary stage of a modelling study of the Kamojang (Indonesia) geothermal field. The first simple model of Kamojang considered was a 2-D vertical slice 3.5 km long , 1.2km deep and 2km thick, consisting of six layers each divided into 7 blocks (see Figs. 1 & 2). The model represents the high permeability vapour-dominated region at Kamojang. The surrounding rock must have a very low permeability to prevent cool water flooding the vapour-dominated zone and therefore for this simple model the vapour-dominated zone was considered to be laterally sealed. Similarly the low permeability cap-rock was approximated by a sealed top. The escape of steam to hot springs and steaming ground was represented by a well on deliverability (discharge proportional to pressure above some cut-off value) located in the top

right (block AAA7). Conductive heat loss through the cap was represented by heat sinks in the top blocks.

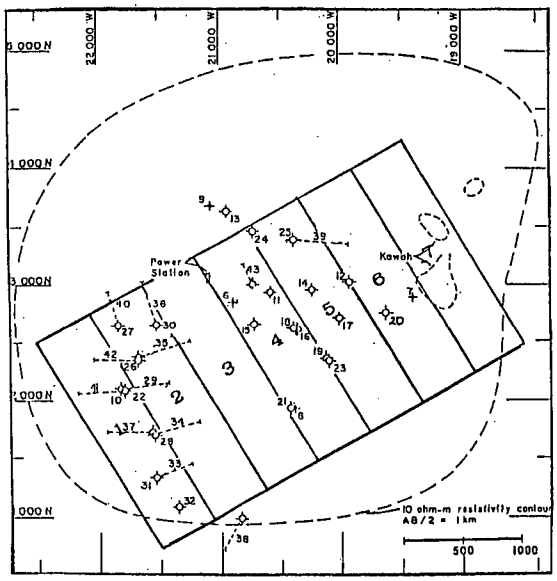

Figure 1. Location of the simple model of Kamojang

This simple model was used to try to set up a natural state representing the pre-exploitation of Kamojang. The basic idea of natural state modelling is to choose a permeability distribution, heat inputs and mass inputs for the model and then run it for a very long time until a steady state pressure and temperature distribution is obtained (see O'Sullivan, 1985, Bodvarsson et al, 1986) for more details. The idea is to simulate the evolution of the geothermal system over geological time to its pre-exploitation state. Comparison of the measured temperatures and pressures in the system with those predicted by the model can then be used to adjust the model parameters.

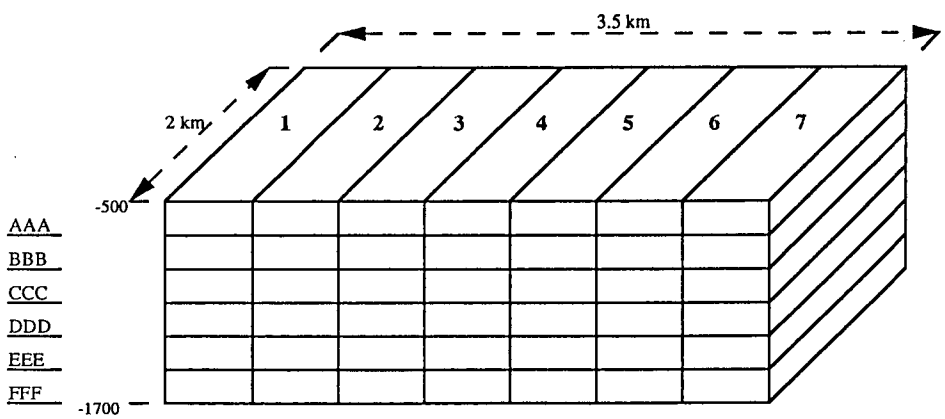

Figure 2. Block structure for the simple model of Kamojang.

Well testing data from Kamojang indicate that the wells can be divided approximately into two categories: shallower wells feeding from very permeable rock and deep wells feeding from moderate permeability rock. Therefore the model was set up with a very simple permeability distribution. The model was assumed to have a high permeability upper half with $k_h = 200$ mD and $k_v = 100$ mD and a medium permeability lower half with $k_h = 40$ mD and $k_v = 20$ mD. Other rock parameters are listed in Table 1.

Table 1 Reservoir Rock Properties

Density	2500 kg/m^3
Porosity	0.10
Thermal conductivity	2.5 W/m.K
Specific heat	1000 J/kg.K
Relative permeability	Straight line
Immobile water	0.3
Fully mobile steam	0.7

The conductive heat losses from the top of the model were represented by heat sinks, removing 0.786 MW , from each of the top blocks. The well representing discharge of steam to the hot springs had the form

$$Q_m = PI\,(p - p_0)/\nu_t$$

where Q_m is mass flow, PI is the productivity index, p is the reservoir pressure, p_0 is the trigger pressure at which the well stops flowing and ν_t is the effective kinematic viscosity of the two-phase mixture of steam and water in the reservoir. The parameters PI and p_0 are not known and have to be selected to give the correct mass flow of 35kg/s to the hot springs and the correct temperature near the top of the vapour-dominated zone of 230 -235°C.

BOUNDARY CONDITIONS AT THE BASE

Using experience from other modelling studies the boundary conditions at the base of the model were first chosen to be constant mass flow and energy flow (Model I). The total mass flow of 35kg/s through the system was divided equally between the seven base block (FFF 1-7) and the enthalpy of the inflow was gradually increased. As the enthalpy of the inflow was increased the reservoir changed from warm water to hot water and then into a liquid -dominated two-phase system. As the enthalpy was increased still further it proved impossible to obtain a steady-state and a vapour-dominated system was not obtained. Eventually it was decided to force the desired vapour-dominated state by specifying a constant pressure, p, and vapour saturation, S, at the base of the model (Model II). These boundary conditions were implemented in the model by having a block with a very large volume at the base. The large volume ensures that the pressure and vapour saturation specified in the block remain constant. With this choice of boundary conditions a stable vapour-dominated steady-state was quickly obtained and after some experimentation with the choice of base pressure and the trigger pressure p_0 in the well on deliverability a good match to the field pressures and temperatures was obtained.

Using the results from this successful steady-state simulation the heat flows Q_{ei} and mass flows Q_{mi}, i = 1, 2,....,7, into the base blocks were calculated. These flows were then used as inputs into model I as bottom boundary conditions. The simulation was run with the vapour-dominated steady-state from model II as initial data. It was found that the vapour-dominated state persisted for some time but eventually changed over to a liquid-dominated state. To investigate this phenomenon further and to check the stability of each model (I and II) they were both re-run with their boundary conditions perturbed by small amounts. Model II (constant p, S at the base) quickly established a new steady state close to the previous one. However Model I could not establish a steady-state, either vapour-dominated or liquid-dominated. Instead an oscillatory state developed. Typical results are shown below where vapour saturation is plotted versus timestep number, Figure 3, and time, Figure 4.

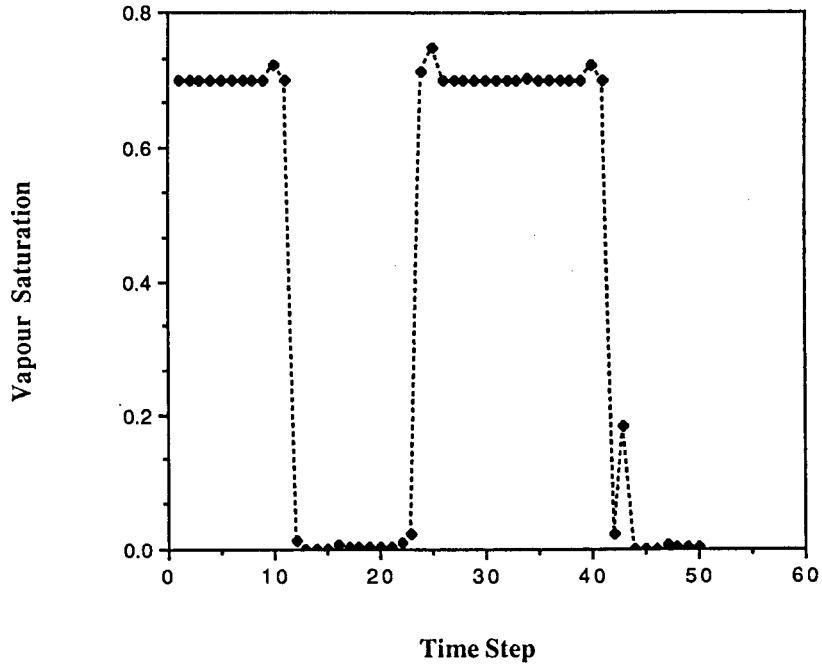

Figure 3. Vapour saturation in block CCC4 vs timestep count.

Fig. 3 clearly shows the cycle of a transition from a vapour-dominated to a liquid-dominated state and then back to a vapour-dominated state. This cycle is repeated periodically. As Fig 4 shows the liquid-dominated part of the cycle is extremely short-lived. The reservoir quickly fills with water, then quickly ejects it, like a giant geyser, and then settles back into a long vapour-dominated period.

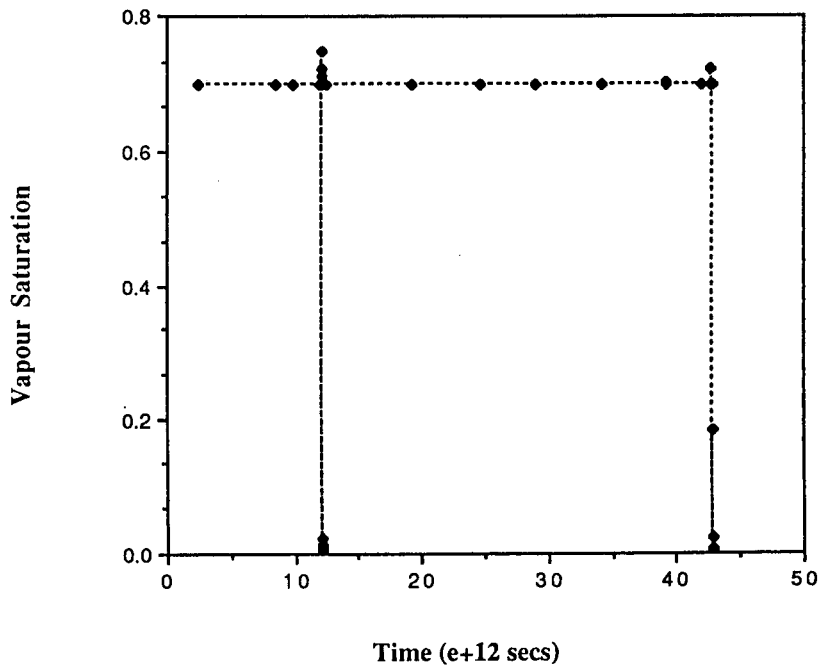

Figure 4. Vapour saturation in block CCC4 vs time.

As the time between eruptions predicted by the model is very long at approximately 10^6 years the vapour-dominated system will certainly appear to be a steady state when observed over a short period of time like 10 - 100 years.

DISCUSSION AND CONCLUSION

These numerical experiments for the 2-D model confirm the numerical and analytic investigations of the 1-D heat pipe and related work by Martin et al., 1976; Schubert and Straus, 1979; Pruess and Truesdell, 1980; Straus and Schubert, 1981; Pruess, 1985; Blakeley, 1986; Ingebritsen, 1986; Pruess et al., 1986; McGuiness and Pruess, 1987; McGuiness, 1988; Ingebritsen and Sorey, 1988. In particular, McGuiness et al, 1990, have considered the stability of the 1-D heat pipe and have shown that a vapour-dominated reservoir is likely to have saturation control at depth.

The use of the constant pressure, constant vapour-saturation boundary conditon at the base of the model raises two important questions: Firstly, what effect does this type of boundary condition have on simulations of the reservoir behaviour under exploitation? And secondly, how does such a boundary condition arise in the real world?

The author has used the simple model above for simulations of future production at Kamojang and found it to be completely unsatisfactory. After quite a short time an equilibrium state is established where the pressure drop between the production wells and the bottom boundary is sufficient to produce a mass flow through the base of the model equal to the production rate. Thereafter the bottom boundary conditions can supply an effectively infinite quantity of high enthalpy steam and the model predicts that the reservoir will last forever. This problem can be solved pragmatically by increasing the number of layers in the model, thus pushing the constant p,S boundary further away from the production zone and delaying the onset of the spurious equilibrium state beyond the 20-30 year production period of interest.

The question remains, however, of what if anything provides the constant p,S control at depth in a vapour-dominated system. Perhaps they are not in a steady equilibrium state at all and the peculiar long-term oscillation shown in Fig. 4 is a real phenomenon.The model described here represented the reservoir as a uniform porous material. Possibly a fracture/matrix model,

similar to that used by Pruess and Narasimham, 1982, would give a better model of a vapour-dominated system.

REFERENCES

Blakeley, M.,1986, *Geothermal Reservoir Modelling*, Ph.D. thesis, Dept. of Theoretical and Applied Mathematics, Auckland University.

Bodvarsson, G.S., Pruess, K. and Lippmann, M.J., 1986, *Modelling of geothermal systems,* J. Petroleum Technology, pp 1007-1021.

GENZL (Geothermal Energy New Zealand Ltd), 1986, *Kamojang reinjection study,* Report for New Zealand Goverment, Ministry of Foreign Affairs.

Ingebritsen, S.E.,1986, *Vapour dominated zones within hydrothermal convection systems: evolution and natural state*, Ph.d. Thesis, Stanford University, Stanford, California.

Ingebritsen, S.E. and Sorey, M.L.,1988, *Vapour dominated zones within hydrothermal convection systems: evolution and narural state,*J.Geophys. Res. **93** No.B11, pp 13635-13655.

McGuiness, M.J.,1988, *Heat Pipe Stability and Upstream Differencing*, in the proceedings of the Tenth New Zealand Geothermal Workshop, Auckland University, pp 117-122.

McGuiness, M.J., Blakeley, M.,Pruess, K. and O'Sullivan, M.J., 1990, *Heat pipe stability and upstream differencing*, to be published.

McGuiness, M.J. and Pruess, K.,1987, *Unstable heat pipes*, in the proceedings of the Ninth New Zealand Geothermal Workshop, Auckland University, pp 147-151.

Martin, J.C., Wegner, R.E. amd Kelsey, F.J.,1976, *One-dimensional convective and conductive geothermal heat flow*, Proc. Second Workshop on Geothermal Reservoir Engineering, Stanford University, pp 251-262.

O'Sullivan, M.J.,1985, *Geothermal reservoir simulation,* Energy Research, **9**, pp 319-332.

Pruess, K.,1985, *A quantitative model of geothermal reservoirs as heat pipes in fractured porous rock,* Transactions of 1985 Symposium on Geothermal Energy, Geothermal Resources Council 1985 Annual Meeting, Volume 9 - Part II, pp 353-362.

Pruess, K. and Narasimham, T.N.,1982, *On fluid reserves and the production of superheated steam from fractured, vapour-dominated geothermal reservoirs*, Journal of Geophysical Research, **87**, no B11, pp 9329-9339.

Pruess, K. and Truesdell, A.H.,1980,*A numerical simulation of the natural evolution of vapour-dominated hydrothermal systems*, Proc., Sixth Workshop on Geothermal Reservoir Engineering, Stanford University, pp 194-203.

Saptadji, N.M.,1987, *Reservoir Simulation of Kamojang field*, project report, Geothermal Institute, University of Auckland.

Schubert, G. and Strauss, J.M.,1979, *Steam-water counterflow in porous media*, J. Geophys. Res., **84**, No B4, pp 1621-1628.

Strauss, J.M. and Schubert, G.,1981, *One-dimensional model of vapour-dominated geothermal systems*, J. Geophys. Res., **86**, pp 9433-9438.

INJECTION OF COLD WATER AND AIR INTO A TWO-PHASE VOLCANIC HYDROTHERMAL SYSTEM

Mario César Suárez Arriaga
Alfredo Mañón Mercado

COMISION FEDERAL DE ELECTRICIDAD
A.P. 31-C, Morelia, Michoacán, 58290 MEXICO.

ABSTRACT

This paper contains a brief description of the thermodynamic effects observed during the injection of cold geothermal water mixed with air into the Los Azufres (México) reservoir. We include an explanation of the idealized processes modeled with TOUGH simulator. The physical problem involves anisotropic flow of heat,liquid,vapor and air within a saturated fractured/porous media with simultaneous injection and production of a two-component fluid (water + air). The three dimensional mesh constructed to represent the reservoir consists of 140 elements distributed in four vertical levels, 273 interfaces connecting them and 29 sinks and sources. We could reproduce the production-injection history of the field and our final results agree well with the observed behaviour of Nitrogen and fluid enthalpy. In this way we could estimate a global value for the absolute permeability existing between injection and production zones.

INTRODUCTION

Los Azufres is a volcanic hydrothermal system intensely fractured and faulted. The field is located in the western part of the Mexican Neo-Volcanic Axis (Fig. 1) at an elevation of about 2800 masl. The reservoir has been discovered in 1972 and the first successful well (Az-1) was drilled by the Comision Federal de Electricidad (CFE) in 1976. Its total explored area using geological, geophysical and geochemical techniques covers about 60 km^2. Today, about 60 wells have been completed and the installed capacity is 90 MWe. Los Azufres is the first Mexican geothermal field that generates electricity from fluids saturating volcanic rocks and is the second energy's producer field in Mexico, after Cerro Prieto, Baja California.

The exploitation of Tejamaniles, the field's southern sector (Fig. 1), started in 1982 subjecting the reservoir simultaneously to mass and heat extraction with reinjection of "cold" fluid and air (temperature of injection: 40-50ºC, at 0.8 bar). This sector is presently under study and is being monitored to detect its response to these parallel processes. Presented herein is a brief, updated resume of the Tejamaniles observed behavior and its numerical simulation. This work corresponds to a most general group of multidisciplinary studies in progress.

THE NATURAL STATE OF THE RESERVOIR

For the last 14 years a large amount of data has been gathered from the Los Azufres reservoir and a quantitative integrated conceptual model of the field is under development. The system consists of a complex andesitic layers series of different textures and rhyolites in the upper levels. The distribution of hydrothermal alteration minerals suggests a geometry for the field corresponding to a main reservoir at depth discharging ascending fluids through convective circulation cells. These cells are closely related to two highly fractured sub-systems which define two connected geothermal zones identified at Los Azufres: Marítaro in the north and Tejamaniles in the south, (Cathelineau et al 1985; Viggiano 1987). A central zone of high resistivity separates the northern and southern portions of the field. In this zone, at shallow levels, the hydrothermal alteration is very low; but deeper (below 1800 m.) there is a continuity in the alteration linking Marítaro with Tejamaniles. This suggests the existence of a deep common aquifer underlying the total area of the reservoir. The field's abnormal geothermal gradient generates a broad, central dome structure which is deformed by hydrothermal alteration brought out by ascending fluids and creating two main zones of alteration and discharge. In Tejamaniles this circulation zone is narrow, bringing out fumaroles, boiling mud pools and steaming ground. These surface

manifestations are scattered between the Agua Fria and Los Azufres faults (Fig. 1). There is no isotopic evidence of mixture of meteoric water or shallow groundwater with geothermal fluid, therefore a caprock must exist and the recharge, if any, may be lateral and deep (Suárez et al.,1989).

In the southern sector,the fluid feeding most of the wells is two-phase in natural state, with a non homogeneous steam saturation, which ranges between 0 to 70 %. Pressure and temperature profiles measured in several Tejamaniles wells, are exhibited in Figures 2 and 3. These profiles clearly show that in this sector, between 1600 and 2500 masl, pressure and temperature gradients are small, indicating a nearly vaporstatic distribution of thermodynamic conditions; but between 0 and 1550 masl the thermodynamic profiles correspond to hydrostatic conditions.

A synthesis of petrophysical measurements performed in 24 drilling cores of 17 wells are presented in Figs. 4,5 and 6 (Contreras et al 1988). The vertical distribution of these properties clearly show that porosity decreases exponentially with depth, while rock density and thermal conductivity increase quadratically with depth. In horizontal planes the same rock properties appear randomly distributed. Los Azufres may be visualized as a discontinuous volume of fractured andesites, intersected by several high permeability faults, with very little permeability in the block matrix and fractured meshes around faults. The permeability is also very low at the top and bottom of the reservoir, but the system permits the communication to the surface by small open conduits (cracks) through the caprock, which is quasi-sealed.

THE FIELD SUBJECT TO EXPLOITATION

Since August 1982, two wellhead non-condensing units, generating 5 MW_e each, were installed at Tejamaniles: Unit 1 connected to wells Az-6 and Az-16D, and Unit 2 connected to well Az-17. In September 1987 Unit 6 has been connected to well Az-18 in order to generate 5 additional MW_e In November 1988 a 50 MW_e unit was installed in Tejamaniles; it is feeding with steam coming from wells Az-22, Az-33, Az-34, Az-35, Az-36, Az-37, Az-38 y Az-46 (Fig.1). These plants have been in continuous operation with a total mass extraction indicated in Table 1. The present pressure and temperature profiles of the production wells exhibit changes. The system as a whole, has started to abandon its natural steady state.

THE RESPONSE OF THE SYSTEM

In the southern sector the wells Az-6, Az-16D and Az-17 have a rich history that shows an interesting chemical evolution. In this region there is a second group of wells (Az-2,33,37 and 46) having less information because they are younger productors. Data from both groups show that chlorides in liquid, Argon and Nitrogen in steam have been growing since June 1986 (Fig. 7); this effect has a close relation with the injection of fluids into the reservoir that induces multiple evaporation of the injected water within the production zones. Molar ratio N_2/Ar has been decreasing with time reaching, in some cases, the same value as in the atmosphere (83.6); this is also a consequence of the continuous injection of fluid into wells Az-7 and Az-8. The air mixed with the fluid could flow through the fractures and high conductivity faults finally arriving to the production zones. This effect extends to wells Az-16D, Az-16, Az-33, Az-37 and Az-46 (Moreno, 1989). Wells Az-22, producing vapor and liquid and well Az-6 (100% steam), do not show any important trend on their chemical behavior.

SIMULATION OF WATER AND AIR INJECTION

We have three implicit purposes in the numerical simulation of Tejamaniles : a)- To integrate data from different sources into a single detailed model. b)- To reproduce the injection/production field's history and c)- To estimate the global or average permeability acting between the injection and production zones. For the last point we have learned, from our own direct experience, that air is a very good and cheap natural tracer. We employed TOUGH (Pruess, 1988) to perform the numerical experiments of a 3-D simplified porous model representing Tejamaniles. Our simulation includes reinjection/production of geothermal water and air with heat injection at the bottom of the reservoir and simultaneous flow of liquid, steam, air and heat into an anisotropic medium.

RESERVOIR CHARACTERISTICS.- Core analysis accomplished at several wells (Contreras et al, 1988), points out that reservoir's porosity varies between 1% and 24%; the matrix permeability is very low (between 0 and 2 microdarcy), but some pressure tests have shown average permeabilities up to 180 md. On the other hand, total lost circulation occur very often during drilling

and must be related to fractured networks around the faults. This indicates an extremely high permeability acting by a multiporosity mechanism. For example, a drilled well's mud column presenting total lost circulation at 1500 m depth, exerts a pressure gradient at the bottom equal to 170 bar/m, producing a mud flow (viscosity of 20 cp, density of 1.1 g/cm^3) into the formation at a linear velocity of about 0.08 m/seg. This corresponds to an effective permeability of about 100 darcy. The real influence of these high permeability conduits has an unknown areal extent.

THE COMPUTATIONAL MESH.- We did not intend to simulate the faults but we have idealized the complex geology of the sector as it is shown in figure 8. The reservoir's volume is divided into 140 elements of different sizes with 273 interfaces between them and distributed in four vertical layers. The deepest layer NIV D, is 1000 m. thick and represents the deep aquifer underlying the whole reservoir's area, having a very small measured porosity (2%). The layer NIV C is the contact region between the production zones of the reservoir and the deep aquifer. NIV B is the transition zone between the two-phase vapor dominated layer NIV A, where most of the wells are producing and the compressed liquid layers. Porosity at each layer was calculated using a simple exponential model obtained from the interpolation of available data. The same operation was done for thermal conductivity and rock density. We assumed all these parameters being a function of depth only. Areal distribution of rock permeability was estimated by numerical trial and error during the modeling of the field's natural state. The values for vertical permeability are shown in Fig. 8 and agree with those obtained from pressure tests.

Simulation of the natural state of the system was performed in order to get a group of coherent initial thermodynamic conditions similar to measured profiles. Some final vertical values are shown in Fig. 8; they are referred to the center of mass of every element. No natural recharge of fluid was considered.

EXTRACTION/REINJECTION MODELING.- We started the exploitation modeling in August 1982, the date at which the first two Tejamaniles' plants started up. The rates of mass extraction and of fluid injection are averaged from those presented in figures 9 and 10. For the rate of air injection we only had two measured values at well Az-8: 35 Kg/h and 250 Kg/h of air in 231 T/h of water. By technical and practical reasons we couldn't make more measurements of air reinjection rate, but performing a global balance of gas N_2 outflowing from the production wells, we estimated the values shown in (Fig. 11)Oxygen coming together with Nitrogen into the reservoir is not taken into account beacause it does not appear in any production well; it must be "consumed" by reducing agents present in the reservoir within reinjection wells' neighborhood. The influence of all the other gases forming the air mixture is neglected.

The calculation begins with a time step of 10 days and convergence is achieved in two or three iterations. The time step grows automatically until a maximum of 320 days with simultaneous extraction/injection. A typical calculation required about 46 seconds for every group of convergent iterations, that means a duration of 38 minutes for a complete run of 50 time steps. The duration of a complete cycle could be four to ten times longer when serious no-convergence problems appear. The calculations were performed on a CYBER-932 a 3.0 mips and 64 bit machine. The simulation was stopped in August 1990.

RESULTS AND CONCLUSIONS

The simulated flow of cold water and air in the Tejamaniles geothermal field, agrees reasonable well with its observed behavior (Fig. 11). When extraction starts simultaneously with reinjection, the air mixed to the injected water propagates very fast through the fractures network and arrives to the producing regions with negligible thermal interference. From figures 9 and 11, one can estimate that the air injected in well Az-7 and/or in well Az-8 takes about 50 days to arrive at well Az-16D, corresponding to an average velocity equal to 22 m/day, and about 35 days to arrive at well Az-17, meaning an average velocity equal to 46 m/day. The distribution of permeabilities (Fig. 12) calculated by trial and error during the production/injection history match, permits to deduce some preferential dispersion paths followed by Nitrogen during its rapid migration from reinjection to extraction zones.

The initial response of the field to exploitation is primarily reflected by geochemical changes. The production history of the sector show some important local alterations. From a thermodynamical point of view, Tejamaniles presents three different vertical zones distinguishables by their vapor saturation. The response of the field to

exploitation is heterogeneous and will require to incorporate more realistic details into future simulations.

MASS BALANCE

The Tejamaniles sector contains initially about 1.44E9 m^3 of liquid water and 0.63E9 m^3 of steam, for a total mass of 1.08E12 kg or 1080 million tons of fluid and no air, saturating about 20 Km^3 of volcanic rock. This rock-fluid volume contains about 2.E16 KJ of thermal energy, 5 % belonging to the fluid. From Tables 2 and 1 we obtain for Tejamaniles:

Qp - Qi = 9,846,840 = 0.9 % of the original fluid mass in place.

REFERENCES

CATHELINEAU M., OLIVER R., NIEVA D., GARFIAS A.,1985. 'Mineralogy and distribution of Hydrothermal Mineral Zones in Los Azufres (Mexico) Geothermal Field'. Geothermics, Vol. 14 No.1, pp. 49-57.

CONTRERAS E.,DOMINGUEZ B.,IGLESIAS E.,GARCIA A.,HUITRON R., 1988. 'Compendio de Resultados de Mediciones Petrofisicas en Nucleos de Perforacion del Campo Geotermico de Los Azufres,Mich.', Geotermia-Revista Mexicana de Geoenergia, Vol.4 No.2, pp. 79-105.

MORENO J.,1989. 'Comportamiento Geoquímico de los pozos Az-16D, Az-17 y Az-6 del Sector Tejamaniles del Campo Geotérmico de Los Azufres'. Dpto. de Exploración. Informe Interno No. 9-89, Diciembre 1989.

NIEVA D.,QUIJANO J.,GARFIAS A.,BARRAGAN R.,LAREDO F.,1983.'Heterogeneity of the Liquid Phase, and Vapor Separation in Los Azufres (Mexico) Geothermal Reservoir'. 9th Workshop on Geothermal Reservoir Engineering, Stanford Ca. pp. 253-260.

NIEVA D.,VERMA M.,SANTOYO E.,BARRAGAN R.,PORTUGAL E.,ORTIZ,J.,QUIJANO J. 1987. 'Estructura Hidrologica del Yacimiento de Los Azufres'. International Symposium on Development and Exploitation of Geothermal Resources. Cuernavaca, Mor., Proceedings, pp. 202-213.

PRUESS K., 1988. 'SHAFT, MULKOM, THOUGH: A Set of Numerical Simulators for Multiphase Fluid and Heat Flow.' Geotermia-Revista Mexicana de Geoenergia, Vol.4, No.1, pp. 185-202.

SUAREZ C.,PRUESS K.,LIPPMANN M., 1989. 'Preliminary Modeling Studies on Los Azufres Geothermal Field: Free Convection in Tejamaniles'. Symposium in the Field of Geothermal Energy. Agreement between U.S. Dept. of Energy and CFE of Mexico (CONF-8904129), April 1989, San Diego, Ca., pp.161-184.

VIGGIANO C., 1987. 'Regimen de Flujo en Base a Mineralogia Autigenica en el Campo Geotermico de Los Azufres,Mich.', Geotermia Vol. 3, No. 3, pp. 191-213.

TABLE 0.- PARAMETERS USED IN THE SIMULATIONS

ROCK/ROMATION PARAMETERS		VALUE
reservoir thickness		2500 m
reservoir permeability tensor (layer NIV A)	Kx	$1.0x10^{-16} m^2$
	Ky	$1.0x10^{-15} m^2$
	Kz	$1.0x10^{-12} m^2$
rock specific heat		1165 J/Kg/°C
reservoir porosity		Fig. 4
reservoir rock density		Fig. 5
rock heat conductivity		Fig. 6
FLUID PARAMETERS		**VALUE**
initial pressure		60 bar
initial temperature		270°C
initial air mass fraction		0%
gravitational acceleration		9.7862 m/s^2
binary diffusion exponent		1.8
residual liquid saturation		0.30
residual vapor saturation		0.05
relative permeability function		corey's curves
capillary pressure		Neglected
EXTRACTION/INJECTION PARAMETERS		**VALUE**
heat injection		0.1 W/m^2
water injection (total)		96.2 Kg/s
air injection (total)		8.2 Kg/s
fluid extraction (total)		222.2 Kg/s

TABLE 1.- LOS AZUFRES INJECTION HISTORY

FLUID FROM	TO WELL	Qi (T/h)	PERIOD	TOTAL MASS INJECTED (T)
SOUTH				
Az- 6 Az-16D Az-17 Prod. Tests	Az- 7	134	Aug. 82 - Nov. 88	7,428,960
Az-18	Az-31	60	Nov. 87 - Dec. 89	1,137,600
Az-22	Az- 8	80	Nov. 88 - Dec. 89	816,000
Az-33	Az- 7	15	Nov. 88. - Dec. 89	153,000
Az-46	Az- 7	30	Nov. 88 - Dec. 89	306,000
Cooling Tower	Az- 8	35	Nov. 88 - Dec. 89	357,000

Qi(North) = 11,947,800 T., Qi(South) = 10,198,560 T., Qi(Total) = 22,146,360 T.

TABLE 2.- LOS AZUFRES PRODUCTION HISTORY.

PLANT	Qp (T/h)	PERIOD	TOTAL MASS EXTRACTED (T)
portable generators			
North	330	Aug. 82 - Dec. 89	21,423,600
South	180	Aug. 82 - Dec. 87	8,532,000
	270	Jan. 88 - Dec. 89	4,730,400
Tejamaniles Unit	665	Nov. 88 - Dec. 89	6,783,000

Qp(North) = 21,423,600 T, Qp(South) = 20,045,400, Qp(Total) = 41,469,000

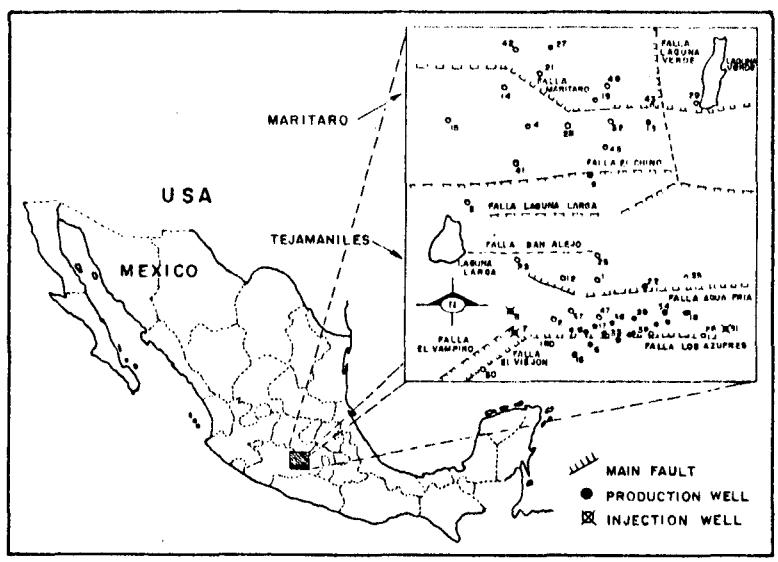

FIG. 1.- LOCATION OF THE LOS AZUFRES GEOTHERMAL FIELD

FIG. 2 PRESSURE VERTICAL PROFILE

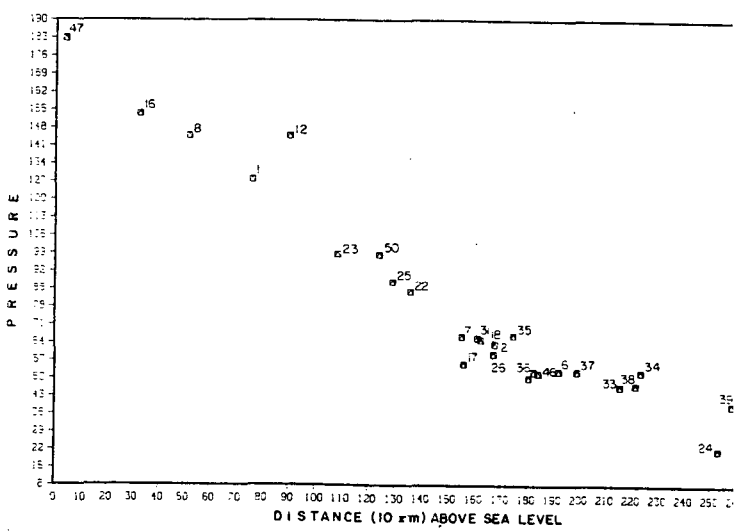

FIG. 3 TEMPERATURE VERTICAL PROFILE

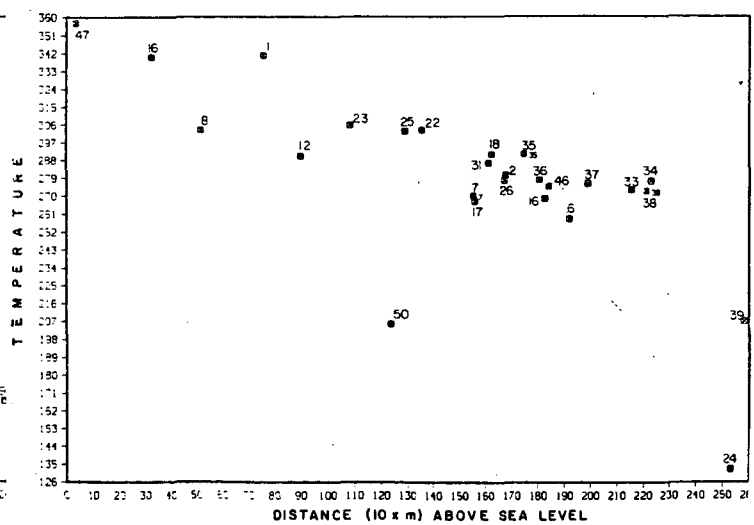

Figure 4. LOS AZUFRES POROSITY DISTRIBUTION

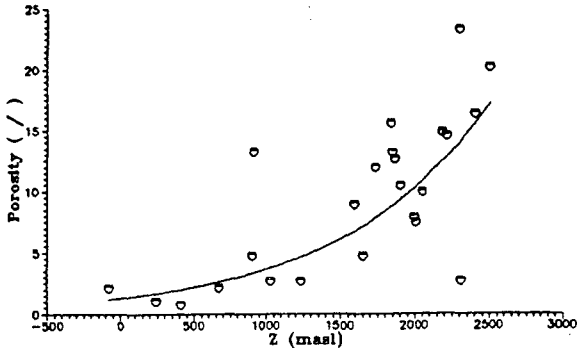

Figure 5. LOS AZUFRES ROCK DENSITY DISTRIBUTION

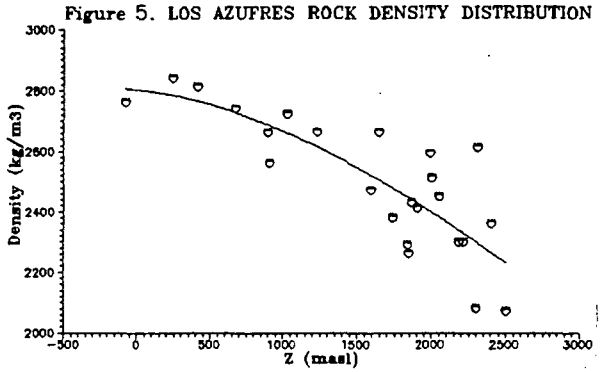

Figure 6. LOS AZUFRES THERMAL CONDUCTIVITY

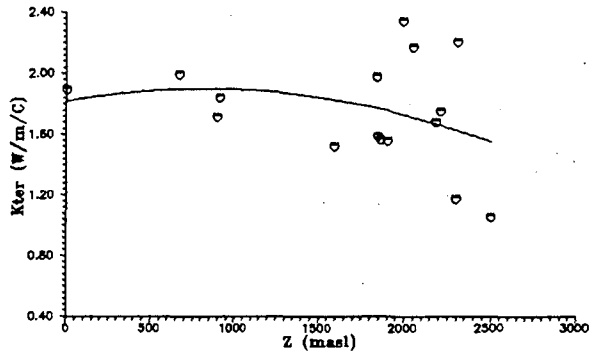

Fig. 7 .- NITROGEN RATE EVOLUTION AT TEJAMANILES WELLS.

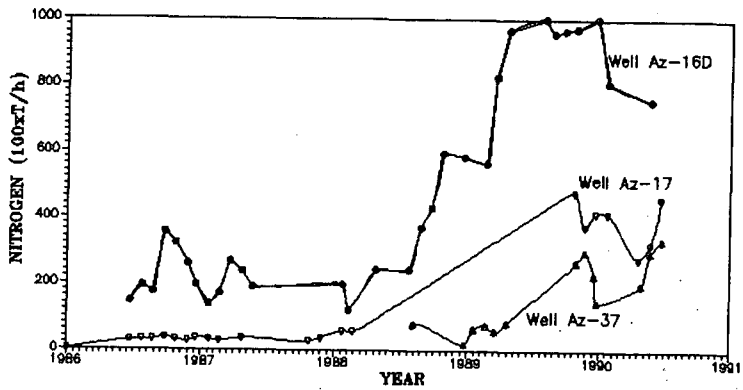

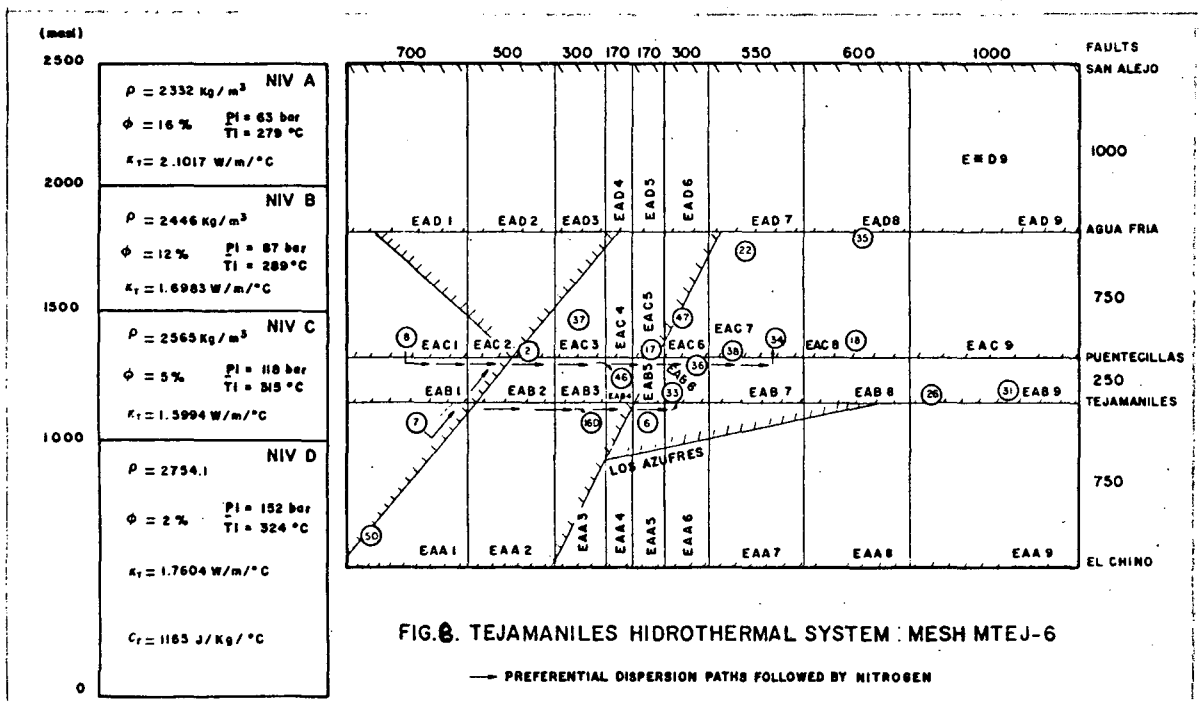

FIG.8. TEJAMANILES HIDROTHERMAL SYSTEM : MESH MTEJ-6

Fig. 9.- TEJAMANILES MASS EXTRACTION.

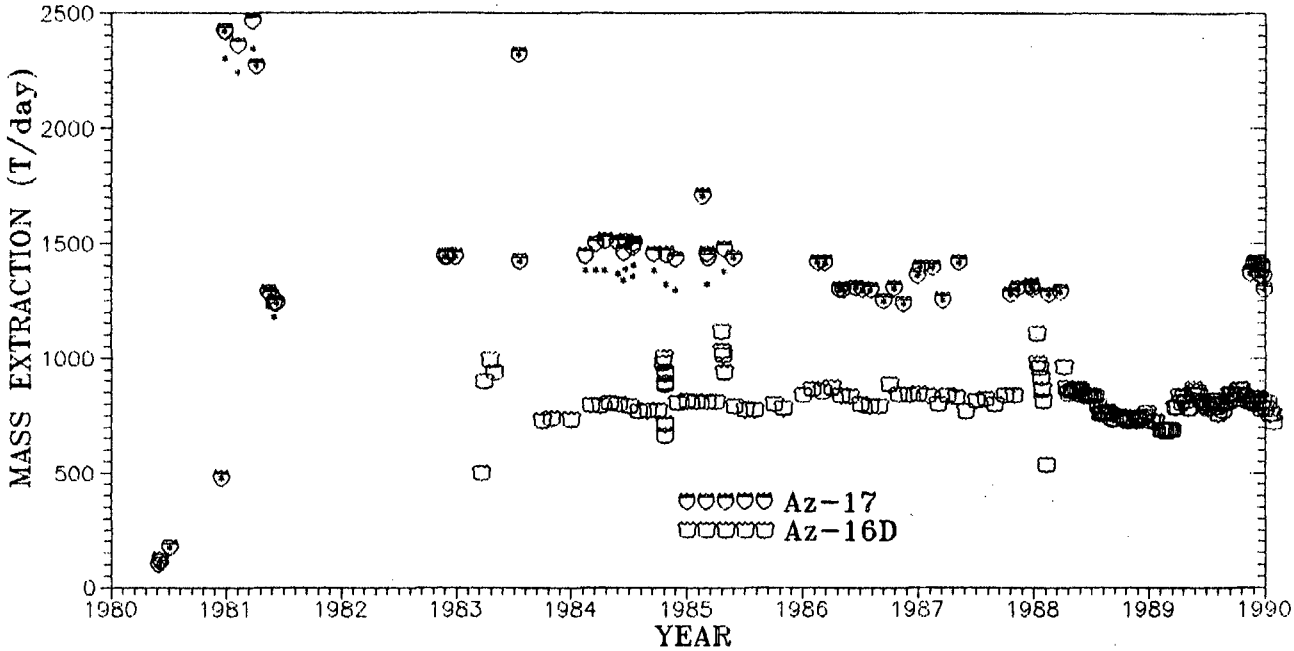

Fig. 10.- RATE OF FLUID INJECTION AT TEJAMANILES.

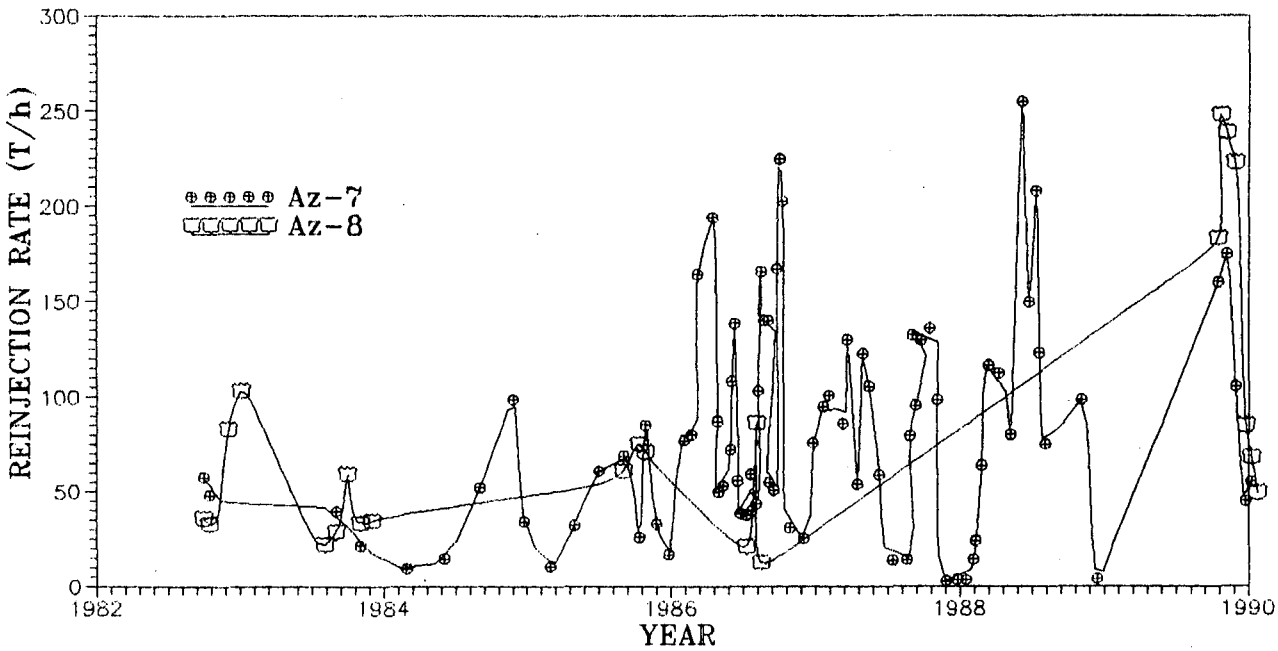

Fig. 11.- TEJAMANILES: EVOLUTION OF AIR MASS IN SITU.

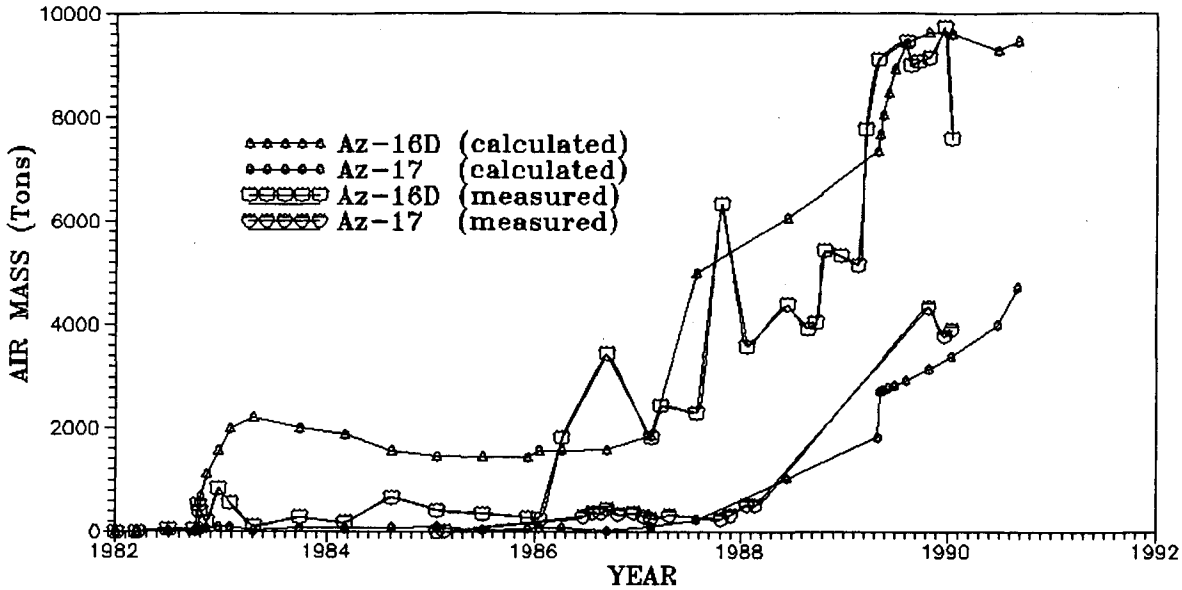

FIG. 12 ESTIMATION OF ABSOLUTE PERMEABILITIES

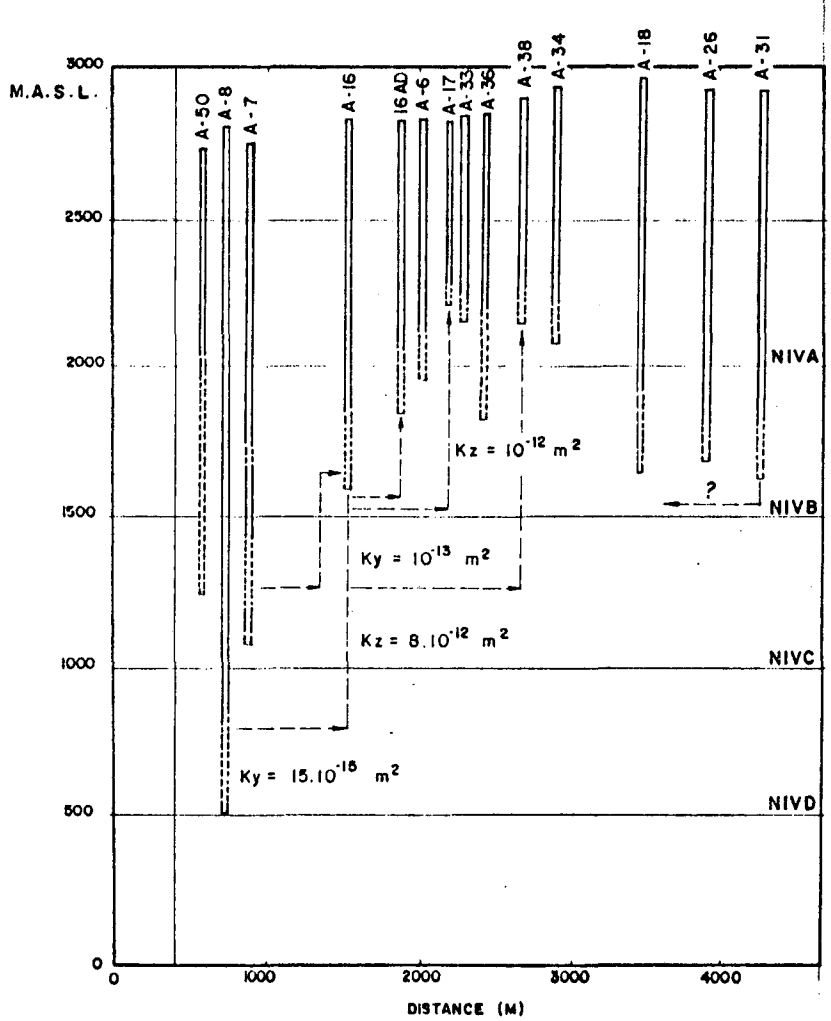

WATER-CO_2 VERSION OF MULKOM CODE: A TOOL FOR STUDYING THE ORIGIN AND TRENDS OF CO_2 IN GEOTHERMAL RESERVOIRS

C. Calore (*), G. Gianelli (*), K. Pruess (+)

(*) Istituto Internazionale per le Ricerche Geotermiche - C.N.R., Pisa, ITALY.
(+) Earth Sciences Division, Lawrence Berkeley Laboratory, Berkeley, USA.

INTRODUCTION

Most wells in the Larderello vapor-dominated geothermal field produce superheated steam, with a non-condensible gas content of 3-10% by weight, of which typically 95% consist of CO_2. For most wells the gas content of the discharge shows remarkably small temporal variations, even as over a period of several decades well flow-rates decline by an order of magnitude.

A study was undertaken in order to obtain useful information on reservoir conditions and processes from observed trends of CO_2 in the well discharges (Pruess et al., 1985). Some general considerations on the amounts of vapor and CO_2 produced from the Larderello field led to the conclusion that the produced CO_2 could not have been stored in the original reservoir fluid. This conclusion was supported by results of numerical simulations, which were carried out by the H_2O-CO_2 version of the Lawrence Berkeley Laboratory general purpose simulator MULKOM (Pruess, 1983; O'Sullivan et al., 1983).

Most of the CO_2 produced at Larderello, therefore, must originate either from external or from internal sources.

The external source hypothesis was considered to be somewhat improbable since observed temporal variations in CO_2 content of discharges are generally small over several decades, whereas the flow-rates of individual wells often change by an order of magnitude or more.

As several authors considered that the non-condensible gas concentrations in geothermal reservoirs, and in particular CO_2 partial pressures, are controlled by equilibrium reactions involving mineral assemblages (Giggenbach, 1981; Cavarretta et al., 1982; Arnorsson et al., 1983; Giggenbach, 1984) it was decided to investigate this by numerical simulations, incorporating an internal CO_2 source into the MULKOM code (Pruess et al., 1985).

In the present paper, after discussing some mineral reactions that could be responsible for buffering the CO_2 partial pressures, P_c, in the reservoir at Larderello, we present the actual implementation of mineral buffers for CO_2 into MULKOM, as an example of incorporating heterogeneous reactions that involve the release or uptake of gaseous constituents. Some simulation results of individual matrix block depletion with mineral buffers proposed for the Larderello reservoir are also presented.

MINERAL BUFFERS FOR CO_2

At Larderello the coexistence of epidote, prehnite, calcite, K-feldspar and of k-mica, calcite, k-feldspar, has led to the proposal of the following reactions as CO_2 partial pressure buffers (Cavarretta et al., 1982):

2 clinozoisite + 2 calcite + 3 quartz + 2 H_2O <---> 3 prehnite + 2 CO_2 (R1)

3 muscovite + 4 calcite + 6 quartz <---> 2 clinozoisite + 3 k-feldspar + 4 CO_2 + 2 H_2O (R2)

These reactions are dominant in the temperature range 230-320 °C. For higher temperatures we can use other mineral reactions involving diopside, tremolite or phlogopite, which occur in the hottest

part of the field as end members in clinopyroxene, clinoamphibole and biotite (Bertini et al., 1985):

3 calcite + tremolite + 2 quartz <---> 5 diopside + 3 CO_2 + H_2O (R3)

2 clinozoisite + 5 calcite + 3 quartz <---> grossular + 5 CO_2 + H_2O (R4)

Figure 1 shows the equilibrium curves for reactions R1 to R4 in a P_c vs temperature diagram. In computing these curves we have used the thermodynamic data of Helgeson et al. (1978) and have taken into account the activity of diopside, tremolite, clinozoisite and muscovite, on the basis of the most frequent composition of clinopyroxene, clinoamphibole, epidote and k-mica present at Larderello (Cavarretta et al., 1980, 1982). Bird and Norton (1981) have emphasized the importance of considering the real mineral compositions in water-rock interaction modeling. In our calculations we have used for epidote the activity-composition relationships given by Bird and Helgeson (1981). For the other minerals we used the relationships proposed by Bird and Norton (1981), Bird et al. (1984) and Bishop and Bird (1987). The variation of equilibrium partial pressure of CO_2 with respect to solid solution compositions can be estimated by considering, for example, reaction R1. Figure 2 shows the dependence of P_c^{eq} on pistacite mole fraction for the reaction R1.

Absolute values of P_c also depend on uncertainties in thermodynamic data. To give some idea of the discrepancies involved we have computed the CO_2 partial pressures controlled by reactions R1 using the data of Helgeson et al. (1978) and Chatterjee et al. (1984). The result, reported in Fig. 3, is that the P_c^{eq} computed with the data of Chatterjee et al. (1984) is about 5 times higher than that computed with the data of Helgeson et al. (1978).

In conclusion, variations in CO_2 partial pressures from the presence of solid solutions and from uncertainties in thermodynamic data are of similar magnitude, and are substantial. The former, however, can be reduced by using reasonable activity-composition relationships for minerals.

IMPLEMENTATION OF A BUFFER FOR CO_2 INTO MULKOM CODE

Since very little is known about the kinetic rates of the above reactions, a first-order rate law was used to study the depletion of a reservoir with a mineral buffer, assuming that the volumetric rate of CO_2 release/uptake from minerals is proportional to the difference between equilibrium and actual partial pressure of CO_2:

$$q_{CO2} = \alpha \, (P_c^{eq} - P_c) \qquad (1)$$

An internal CO_2 sink/source, as given by Equation (1), was incorporated into the MULKOM simulator.

The buffering of CO_2 partial pressure by mineral assemblages is a prototype for heterogeneous reactions that involve the release or uptake of gaseous constituents. Because of the broad significance of such processes in subsurface flows, a code fragment showing the programming of the reaction into subroutine MULTI is reproduced in the Appendix. This can serve as a guide in implementing other fluid-mineral reactions.

The buffering of CO_2 can be performed by using a constant or temperature-dependent CO_2 equilibrium partial pressure (PCEQX). The temperature dependence of P_c^{eq} is expressed by empirical fits to data for the various reactions. The relationships for reactions R1 (curve c) and R2 (curve a) are now implemented (Equations 1 and 2, below).

A library of mineral buffers for CO_2 can be provided by coding the appropiate relationships for P_c^{eq}. The choice of the reaction is made by supplying an integer parameter in the input deck; the kinetic rate constant α is also provided in the input deck (parameter EQ in MULTI).

Since the mineral buffer reactions are believed to proceed only in the presence of liquid water, the mineral buffer segment is not performed for elements having $S_l = 0$. It is also assumed

that the rate constant should go to zero for S_l --> 0. This is achieved by replacing α with $\alpha \cdot S_l$ /SLEQ for $S_l \leq$ SLEQ (the parameter SLEQ is supplied in the input deck; we used a value of 0.05).

Changes in reservoir porosity and permeability from the mineral reaction are neglected here. Such changes would depend on the total cumulative CO_2 release/uptake, calculated, after convergence is achieved, in subroutine CONVER (see Appendix). Implementation of this would be no problem from the coding standpoint, but little is known about the porosity-permeability relationship in real subsurface media.

In the present version of the code no allowance is made for using different equilibrium reactions in different grid elements, for changing the reaction for temperatures above or below the range of validity, or for exhausting the reagents.

NUMERICAL SIMULATIONS WITH AN INTERNAL CO_2 SOURCE

At the beginning of the study, with little detailed information on possible mineral buffers at Larderello, Pruess et al. (1985) implemented a buffer as given by reaction R1 (curve c in Fig.1) to investigate physical processes, mechanisms and numerical performance of the code, and assumed that it was valid for the entire reservoir and in a wider temperature range. The temperature dependence of the equilibrium partial pressure of CO_2 for curve c is expressed by the relatioship:

$$\log P_c^{eq} = 1.437 \times 10^{-2}\ T - 1.4 \times 10^{-5}\ T^2 - 2.81 \qquad (2)$$

This relationship has the peculiarity of giving, over the temperature interval 200-300 °C, P_c^{eq} values such that the ratio between P_c^{eq} and the saturated vapor pressure is practically constant, thus implying that equilibrium CO_2 mass fractions in vapor are independent of temperature.

We then implemented in the code the other CO_2 buffer given by reaction R2 (curve a) that is valid in the range of temperatures present in most of the Larderello exploited reservoir. The temperature dependence of P_c^{eq} for curve a is expressed by the relationship:

$$\log P_c^{eq} = 3.115 \times 10^{-2}\ T - 2.48 \times 10^{-5}\ T^2 - 6.31 \qquad (3)$$

The equilibrium partial pressure of CO_2 given by the above equation decreases more rapidly than the saturated vapor pressure as temperature decreases. We thus expect that the CO_2 discharged from matrix blocks will tend to decrease with time, after an initial rise due to diminishing liquid phase flow, as a consequence of the decrease in temperature due to boiling of liquid.

Some simulation results of the depletion of individual matrix blocks using Equation (3) and different values of α are shown in Figure 4, which also reports the results obtained by Pruess et al. (1985) with reaction R1. The simulation parameters are given in Table 1 of Pruess et al. (1985), except for initial temperature, T = 280 °C, and initial partial pressure of CO_2, which was assumed equal to the equilibrium value at 280 °C (2.9355×10^5 Pa). The results for simulated block depletion with the two buffers are similar, although, as expected, even with high α we obtained a decline of CO_2 concentrations with time with reaction R2, due to the decrease in temperature. A description of the simulation results with reaction R1 is given in Pruess et al. (1985).

A faster increase in the discharged enthalpy can also be achieved with a lower permeability (Fig. 5) instead of a lower initial liquid saturation (Pruess et al. 1985), thus avoiding the reduction in the depletion time.

Although the parametric analysis has still to be completed and we have considered only the depletion of individual matrix blocks, reaction R1 seems the best candidate for mantaining the CO_2 concentrations in the reservoir that will produce the small temporal variations in CO_2 content of well discharges. Higher simulated values of CO_2 concentrations can be obtained by considering different equilibrium curves for reaction R1. Equation (2) used in the simulations gives lower P_c^{eq} than the

other possible curves computed with different solid solution compositions and thermodynamic data sets (Fig. 3). Since these curves are almost parallel to curve c, we should obtain similar CO_2 trends but with higher values.

On the other hand, we cannot a priori exclude a buffer for CO_2 as given by Equation (3). Observed CO_2 concentrations in the field represent an average of fluid discharge from many matrix blocks. As the drainage volume of a well expands with time, matrix blocks at greater distance from the well will contribute increasing CO_2 concentrations, while matrix blocks near the well will discharge fluids of declining CO_2 content.

CONCLUSIONS

The MULKOM simulator incorporating a buffer for CO_2 has proved a valuable tool for improving our knowledge of the physical processes and mechaninisms occuring in reservoirs in which the partial pressure of CO_2 is controlled by a mineral buffer.

Block depletion simulations suggested that reaction R1 is a very likely candidate for generating CO_2, as observed in the central zones of the Larderello field. This is also supported by the fact that the mineral assemblage involved in reaction R1 is found more frequently in the parts of the reservoir with temperature in the interval 250-320 °C. Through an appropriate choise of formation parameters, initial conditions and kinetic rate factors for CO_2 release, it is possible to adequately represent the observed trends of non-condensible gas content and produced enthalpy. Unfortunately, it is not possible to make reliable predictions for absolute partial pressures of CO_2, as these are strongly affected by relatively minor uncertainties in thermodynamic data as well as in solid solution cmpositions.

Further constraints will probably emerge when we consider the long-term trends in temperature in linear depletion models.

Improvements to the simulator should include:

- the implementation of a two-phase front-tracking technique to limit the oscillations in CO_2 concentrations and consequently the need for finer space discretization;
- an option to use different mineral buffers for different parts of the reservoir;
- an option to change the buffer for temperatures above or below its range of validity.

ACKNOWLEDGEMENTS

The authors are indebted to Romano Celati (deceased), for helpful discussions in the earlier phase of this work. Karsten Pruess gratefully acknowledges the hospitality of the Istituto Internazionale per le Ricerche Geotermiche.

REFERENCES

- Arnorsson S., Gunnlaugsson E., and Svavarsson H. (1983). The Chemistry of Geothermal Waters in Iceland. III. Chemical Geothermometry in Geothermal Investigations. Geochim. Cosmochim. Acta, Vol. 47, pp. 567-577.

- Bertini G., Gianelli G., Pandeli E., and Puxeddu M. (1985). Distribution of Hydrothermal Minerals in Larderello - Travale and Mt. Amiata Geothermal Fields (Italy). Geothermal Resources Council Transactions, Vol. 9-Part I, pp. 261-266.

- Bird D.K., and Helgeson H. (1981). Chemical Interaction of Aqueous Solutions with Epidote-Feldspar Mineral Assemblages in Geologic Systems. II. Equilibrium Constraints in Metamorphic/Geothermal Processes. Am. J. Sci. Vol. 281, pp. 576-614.

- Bird D.K., and Norton D. (1981). Theoretical Prediction of Phase Relations among Aqueous Solutions

and Minerals: Salton Sea Geothermal System. Geochim. Cosmochim. Acta, Vol. 45, pp. 1479-1493.

- Bird D.K., Schiffman P., Elders W.A., Williams A.E., and McDowell S.D. (1984). Calc-Silicate Mineralization in Active Geothermal Systems. Econ. Geol. Vol. 79, pp. 671-695.

- Bishop B.P., and Bird D.K. (1987). Variation in Sericite Compositions from Fracture Zones within the Coso Hot Springs Geothermal System. Geochim. Cosmochim. Acta, Vol. 51, pp. 1245-1256.

- Cavarretta G., Gianelli G., and Puxeddu M. (1980). Hydrothermal Metamorphism in the Larderello Geothermal Field. Geothermics, Vol. 9, pp. 297-314.

- Cavarretta G., Gianelli G., and Puxeddu M. (1982). Formation of Authigenic Minerals and their Use as Indicators of Physico-Chemical Parameters of the Fluids in the Larderello-Travale Geothermal Field. Econ. Geol., Vol. 77, pp. 1071-1084.

- Chatterjee N.D., Johannes W., and Leistner H. (1984). The system $CaO-Al_2O_3-SiO_2-H_2O$: New Phase Equilibria Data, Some Calculated Phase Relations and their Petrological Applications. Contrib. Mineral. Petrol., Vol. 88, pp. 1-13.

- Giggenbach W.F. (1981). Geothermal Mineral Equilibria. Geochim. Cosmochim. Acta, Vol. 45, pp. 393-410.

- Giggenbach W.F. (1984). Mass Transfer in Hydrothermal Alteration Systems - A Conceptual Approach. Geochim. Cosmochim. Acta, Vol. 48, pp. 2693-2711.

- Helgeson H., Delaney J.M., Nesbit H.W., and Bird D.K. (1978). Summary and Critique of the Thermodynamic Properties of Rock-Forming Minerals. Am. J. Sci., Vol. 278A, pp. 1-229.

- O'Sullivan M.J., Bodvarsson G.S., Pruess K., and Blakeley M.R. (1983). Fluid and Heat Flow in Gas-Rich Geothermal Reservoirs. Paper SPE-12102, presented at the Society of Petroleum Engineers 58th Annual Technical Conference and Exhibition, San Francisco, Ca., October 1983.

- Pruess K. (1983). Development of the General Purpose Simulator MULKOM. Annual Report 1982, Earth Sciences Division, Lawrence Berkeley Laboratory Report LBL-15500, Berkeley, California.

- Pruess K., Celati R., Calore C., and D'Amore F. (1985). CO_2 Trends in the Depletion of the Larderello Vapor-Dominated Reservoir. Proc. Tenth Workshop Geothermal Reservoir Engineering, Stanford, California, pp. 273-278.

APPENDIX

```
      SUBROUTINE MULTI
            |
            |
C     ADD ROCK ENERGY
      ENR = CD * PAR(NLM2+NSEC-1)
      D(NK1,M) = D(NK1,M) + ENR
C**************** BUFFER FOR CO2 PARTIAL PRESSURE ****************
      QCO2(M) = 0.
      IF(EQ.EQ.0..OR.PAR(NLOC2+NBK+1).EQ.0.) GO TO 101
      PCEQX = PCEQ
      IF(PCEQ.NE.0.) GO TO 99
C*********** COME HERE TO COMPUTE T-DEPENDENT PCEQX *********
      TX = PAR(NLM2+NSEC-1)
```

```
      IF(MOP(18).EQ.2)  GO TO 555
      ELOGPC  =  -1.4E-5*TX**2  +  1.437E-2*TX  -  2.81
      PCEQX = 10.**ELOGPC * 1.E5
      GO TO 99
  555 ELOGPC  =  -2.48E-5*TX**2  +  3.115E-2*TX  -  6.31
      PCEQX = 10.**ELOGPC * 1.E5
   99 CONTINUE
      PCO2 = X(NLOC+3) + DX(NLOC+3)
      IF(M.EQ.4) PCO2 = PCO2 + DELX(NLOC+3)
      EQX = EQ
      IF(PAR(NLOC2+NBK+1).GE.SLEQ.OR.SLEQ.EQ.0.) GO TO 137
C*********** COME HERE TO INTERPOLATE RATE CONSTANT *******
      SL = PAR(NLM2+NBK+1)
      EQX = EQ * SL/SLEQ
  137 CONTINUE
      QCO2(M) = EQX * (PCEQX - PCO2)
  101 CONTINUE
      QC(N) = QCO2(1)
C ***********************************************************************
      IF(MOP(3).GE.4) PRINT 200, ELEM(N), ((D(K,M), K=1,NK1), M=1,NEQ1)
  200 FORMAT(/' ACCUMULATION TERMS AT ELEMENT 'A5/(10(1XE12.6)))
                |
                |
C-----AT BEGINNING OF TIME STEP, ACCUMULATION TERM CONTRIBUTION TO
C     RESIDUAL IS ZERO.
      IF(ITER.NE.1)  R(NLOC+K) = R(NLOC+K) + D(K,1) - DOLD(NLOC+K)
      IF(K.EQ.2)  R(NLOC+2) = R(NLOC+2) - QCO2(1) * FORD
C-----SET DOLD(NLOC+K) AT BEGINNING OF TIME STEP.
                |
                |
C-----COMPUTE MATRIX ELEMENT ARISING FROM DEPENDENCE OF COMPONENT K
C     UPON PRIMARY VARIABLE L.
      IRN(NZ+1) = NLOC + K
      IF(IAB.EQ.0)  ICN(NZ+1) = NLOC + L
      IF(IAB.NE.0)  JVECT(NZ+1) = NLOC + L
      CO(NZ+1) =  - (D(K,L+1) - D(K,1)) / DELX(NLOC+L)
      IF(K.EQ.2)  CO(NZ+1) = CO(NZ+1) + FORD * (QCO2(L+1) - QCO2(1)) / DELX(NLOC+L)
      IF(PHINN.EQ.0..AND.K.EQ.L.AND.K.NE.NEQ)  CO(NZ+1) = 1.
  106 NZ = NZ+1
                |
                |
      SUBROUTINE CONVER
                |
                |
      DPHI = PHIN * (COM(NMAT) * DX(NLOC+1) + EXPAN(NMAT) * (PAR(NLOC2+NSEC-1) - T(N)))
      PHI(N) = PHIN + DPHI
C************** COMPUTE CUMULATIVE CO2 RELEASE/UPTAKE ***************
      QCI(N) = QCI(N) + QC(N) * DELTEX
C-----INCREMENT PRIMARY VARIABLES.
      DO 3 M=1,NEQ
```

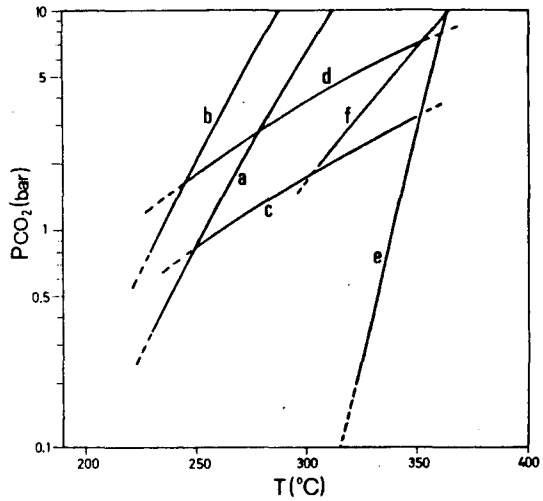

Fig.1 P_{CO2}-temperature equilibrium curves for possible mineral buffers at Larderello. Curve a and b refer to the reaction R2, c and d to reaction R1, e to R4 and f to R5. The composition of the minerals refers to the pure phase, with the exception of muscovite (X_{mu}=0.6) for curve a, tremolite (X_{tr}=0.5) and diopside (X_{dio}=0.5) for curve e, epidote (X_{ps}=0.275) for curves a,b,c, and epidote (X_{ps}=0.2) for curve d. X denotes mole fractions and X_{ps} the mole fraction of the pistacite component in epidote.

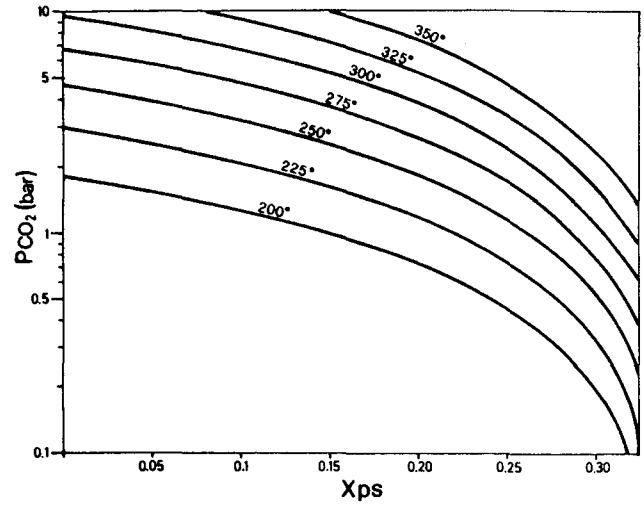

Fig. 2 CO_2 partial pressure vs pistacite mole fraction in epidote solid solutions at different temperatures. Curves refer to the reaction R1.

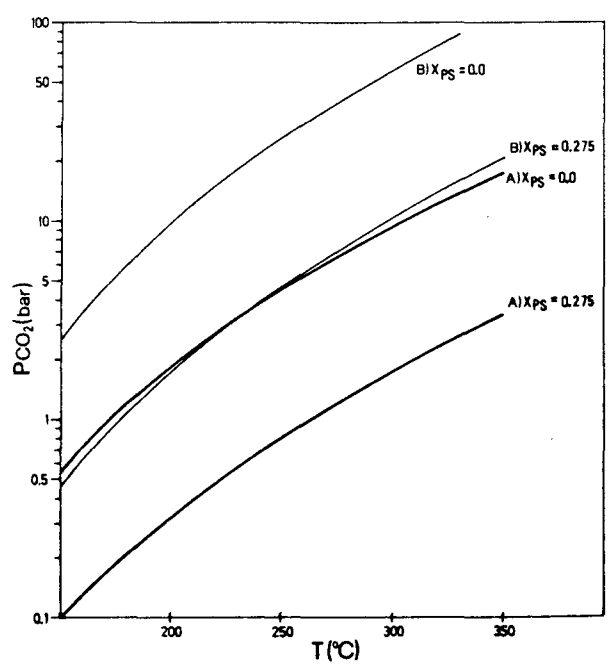

Fig. 3 P_{CO2} - temperature diagram for reaction R1. Curves are computed using different epidote compositions and different thermodynamic data: A) after Helgeson et al. (1978), B) after Chatterjee et al. (1984).

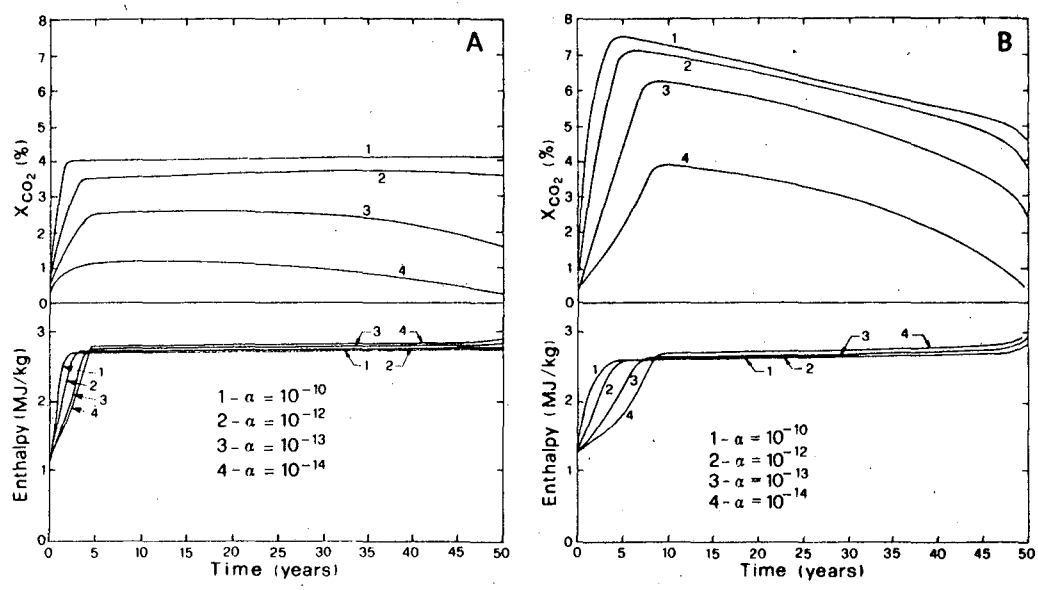

Fig. 4 Block depletion model with mineral buffer: CO_2 mass fractions and enthalpy trends for the discharged fluid. A) with mineral buffer given by Equation (2) and initial temperature of 240°C; B) with mineral buffer given by Equation (3) and initial temperature of 280 °C. Cases 1 to 4 with a kinetic rate constant of 10^{-10}, 10^{-12}, 10^{-13} and 10^{-14} kg/(m^3 ·s· Pa) respectively.

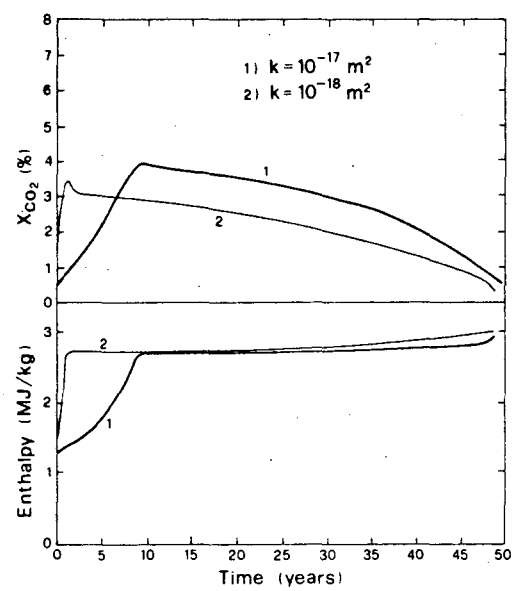

Fig. 5 Simulated CO_2 and enthalpy transients for fluid discharge from a porous block with mineral buffer given by Equation (3) and a kinetic rate constant of 10^{-14} kg/(m^3· s· Pa). Cases 1 and 2 with a matrix permeability of 10^{-17} and 10^{-18} m^2 respectively.

Case Study Using Faster TOUGH

Takashi Okabe, Kazumi Osato and Shinji Takasugi

Department of Technology, Geothermal Energy Research and Development Co., Ltd., Tokyo 103, Japan

Abstract

The original version of TOUGH (OLD TOUGH) requires a large amount of CPU time for large 2D or 3D problems. This has prevented us from using OLD TOUGH on several actual field simulations. OLD TOUGH has been modified to use less CPU time, mainly by using two new matrix inversion methods, allowing us to use the NEW TOUGH on large problems.

In this report, we first check NEW TOUGH for accuracy and speed, and we then use the NEW TOUGH to optimize a porous medium model before applying this model in a case study. In the case study we try to simulate build-up data from PTS (Pressure/Temperature/Spinner) logging. In this report we examine in particular how to choose grids when modeling porous media, and the application of such an optimized grid in a field simulation.

1. Introduction

1-1. Analysis of Build-up Data

Build-up data are obtained from either PTS logging or pressure monitoring, in most cases. When analysis build-up data, in the single-phase case, we use a "Multi-Well Multi-Rate" simulator. The assumptions made in this simulator are that the reservoir is unbounded (no closed or constant pressure boundaries laterally), homogeneous (field parameters are constant), isotropic (flow independent of direction) and confined above and below (no leakage). Because we use an "Early Time Analysis" option the reliability of the results is excellent. If two-phase conditions occur in the reservoir, it is necessary to use a simulator like TOUGH. We also find that the wellbore simulator we use is useful in both single-phase and two-phase cases.

1-2. OLD TOUGH Limitations and Modifications

(1) Limitations

OLD TOUGH could not be used for actual field simulations because it required too much CPU time and did not allow enough elements to give the resolutions we required.

(2) Modifications

Modifications to TOUGH were done in cooperation with the New Zealand Department of Scientific and Industrial Research (DSIR). The aims of the modifications were to

- reduce the CPU time needed to solve problems
- increase the number of elements that could be included in TOUGH simulations

These aims were motivated by the desire to perform the actual field simulation described later in this report.

1-3. Contents of this Report

(1) Assessment of this report

Two aspects of the NEW TOUGH have been assessed, the accuracy and the speed improvement. To check accuracy, Garg's model as specified in the TOUGH user's guide was used. To check speed, 1D, 2D and 3D model were used.

(2) Analysis of build-up data

Before analysing build-up data, the model was optimized. The model assumes 1D radial flow, and includes the well block. Optimization involved the construction of find grids near the well, and consideration of the build-up response. And we tried to match with the actual PTS data. The PTS data obtained by PTS logging in Japan.

2. Improvements to TOUGH, and Assessment

2-1. Improvements

The following improvements were made to TOUGH, to reduce CPU time and to allow more complex simulations:

(1) To reduce CPU time used by TOUGH

In OLD TOUGH, when the number of connections is large, much of the CPU time is spent inverting the matrix directly with subroutine MA28. Two new matrix inversion methods are made available in NEW TOUGH. One method is a direct one for 1D problems such as a one layer radial flow problem, and the other is a modified Successive Over-Relaxation (SOR) method, intended for use on 2D and 3D problems with a large number of elements.

(2) To increase the size of problem that could be solved

The improved speed of NEW TOUGH allows a larger number of element. The iterative SOR method for matrix inversion requires significantly less storage space than the Harwell subroutine MA28. With these improvements, we can now handle problems with 2500 elements and 6,000 connections.

2-2. Assessment of NEW TOUGH

(1) Accuracy

To verify accuracy, Garg's model as specified in the TOUGH user's guide was used. Figure-1(a) shows the results of this calculation. NEW and OLD TOUGH are in good agreement with each other, and also match Garg's semi-analytical theory. The NEW TOUGH was 1.9 times faster than OLD TOUGH.

In the 1980 Stanford Geothermal Workshop, there was a DOE comparison of existing geothermal simulators and analytical solutions. We have compared NEW TOUGH with these reported results. Figure-1(b) shows the results of this comparison in enthalpy, for two-phase radial flow in a porous medium.

(2) Speed

A comparison of CPU time is shown in Table-1. A speed improvement is observed, with simulations being 1.9 times faster for the 1D problem, 1.5 times faster for the 2D problem and 23 times faster for the 3D problem. The nature of the problems simulated is indicated in Table-1.

3. Build-up Analysis of PTS Logging Data

3-1. PTS Data and Analysis

PTS logging has been available for five years, and has been used in many geothermal regions in Japan. The quality of PTS data is excellent, and the analysis of such data is very useful for reservoir evaluation. Methods for analysing PTS data are mentioned in Introduction.

3-2. Optimization of the Model

Before running the case study we optimized the grid used to model the area surrounding the well.

We assume radial flow in a uniform porous medium towards a well of radius 0.2 meters.

The initial grid consisted of a well block, 500 equal thickness (1 meter) cylindrical blocks followed by 100 elements of gradually increasing thickness.

This grid was optimized in the following way.

(1) Calculation of drawdown and confirmation of thermal front

Using the initial grid, pressure drawdown was calculated and the presence of a thermal front was confirmed. The grid was then refined out as the thermal front and the calculation repeated.

Figures-2a and -2b show pressure and temperature curves after 20 days production for various block thicknesses. As can be seen the thermal front lies between 1.75 and 2 meters from the well block.

Refining the grid around the well smooths the curves out to the thermal front but has little effect past the front.

The temperature and pressure calculated using the finest grid were used as initial conditions for the pressure build up calculation.

(2) Calculation of pressure and temperature build-up, and confirmation of convergence

Figure-3 shows pressure and temperature curves for various block sizes 8,000 seconds after well shutdown. As block size is reduced these curves converge to a limit. It is apparent from these curves that there is little benefit in reducing the blocksize below 0.5 meters.

The 0.5 meters blocksize model is used as an optimized model for the case study.

3-3. Case Study

Data used in this case study was acquired by PTS logging in September 1989. At that time the well was in a two phase condition and flashing was in the formation. Before shutdown the pressure and temperature at the main feedpoint (1,940 meters) were 3.4 MPa and 237.4 deg. C respectively, and flow rate was 13.94 kg/s. After shutdown we recorded PTS data at the feedpoint in the well for 137 minutes. In this time the pressure recovered to 6.2 MPa and temperature to 271.9 deg. C.

4. Conclusions and Future Task

We drew the following conclusions from the work described in this report.

(1) We confirmed the speed increase and accuracy of NEW TOUGH. The speed increase was most dramatic for 3D problems. Here NEW TOUGH was 23 times faster than OLD TOUGH.

(2) Grids were optimized using a uniform porous medium model. Using the optimized grids, we tried to match with actual PTS data.

In this report we have mainly discussed optimization of the porous model. We will use this method of simulation in the future. As a future task we will try to match this PTS data using a double porosity model.

5. References

Pruess, K. (1987): TOUGH USER'S GUIDE, LBL-20700.

Stanford Geothermal Program (SGP) (1981): Proceedings of the Special Panel on Geothermal Model Intercomparison Study, Rep. SGP-TR-42. Stanford University, Stanford, California.

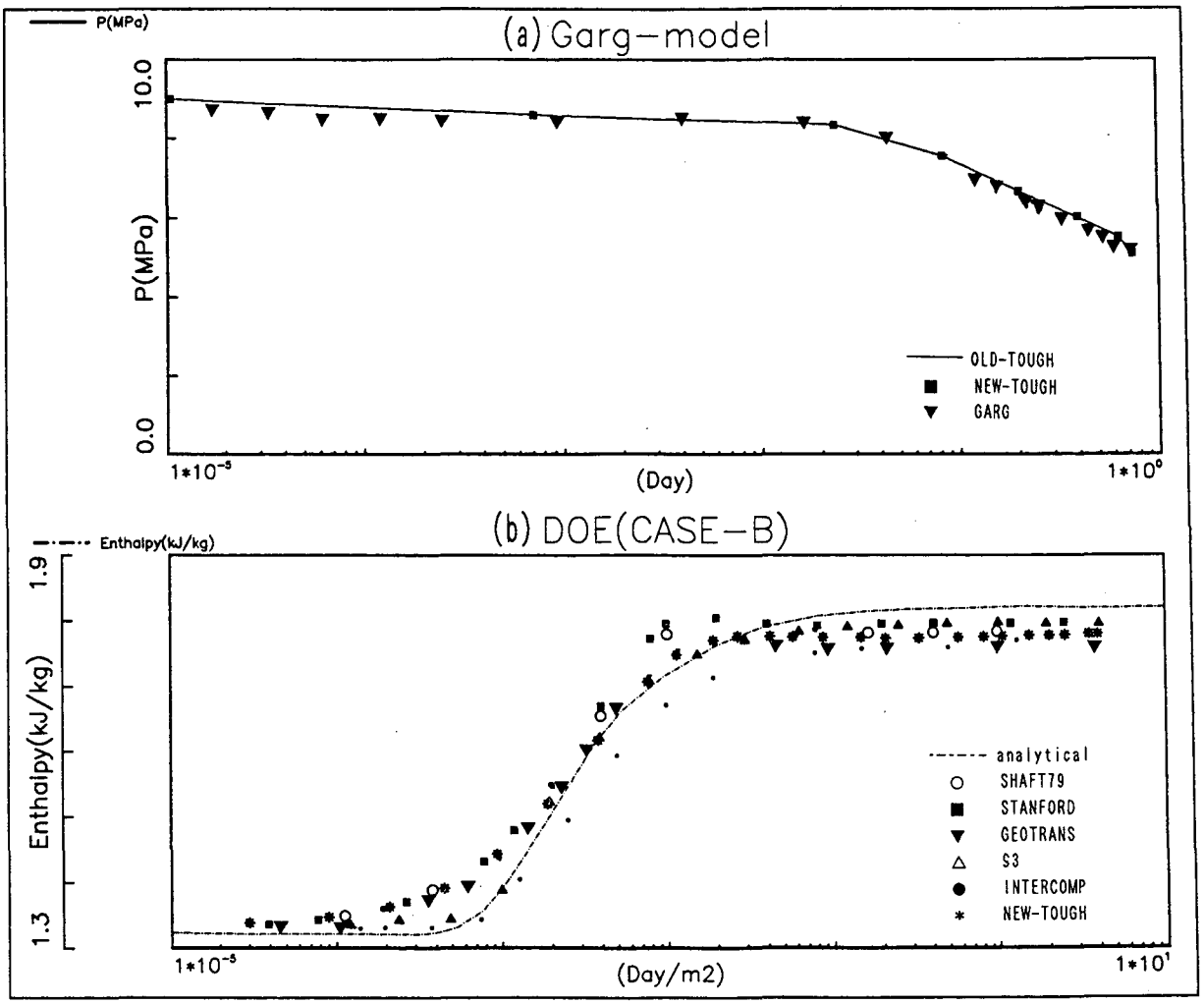

Figure-1 Comparison of NEW TOUGH with Garg's Model and DOE (Case-B)

Table-1 Comparison of CPU Time

Dimension	Elements	Connections	CPU Time (sec)		Remarks
			OLD	NEW	
1 D	50	49	215.9	114.4	Garg's model
2 D	164	289	348.4	224.3	2D Infiltration problem
3 D	196	459	2076.6	89.9	Cubic model

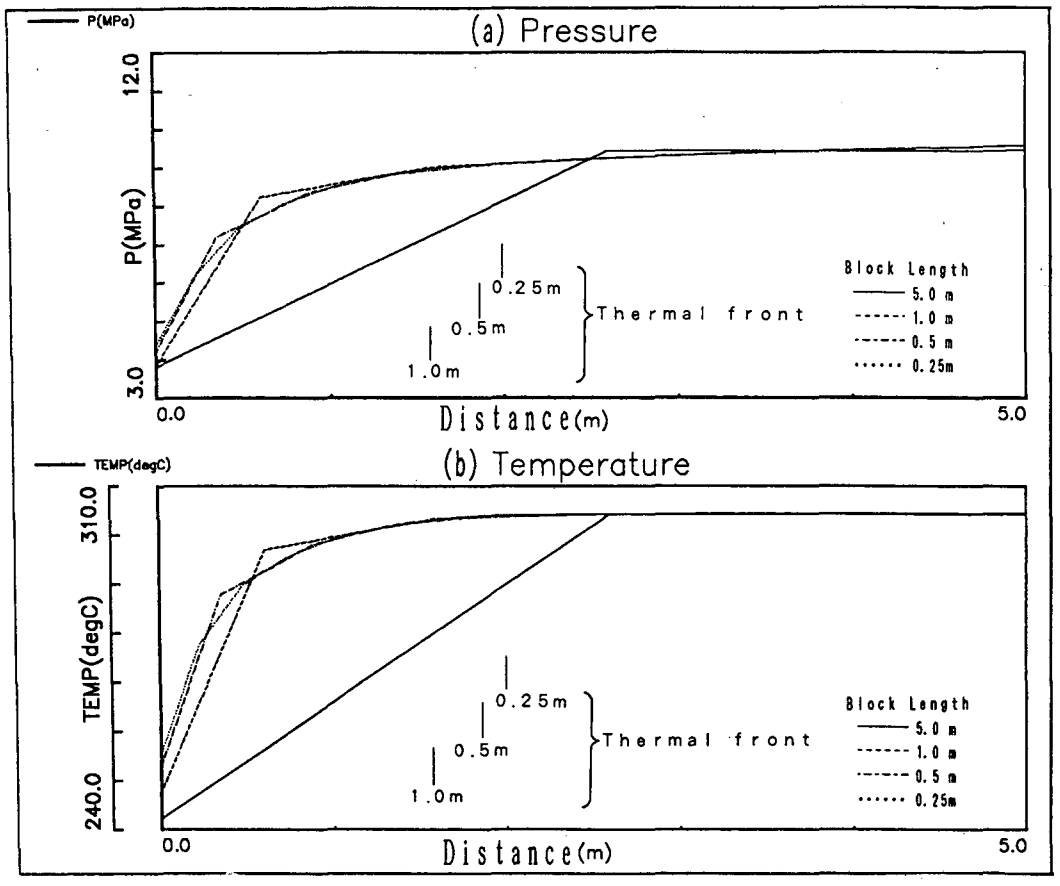

Figure-2 Draw-Down Curves for Various Block Length

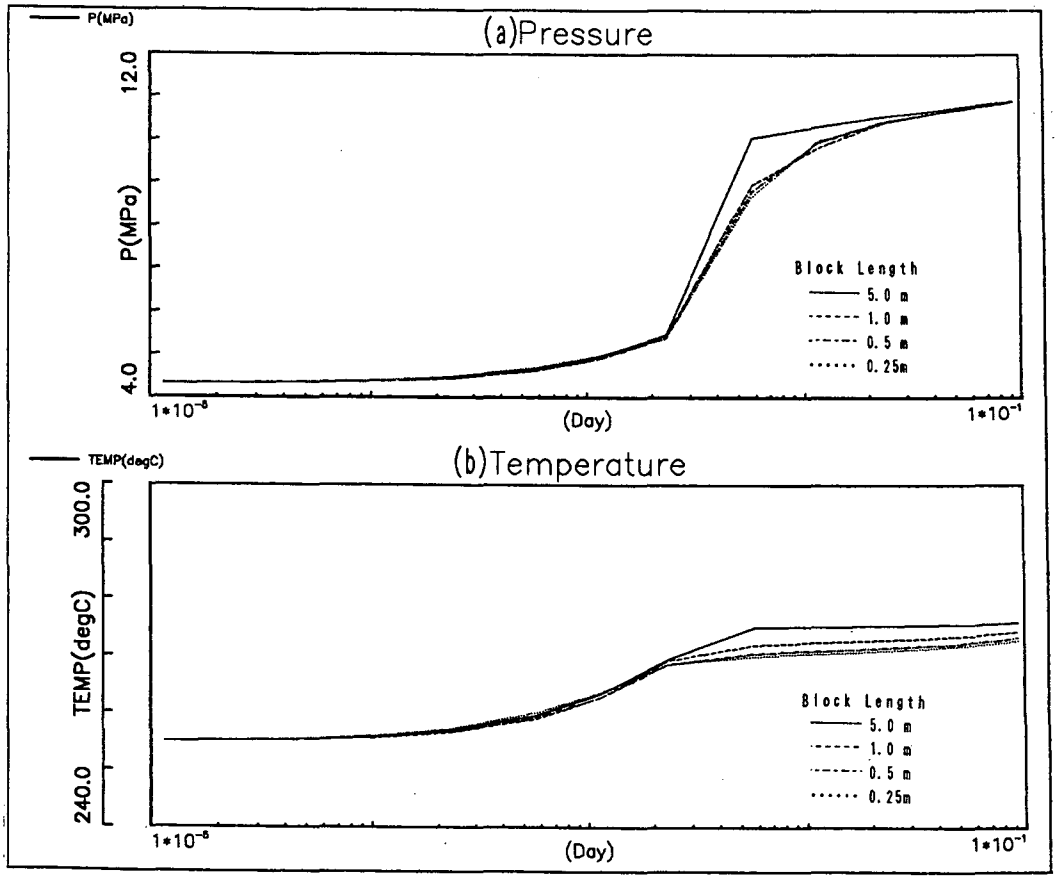

Figure-3 Build-Up Curves for Various Block Length

Incorporation into TOUGH of an Analytical Source/Sink Term for Fracture/Matrix Flow

Robert W. Zimmerman and Gudmundur S. Bodvarsson
Earth Sciences Division
Lawrence Berkeley Laboratory
University of California
Berkeley, CA 94720

Introduction

The proposed underground radioactive waste repository at Yucca Mountain would be located in the unsaturated zone above the water table, in a region consisting of highly fractured volcanic tuff. As part of the process of characterizing the site for the purposes of determining its suitability for the repository, it is necessary to develop models for studying the flow of water in an unsaturated fractured rock mass with low matrix permeability. For quasi-steady-state processes, the fractured/porous medium can be treated as an equivalent porous medium. For transient processes, such as the infiltration that would occur after a precipitation event, the "dual-porosity" nature of the medium must be accounted for. Large-scale simulations accomplished by explicit treatment of the fractures and matrix blocks in a numerical simulator such as TOUGH (Pruess, 1987) would require an impractical number of computational cells. Our approach is to treat flow between the fractures and matrix via an analytical source/sink expression, in which case we need to explicitly discretize only the fracture system. Absorption into the matrix is described by a single analytical expression that relates the cumulative influx into a matrix block to the elapsed time of absorption, the hydraulic properties of the matrix block, the initial saturation of the matrix block, and the surface/volume ratio of the matrix block. This method has been used on the problem of water infiltrating into a planar fracture, with transverse leakage into the formation. The computational mesh consists only of "fracture elements", with leakage treated as a source/sink term for each element. The agreement between the results calculated using both a fully-discretized fractured/porous medium and the source/sink approach is excellent, with a savings in CPU time on the order of a factor of ten.

Absorption into a Matrix Block: Formulation of Problem

The basic analytical ingredient needed for the dual-porosity model is a closed-form expression for the rate of imbibition of water into a matrix block that is surrounded by saturated fractures. Absorption of water into a matrix block is governed by the highly nonlinear Richards' equation (Hillel, 1980):

$$\mathrm{div}\left[\frac{kk_r(\psi)}{\mu\phi}\,\mathrm{grad}\,\psi\right] = \frac{\partial S(\psi)}{\partial t}\,, \tag{1}$$

in which ψ represents the pressure potential of the water in the block, S represents the liquid saturation, k is the absolute permeability of the block, μ is the viscosity of the water, ϕ is the porosity of the block, and k_r is the "relative permeability" function. Equation (1) embodies the principle of conservation of mass for the water, with the left hand side representing the local net influx of water (through a modified form of Darcy's law), and the right hand side representing the change in the volumetric water content. Each porous medium has its own set of characteristic curves that describe the relationships between S, ψ and k_r. The functional forms of the characteristic functions that we have used to represent the hydraulic properties of the volcanic tuffs at Yucca Mountain are those proposed by van Genuchten (1980):

$$S = S_r + (S_s - S_r)[1 + (\alpha|\psi|)^n]^{-m} , \tag{2}$$

$$k_r = \frac{\{1 - (\alpha|\psi|)^{n-1}[1 + (\alpha|\psi|)^n]^{-m}\}^2}{[1 + (\alpha|\psi|)^n]^{m/2}} , \tag{3}$$

where α is a scaling parameter that has dimensions of 1/pressure, and m and n are dimensionless parameters that are related by $m = 1 - 1/n$, $n > 1$.

The basic problem to be solved is that of a block of porous material which is initially at some uniform saturation, S_i. Through (2), this corresponds to some initial potential ψ_i. In the field, the initial saturation (under equilibrium conditions) will generally vary with depth. At Yucca Mountain, however, the fracture spacing is small enough (less than 1 m) that any individual matrix block can be considered to be initially at a uniform saturation (Rulon et al., 1986). At some time $t = 0$, the fractures that form the boundary of the block become saturated at zero potential. Since the permeability of the fractures greatly exceeds that of the matrix blocks, we assume that this boundary condition is established instantaneously. If the block occupies a region of space denoted by Ω, with boundary $\partial\Omega$ (Fig. 1), the boundary and initial conditions are

$$\psi(\vec{x}, t = 0) = \psi_i \quad \text{for all } \vec{x} \in \Omega , \tag{4}$$

$$\psi(\vec{x}, t > 0) = 0 \quad \text{for all } \vec{x} \in \partial\Omega . \tag{5}$$

For a given block geometry Ω, the imbibition process is defined by equations (1-5).

Development of Source/Sink Expression

There are two difficulties with developing a general expression to represent imbibition into a block of arbitrary shape. One is that of accounting for irregular block geometries, and the other is that of treating the inherent nonlinearity of the imbibition process. We can conceptually break up this problem into a few different steps, however, in order to arrive at a general method of representing imbibition into porous matrix blocks. First, dimensional considerations (and analogy with saturated flow

problems) show that the process is governed by a dimensionless time proportional to $kt/\alpha\mu\phi L^2$, where L is some characteristic length of the block. An obvious choice for L is V/A, where V is the volume of the block, and A is the outer surface area of the block.

Next we consider imbibition into a block of simple geometry, namely a thin slab, which can be treated by the integral method (Zimmerman et al., 1989). Although this method leads only to approximate results, it does reveal the manner in which the imbibition rate depends on parameters such as the initial saturation, S_i, and the hydraulic parameters S_s, S_r, α, m, and n. This solution shows that, at least until the wetting front reaches the midplane of the slab, the fractional uptake of water is given by

$$\frac{Q}{Q_\infty} = \left[\frac{2nk(S_s-S_i)^{-m}t}{\alpha\mu(n+1)\phi[m(S_s-S_r)]^{1/n}(V/A)^2}\right]^{1/2}, \tag{6}$$

where Q_∞ is the amount of water absorbed when imbibition is complete. Numerical simulations using TOUGH (Zimmerman and Bodvarsson, 1989) show that (6) overestimates the flux by a few percent. We assume, however, that this approximate expression correctly accounts for the effects of the hydraulic parameters, as well as the initial saturation, and that the error is only in the numerical coefficient 2 that appears in the numerator.

We now note that, regardless of the shape of the block, the penetration depth of the wetting front will initially grow as $\sqrt{t}$ (Philip, 1969). Since this occurs over an area A, the total liquid uptake will be proportional to $A\sqrt{t}$. When the imbibition process is complete, the total liquid uptake will equal $\phi V(S_s-S_i)$. Hence for small times, the fractional uptake Q/Q_∞ will be proportional to $\sqrt{t}/(V/A)$, regardless of the shape of the block. The next assumption is to assume that the dependence follows that given by (6), with a different numerical factor in place of the 2. Hence we are led to define a dimensionless time τ as

$$\tau = \frac{nk(S_s-S_i)^{-m}t}{\alpha\mu\phi(n+1)[m(S_s-S_r)]^{1/n}(V/A)^2}, \tag{7}$$

and postulate that, for small times, $Q/Q_\infty = \text{constant}\times\sqrt{\tau}$, where the constant is independent of the block geometry. By plotting the results of numerical simulations for imbibition into spherical and cylindrical blocks in log-log form, we see that the cumulative uptake eventually increases at a slower rate than $\tau^{1/2}$. Since we know that the next term in an exact series solution would be proportional to t^1, the simplest functional form to use to fit the results over the entire range of τ is

$$\frac{Q}{Q_\infty} = C_1\sqrt{\tau} - C_2\tau\,. \tag{8}$$

The numerical value of the coefficients C_1 and C_2 can be found by fitting (8) to the results of a numerical simulation for, say, a spherical block. If this is done, we find that $C_1 = 1.25$ and $C_2 = 0.39$. Sensitivity studies performed with TOUGH by varying the initial saturation, the n parameter, and the block shape show that with these values for C_1 and C_2, equation (8) fits the imbibition data very well (Fig. 2). Equation (8) is of course used only until $Q/Q_\infty = 1$, which occurs at $\tau = 2.55$; at times greater than this, the instantaneous flux is zero.

All computational blocks used during a "dual-porosity" simulation are assumed to represent fracture elements. Flow into adjacent matrix blocks is calculated as a source/sink term. The GENER block is modified to accept a new "type" of source/sink, called "MTRX". The surface area of the interface between the fracture element and the matrix block, as well as the volume of the matrix block, is also an input in the GENER block. Another of the input variables in GENER is used to specify a minimum saturation in the fracture at which absorption into the matrix is assumed to commence. Calculation of the magnitude of the influx term takes place in the subroutine QU. The total influx between time steps t_1 and t_2, for example, is found by first calculating τ_1 and τ_2 from equation (7), and then calculating $Q(\tau_2) - Q(\tau_1)$ from equation (8).

Flow Along a Single Fracture with Leakage to the Matrix

One basic problem which has much relevance to understanding the hydrological behavior of the Yucca Mountain site is that of water flowing down a fracture with leakage into the adjacent matrix. This problem has been studied by Martinez (1988) and Nitao and Buscheck (1989), using ad hoc numerical/analytical approaches. These methods are somewhat "inverse" to our method, in that the leakage was treated numerically, while the flow along the fracture was treated analytically. A schematic drawing of this problem is shown in Fig. 3. Flow into the fracture is driven by an imposed potential at the $y = 0$ boundary, which could represent ponded water under a very small hydraulic head. This problem represents a simple case of the type of problem to which a dual-porosity code should be well-suited.

For simplicity in our sample problem, we use the same characteristic curves for both the fracture and the matrix, but take their absolute permeabilities to be 3.9×10^{-10} and 3.9×10^{-20}, respectively. The van Genuchten parameters are taken to be $S_s = 0.984$, $S_r = 0.318$, $\alpha = 1.147 \times 10^{-5}$/Pa, $n = 3.04$, and $m = 0.671$ (for Topopah Spring unit; see Rulon et al., 1986). The initial saturation is taken to be 0.676. The fracture is discretized into 10 elements, each 1 m long and 100 μm thick. Each of these elements has a "sink" term represented by (8). The matrix block that is adjacent to each fracture element is taken to have infinite volume; note that if we multiply (8) through by Q_∞ to solve for Q, we see that it does not break down if $(V/A) \rightarrow \infty$, but merely that the C_2 term drops out. As a comparison, the problem has also been solved without the source/sink expressions, but with five computational blocks extending into the matrix adjacent to each fracture element. The matrix elements extend 100 μm into the formation, which, for the time scale of the problem, is sufficient to simulate a semi-infinite region, since the wetting front does not reach the outermost matrix element. The saturation profile in the fracture after an elapsed time of 4×10^3 s is shown in Fig. 4, according to both methods of calculation. The agreement is excellent, and

the savings in CPU time (on a CRAY-XMP) obtained using the source/sink approach was roughly a factor of ten. Note that after 4×10^3 s, about 30% of the fluid that entered the fracture at the inlet $y=0$ has leaked off into the formation, so the effect that is being modeled is not insignificant.

Conclusions

We have developed an approximate expression to predict the rate of imbibition into a matrix block that is surrounded by saturated fractures. The imbibition rate is expressed as a function of a dimensionless time that depends on the hydraulic parameters of the medium, the initial saturation of the block, and the surface/volume ratio of the block. This expression has been incorporated onto TOUGH as a source/sink term for discrete ''fracture elements'', and has been tested for the problem of flow along a single fracture with transverse leakage into the matrix. Our next step is to extend the use of this method to computational blocks that represent a ''fracture continuum'', as opposed to a single fracture, and which have a distribution of block sizes and shapes in each individual block.

Acknowledgments

This work was done under U.S. Department of Energy Contract DE-AC03-76SF00098, administered by the Nevada Operations Office, in cooperation with the U.S. Geological Survey, Denver.

References

Hillel, D., *Fundamentals of Soil Physics*, Academic Press, New York, 1980.

Martinez, M. J., Capillary-driven flow in a fracture located in a porous medium, *Report SAND84-1697,* Sandia National Laboratories, Albuquerque, N.M., 1987.

Nitao, J. J., and Buscheck, T. A., Movement of a liquid front in an unsaturated, fractured porous medium, Part 1 (Physical theory) and Part 2 (Mathematical analysis), *Reports UCRL-101005 and 101006,* Lawrence Livermore National Laboratory, Livermore, Calif., 1989.

Philip, J. R., Theory of infiltration, *Adv. Hydrosci.*, Vol. 5, pp. 215-296, 1969.

Pruess, K., TOUGH User's Guide, *Report LBL-20700,* Lawrence Berkeley Laboratory, Berkeley, Calif., 1987.

Rulon, J., Bodvarsson, G. S., and Montazer, P., Preliminary numerical simulations of groundwater flow in the unsaturated zone, Yucca Mountain, Nevada, *Report LBL-20553,* Lawrence Berkeley Laboratory, Berkeley, Calif., 1986.

van Genuchten, R., A closed-form equation for predicting the hydraulic conductivity of unsaturated soils, *Soil Sci. Soc. Amer. J.*, Vol. 44, pp. 892-898, 1980.

Zimmerman, R. W., and Bodvarsson, G. S., An approximate solution for one-dimensional absorption in unsaturated porous media, *Water Resour. Res.*, Vol. 25, pp. 1422-1428, 1989.

Zimmerman, R. W., Bodvarsson, G. S., and Kwicklis, E. M., Absorption of water into porous blocks of various shapes and sizes, *Water Resour. Res.*, in press.

Fig. 1. Schematic diagram of the basic boundary-value problem for absorption into a porous matrix block.

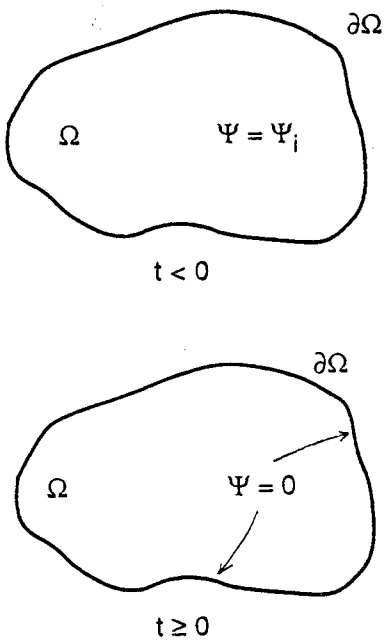

Fig. 2. Cumulative liquid flux into three differently-shaped blocks (from TOUGH simulations), compared with eqn. (8).

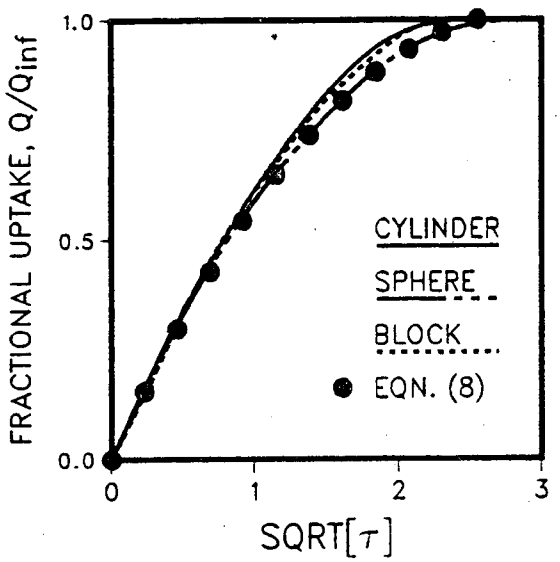

Fig. 3. Schematic diagram of flow along a fracture with transverse leakage into the adjacent formation.

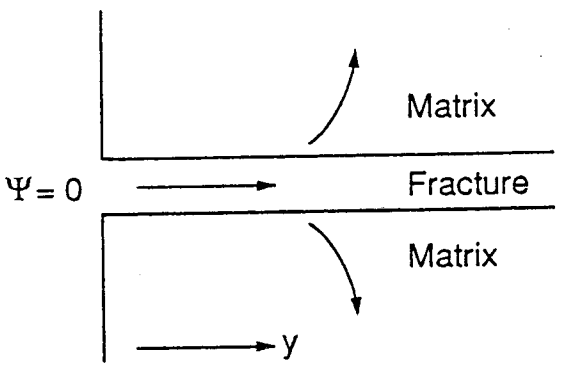

Fig. 4. Saturation profile in fracture, for problem illustrated in Fig. 2.

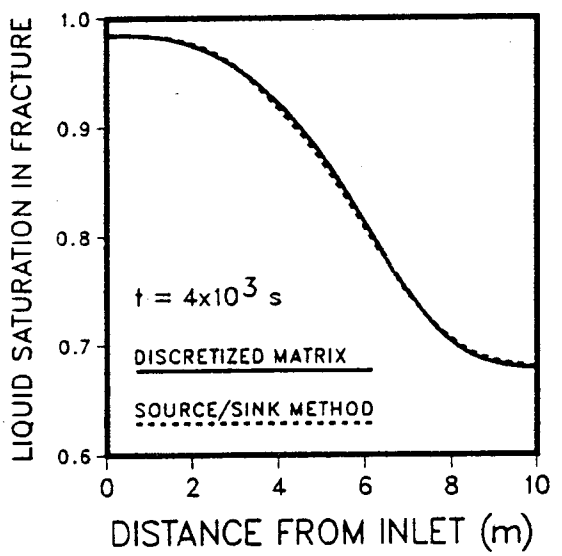

ON VERIFICATION, USE AND TREATMENT ON NON-NEWTONIAN BEHAVIOR OF THE NUMERICAL SIMULATOR MULKOM-GWF

Yu-Shu Wu
HydroGeoLogic, Inc.
503 Carlisle Drive
Herndon, VA 22070

Karsten Pruess
Lawrence Berkeley Laboratory
University of California
Berkeley, CA 94720

INTRODUCTION

The numerical simulator - MULKOM-GWF for isothermal gas-water-foam flow in porous media is a modified version of MULKOM (Pruess, 1983). It has the capability of modeling multiple-phase flow of gas, water and foam in porous media and includes a treatment of non-Newtonian behavior of the foam solution under a wide range of operation conditions (Pruess and Wu, 1988). The validity of the numerical results from this code has been tested here by comparison of the numerical calculations with analytical solutions.

The sample problems reported for code verification and applications are:

i) immiscible displacement of a Newtonian fluid by a power-law non-Newtonian fluid;

ii) transient flow of single-phase Bingham fluids; and

iii) three-phase immiscible flow.

TREATMENT OF NON-NEWTONIAN BEHAVIOR

The flow of foam in porous media is a focus of current research in many fields. Foam has been shown to be one of the most promising fluids for mobility control in underground natural resource recovery or in storage projects. On a macroscopic scale, flow behavior of foam in porous media is non-Newtonian. The "power law" is generally used to correlate the apparent viscosities of foam with other flow properties for a given porous medium and a given surfactant (Patton et al., 1983; Hirasaki and Lawson, 1970). The Bingham flow behavior for foam to flow in porous media has also been observed experimentally, i.e, foam will start to flow in a porous medium only after the applied pressure gradient exceeds a certain threshold value (Albrecht and Marsden, 1970; Witherspoon et al., 1989).

The special numerical treatment on power-law and Bingham non-Newtonian fluids will be discussed as follows.

a. Power-law Fluid

To date the power-law, or the Ostwald-de Waele model (Bird et al., 1960), is the most widely used rheological model for non-Newtonian flow problems in porous media.

Originally formulated from an empirical curve-fitting function, the power law is represented in fluid mechanics as,

$$\tau = -H\dot{\gamma}^n \tag{1}$$

where τ is the shear stress; $\dot{\gamma}$ is the shear rate; n is the power-law index; and H is called the consistence coefficient. For n = 1, the fluid becomes Newtonian. Because of its inherent simplicity, the power-law is of considerable interest in applications and is used to approximate the rheological behavior of both shear-thinning or pseudoplastic (n < 1) and shear-thickening or dilatant (n > 1) fluids over a large range of flow conditions.

The modified Darcy's equation for flow of single-phase power-law fluids in porous media was derived by Christopher and Middleman (1965) and generalized by Wu (1990) as

$$\vec{u} = -\frac{K}{\mu_{nn}} \nabla\Phi \tag{2}$$

where **u** is the Darcy's velocity; K is permeability; Φ is the flow potential, and the apparent viscosity for power-law fluids μ_{nn} is defined by

$$\mu_{nn} = \mu_{eff} \left[\frac{K}{\mu_{eff}} |\nabla\Phi| \right]^{\frac{n-1}{n}} \tag{3}$$

and μ_{eff} is given by

$$\mu_{eff} = \frac{H}{12} \left[9 + \frac{3}{n} \right]^n (150K\phi)^{\frac{(1-n)}{2}} \tag{4}$$

Note that μ_{eff} does not have the units of viscosity.

The power-law model, Equation (2), is the most widely used theological model to describe the non-Newtonian property of shear-thinning fluids in porous media, such as polymer

and foam solutions. The power-law index n ranges between 0 and 1 for a shear thinning fluid, and the viscosity becomes infinite as the flow potential gradient tends to zero for $n < 1$. Therefore, direct use of Equation (3) in the calculation will cause numerical difficulties. A formulation incorporated in the code for a power-law fluid is to use a linear interpolation when the potential gradient is very small. As shown in Figure 1, the viscosity for a small value of potential gradient is calculated by

$$\mu_{nn} = \mu_1 + \frac{\mu_1 - \mu_2}{\delta_1 - \delta_2} (|\nabla\Phi| - \delta_1) \tag{5}$$

for $|\nabla\Phi| \leq \delta_1$. Where the interpolation parameters δ_1 and δ_2 are defined in Figure 1. If the potential gradient is larger than δ_1 Equation (3) is used in the code. In order to maintain the continuities in the viscosity and its derivative at (δ_1, μ_1), the difference in values of δ_1 and δ_2 should be chosen sufficiently small. Then, the values for μ_1, and μ_2 may be taken as

$$\mu_j = \mu_{eff} \left[\frac{K}{\mu_{eff}} \delta_j \right]^{\frac{n-1}{n}} \quad (j = 1, 2) \tag{6}$$

The numerical tests show that the treatment of power-law fluids by Equation (5) works very well for a power-law fluid flow problem with various potential gradients. The accuracy of this scheme has been confirmed by a number of runs. In the numerical studies of transient flow problems of power-law fluids, the values of the interpolation parameters are taken as $\delta_1 = 10$(Pa/m), and δ_1-$\delta_2 = 10^{-7}$ (Pa/m).

b. Bingham Fluid

The rheological equation for a Bingham plastic fluid is (Bird et al., 1960)

$$\tau = \tau_y - \mu_b \dot{\gamma} \tag{7}$$

where τ_y is the yield stress; μ_b is the Bingham plastic coefficient.

For flow problems in porous media involving non-Newtonian Bingham fluids, the formulation of Darcy's law has been modified (Bear, 1972; Scheidegger, 1974) to,

$$\vec{\mu} = -\frac{K}{\mu_b} \left[1 - \frac{G}{|\nabla\Phi|} \right] \nabla\Phi \quad \text{for } |\nabla\Phi| > G \tag{8a}$$

$$\vec{\mu} = 0 \qquad \text{for } |\nabla\Phi| \leq G \tag{8b}$$

where G is the minimum pressure gradient. The two Bingham fluid parameters G and μ_b in Equation (8a) are determined by laboratory experiments or well tests for a porous media flow problem.

The flow of Bingham fluids is treated in the code by introducing an effective potential gradient $\nabla\Phi_e$, whose scalar component in the flow direction, assumed to be the x direction, is defined as

$$\left(\nabla\Phi_e\right)_x = \begin{cases} (\nabla\Phi)_x - G & (\nabla\Phi)_x > G \\ (\nabla\Phi)_x + G & (\nabla\Phi)_x < -G \\ 0 & -G \leq (\nabla\Phi)_x \leq G \end{cases} \tag{9}$$

as shown in Figure 2. Darcy's law for a Bingham fluid is used in the code in the form

$$\vec{\mu} = \frac{K}{\mu_b} \nabla\Phi_e \tag{10}$$

This treatment is much more efficient for simulation of Bingham fluid flow in porous media than the direct use of a highly nonlinear apparent viscosity as in Equation (8a).

COMPARISON WITH THE ANALYTICAL SOLUTION FOR POWER-LAW FLUID DISPLACEMENT

The power-law non-Newtonian fluid has been used extensively in study of non-Newtonian fluid flow through porous media theoretically and experimentally (Savins, 1969), so we take a power-law liquid as a displacing agent to drive the initially saturated Newtonian liquid in the porous medium. A Buckley-Leverett type analytical solution developed for immiscible displacement with non-Newtonian fluids in porous media (Wu, 1990) is used to check the numerical code for simulation of power-law non-Newtonian displacement.

The physical flow problem is a one-dimensional linear flow case of two incompressible fluids in a semi-infinite, horizontal, homogeneous and isotropic porous medium. A constant injection rate of a power-law liquid is maintained at the inlet (x=0) from time t=0. Initially, the reservoir is fully saturated with only the displaced Newtonian liquid. The relative permeability curve used for both the analytical and numerical calculations is shown in Figure 3. The capillary effects are assumed to be negligible, and the reservoir and fluid properties are summarized in Table 1.

In order to reduce the effects of space discretization and ends of a finite system on the accuracy of numerical results, a long and constant cross-sectional physical flow model is used. Very fine spacing meshes ($\Delta x=0.01m$) are chosen for the first 300 grids, then the mesh spacings increase by a factor of 1.5 to the 350th one. A comparison of the saturation profiles from the numerical and the analytical calculations is given by Figure 4 using the input data of Table 1. Figure 4 shows that the numerical results are in good agreement with the Buckley-Leverett type solution. Therefore, the numerical results for the Buckley-Leverett-type problem converge to a correct answer.

COMPARISON WITH INTEGRAL SOLUTION FOR TRANSIENT FLOW OF SINGLE-PHASE BINGHAM FLUIDS

The Bingham non-Newtonian flow behavior of foam, heavy oil and other fluids in porous media have been reported in the literature. The capability of MULKOM-GWF to model the flow of Bingham fluids is checked by comparison with the integral analytical solution (Wu et al., 1990) for transient single-phase flow. An example of the application is to analyze well testing data from a Bingham-type heavy oil reservoir.

The input data are given in Table 2 and it is a single-well radial flow problem with production of a Bingham fluid. The wellbore flowing pressures calculated from the numerical and integral solutions are shown in Figure 5, and the agreement of the numerical and integral analytical solutions is excellent.

THREE-PHASE IMMISCIBLE FLOW

This example is to demonstrate the application of the simulator to three-phase immiscible flow problems, since the simulator has the capability of modeling three-phase flow of gas, water and foam in porous media. The problem is foam injection into a one-dimensional linear horizontal system, which is initially saturated with uniform three mobile phases of gas, water and foam. The meshes used for the reservoir are the same as for the Buckley-Leverett case, and the parameters are given in table 3. The foam relative permeability is calculated by Stone function (Pruess and Wu, 1988) for this three-phase flow problem.

In this problem, the foam phase has been treated as a Newtonian fluid with constant viscosity $\mu=5cp$. After one hour of injection of foam, the saturation profiles in the system are shown in Figure 6.

SUMMARY

In conclusion, the simulator MULKOM-GWF has been checked by comparison of the simulation results with the analytical solutions for power-law fluid displacement and single-phase Bingham fluid flow problems. In both cases, the excellent agreement has been obtained between the numerical and analytical solutions. Also, a test run on three-phase flow has been performed.

REFERENCES

Albrecht, R. A. and Marsden, S. S. (1970): "Foams as Blocking Agents in Porous Media," Soc. Pet. Eng. J., 51.

Bear, J.: Dynamics of Fluids in Porous Media, American Elsevier, New York (1972).

Bird, R. B., Steward, W. E. and Lightfoot, E. N. (1960): Transport Phenomena, Wiley, New York.

Buckley, S. E. and Leverett, M. C. (1942): " Mechanism of Fluid Displacement in Sands, " Trans., AIME Vol.146, 107-116.

Christopher, R. H. and Middleman, S. (1965): "Power-Law Flow through a Packed Tube," I & EC Fundamentals, Vol. 14, No. 4, 422-426.

Hirasaki, G. J. and Lawson, J. B. (1985): "Mechanisms of Foam Flow in Porous Media: Apparent Viscosity in Smooth Capillaries," Soc. Pet. Eng. J., 176-190.

Patton, J. T., Holbrook, S. T. and Hsu, W. (1983): "Rheology of Mobility-Control Foams," Soc. Pet. Eng. J., 456-460.

Pruess, K. (1983): " Development of the General Purpose Simulator MULKOM, " Annual report, Earth Sciences Division, report LBL-15500, Lawrence Berkeley Laboratory.

Pruess, K. and Wu. Y. S. (1988): " On PVT-Data, Well treatment, and Preparation of Input Data for an Isothermal Gas-Water-Foam Version of MULKOM," report LBL-25783, UC-403, Earth Sciences Division, Lawrence Berkeley Laboratory. Savins, J. G. (1969): " Non-Newtonian Flow through Porous Media," Ind. Eng. Chem., 61, 18-47.

Scheidegger, A. E. (1974): The Physics of Flow through Porous Media, University of Toronto Press.

Witherspoon, P. A., Benson, S., Persoff, P., Pruess, K., Radke, C. J. and Wu, Y. S. (1990): "Feasibility Analysis and Development of Foam Protected Underground Natural Gas Storage Facilities," Final Report, LBL-28594, GRI-90/0211, Earth Sciences Division,

Lawrence Berkeley Laboratory, University of Californian, Berkeley, CA.

Wu, Y. S. (1990): " Theoretical Studies of Non-Newtonian and Newtonian Fluid Flow through Porous Media, " Ph. D. Thesis, LBL-28642, Earth Sciences Division, Lawrence Berkeley Laboratory, University of California.

Wu, Y. S., Pruess, K. and Witherspoon, P. A. (April, 1990): "Flow and Displacement of Bingham Non-Newtonian Fluids in Porous Media," Paper SPE 20051, Presented at the 60th California Regional Meeting of AIME-SPE, Ventura, CA.

Table 1
Parameters for Linear Power-law Fluid Displacement

Porosity	ϕ=0.20
Permeability	K=100 md
Cross-Sectional Area	1 m^2
Injection Rate	q=5.0x$10^{-6}m^3/s$
Injection Time	T=20 hrs
Displaced Phase Viscosity	μ_{ne}=5.00 cp
Irreducible Saturation	S_{ir}=0.20
Power-Law Index	n=0.5
Consistence Coefficient	H=0.01 Pa· s^n

Table 2
Parameters for Single Phase Bingham Fluid Flow

Initial pressure	P_i=100.00 bars
Initial Porosity	ϕ_i=0.20
Initial Fluid Density	ρ_i=975.9 kg/m_3
Formation Thickness	h=1.00 m
Bingham Coefficient	μ_b=5.00 cp
Fluid Compressibility	C_f=4.557 x 10-$^{10}Pa^{-1}$
Rock Compressibility	C_r=2.5443 x $10^{-9}Pa^{-1}$
Mass Injection Rate	Q_m=0.1 kg/s
Permeability	K=9.869 x $10^{-13}m^2$
Wellbore Radius	r_w=0.1 m
Minimum Pressure Gradient	G=10^3Pa/m

Table 3
Parameters for Three-Phase Immiscible Flow

Porosity	ϕ=0.20
Permeability	K=1 darcy
Cross-Sectional Area	1 m^{-2}
Foam Mass Injection Rate	q=1.0x10^{-3}kg/s
Injection Time	T=1.0 hrs
Water Viscosity	μ_w=0.3513 cp
Gas Viscosity	μ_g=0.0187 cp
Foam Viscosity	μ_f=5.0000 cp
Initial Water Saturation	S_w=0.30
Initial Gas Saturation	S_g=0.40
Initial Foam Saturation	S_f=0.30
Initial Formation Pressure	P_i=100.00 bars
Formation Temperature	T=80.33 °C

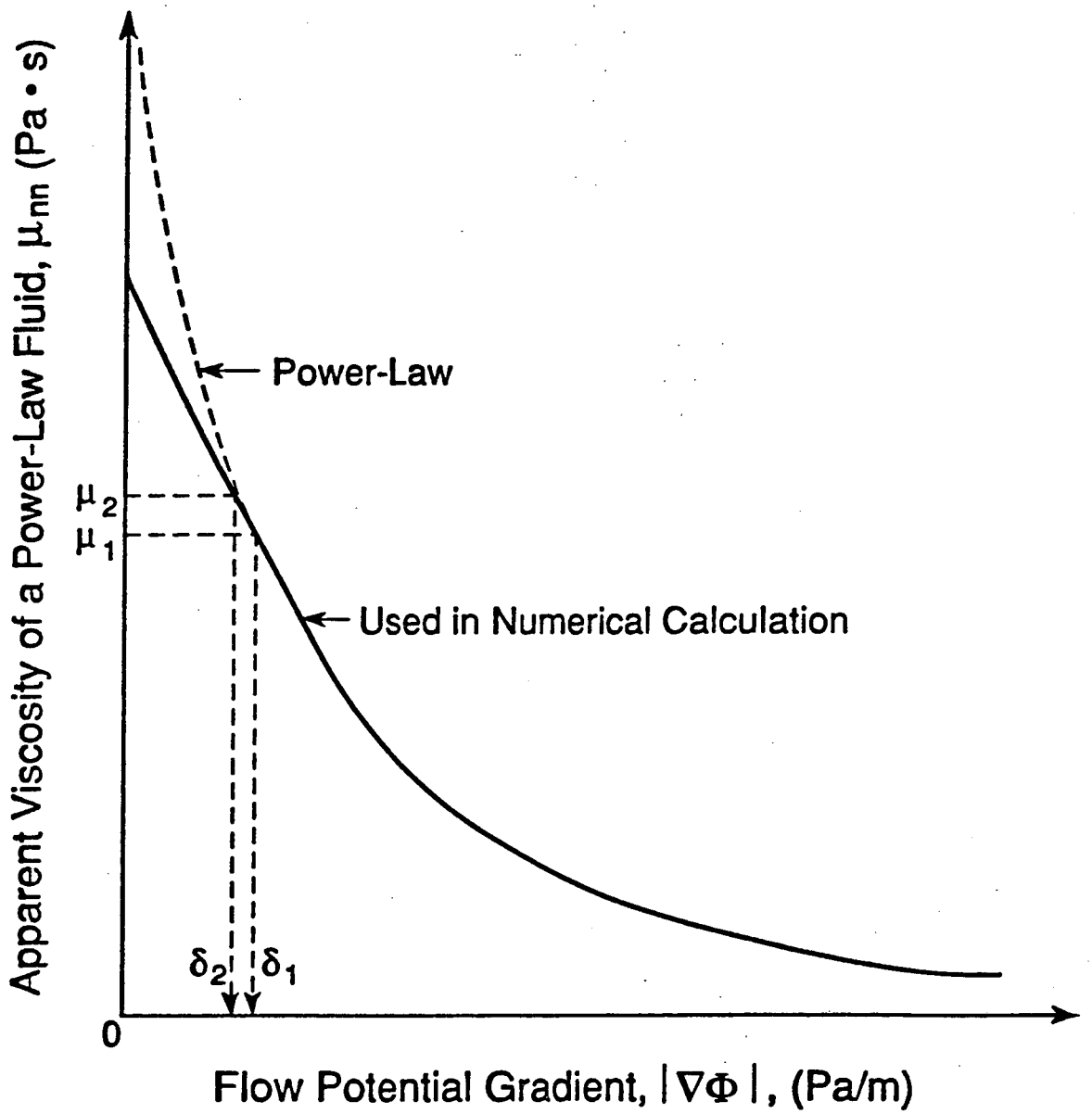

Figure 1. Schematic of Linear Interpolation of Viscosities of Power-Law Fluids with Small Flow Potential Gradient.

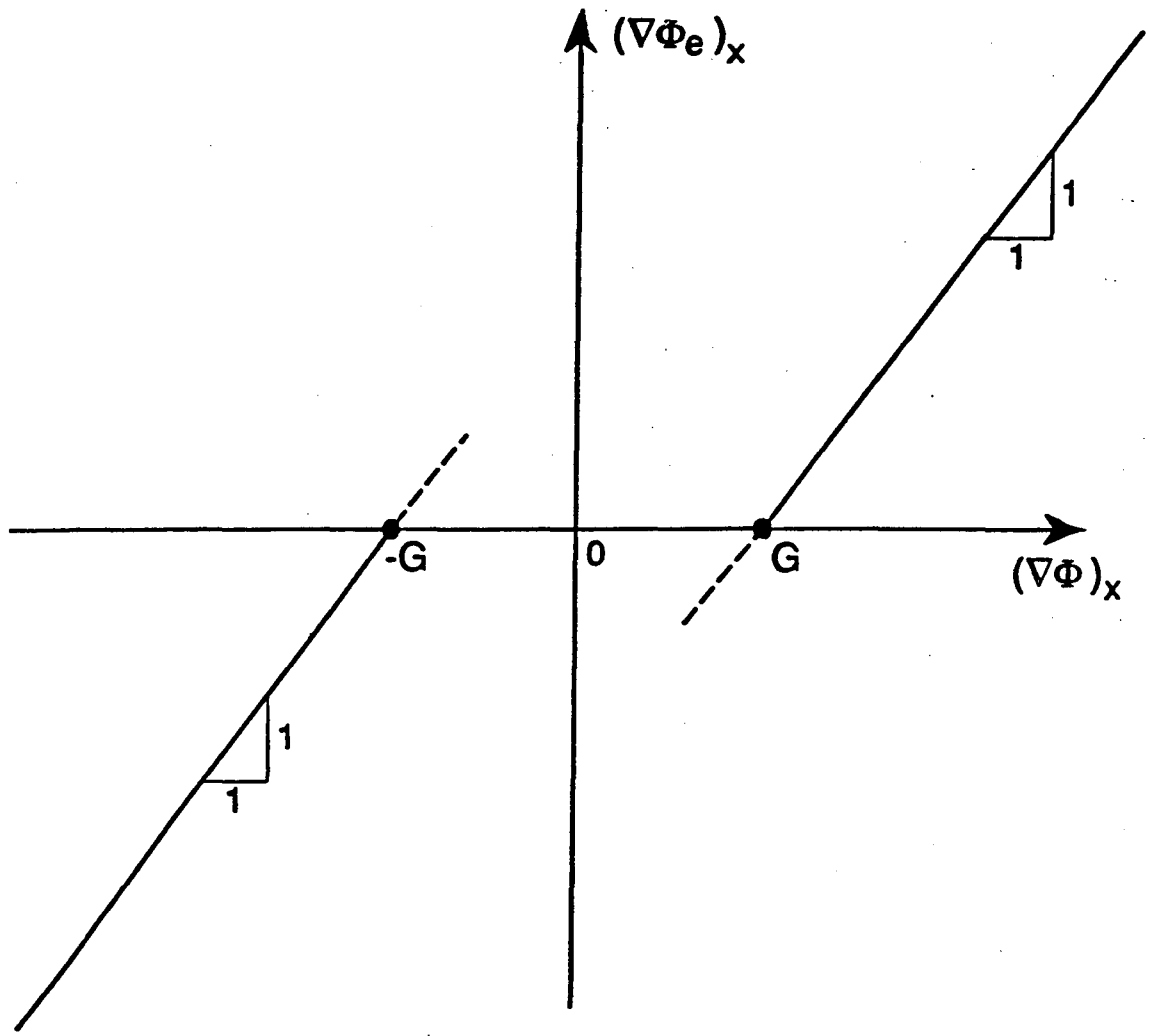

Figure 2. Effective Potential Gradient of Bingham Fluids, the Dashed Linear Extension for Numerical Calculation of Derivatives When $(\nabla\Phi)$ is near +G or -G.

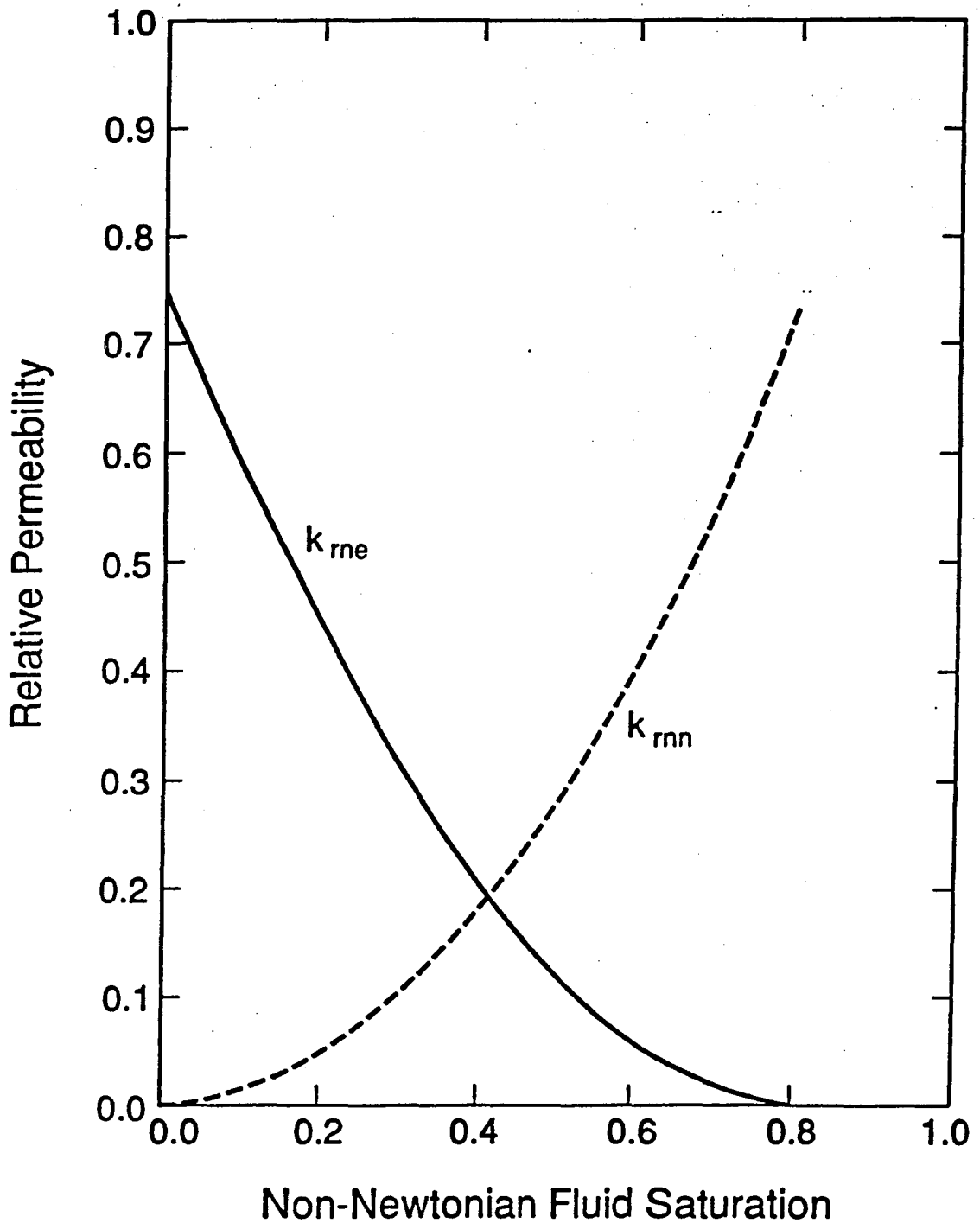

Figure 3. Relative Permeabilities for Power-Law Fluid Displacement.

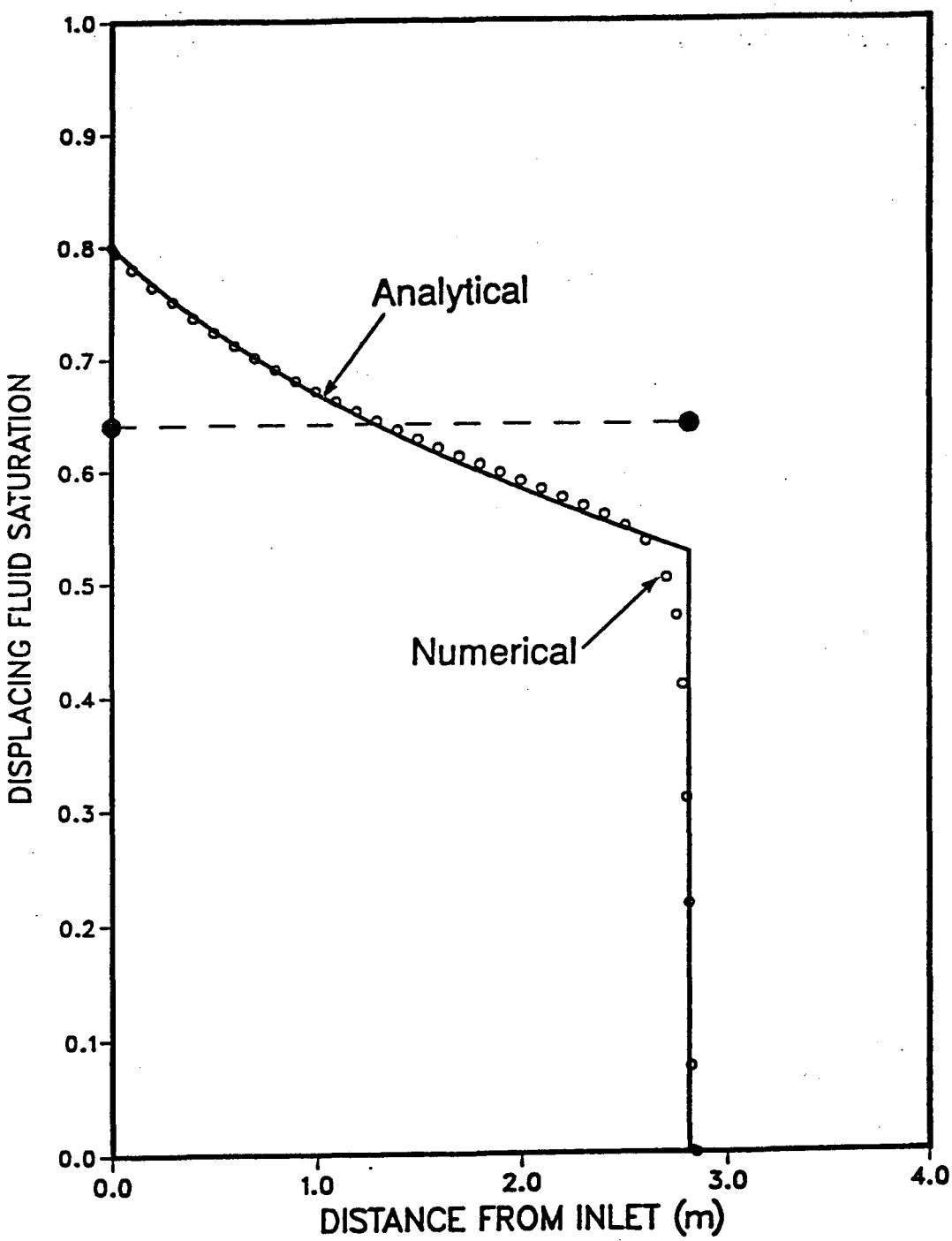

Figure 4. Comparison of Saturation Profiles calculated from Analytical and Numerical Solutions after 20 Hours of Injection of Power-Law Fluid.

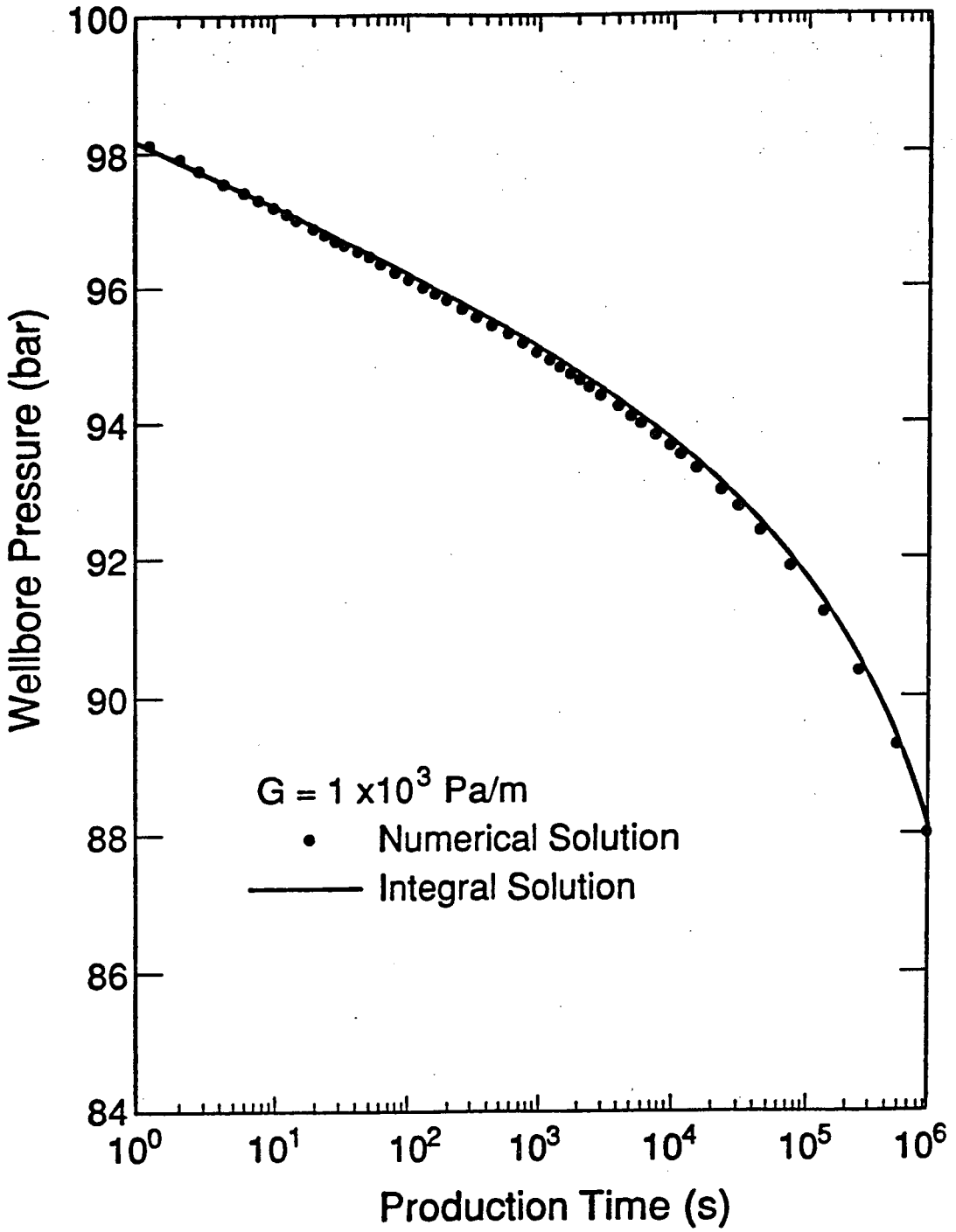

Figure 5. Comparison for Wellbore Pressures during Bingham Fluid Production, Calculated from the Numerical Solution and the Integral Solution (G=1000 Pa/m).

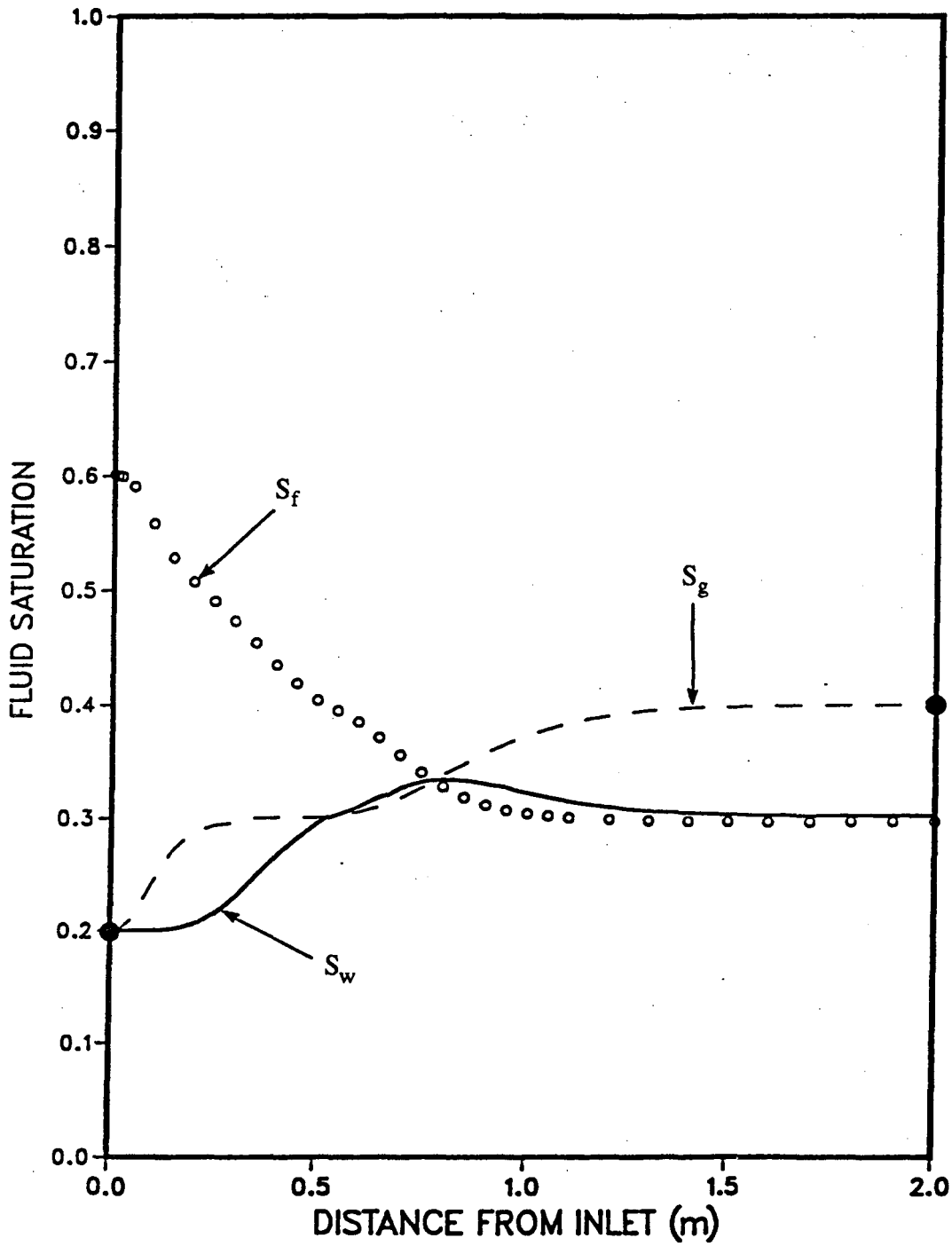

Figure 6. Saturation Profiles of Three-Phase Displacement After One Hour of Foam Injection (w = water, f = foam, g = gas).

Overview of TOUGH2, A General-Purpose Numerical Simulator for Multiphase Nonisothermal Flows†

Karsten Pruess

Earth Sciences Division, Lawrence Berkeley Laboratory
University of California, Berkeley, CA 94720

Introduction

Numerical simulators for multiphase fluid and heat flows in permeable media have been under development at Lawrence Berkeley Laboratory for more than ten years. The initial focus of this work was mostly on geothermal reservoir simulation, but efforts later broadened to include flow problems arising in the context of high-level nuclear waste isolation, oil and gas recovery and storage, and the management and protection of groundwater resources.

Several interrelated numerical codes have been developed. The first of these was SHAFT79 (Pruess and Schroeder, 1980), which was designed for simulating water/vapor flows in geothermal reservoirs, including heat flows and phase change effects. Real geofluids contain non-condensible gases and dissolved solids in addition to water, however, and the desire to model such "compositional" systems led to the development of a flexible multicomponent, multiphase simulation architecture known as "MULKOM" (Pruess, 1983b; see Fig. 1). The design of MULKOM was based on the recognition that the mass- and energy-balance equations for multiphase fluid and heat flows in multicomponent systems have the same mathematical form, regardless of the number and nature of fluid components and phases present. Hence, MULKOM can simulate flows in which an arbitrary number of components is distributed among several coexisting fluid phases. Application of MULKOM to different fluid mixtures, such as water and air, or water, oil, and gas, is possible by means of appropriate "equation-of-state" (EOS) modules, which provide all thermophysical and transport parameters of the fluid mixture and the permeable medium as a function of a suitable set of primary thermodynamic variables. Although the design of MULKOM is based on simple and straightforward concepts, the code has never been easy to use because various research applications have led to a proliferation of specialized program modules and options. Investigations of thermal and hydrologic effects from emplacement of heat-generating nuclear wastes into partially water saturated formations prompted the development and release of a specialized version of MULKOM for nonisothermal flow of water and air, named TOUGH (Pruess,

† Paper presented at TOUGH Workshop, Lawrence Berkeley Laboratory, September 1990.

1987). TOUGH[&] is an acronym for "transport of unsaturated groundwater and heat," and is also an allusion to the tuff formations at Yucca Mountain, Nevada, which are presently being evaluated by the U.S. Department of Energy for their suitability as a host medium for a high-level nuclear waste repository.

A more detailed discussion of the interrelation between LBL's multiphase flow codes can be found in (Pruess, 1988); a critical evaluation of simulation capabilities with special reference to geothermal applications is available in (Pruess, 1990).

The TOUGH2 code is intended to supersede TOUGH. It offers all the capabilities of TOUGH and it includes a considerably more general subset of MULKOM modules with added capabilities. TOUGH2 can interface with different EOS modules, and thereby model different fluid mixtures that consist of a variable number of components distributed among several phases. It also contains facilities for mesh generation and internal processing of geometric data, including multiple interacting continua discretization of fractured media (Pruess and Narasimhan, 1982, 1985; Pruess, 1983a), and it provides a tight and visible version control system for meeting stringent demands on reliability and referenceability of code applications. Except for the added flexibility and user features, TOUGH2 is subroutine-for-subroutine actually very similar to TOUGH. TOUGH2 input formats are similar to and upwardly compatible with TOUGH, facilitating the maintenance of existing TOUGH applications.

The development of TOUGH2 was carried out on CDC-7600 and Cray X-MP computers. The coding complies with the ANSI X3.9-1978 (FORTRAN77) standard. 64-bit word length is required for successful execution. The TOUGH2 source code and documentation is presently undergoing internal review and testing. After this is completed the code will be released to the public through the National Energy Software Center. It is expected that in the future additional MULKOM modules will be documented and included into the TOUGH2 package.

Simulation Methodology

For a multiphase flow system with NK mass components and one heat "pseudo-component," the (NK + 1) coupled mass- and energy-balance equations can all be written in the following general form.

$$\frac{d}{dt}\int_{V_n} M^{(\kappa)}\,dV = \int_{\Gamma_n} \mathbf{F}^{(\kappa)}\cdot\mathbf{n}\,d\Gamma + \int_{V_n} q^{(\kappa)}\,dV \qquad (1)$$

$$\kappa = 1, \ldots, NK+1$$

The integration is over an arbitrary subdomain V_n ("grid block" in finite difference parlance) of the flow system under study, which is bounded by the closed surface Γ_n. The left hand side represents the "accumulation term," with M denoting the amount of component κ (κ = water, air, heat, ...) present per unit volume of the flow system. **F** is the flux of component κ entering V_n on the closed surface Γ_n around V_n, and q represents sinks and sources, through which mass or heat is injected into or removed from the system.

& The TOUGH code and associated documentation is available from the National Energy Software Center, c/o Argonne National Laboratory, 9700 South Cass Ave., Argonne, IL 60439.

Thus, Eq. (1) expresses the simple fact that the rate of change in the amount of κ within V_n is equal to the total rate at which κ flows across the surface Γ_n of V_n, plus the contribution of sinks and sources from within V_n. (We mention in passing that the heat "component" is not strictly conserved because of the possibility of conversion of heat into mechanical work and vice versa; this fine point is immaterial for the present discussion.)

Note that the conservative quantities for which Eqs. (1) are written are not the phases but the components (different chemical species, or mixtures of species, such as air, which can be treated as a single "pseudo-component" for the processes of interest). The accumulation term M is a sum over contributions from the various phases (liquid, gaseous, solid) in which component κ is present. This formulation automatically includes the description of phase change processes subject to the constraint of "local thermodynamic equilibrium" between all phases. Description of non-equilibrium phase change effects would require separate conservation equations for different phases, with appropriate sink and source terms to represent phase transformations. The flux terms **F** are likewise sums of the separate contributions made by the different flowing phases, the main term being a multiphase version of Darcy's law, that includes relative permeability and capillary pressure effects. In addition, diffusive and dispersive mass fluxes can be present. Heat flux includes conductive and convective components; the latter includes latent heat effects represented by different specific enthalpies of different phases.

The transport Eqs. (1) need to be complemented with constitutive relationships, which express all thermophysical parameters as functions of a set of primary thermodynamic variables. Thermophysical property modules developed for MULKOM are listed in Table 1; modules included in the present TOUGH2 package are marked with an asterisk.

For numerical solution, the mass and energy balance Eqs. (1) must be discretized in space and time. In MULKOM and TOUGH2, space discretization is made directly from the integrals, without first converting Eqs. (1) into partial differential equations. This "integral" finite difference method, pioneered by Edwards (1972) and Narasimhan and Witherspoon (1976), avoids any reference to a global system of coordinates, and thus offers the advantage of being applicable to regular or irregular discretizations in one, two, or three dimensions. It also facilitates implementation of higher-order differencing methods and applications to fractured media. For systems of regular grid blocks referred to global coordinates, the integral finite difference method is equivalent to conventional finite differences. Time is discretized fully implicitly as a first-order backward finite difference. This together with 100% upstream weighting of flux terms at interfaces is necessary to achieve unconditional stability (Peaceman, 1977), and to avoid impractical time step limitations for multiphase flow problems in fractured media with their usually small but highly active fracture volume. Space and time discretization results in a set of nonlinear algebraic equations. These are usually strongly coupled and are solved completely simultaneously by means of Newton/Raphson iteration. If convergence is not achieved within a predetermined number of iterations (typically eight), the time step size is automatically reduced. The linear equations arising at each iteration step are solved with a sparse version of LU-decomposition and backsubstitiution (Duff, 1977).

TOUGH2 User Features

As mentioned above the TOUGH2 input formats are upwardly compatible with those of TOUGH. Much of the available parameter choices is documented in the printed output, which otherwise is similar to that of TOUGH. Several additional parameters are provided through TOUGH data blocks for modeling additional processes and effects. These include a provision for the Klinkenberg (1941) effect, an account of vapor diffusion enhancement from pore-level phase change effects, and a capability to model heat exchange with impermeable confining layers by means of a semi-analytical method (Vinsome and Westerveld, 1980).

A new feature in TOUGH2 is the concept of "inactive elements." By convention, volume elements or grid blocks encountered in data block "ELEME" are taken to be "active" until the first element entry with a volume of zero or negative is encountered. The first element with volume zero or negative, and all subsequent elements, are taken to be "inactive." For the inactive elements no mass or energy balance equations are set up, and their primary thermodynamic variables are not included in the list of unknowns. Otherwise, however, inactive elements can appear in flow connection and initial condition specifications like all other elements. This feature can be conveniently used to specify Dirichlet boundary conditions, by gathering all elements beyond the desired flow domain boundary at the end of the ELEME-block, and inserting a "dummy" volume element of zero volume in front of them. TOUGH2 features dynamic dimensioning of major (problem-size dependent) arrays, by means of PARAMETER statements in the main program. Allowable problem size data are printed in the output.

Further enhancements in comparison to TOUGH can be invoked by means of new data blocks (Fig. 2). The keyword 'MESHM' calls up a MESHMAKER module for mesh generation and processing, which itself has a modular structure and can call several submodules. Present capabilities include generation of two-dimensional R-Z grids, and one, two, or three-dimensional rectilinear grids. MESHMAKER can also be used to sub-grid a porous medium mesh for fractured media according to the method of "multiple interacting continua," which includes double-porosity and dual-permeability models as special cases.

A new data block 'MULTI' can be used for various choices in the EOS-modules. The balance equations solved by TOUGH2 are ordered in such a fashion that, for a system with NK mass components, the NK mass balance equations appear first, followed by an energy balance. For nonisothermal problems, therefore, the number of equations per grid block is NEQ = NK + 1. In many problems heat effects are unimportant, however, and it would be desirable to avoid the expenditure of computing resources on solving a system of equations in which the energy balance reduces to the trivial statement dT/dt = 0. For several of the EOS modules it is possible to specify NEQ = NK, in which case no energy balances will be set up. As computing work typically is proportional to NEQ**2, this can provide substantial savings.

In addition to specifying initial conditions by default for the entire flow domain, or in element-for-element fashion, TOUGH2 permits specification of default initial conditions for reservoir subdomains (data block 'INDOM').

The version control system in TOUGH2 works as follows. At the end of the assignment statements, each subroutine has a code section such as:

```
      DATA ICALL/0/
      ICALL=ICALL+1
      IF(ICALL.EQ.1) WRITE(11,899)
  899 FORMAT(/6X,'EOS      1.0   15 AUGUST   1990',6X,
     X'*EOS1* ... THERMOPHYSICAL PROPERTIES MODULE FOR WATER')
```

Thus, on first call to each subroutine, a one-line informative message will be printed to unit 11 (disk file 'VERS'), identifying the program unit, its version number and date, and the function performed by the program unit. At the end of a TOUGH2 simulation run, the contents of file 'VERS' will be copied to (default) OUTPUT, see the example in Fig. 3. Besides documenting the versions and dates of subroutines used, this listing is instructive as a record of the calling sequence of program units during execution. When making code modifications, these version messages should be appropriately updated to maintain a traceable and referenceable record of source code developments and applications. Printing of version information can be optionally suppressed by means of a keyword 'NOVER'.

Keyword 'ENDFI' can be used as an alternative to 'ENDCY' for terminating input data. 'ENDFI' will cause the flow simulation to be bypassed; this option is useful when only mesh processing is desired.

Concluding Remarks

TOUGH2 is a more powerful successor to TOUGH. The code implements the general MULKOM architecture that separates and interfaces the flow and transport aspects of the problem (which do not depend on the nature and number of fluid components and phases) from the fluid property and phase composition aspects (which are specific to the particular fluid mixture under study).

The emphasis in the development of the MULKOM concept, and its implementation in the TOUGH2 code, has been on flexibility and robustness. TOUGH2 is an adaptable research tool; in its present form the TOUGH2 package includes the ''core'' modules of MULKOM for simulation studies in the fields of geothermal reservoir engineering, nuclear waste isolation, and hydrology. Examples of applications can be found in several papers presented at the TOUGH Workshop (Tsang and Pruess, 1990b; Calore *et al.*, 1990; Doughty and Pruess, 1990). MULKOM fluid property modules to be included in future releases would allow applications to problems in petroleum engineering, natural gas recovery and storage, and environmental monitoring and remediation. Further enhancements of the code are desirable, including a more comprehensive description of multiphase processes, improved execution speed, and a simpler more graphically oriented user interface.

TOUGH2 is intended to be a ''general purpose'' simulator. Applications to many different kinds of flow problems are possible, but should be made with caution. The diversity of multiphase fluid and heat flow problems is enormous, and careful consideration must be given to the peculiar features of any given problem if a reasonably accurate and efficient solution is to be obtained. A case in point is multiphase flow in composite

(layered) media, in which discontinuous permeability changes occur at the boundaries between different geologic units. It is well known that for single phase flow, the appropriate interface weighting scheme for absolute permeability is harmonic weighting. For two-phase flow, the added problem of relative permeability weighting arises; it has been established that for transient flow problems in uniform media, relative permeability must be upstream weighted, or else phase fronts may be propagated with erroneous speed (Aziz and Settari, 1979). Recent studies at Lawrence Berkeley Laboratory have shown that for transient two-phase problems in composite media, both absolute and relative permeability must be fully upstream weighted to avoid the possibility of gross errors (Tsang and Pruess, 1990a; Wu, Pruess and Chen, 1990). The applicable weighting schemes for different flow problems are summarized in Fig. 4. Our somewhat disturbing conclusion is that there is no single weighting scheme for general two-phase flows in composite media that would at the same time preserve optimal accuracy for single-phase or steady two-phase flows. Another interesting problem is the weighting scheme for interface densities. For proper modeling of gravity effects, it is necessary to define interface density as the arithmetic average between the densities of the two adjacent grid blocks, regardless of nodal distances from the interface. An unstable situation may arise when phases (dis–)appear, because interface density may then have to be ''switched'' to the upstream value when the phase in question is not present in the downstream block. For certain flow problems spatial interpolation of densities may provide more accurate answers.

These examples are by no means exhaustive; they are simply intended to illustrate potential subtle and not so subtle pitfalls in the modeling of multiphase flows. Generally speaking, in the design and implementation of numerical schemes for such flows, there appears to be a trade-off between accuracy and efficiency on the one hand, and flexibility and robustness on the other. For any given problem, small modifications in the source code will often allow substantial gains in accuracy and efficiency.

Acknowledgement

The author is deeply indebted to Paul Witherspoon, whose foresight and continual interest and encouragement made the developments described in this article possible. He also appreciates the many stimulating discussions with colleagues at the Lawrence Berkeley Laboratory. The development of LBL's multiphase simulation capabilities received initial support from the Office of Basic Energy Sciences, and was subsequently primarily funded by the Geothermal Technology Division, U.S. Department of Energy, under Contract No. DE-AC03-76SF00098. Additional support for documentation and maintenance of the TOUGH and TOUGH2 codes was provided by the Nuclear Regulatory Commission, and by the Yucca Mountain Project through Sandia National Laboratories.

References

Aziz, K. and Settari, A., 1979, Petroleum Reservoir Simulation, Elsevier, London and New York.

Calore, C., Gianelli, G. and Pruess, K., 1990, Water-CO_2 Version of MULKOM Code: A Tool for Studying the Origin and Trends of CO_2 in Geothermal Reservoirs, paper presented at TOUGH Workshop, Lawrence Berkeley Laboratory, Berkeley, CA.

Doughty, C. and Pruess, K., 1990, Verification of TOUGH2 Against A Semianalytical Solution for Transient Two-phase Fluid and Heat Flow in Porous Media, paper presented at TOUGH Workshop, Lawrence Berkeley Laboratory, Berkeley, CA.

Duff, I. S., 1977, MA28 - A Set of FORTRAN Subroutines for Sparse Unsymmetric Linear Equations, AERE Harwell Report R 8730.

Edwards, A. L., 1972, TRUMP: A Computer Program for Transient and Steady State Temperature Distributions in Multidimensional Systems, National Technical Information Service, National Bureau of Standards, Springfield, VA.

Klinkenberg, L. J., 1941, The Permeability of Porous Media to Liquids and Gases, *in:* API Drilling and Production Practice, pp. 200–213.

Narasimhan, T. N. and Witherspoon, P. A., 1976, An Integrated Finite Difference Method for Analyzing Fluid Flow in Porous Media, *Water Res. Res., 12*, (1), 57–64.

Peaceman, D. W., 1977, *Fundamentals of Numerical Reservoir Simulation*, Elsevier, Amsterdam.

Pruess, K., 1983a, GMINC—A Mesh Generator for Flow Simulations in Fractured Reservoirs, Lawrence Berkeley Laboratory report LBL-15227, Berkeley, CA.

Pruess, K., 1983b, Development of the General Purpose Simulator MULKOM, Annual Report 1982, Earth Sciences Division, Lawrence Berkeley Laboratory report, LBL-15500.

Pruess, K., 1987, TOUGH User's Guide, Nuclear Regulatory Commission, report NUREG/CR-4645 (also Lawrence Berkeley Laboratory report LBL-20700, Berkeley, CA).

Pruess, K., 1988, SHAFT, MULKOM, TOUGH: A Set of Numerical Simulators for Multiphase Fluid and Heat Flow, *Geotermia, Rev. Mex. Geoenergia, 4*, (1), 185–202 (also Lawrence Berkeley Laboratory report LBL-24430).

Pruess, K., 1990, Modeling of Geothermal Reservoirs: Fundamental Processes, Computer Simulations, and Field Applications, *Geothermics, 19*, (1), 3–15.

Pruess, K. and Narasimhan, T. N., 1982, On Fluid Reserves and the Production of Superheated Steam from Fractured Vapor-dominated Geothermal Reservoirs, *J. Geophys. Res., 87*, (B11), 9329–9339.

Pruess, K. and Narasimhan, T. N., 1985, A Practical Method for Modeling Fluid and Heat Flow in Fractured Porous Media, *Soc. Pet. Eng. J., 25*, 1, 14–26.

Pruess, K. and Schroeder, R. C., 1980, SHAFT79 User's Manual, Lawrence Berkeley Laboratory report LBL-10861, Berkeley, CA.

Tsang, Y. W. and Pruess, K., 1990a, Further Modeling Studies of Gas Movement and Moisture Migration at Yucca Mountain, Nevada, Lawrence Berkeley Laboratory, report LBL-29127, Berkeley, CA.

Tsang, Y. W. and Pruess, K., 1990b, Modeling Studies of Gas Movement and Moisture Migration at Yucca Mountain, Nevada, paper presented at TOUGH Workshop, Lawrence Berkeley Laboratory, Berkeley, CA.

Vinsome, P. K. W. and Westerveld, J., 1980, A Simple Method for Predicting Cap and Base Rock Heat Losses in Thermal Reservoir Simulators, *J. Canadian Pet. Tech.*, pp. 87–90, July–September.

Wu, Y. S., Pruess, K. and Chen, Z. X., 1990, Buckley-Leverett Flow in Composite Media, submitted to *Water Res. Res.*, May.

Table 1. MULKOM/TOUGH2 Fluid Property Modules

Number of Components	Components	Applications
1	water*	hydrology
2	water, heat*	geothermal, lab experiments
	near-critical water, heat	geothermal
3	water, tracer, heat*	geothermal, hydrology
	water, CO_2, heat*	geothermal
	water, air, heat*, §	nuclear waste, geothermal, compressed air energy storage
	water, H_2, heat*	nuclear waste
	water, SiO_2, heat	nuclear waste, geothermal
	water, NaCl, heat	geothermal
	water, CH_4, foam	aquifer gas storage, environmental
	water, NAPL‡, heat	environmental
4	water, CO_2, NaCl, heat	geothermal
	water, light oil, heavy oil, heat	enhanced oil recovery (steam flooding)
N + 1	water, N-component NAPL‡	environmental

*TOUGH2

§TOUGH

‡NAPL = non-aqueous phase liquid, such as organic solvents or fuels

Figure Captions

Figure 1. Modular architecture of MULKOM and TOUGH2.

Figure 2. Input formats for new TOUGH2 data blocks.

Figure 3. An example of the version identification printout from TOUGH2.

Figure 4. Weighting procedures for absolute (k) and relative permeability (kr) at grid block interfaces.

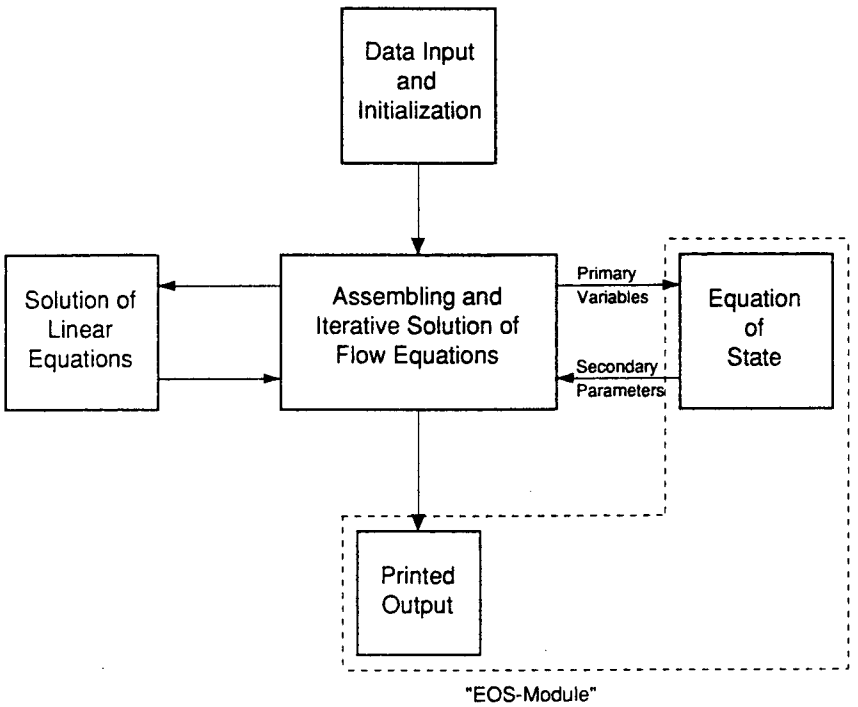

Figure 1. Modular architecture of MULKOM and TOUGH2.

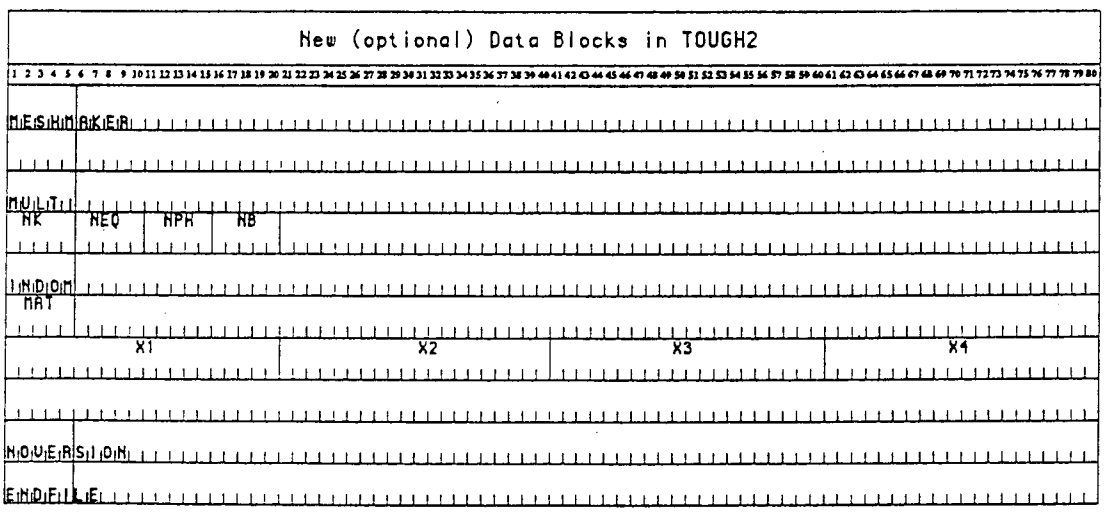

Figure 2. Input formats for new TOUGH2 data blocks.

```
1*************************************************************************************************************************

                    SUMMARY OF PROGRAM UNITS USED

     UNIT     VERSION      DATE                    COMMENTS
 ------------------------------------------------------------------------------------------------------------------------

     TOUGH2     1.0      8 JUNE        1990      MAIN PROGRAM
     IO         1.0     22 JANUARY     1990      OPEN FILES *MESH*, *INCON*, *GENER*, *SAVE*, *LINEQ*, AND *TABLE*

     INPUT      1.0     24 MAY         1990      READ ALL DATA PROVIDED THROUGH FILE *INPUT*

     MESHM      1.0     24 MAY         1990      EXECUTIVE ROUTINE FOR INTERNAL MESH GENERATION
     RZ2D       1.0     22 JANUARY     1990      CALCULATE 2-D R-Z MESH FROM INPUT DATA
     WRZ2D      1.0     25 MAY         1990      WRITE DATA FOR 2-D R-Z MESH ON FILE *MESH*
     RFILE      1.0     24 MAY         1990      INITIALIZE DATA FROM FILES *MESH* OR *MINC*, *GENER*, AND *INCON*

     CYCIT      1.0     22 JUNE        1990      EXECUTIVE ROUTINE FOR MARCHING IN TIME

     EOS        1.0      5 FEBRUARY    1990      ASSIGN ALL THERMOPHYSICAL PROPERTIES ("SECONDARY PARAMETERS")
     SAT        1.0     22 JANUARY     1990      STEAM TABLE EQUATION: SATURATION PRESSURE AS FUNCTION OF TEMPERATURE
     COWAT      1.0     22 JANUARY     1990      LIQUID WATER DENSITY AND INT. ENERGY AS FUNCTION OF TEMPERATURE AND PRESSURE
     SUPST      1.0     29 JANUARY     1990      VAPOR DENSITY AND INTERNAL ENERGY AS FUNCTION OF TEMPERATURE AND PRESSURE
     VISW       1.0     22 JANUARY     1990      VISCOSITY OF LIQUID WATER AS FUNCTION OF TEMPERATURE AND PRESSURE

     VISCO      1.0      1 FEBRUARY    1990      CALCULATE VISCOSITY OF VAPOR-AIR MIXTURES

     COVIS      1.0      1 FEBRUARY    1990      COEFFICIENT FOR GAS PHASE VISCOSITY CALCULATION
     VISS       1.0     22 JANUARY     1990      VISCOSITY OF VAPOR AS FUNCTION OF TEMPERATURE AND PRESSURE
     RELP       1.0     25 JANUARY     1990      LIQUID AND GAS PHASE RELATIVE PERMEABILITIES AS FUNCTIONS OF SATURATION
     PCAP       1.0     22 JANUARY     1990      CAPILLARY PRESSURE AS FUNCTION OF SATURATION

     BALLA      1.0      1 FEBRUARY    1990      PERFORM SUMMARY BALANCES FOR VOLUME, MASS, AND ENERGY
     TSTEP      1.0     22 JANUARY     1990      ADJUST TIME STEPS TO COINCIDE WITH USER-DEFINED TARGET TIMES

     MULTI      1.0     24 MAY         1990      ASSEMBLE ALL ACCUMULATION AND FLOW TERMS
     QU         1.0     22 JANUARY     1990      ASSEMBLE ALL SOURCE AND SINK TERMS
     LINEQ      1.0     22 JANUARY     1990      INTERFACE FOR THE LINEAR EQUATION SOLVER MA28
     MC19A                                       HARWELL SUBROUTINE FOR SCALING MATRIX
     CONVER     1.0     22 JANUARY     1990      UPDATE PRIMARY VARIABLES AFTER CONVERGENCE IS ACHIEVED

     PP         1.0      1 FEBRUARY    1990      CALCULATE VAPOR PRESSURE, DENSITY, INT. ENERGY AS F(P,T,X)

     OUT        1.0      1 FEBRUARY    1990      PRINT RESULTS FOR ELEMENTS, CONNECTIONS, AND SINKS/SOURCES
     WRIFI      1.0     22 JANUARY     1990      AT THE COMPLETION OF A TOUGH2 RUN, WRITE PRIMARY VARIABLES ON FILE *SAVE*

*************************************************************************************************************************

END OF TOUGH2 SIMULATION RUN --- ELAPSED TIME =  162.699 SEC-- CALCULATION TIME =  162.314 SEC-- DATA INPUT TIME =    0.285 SEC
```

Figure 3. An example of the version identification printout from TOUGH2.

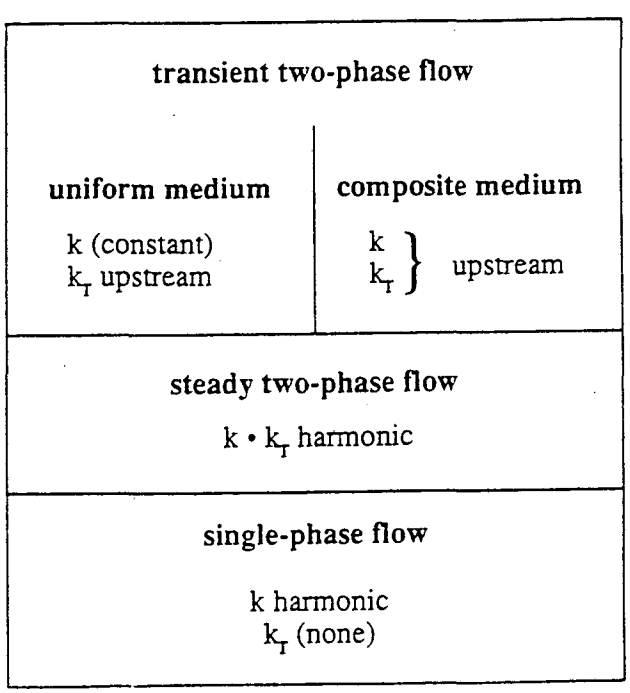

ESD-905-0007

Figure 4.

Weighting procedures for absolute (k) and relative permeability (kr) at grid block interfaces.

Extended abstract for TOUGH User's Workshop, September 13-14, 1990

Modeling Studies of Gas Movement and Moisture Migration at Yucca Mountain, Nevada

Y. W. Tsang and K. Pruess

Lawrence Berkeley Laboratory

Introduction

We have carried out modeling studies on moisture redistribution processes that are mediated by gas phase flow and diffusion. We specifically address the effect of a lowered humidity of the soil gas at the land surface to moisture removal from Yucca Mountain, the potential site for a high level nuclear waste repository. At the land surface, humid formation gas contacts much drier atmospheric air. Near this contact, the humidity of the soil gas may be considerably lower than at greater depth, where we expect equilibrium with the liquid phase and close to 100% humidity. The lower relative humidity of the soil gas may be modeled by imposing, at the land surface, an additional negative capillary suction corresponding to vapor pressure lowering according to Kelvin's Equation (Edlefsen and Anderson, 1943), thus providing a driving force for the upward movement of moisture in both the vapor and liquid phases. Sensitivity studies show that moisture removal from Yucca Mountain arising from the lowered-relative-humidity boundary condition is controlled by vapor diffusion. The lowered-humidity boundary condition implies a composition gradient in the gas phase, giving rise to a downward diffusive flux of air and an upward flux of vapor. The binary diffusion gas flux is described by

$$\mathbf{F}^{\kappa} = -D_{va}\rho_g \nabla \chi_g^{\kappa}, \tag{1}$$

where κ is the component index for the gas phase (κ=air or vapor), χ_g^{κ} is the mass fraction of the κth component in the gas phase, and D_{va} is the diffusion coefficient for the vapor-air mixture in a porous medium, given by (Vargaftik, 1975; Walker et al., 1981)

$$D_{va} = \tau\phi S_g D_{va}^{o} \frac{P_o}{P}\left[\frac{T}{T_o}\right]^{\theta}. \tag{2}$$

D_{va}^{o} is the diffusion coefficient in free gas phase at standard conditions of $P_o = 1$ bar and T_o = 273.15 K. The parameter group $\beta = \tau\phi S_g$, where S_g is the gas saturation, τ is the tortuosity, and ϕ is the porosity, specifies properties relevant to binary diffusion in a porous medium. For typical values of porosity and saturation in geological formations, β falls in the range of .001 to .01. However, there is much experimental evidence in the soil literature (e.g. Jury and Letey, 1979) that diffusion of vapor is enhanced due to pore-level phase change effects by a few orders of magnitude, so that β may take on values on the order of 1 regardless of media properties and gas saturation. Modeling results presented here will account for this enhancement in vapor diffusion.

Simulation Results for a Medium with Uniform Hydrological Properties

Calculations were carried out by means of an in-house version of the numerical simulator "TOUGH" (Transport Of Unsaturated Goundwater and Heat; Pruess, 1987), which includes vapor pressure lowering effects. To focus on the vertical movement of fluxes, the simulation was carried out in one dimension, in a vertical tuff column of 600 m, which is the approximate distance from the land surface to the water table at the proposed repository site. We first employed a highly simplified stratigraphic description, assuming uniform hydrologic parameters that were representative of the proposed repository host formation (the Topopah Spring welded unit). The welded tuff unit is intensely fractured, with an average continuum fracture permeability about four orders of magnitude larger than the matrix permeability. We use an effective continuum approximation which allowed us to use one set of hydrological parameters for the description of fluid flow in the fractured porous medium. This is accomplished by coding effective continuum characteristic curves as given in Appendix A into TOUGH. The numerical computation is first carried out without the imposition of a lowered humidity boundary condition. The ground surface and the water table serve as constant temperature boundaries maintained at 286 K and 304 K, respectively. The water table serves also as a pressure boundary with the constant pressure P_o of 1 bar, while a "no flow" boundary is imposed at the top, so that the gas pressure at each elevation will adjust itself to $P_o - \rho_g gz$, whereas the equilibrium liquid pressure depends also on the capillary suction. Then the lowered-humidity boundary condition is implemented at the land surface for the second part of the calculations.

In Figure 1 we show the fluxes in the liquid and gas phase. Results obtained prior to imposition of reduced-humidity boundary conditions are labeled "reference case", and those with imposed humidity boundary condition are labeled accordingly by "50% humidity". Units of flux are in both kg/m^2-s (bottom scale) and mm/yr of water (top scale). The label "vapor" in the figures denotes the total vapor flux arising from binary diffusion, as represented by Equation 1, as well as pressure-driven Darcy flow. The figures display the fluxes as a function of elevation, with positive values for upward fluxes, and negative values for downward fluxes. Figure 1 shows result with the enhanced value of β=1 for vapor diffusion, and the value corresponding to material properties $\tau\phi S_g$ = .0018 for the air diffusion. For the "reference case", the upward vapor flux is balanced by the downward flow of the condensed liquid, resulting in zero net moisture migration. The larger magnitude of the vapor fluxes at depth arises from the geothermal gradient. With the imposition of a 50% relative humidity boundary condition, both the liquid flux and the vapor flux are upward, giving rise to a net upward migration of moisture. Vapor flux first decreases with elevation from the water table because of the decrease of temperature; at 300 m above the water table, vapor pressure lowering effects come into play from the lowered humidity boundary condition applied at the land surface, and the magnitude of vapor flux increases with elevation. The moisture flux from the upper portion of the formation consists almost entirely of vapor. The decrease of liquid flux with elevation arises from non-linear liquid-flow effects, since the lower liquid saturation with elevation from the imposed boundary condition, while giving rise to a stronger upward capillary driving force, also results in a rapid decrease in liquid relative permeability. The total upward moisture flux is seen to be approximately .04 mm yr^{-1} in Figure 1b.

Simulations were also carried out for three other values of β= .0018, .05, and .33. The simulated results are summarized in Figure 2, which is a log-log plot of fluxes versus the vapor diffusion strength β. The upward vapor fluxes plotted are the simulated values at 2.5 m below the land surface. when no lowered humidity boundary condition is present, the vapor fluxes fall on a straight line of unit slope on the log-log plot, illustrating the linear dependence of the diffusion vapor flux on β, which follows from Equations 1 and 2. With the 80 % humidity boundary condition at the land surface, the upward moisture flux is predominantly carried by the vapor phase when β is larger than .05. Only for the smallest value of β=.0018 does the liquid phase flux contribute significantly to the total upward moisture flux. For the range of values of β examined, the rate of moisture removal ranges from about .002 mm/yr to .04 mm/yr with the lowered humidity boundary condition of 80%. Similar results were obtained for the humidity boundary condition of 50%. Figure 2 therefore summarizes the following: (1) For the reference case, the vapor flux increases linearly with β. In the absence of an imposed lowered humidity boundary condition, the upward vapor flux is balanced by the downward condensed liquid flux, resulting in no net loss of moisture from the formation. (2) With the lowered-humidity boundary condition at the surface, the magnitude of the total moisture flux is larger than, but of the same order of magnitude as, the vapor flux of the reference case. Hence the strength of the vapor diffusion both controls, and gives a good estimate, of the amount of moisture which is removed from the formation under an imposed lowered relative humidity boundary condition.

By varying β over a large range up to the greatly enhanced value of 1, we have bracketed the possible range of magnitude of moisture flux out of a column of welded tuff. Since the value of β dictates the rate of vapor-dominated moisture removal from humidity boundary conditions, our estimates for a column of welded tuff remain pertinent to the actual formation with layers of different hydrological properties. To substantiate our claim, we now turn to sample calculations where the effects of stratigraphy are included.

Inclusion of Stratigraphy in 1-D Column Simulations

We included a simplified stratigraphy consisting of alternating layers of welded and non-welded tuff, in our simulations. The division of hydrologic units and spatial discretization for numerical simulation are shown in Figure 3a. The non-welded units of tuff are only sparsely fractured and may be treated as a porous medium, while the effective continuum approximation still applies for the highly fractured welded units. For choice of layer thickness, material properties and characteristic curves we refer the reader to our detailed report (Tsang and Pruess, 1990). In Figure 3b we show the steady-state liquid satuation profile for the reference case, which clearly demonstrates the effects from different hydrological properties in the alternating layers. Simulated results for fluxes are shown in Figure 4, those for the "reference case" prior to the imposition of humidity boundary conditions in 4a, and those when a boundary condition of 50% humidity is imposed in Figure 4b. Figure 4b shows that, whereas in the welded unit both the liquid and vapor flow contribute to the upward transport of moisture, in the top 250 m the removal of moisture from the formation comes mostly from the vapor flow. In comparing the fluxes for the layered column with different characteristic curves (Figure 4) to those for the 1-D welded column with no stratigraphy

(Figures 1), it is clear that the moisture removal from the formation is of the same order of magnitude, confirming our earlier claim that vapor diffusion strength is the controlling factor for the amount of moisture that is removed from the formation with a lowered humidity boundary condition.

These results show that the presence of a realistic stratigraphy of alternating layers of nonwelded and welded units with very different hydrological properties has minor effects on the magnitude of moisture removal due to the "humidity" boundary condition. With a typical enhanced vapor diffusion strength of $\beta=1$, our studies show that the amount of upward moisture flux (predominantly vapor) from the tuff column is equivalent to $\approx$ .04 mm/yr of water. We therefore conclude from our calculations that the rate of moisture removal from vapor transport has an upper limit of about .1 mm/yr.

Upstream Weighting Scheme for a Stratigraphic Interface

In the course of our study on stratigraphic columns with alternate layers of nonwelded and welded units, we discovered that order-of-magnitude discontinuities in absolute and relative permeabilities at a lithologic contact give rise to artificially large resistance to flow with the usual numerical scheme of harmonic weighting of absolute permeability and upstream weighting of relative permeability. We carried out extensive investigations into the treatment of flow at stratigraphic interfaces (between porous/porous fractured media) in numerical studies. Our conclusion is that there is no single interface weighting scheme that would be optimal for all conditions. The only generally applicable weighting scheme which avoids gross errors in general two phase flow in composite media is the complete 100% upstream weighting of the effective permeability (product of absolute and relative permeability), which we employed to resolve the numerical difficulty in our calculations.

References

Edlefsen, N. E., and A. B. C. Anderson, Thermodynamics of soil moisture, Hilgardia, 15(2), 31-298, 1943.

Jury W. A. and J. Letey, Jr., Water vapor movement in soil: Reconciliation of theory and experiment, Jour. Soil Sci. Am., 43(5), 823-827, 1979.

Pruess, K. TOUGH Users's Guide, rep. LBL-20700, Lawrence Berkeley Laboratory, Berkeley, CA. June 1987.

Pruess, K., J. S. Y. Wang, and Y. W. Tsang, On thermohydrologic conditions near high-level nuclear wastes emplaced in partially saturated fractured tuff 2. Effective continuum Approximation, Water Resour. Res., 26(6), 1249-1261, 1990.

Tsang, Y. W. and K. Pruess, Further modeling studies of gas movement and moisture migration at Yucca Mountain, Nevada, rep. LBL-29127, Lawrence Berkeley Laboratory, Berkeley, CA. May 1990.

Vargaftik, N. B., Tables on the thermophysical properties of liquids and gases, 2nd ed., John Wiley, NY, 1975.

Walker, W R., J. D. Sabey and D. R. Hampton, Studies of heat transfer and water migration in soils, Final report, Deprtment of agricultural and Chemical Engineering, Colarado University, Fort Collins, CO, April 1981.

APPENDIX A

Effective Continuum Characteristic Curves

In the effective continuum approximation, one set of hydrological parameters is defined for the description of fluid flow in the fractured porous medium. The effective continuum parameters are: permeabilities to the liquid and gas phase, k_l and k_g, relative permeabilities k_{rl}, k_{rg}, and the capillary suction P_{suc}, all expressed in terms of the independent variable, effective continuum liquid saturation S_l. When an effective continuum approximation is applicable, it is necesary to define the effective continuum parameters in terms of matrix and fracture parameters. The corresponding parameters for the fracture and matrix media will be denoted by subscript f and m respectively.

(1) Threshold liquid saturation

Let S_l be the liquid saturation of the effective continuum. It is expressed in terms of the matrix and fracture saturations as follows (Pruess et al., 1990):

$$S_l = \frac{S_{lm}\bar{\phi}_m + S_{lf}\bar{\phi}_f}{\bar{\phi}_m + \bar{\phi}_f} \tag{A-1}$$

where both $\bar{\phi}_m$ and $\bar{\phi}_f$ are void fractions defined in terms of the total volume,

$$V_{tot} = V_m + V_f \,. \tag{A-2}$$

Total effective porosity is $\bar{\phi} = \bar{\phi}_m + \bar{\phi}_f$. The threshold saturation, S_{th} is defined as the continuum liquid saturation at the juncture when the matrix is fully saturated and the fracture is dry, that is, S_{th} is the value of S_l in Equation (A-1) where S_{lm} is 1 and S_{lf} is 0,

$$S_{th} = \frac{\bar{\phi}_m}{\bar{\phi}_m + \bar{\phi}_f} = 1 - \frac{\bar{\phi}_f}{\bar{\phi}}. \tag{A-3}$$

The reasoning which leads to the definition of threshold liquid saturation is as follows. An effective continuum concept is only applicable when approximate local thermodynamic equilibrium exists between matrix and fractures. Because the capillary suction in the matrix is much stronger than that in the fracture, local equilibrium implies that the liquid saturation in the fracture will remain near zero until matrix saturation reaches 100%. The concept of a liquid threshold saturation as defined by Equation (A-3) is based on the approximation that the enormous disparity of the strength of capillary suction in the matrix and fractures will cause the fractures to remain completely dry until the matrix becomes fully saturated during imbibition; and for the fractures to be completely drained before the matrix begins to desaturate during drainage. We have found the above approximation to be an excellent one from running 2-D simulations of discrete fracture and matrix systems with infiltration.

From Equation (A-1), given the liquid saturation of the effective continuum, S_l, the matrix and fracture liquid saturation are as follows:

$$S_{lm} = S_l/S_{th}, \quad S_{lf} = 0; \qquad \text{for } S_l \le S_{th}$$

$$S_{lm} = 1, \quad S_{lf} = \frac{(S_l - S_{th})}{(1 - S_{th})}; \qquad \text{for } S_l > S_{th} \tag{A-4}$$

(2) Effective Continuum Capillary Suction

The capillary suction for the effective continuum in terms of the continuum saturation S_l is

$$P_{suc}(S_l) = P_{suc}(S_{lm} - \delta) \qquad \text{for } S_l < S_{th}$$
$$= P_{suc}(1-\delta) \cdot \frac{(1-S_l)}{(1-S_{th})} \qquad \text{for } S_l \geq S_{th} \qquad \text{(A-5)}$$

The matrix characteristic curve is used for P_{suc}. The formulation in Equation (A-5) gives a continuous curve as the continuum liquid saturation passes through the threshold value. Below the threshold, it follows the suction curve for the matrix; above the threshold, the capillary suction in the fracture varies linearly with S_l. The parameter δ is introduced to represent air entry effects; i.e., a finite suction is required to reduce the matrix saturation from $S_{lm} = 1$. It gives the added advantage that the slope of dP_{suc}/dS_{lm} remains finite at S_{th}. The infinite slope of dP_{suc}/dS_{lm} at $S_{lm} = 1$ would have made the transition across the threshold impossible physically and numerically. A choice of δ corresponding to a suction pressure of 2000 Pascals (.2 m of H_2O) is sufficient to render the numerical computation possible.

(3) Effective Continuum Liquid and Gas Permeability

The effective continuum liquid and gas permeabilities as functions of the effective continuum liquid saturation are defined in terms of the permeabilities in the matrix and fracture continua (Pruess et al., 1990).

$$k_l(S_l) = \bar{k}_m(1-\bar{\phi}_f)k_{rm}(S_{lm}) \qquad \text{for } S_l \leq S_{th}$$
$$= \bar{k}_m(1-\bar{\phi}_f) + \bar{k}_f k_{rf}(S_{lf}) \qquad \text{for } S_l > S_{th} \qquad \text{(A-6)}$$

Equation (A-6) makes use of the fact that below S_{th}, the liquid saturation in the fracture continuum is 0 and therefore the relative permeability to the liquid in the fracture is zero; whereas above S_{th}, the matrix continuum is fully saturated with relative permeability equals 1. The $\bar{k}_m$ and $\bar{k}_f$ are respectively the saturated continuum permeabilities for the matrix and fracture. The effective continuum permeability to the gas is approximated as the difference between the saturated permeability of the effective continuum and the permeability to the liquid phase, that is,

$$k_g(S_l) = [\bar{k}_m(1-\bar{\phi}_f) + \bar{k}_f] - k_l(S_l). \qquad \text{(A-7)}$$

where the expression in the square bracket is the saturated permeability of the effective continuum.

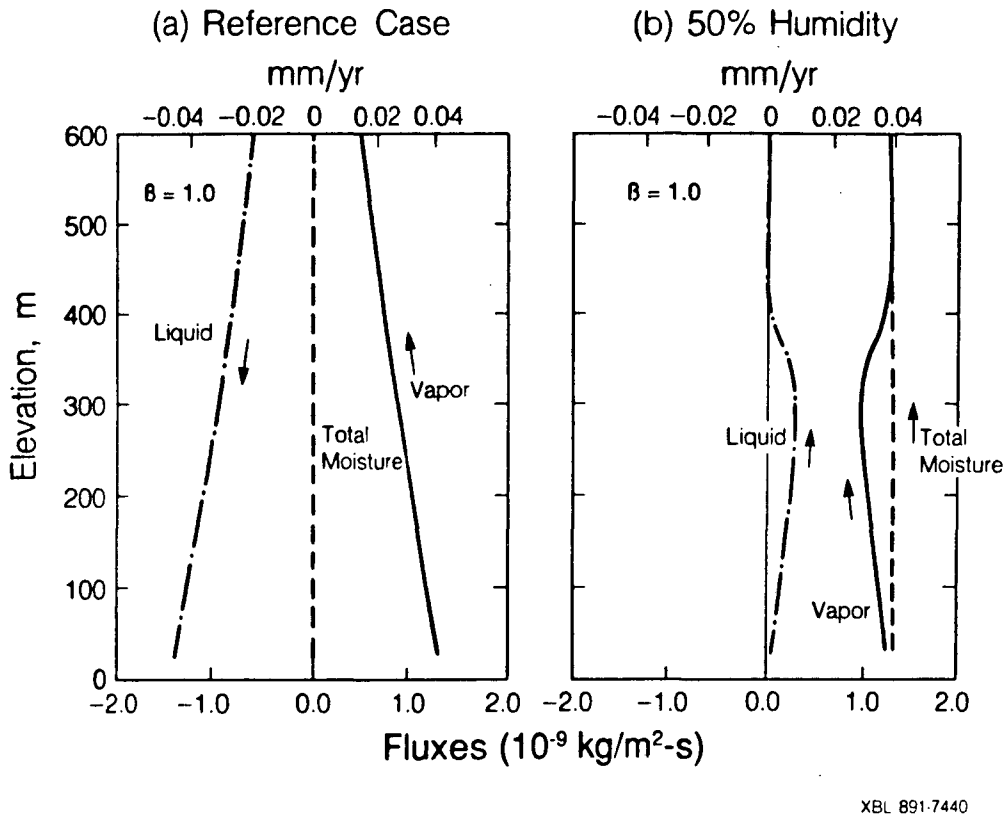

Figure 1. Fluxes in a column of welded tuff with vapor diffusion strength $\beta = 1$, and air diffusion strength $\beta = 0.0018$.

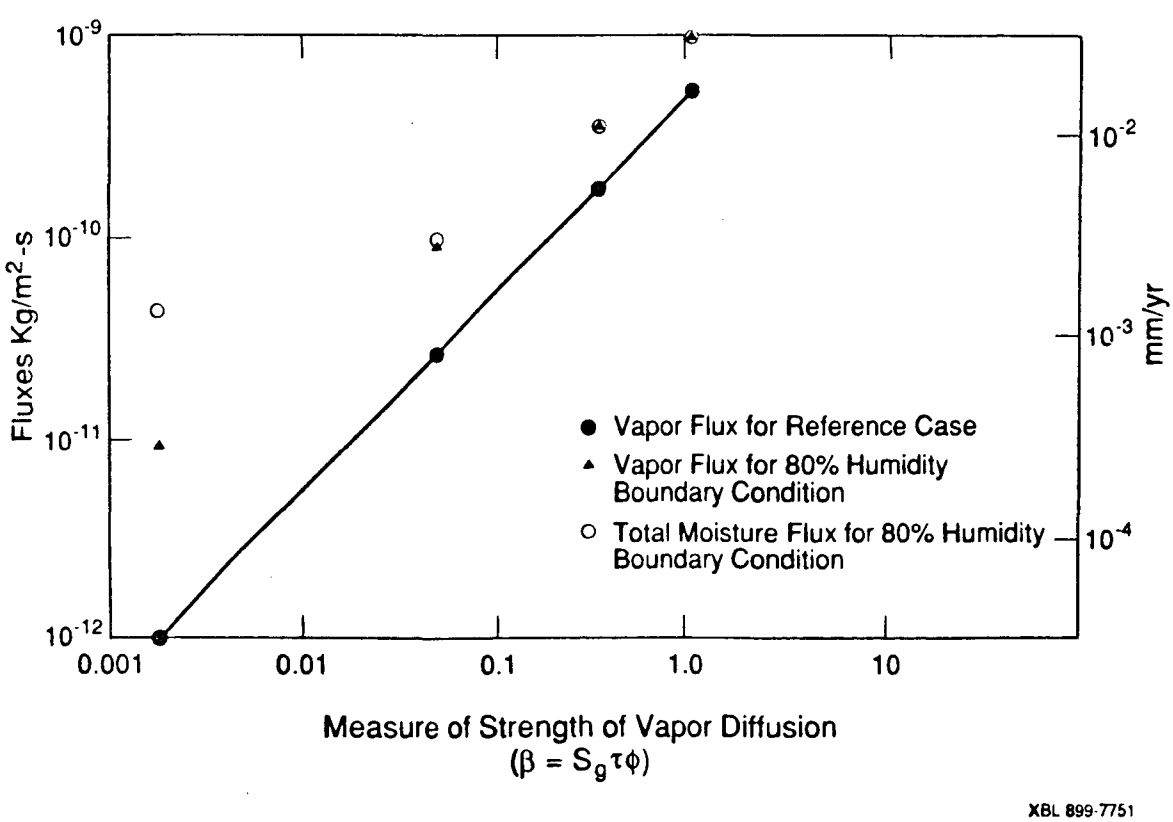

Figure 2. Fluxes at land surface as a function of vapor diffusion strength.

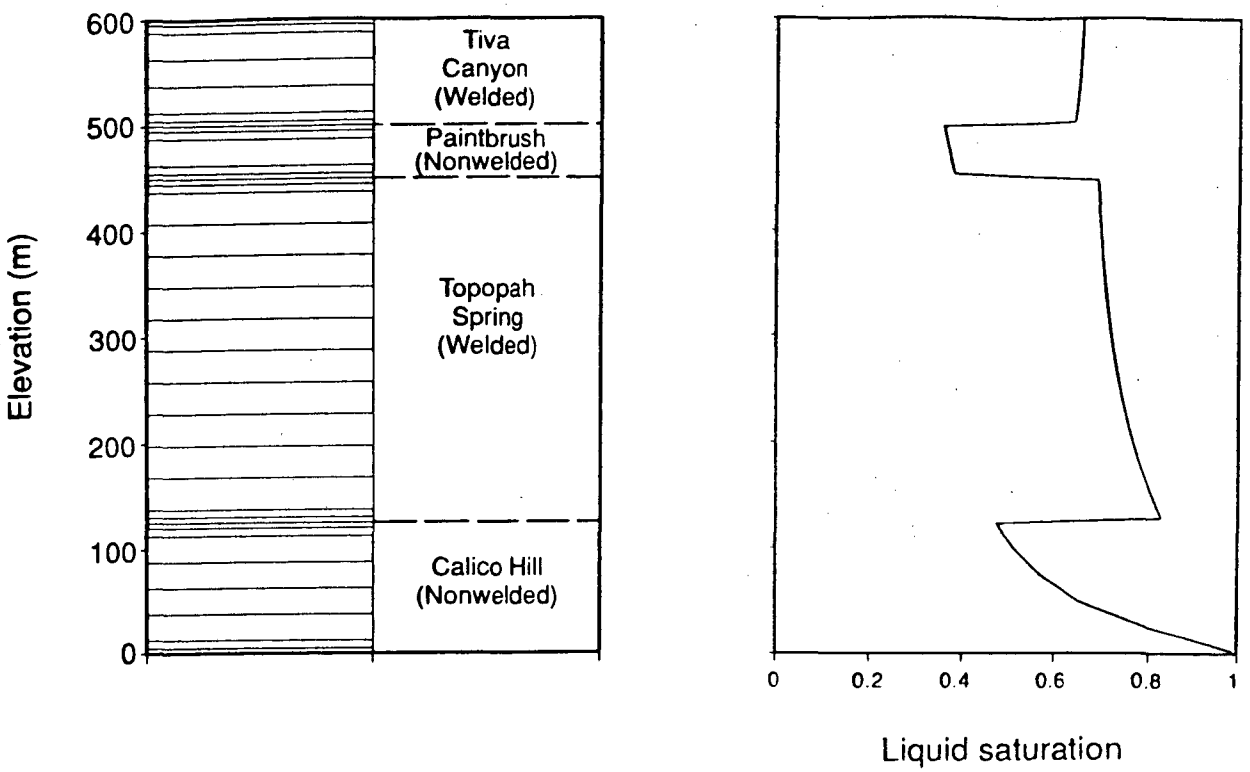

Figure 3. (a) Division of hydrologic units and spatial discretization for numerical simulation and (b) Liquid saturation profile for a layered column of welded and nonwelded tuff.

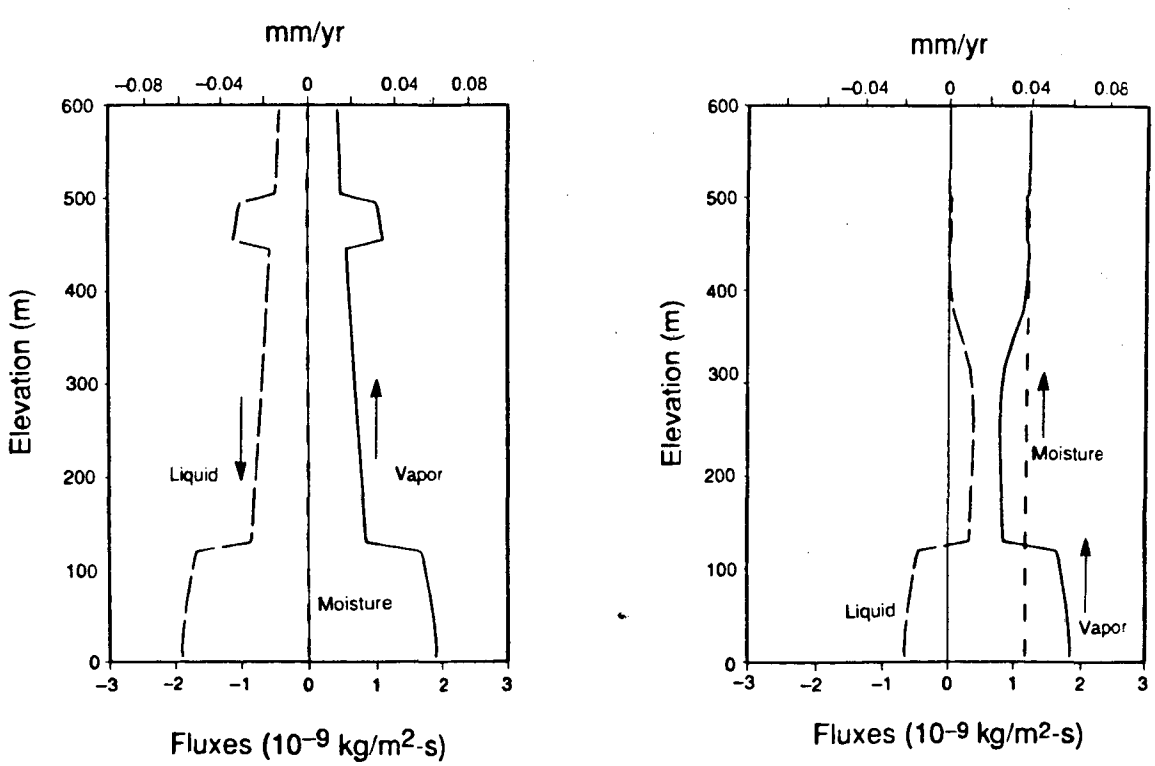

Figure 4. Fluxes for a layered column in (a) the "reference case" and (b) with 50% humidity boundary condition imposed. Vapor diffusion strength is $\beta = 1$.

SAND90-1071C

Phasic Pressure Difference Effects In Two-Phase Flow For Dissolved Gas Exsolution*

by
Stephen W. Webb[1] and John C. Chen[2]

INTRODUCTION

Two-phase flow in porous media exists at the Waste Isolation Pilot Plant (WIPP) in the salt surrounding the repository. Under undisturbed conditions, the salt is probably brine saturated. However, dissolved gases are expected to come out of solution as the brine pressure decreases due to mining activities. The pressure in the gas bubbles will be much greater than that in the brine due to surface tension effects.

The pressure difference between the phases is traditionally based on a capillary pressure curve. However, this relationship is not appropriate for the case of dissolved gas coming out of solution. The capillary pressure curve is a measure of the pressure difference between the liquid in the porous medium and gas at the boundary; it is not a measure of the pressure difference between the fluid and trapped gases. The difference between these two curves is illustrated in Figure 1. The capillary pressure curve is especially appropriate at low liquid saturations where the gas phase is the continuum. The gas exsolution pressure curve is appropriate for trapped gas bubbles at high liquid saturations (low gas saturations) where the liquid phase is the continuum. As can be seen in Figure 1, the two curves are applicable at opposite ends of the liquid saturation scale and have opposing shapes.

Similar problems exist in solution-gas-drive reservoir simulations where dissolved gas comes out of solution and in the wetting and drying cycles of a porous medium where gas can become trapped. No study of the phasic pressure difference for solution-gas-drive reservoirs has been found. However, for the trapped gas case, the recognition that the trapped gas exists at a higher pressure than the gas pressure used for the capillary curve has been recognized for a long time (Peck, 1960; Chahal, 1964). Recent experimental results of Stonestrom and Rubin (1989a, 1989b), who measured trapped gas fractions and relative permeabilities for wetting and drying cycles, indicate that trapped gas can occupy a considerable fraction of the pore space (up to 10% or more).

MODEL DEVELOPMENT

In order to evaluate the effects for the WIPP, a preliminary model for the phasic pressure difference between the gas coming out of solution (gas exsolution) and the liquid phase has been developed. The phasic pressure difference can be written as

$$\Delta P = P_{bub} - P_{brine} = \frac{2\,\sigma}{r_e}. \qquad (1)$$

1 - Sandia National Laboratories, Albuquerque, NM.
2 - Lehigh University, Bethlehem, PA.

* This work is sponsored by the U. S. Department of Energy under Contract No. DE-AC04-76-DP00789.

Relating r_e to the amount of gas present and assuming that the gas is in a constant number of equal size spherical bubbles (obviously a very simple analysis),

$$S_g \ \alpha \ V_{gas} \ \alpha \ r_e^3 \tag{2}$$

$$\Delta P \ \alpha \ r_e^{-1} \ \alpha \ S_g^{-1/3} = C \ S_g^{-1/3}. \tag{3}$$

In order to evaluate the proportionality constant, the conditions at incipient formation of a gas continuum from a fully liquid saturated condition, or the mobile gas fraction, have been used. The capillary pressure at this condition is commonly called the breakthrough pressure (Dullien, 1979), so

$$C = \Delta P \ S_g^{1/3} = P_{br} \ S_{g,mob} \tag{4}$$

and

$$\Delta P = P_{bub} - P_{brine} = P_{br} \left(\frac{S_{g,mob}}{S_g} \right)^{1/3} \tag{5}$$

where P_{br} and $S_{g,mob}$ are the breakthrough pressure and the mobile gas saturation, respectively. The conditions of interest in the present application are those in the halite surrounding the WIPP repository. According to Davies (1990a, 1990b), the best estimate intrinsic permeability is 10^{-21} m^2 with an approximate breakthrough pressure of 10. MPa, and the mobile gas saturation value is 0.20. The threshold pressure referred to by Davies (1990a) is the same as the breakthrough pressure discussed above and is equivalent to a 0.016 μm pore radius. Based on these values, the phasic pressure difference is given by

$$\Delta P = 5.85 \ S_g^{-1/3} \ \text{MPa}. \tag{6}$$

This relationship is obviously a major simplification of the actual process, but it should give qualitative results.

The above relationship relates the phasic pressure difference to the local saturation. However, there are additional physical limits on the actual bubble pressure. The total pressure in the bubble is the sum of the gas and vapor pressures, or

$$P_{bub} = P_{gas} + P_{vap}. \tag{7}$$

The maximum gas pressure in the bubble is the pressure at which the liquid is saturated with dissolved gas. For the WIPP, an upper bound pore pressure is approximately 15 MPa (Nowak, et al., 1988). For the present analysis, the liquid will be assumed to be saturated with dissolved gas at this pressure.

As stated above, the bubble pressure consists of the gas pressure plus the vapor pressure. Unlike the gas pressure, the vapor pressure is affected by the presence of the curved bubble surface and by the presence of dissolved gas in the liquid as discussed by Ward, et al. (1970). However, in the present situation, the saturation vapor pressure at 30°C is only 4.2 kPa, or 0.0042 MPa, which is negligible compared to the maximum gas pressure value of 15 MPa. Therefore, any vapor pressure lowering effects due to curved surfaces or dissolved gas will be neglected.

EVALUATION

One of the more important parameters in the performance assessment for the WIPP is the brine flow rate into the repository since it affects the rate of gas generation in the repository and is the vehicle for radionuclide transport. The effect of this phasic pressure difference is illustrated by computation of the 1-D radial brine inflow rate to an isolated tunnel with a 4.5 m radius. This configuration is a simplification of a reference waste disposal room in the WIPP and has been used for earlier brine inflow rate studies (Nowak, et al., 1988). Two limiting cases for brine inflow are no dissolved gas (the smallest possible gas volume) and brine saturated with dissolved gas assuming equal phasic pressures (the maximum gas volume). Note that equal phasic pressures is the default model in the TOUGH code. Between these two cases is the situation where the phases are at different pressures. The phasic pressure difference will be evaluated by the present model. This analysis of the brine inflow rate has been performed by a modified version of the TOUGH code (Pruess, 1987). The maximum bubble pressure is the dissolved gas saturation value (15 MPa) plus the local vapor pressure; if a lower pressure is calculated by TOUGH, that value is used. The parameters used in the analysis are summarized in Table 1. A constant capillary pressure was used to eliminate this effect as a driving force for flow. The Sandia functions (Pruess, 1987) were used for the relative permeability to include the effect of zero gas relative permeability below 20% gas saturation. In addition to the parameters given in Table 1, the absolute error convergence criteria, RE2, was decreased from its default value of 1.0 to 1.E-4 in order to more efficiently resolve the dissolved gas exsolution.

The results of this analysis are presented in Figure 2. This figure presents the ratio of the cumulative brine inflow for two-phase conditions to the total brine inflow for the case of no dissolved gas. For the case of equal phasic pressures, which is the default model in TOUGH, the cumulative brine inflow can be up to 2.1 times the value with no dissolved gas. Note that in this case, the mobile gas saturation of 20% is reached late in the simulation at 3.9×10^9 seconds (120 years). Before this time, the gas stays in place in the salt. If the present phasic pressure difference model is used, the cumulative brine inflow is only up to 1.5 times the no dissolved gas case, or less than half the increase seen for equal phasic pressures. Gas flow does not occur in this case as the local gas saturation value is always significantly below the mobile gas saturation value. Thus, the influence of phasic pressure difference can be significant on the integrated brine inflow rate for the WIPP.

Table 1
Problem Parameters

Problem Geometry	1-D Radial
Problem Fluids	Water, Air
Repository Conditions	
Radius	4.5 m
Pressure	0.1 MPa
Gas Saturation	1.0
Salt Conditions	
Porosity	0.01
Permeability	10^{-21} m^2
Initial Pressure	15 MPa
Gas Saturation	0.0 (All Brine)
Dissolved Gas	Saturated
Compressibility	Incompressible Matrix
Capillary Pressure	Constant
Relative Permeability	Sandia functions λ=0.45, S_{lr}=0., S_{ls}=0.8

SUMMARY AND CONCLUSIONS

In the salt surrounding the WIPP repository, two-phase flow may exist due to dissolved gas exsolution. Due to surface tension effects, these two phases may exist at significantly different pressures. Based on a simplified phasic pressure difference model, this effect has been evaluated using a simplified repository model. For the case of brine saturated salt, exsolution of dissolved gas may increase the cumulative flow rate into the repository by a factor of 2.1 if equal phasic pressures are assumed; note that equal phasic pressures are assumed in TOUGH. If the current phasic pressure difference model is used, the integrated brine inflow only increases by a factor of 1.5, or less than half of the increase for the equal phasic pressure case. Thus, the phasic pressure difference effect may be significant for brine inflow into the WIPP.

REFERENCES

Chahal, R. S. (1964), "Effect of Temperature and Trapped Air on the Energy Status of Water in Porous Media," Soil Sci., 104(3), 174-180.

Davies, P. (1990a), "Evaluation of the Role of Threshold Pressure in Controlling The Flow of Waste-Generated Gas into the Bedded Salt Surrounding the WIPP Repository," SAND Report in preparation.

Davies, P. (1990b), personal communication, June 29, 1990.

Dullien, F. A. L. (1979), Porous Media Fluid Transport and Pore Structure, Academic Press, New York.

Nowak, E. J., D. F. McTique, and R. Beraun (1988), "Brine Inflow to WIPP Disposal Rooms: Data, Modeling, and Assessment," SAND88-0112.

Peck, A. J. (1960), "Change of Moisture Tension With Temperature and Air Pressure, Theoretical," Soil Sci., 89(6), 303-310.

Pruess, K. (1987), "TOUGH User's Guide," NUREG/CR-4645, SAND86-7104, LBL-20700.

Stonestrom, D. A., and J. Rubin (1989a), "Water Content Dependence of Trapped Air in Two Soils," Water. Resour. Res., 25(9), 1947-1958.

Stonestrom, D. A., and J. Rubin (1989b), "Air Permeability and Trapped-Air Content in Two Soils," Water. Resour. Res., 25(9), 1959-1969.

Ward, C. A., A. Balakrishnan, and F. C. Hooper (1970), "On the Thermodynamics of Nucleation in Weak Gas-Liquid Solutions," Trans. ASME, J. Basic Eng., 695-704.

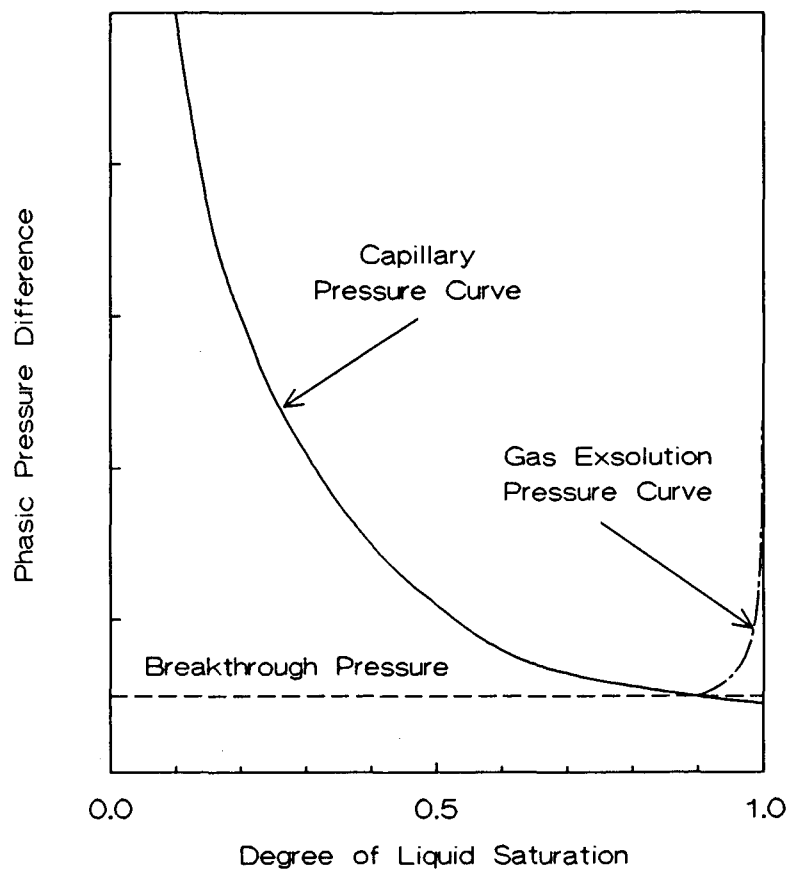

Figure 1 Phasic Pressure Difference Curves

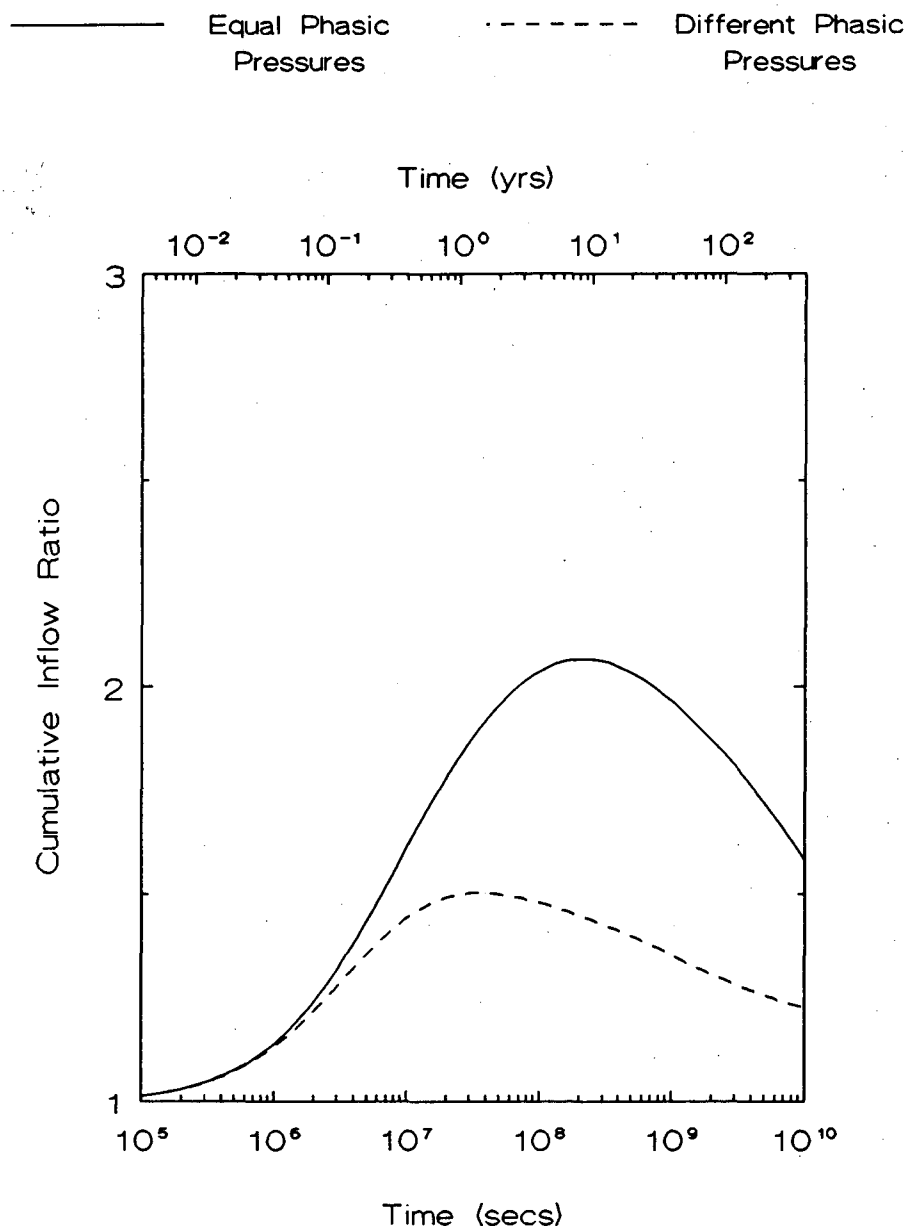

Figure 2
Ratio of Cumulative Brine Inflow
With and Without Dissolved Gas

Verification of TOUGH2 Against a Semianalytical Solution for Transient Two-phase Fluid and Heat Flow in Porous Media

Christine Doughty and Karsten Pruess
Earth Sciences Division
Lawrence Berkeley Laboratory

Introduction

A semianalytical solution for transient two-phase fluid and heat flow in a uniform porous medium surrounding a constant-strength linear heat source has been developed, using the similarity transformation $\eta = r/\sqrt{t}$ to convert the governing equations from partial differential equations to ordinary differential equations. Although the similarity solution requires a simplified geometry, it incorporates all the two-phase fluid and heat flow processes present in the numerical model TOUGH [*Pruess*, 1987], including non-linear thermophysical fluid and material properties.

The solution has been applied to partially saturated porous media initially at temperatures well below saturation temperature. At early times, heat transfer from the heat source is primarily conductive, but as temperature increases to near the saturation temperature, vaporization of liquid phase and convective heat transport of gas-phase flow away from the heat source become important. Capillary forces drive a backflow of liquid phase toward the heat source, setting up a counterflow known as a heat pipe. As time progresses the heat pipe moves away from the heat source, leaving a gas-phase zone where heat transfer is again primarily conductive.

This complex flow pattern provides a rigorous test of many of the capabilities of TOUGH and of a more recent successor code, TOUGH2. Comparisons to date have shown excellent agreement between TOUGH2 and the similarity solution for a variety of conditions. Additionally, much insight has been gained by comparing the numerical and semianalytical approaches to solving this problem.

The primary motivation for the development of the similarity solution is the need to study conditions that might develop within and around the proposed geologic repository for high-level nuclear waste at Yucca Mountain, Nevada, which would be located in a partially-saturated, highly-fractured volcanic formation. In this application, a string of cylindrical waste canisters is modeled as a linear heat source. The similarity solution may be applied to study heat and mass transfer for a variety of other heat sources, such as buried power-transmission cables, volcanic dikes, agricultural root-zone heating operations, or underground thermal energy storage systems.

Physical Processes

The conditions surrounding a waste canister at some time after emplacement are shown schematically in Figure 1. In the heat-pipe region, heat transfer is primarily convective. Near the heat source liquid water vaporizes, causing pressurization of the gas phase and gas-phase flow away from the heat source. The water vapor condenses

in cooler regions away from the heat source, depositing its latent heat of vaporization there. This sets up a saturation profile, with liquid saturation increasing away from the heat source. The saturation gradient drives the backflow of the liquid phase toward the heat source through capillary forces. The liquid then vaporizes again and repeats the cycle. This convective heat transfer is very efficient compared to conduction, so it occurs under nearly isothermal conditions. In contrast, in the conductive regions large temperature gradients exist, so the length of the heat pipe strongly influences the temperature conditions at the canister. The transient liquid- and gas-phase flows are subject to highly nonlinear relative permeability effects, and fluid properties depend in nonlinear fashion on temperature and pressure.

Mathematical Model

When gravity effects are neglected and the heat source is considered to be infinitely long, the system has a one-dimensional radial symmetry. For an infinite homogeneous medium, with uniform initial conditions, surrounding a heat source of constant (time-independent) strength, the coupled partial differential equations governing fluid and heat flow can be transformed into simpler ordinary differential equations through the use of a similarity variable, $\eta = r/\sqrt{t}$. This change of variable is known as the Boltzmann transformation in heat conduction problems. It has been applied to the thermohydrologic behavior of geologic media by *O'Sullivan* [1981], who used it to analyze geothermal well-test data. Other researchers also have used the similarity concept for this purpose, but limited themselves to simplified thermodynamic relationships to allow quasi-analytic solutions.

Following *O'Sullivan* [1981], we consider the fully non-linear problem with realistic thermodynamic relationships, which requires a numerical integration of the coupled differential equations. The present work differs from O'Sullivan's treatment in that the mass flux boundary condition at $r = 0$, appropriate for geothermal production or injection wells, is here replaced by a heat flux boundary condition. Furthermore we include capillary pressure, heat conduction effects, and an air component. These are unimportant for the geothermal well test problem, but are essential for the heat-driven problem in a partially saturated medium considered here.

After the similarity transformation, the problem is posed as a set of six coupled first-order nonlinear ordinary differential equations, for six unknowns: pressure, temperature (or saturation), air partial pressure, heat flux, mass flux of water, and mass flux of air. Details of the mathematical derivation are given in *Doughty and Pruess* [1990]. Solution of the equations is straightforward in principle, by numerically integrating from $\eta = 0$ to $\eta = \infty$, but in practice several complications arise that require special numerical techniques. One difficulty is posed by the nature of the boundary conditions, which specify the value of some variables at $\eta = 0$ and others at $\eta = \infty$; thus no complete set of starting values is available for integration. The solution to this problem is to use an iterative integration scheme, known as the shooting method [*Press et al.*, 1986]. At the lower limit of the integration values are guessed for the missing boundary conditions, and the numerical integration is carried out. At the upper limit of the integration, the values of the variables are compared to the specified boundary conditions. A Newton-Raphson iteration is used to find improved values for the missing boundary conditions at $\eta = 0$ and the integration is repeated. This

procedure continues until the value of each variable at $\eta = \infty$ matches the specified boundary condition there. A second complication arises from the need for a different set of primary variables depending on phase conditions. Under single-phase conditions pressure, temperature, and air partial pressure constitute a set of primary variables, while under two-phase conditions saturation replaces temperature, which depends on pressure and saturation. Thus the integration procedure must keep track of the phase conditions and make a change of primary variables at phase-change points.

Illustrative Results

The boundary and initial conditions and the material properties for a sample problem comparing TOUGH2 and the similarity solution are shown in Table 1. The boundary conditions represent a "closed hole" or backfilled waste canister; that is, there is no water or air flow at the canister ($Q_w = Q_a = 0$). Heat source strength is specified by the variable Q_e. For the most part, the parameters in Table 1 are typical of the Yucca Mountain site, with the exception that intrinsic permeability has been increased by a factor of 10,000 and capillary suction decreased correspondingly by a factor of $\sqrt{10{,}000} = 100$ to create a problem that conveniently illustrates some interesting features of the solution. Neither change is necessary for either TOUGH2 or the similarity solution to work in general. Figure 2 shows TOUGH2 results superposed on the output of the similarity solution. The agreement is excellent. Details of the TOUGH2 calculation will be described below, following a description of some of the general features of the solution. The horizontal axis is $z = \ln(\eta) = \ln(r/\sqrt{t})$, so these profiles may be viewed as spatial profiles for a given time, with radial distance increasing from left to right, or a time sequence for a given point in space, with time increasing from right to left. Figure 2a shows temperature, pressure, air-mass-fraction, and liquid-saturation profiles. The large linear temperature gradient in the single-phase gas zone ($z < -8.5$) indicates that heat transfer is conduction-dominated there. The more gradual temperature decline for $-8.5 < z < -8.0$ indicates that convective heat transfer, the heat-pipe process, accounts for much of the heat transfer in this region, while for $z > -8$ conduction again dominates. The sharp air-mass-fraction profile that coincides with the outer edge of the heat pipe illustrates how the heat pipe effectively purges the near-canister region of air. Figure 2b shows heat-flow and water-flow profiles; at this scale air flow is too small to see. Mass flows are largest in the heat-pipe region, where a countercurrent flow of liquid and vapor is seen. Total water flow, Q_w, the sum of liquid and vapor flows, $Q_w = Q_l + Q_v$, is positive, but quite small by comparison. In the region beyond the heat pipe ($z > -8$) Q_w is also positive; this net flow away from the heat source arises because the vapor forming near the heat source is much less dense than the liquid water it replaces.

A one-dimensional radial mesh with 108 elements, the 'fine mesh', was used for the TOUGH2 calculation shown in Figure 2. The mesh spacing is nonuniform, with finest spacing (0.03 m) used where the similarity solution predicts sharp gradients. The TOUGH2 calculation was carried out for 6.3 years, requiring 800 time steps and 8.5 minutes of CPU time on the Cray X-MP at the National Energy Research Supercomputer Center at Lawrence Livermore National Laboratory.

In addition to the calculation shown in Figure 2, two additional TOUGH2 runs were made for this problem, using different discretizations in order to study mesh

effects. These meshes were designed with steadily increasing spacing, to reflect the radial geometry of the problem, but do not account for the details of the solution, as does the fine mesh. The 'medium mesh' has 122 elements, with a minimum mesh spacing of 0.10 m, and the 'coarse mesh' has 121 elements, with a minimum mesh spacing of 0.30 m. The results of all three TOUGH2 runs are shown in Figure 3, indicating that except at the inner edge of the heat pipe, all three meshes give identical results. However, the length of the heat pipe, slightly increasing for the coarser meshes, has a strong effect on temperature conditions at the heat source so it may be important to get an accurate solution there. A 4-year calculation period requires 510, 226, and 99 time steps for the fine, medium, and coarse meshes, respectively. Because the meshes all have roughly the same number of elements, the computation time scales approximately linearly with the number of time steps. The use of the similarity solution to optimize the mesh for the TOUGH2 calculation illustrates the useful interaction of numerical and semianalytical approaches to the problem.

Current Work

Several new features that are included in TOUGH2 have recently been added to the similarity solution: vapor pressure lowering, enhanced vapor diffusion from pore-level phase change effects, and Knudsen diffusion using the Klinkenberg *b* factor. Additionally, the capability to use an effective continuum to represent a fractured/porous medium has been added, which is necessary for a realistic treatment of the Yucca Mountain site. TOUGH2 calculations including these new features will be verified against the similarity solution in the near future.

Acknowledgements

This work was carried out under U.S. Department of Energy Contract No. DE-AC03-76SF00098, administered by the DOE Nevada Office, in cooperation with Sandia National Laboratories, Albuquerque, New Mexico, and was supported in part by the Director, Office of Energy Research, Office of Basic Energy Sciences, Engineering and Geosciences Division.

References

Doughty, C. and Pruess, K., 1990. A similarity solution for two-phase fluid and heat flow near high-level nuclear waste packages emplaced in porous media. In press, *Int. J. Heat Mass Transfer.*

O'Sullivan, M. J., 1981. A similarity method for geothermal well test analysis. *Water Resour. Res.* 17(2), 390-398.

Press, W. H., Flannery, B. P., Teukolsky, S. A., and Vetterling, W. T., 1986. *Numerical Recipes: The art of scientific computing.* Cambridge University Press, New Rochelle, New York, Ch. 16.

Pruess, K., 1987. TOUGH user's guide. Rep. NUREG/CR-4645, Nuclear Regulatory Commission, Washington, D.C. (Also avail. as Lawrence Berkeley Laboratory Report LBL-20700.)

van Genuchten, M. Th., 1980. A closed-form equation for predicting the hydraulic conductivity of unsaturated soils. *Soil Sci. Soc. Am. J.* 44, 892-898.

Table 1. Specifications for the problem shown in Figures 2 and 3.

Boundary and Initial Conditions		
TOUGH2	Similarity Solution	
$r=0$, all t	$z=\ln(\eta)=\ln(r/\sqrt{t})=-\infty$	$Q_e=667$ W/m $Q_w=0$ $Q_a=0$
$t=0$, all $r\neq 0$ and $r=\infty$, all t	$z=\ln(\eta)=\ln(r/\sqrt{t})=+\infty$	$P=1$ bar $T=18°C$ $S_l=0.8$

Material Properties			
permeability	20×10^{-15} m^2	thermal conductivity	2 W/m K
porosity	0.10	tortuosity	0.5
density	2550 kg/m^3	binary diffusion strength	2.6×10^{-5} m^2/s
heat capacity	800 J/kg K		

Characteristic Curves [*van Genuchten*, 1980]			
k_{rl}	$\sqrt{S_l^*}\left[1-(1-(S_l^*)^{1/\lambda})^{\lambda}\right]^2$	S_{lr}	9.6×10^{-4}
k_{rg}	$1-k_{rl}$	S_{ls}	1.0
P_c	$-P_0\left[(S_l^*)^{-1/\lambda}-1\right]^{1-\lambda}$	λ	0.45
S_l^*	$(S_l-S_{lr})/(S_{ls}-S_{lr})$	P_0	0.125 bars

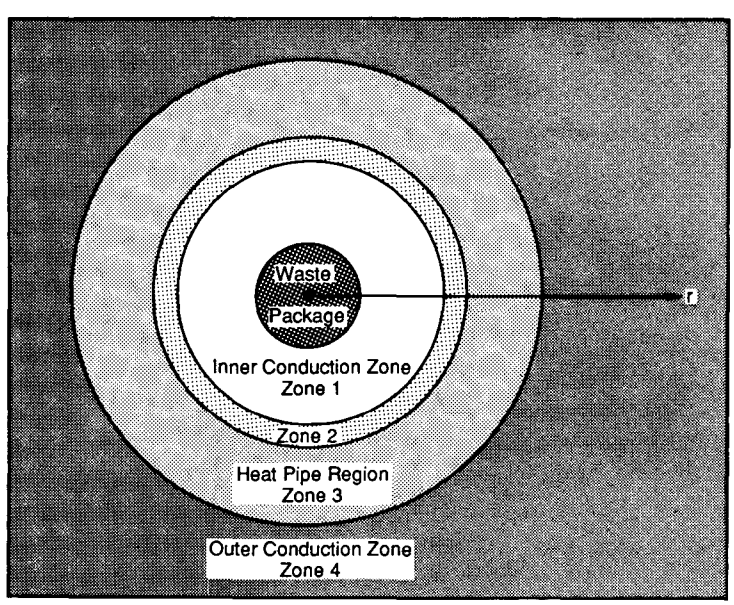

Figure 1. Schematic of the conditions achieved at some time after waste emplacement (not to scale). Water is primarily in the liquid phase in zone 4, because $T<T_{sat}$; two-phase conditions prevail in zones 2 and 3, with $T\approx T_{sat}$; fluid in zone 1 is in the gas phase, with $T>T_{sat}$. In zone 2 the liquid phase is immobile ($S_l<S_{lr}$), while in zone 3 the liquid phase is mobile ($S_l>S_{lr}$), allowing heat-pipe development.

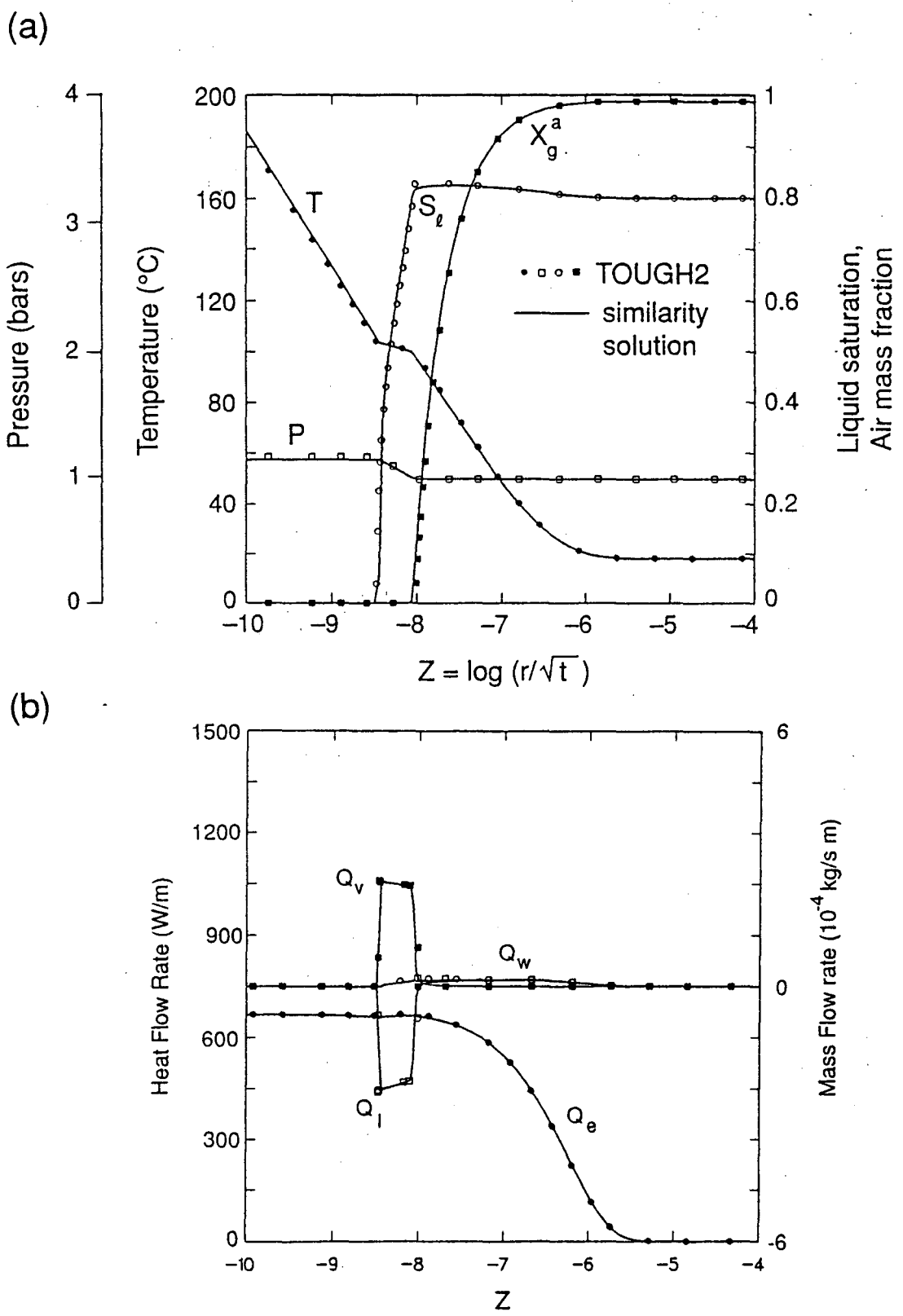

Figure 2. Temperature T, pressure P, air-mass-fraction X_g^a, and liquid-saturation S_l profiles (2a), and profiles of heat flow (Q_e, closed circles), water flow (Q_w, open circles), liquid flow (Q_l, open boxes), and vapor flow (Q_v, closed boxes) (2b), for the problem described in Table 1. For clarity of presentation, not all points calculated with TOUGH2 are shown; those shown include values from profiles at 4 and 6.3 years.

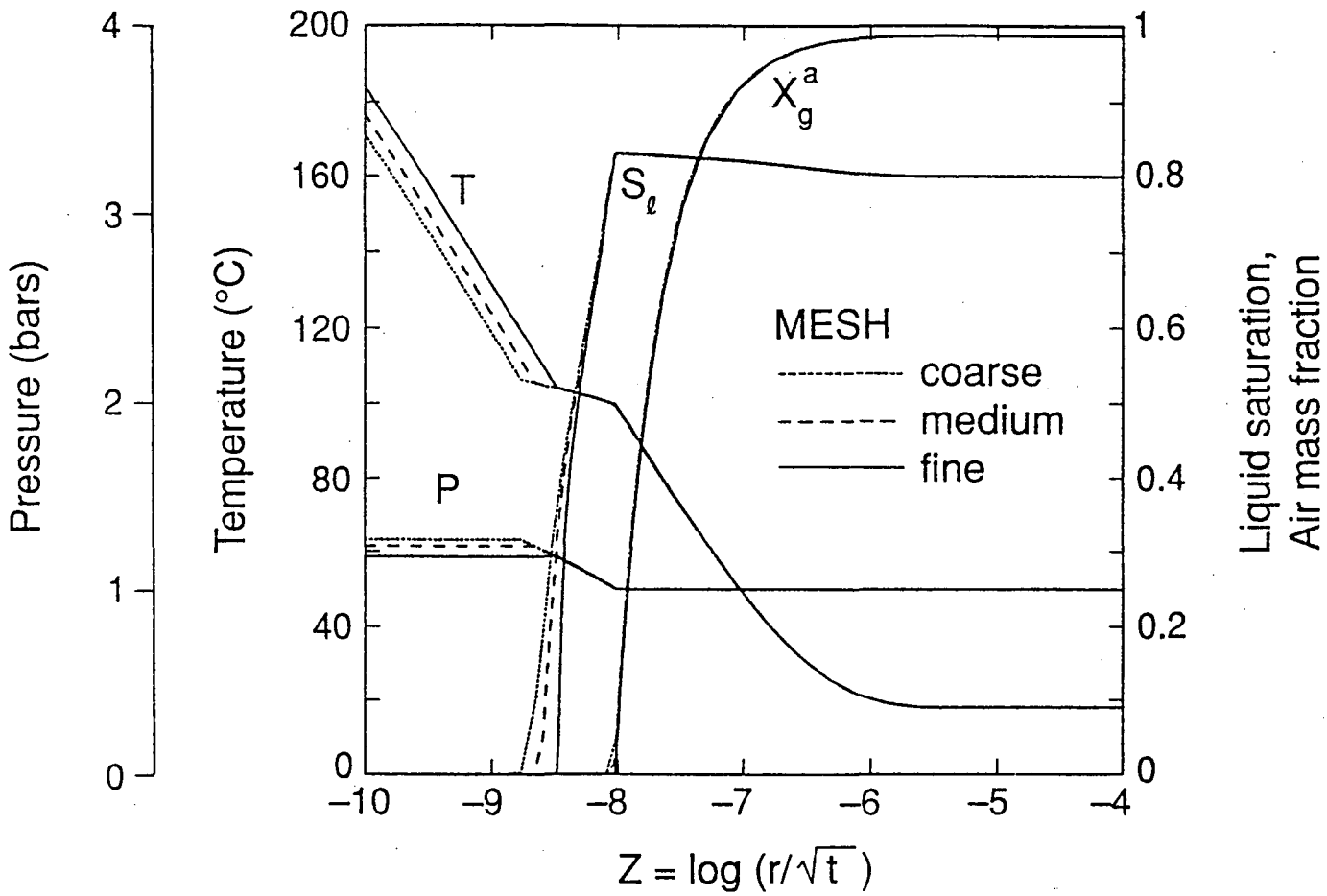

Figure 3. Temperature, pressure, air-mass-fraction, and liquid-saturation profiles calculated using TOUGH2 with three different mesh discretizations. The fine-mesh results are those shown in Figure 2.

TOUGH Users Group Workshop

USE OF TOUGH COMPUTER CODE TO SIMULATE A LABORATORY-SCALE EXPERIMENT

by
Ronald T. Green, Ronald H. Martin and Steve Svedeman
CNWRA, San Antonio, TX.

I. Introduction

Thermohydrological processes as related to a high-level waste repository are investigated by performing non-isothermal experiments on partially-saturated media. The objective is to better understand the processes that contribute to the complex flow phenomena expected to be present close to buried high-level waste. An effort will be made to see if the observed results can be simulated by the TOUGH code.

Presented in this paper are the preliminary results of the laboratory experiments and numerical simulations performed using a modified version of the TOUGH code. The intention of performing the simulation is to evaluate the theory incorporated into the TOUGH code.

II. Experimental Setup

The laboratory experimental apparatus consisted of two differently-sized and planar-shaped plexiglass test chambers constructed with heat exchangers attached to two opposing ends. The media consisted of various mixes of silica glass beads with pre-determined levels of water saturation. Several tests have been conducted with these apparatus, one of which is described as follows.

Test 5 was the last experiment conducted as part of this exercise. The test chamber used for this experiment was a plexiglass-sided container with dimensions of 5.75 in. x 8.15 in. x 0.75 in (Figure 1). The end plates were anodized aluminum of which two were heat exchangers to permit the circulation of fluids at specified temperatures. The side walls of the container were insulated with 0.75 in. thick styrofoam to minimize heat loss and attendant fluctuations in temperature.

The medium for Test 5 consisted of a mixture of equal volumes of 40- and 80-micron diameter glass beads. The beads were mechanically mixed and then saturated to a degree of 60%. After the container was filled halfway with the bead mixture, an artificial fracture was emplaced by sprinkling 160-micron diameter glass beads at an average thickness of 500 microns across the surface of the bead mixture. A uniformly-thick fracture was not possible, however, by the nature in which the larger-sized beads were emplaced. The remaining half of the container was then filled with the pre-mixed, partially-saturated glass beads.

After filling with the glass bead mixture, the container was closed except for two ports located in the side walls. The ports were used for injection of colored dyes into the medium. When not in use, the ports were sealed.

The two vertically-oriented end plates contained the heat exchangers whose temperatures were adjusted to impose a horizontal temperature gradient across the test chamber. The maximum temperature differential between the end plates was 40°C (with the end plates at 20 and 60°C) for a temperature gradient of 2.7°C/cm. The left end plate was initially raised to 60°C, however soon in the experiment the temperature gradient was reversed so that the temperature of the right end plate was set at 60°C and the left at 20°C. This imposed temperature gradient was maintained for the duration of the experiment.

The movement of water moisture was monitored visually (and photographed) by removing the styrofoam insulation for short periods of time and through use of a gamma-ray densitometer that periodically scanned the test container throughout the course of the experiment. The densitometer had a 500 millicurie Cesium-137 source with a Ludlum Instruments NaI detector.

III. Experimental Results

The porosity of the bead mixture medium was calculated to be approximately 34.5%. The hydrological characteristics of the test medium were measured by conducting a positive-pressure, porous-plate experiment (ASTM Method D 2325) on the glass beads. The saturated bead mixture was subject to positive pressures up to 29,400 Pascals (3 meters of water). Because of the relatively coarse nature of the medium, most non-residual moisture was driven from the medium under this pressure. The van Genuchten parameters were determined by regression to the observed data (van Genuchten, 1978). The van Genuchten-Mualem parameters were calculated as follows: alpha = 0.7586; n = 7.3819 and residual saturation = 0.095.

Although densitometer measurements correlated positively with moisture movement observed in the test chamber, moisture content levels in the test chamber measured with the densitometer had insufficient resolution to be used quantitatively. Information gathered during the experiment that proved to be more useful was photographs of the locations of the dyes injected into the medium in order to visibly track the movement of water. Photographs illustrating the locations of the dyes at days 7, 14 and 23 of the experiment are included as Figures 2, 3 and 4.

Test 5 of the separate effects experiments produced results of interest in two areas, both of which are associated with the nature of flow of water through porous media with a simulated fracture. The initial direction of dye flow next to the heated end plate was downward to the bottom of the container then toward the interior of the chamber until the simulated fracture was encountered. As evidenced by the dye, water did not cross the fracture. Rather, it moved upward thus forming what appeared to be a convection cell. The dye became too diluted beyond this point to be useful as an indicator of water flow direction or of the existence of the upper portion of the suspected convection cell.

The second observation of interest in Test 5 was the effect that the simulated fracture had upon flow within the test container. Water appeared to flow up to but not across the fracture during the early stages of the experiment. Late in the experiment, after sufficient water had migrated to the cool side of the test container, the moisture content of the bead mixture medium next to the fracture became sufficiently high so that the relatively larger sized pores of the simulated fracture became saturated and water appeared to traverse the fracture to the other side of the container.

IV. Simulation of Experiment Using TOUGH (CTUFF)

A version of TOUGH that was adapted for use for the NRC (MCTUFF) has been further adapted for use at the CNWRA (CTUFF). MCTUFF has been modified to facilitate data entry and interpretation of the simulation results. Planned modifications include replacing the MA matrix solver with the ITPACK solver developed at the University of Texas-Austin and incorporating table look-ups instead of equation solving in determining the thermophysical properties.

The CTUFF version of TUFF was used in the numerical simulation experiments using a VAX 8700. The results of the CTUFF version were initially compared to published results (Pruess, 1987) for test examples Sam01 through Sam06. No significant difference between the two sets of results was observed.

In particular, it is the intention of these numerical exercises to evaluate the capabilities of TOUGH to simulate the two significant flow patterns observed in Test 5, the apparent formation of a convection cell and the reluctance to flow across the simulated fracture under less-than-saturated conditions. Although the difficulty of simulating these complex processes have been documented (Runchal et al., 1985; studies by Nitao and Buscheck; and Pruess et al. for examples), it is thought that such an assessment will provide valuable insight into the thermohydrological phenomena expected in the geologic medium near high-level waste.

The simulated medium is a vertically-oriented, two-dimensional (8.15 in. by 5.75 in.) grid with variably-sized elements that decrease in width proximal to the vertically-oriented, simulated fracture. The two vertical edges of the container are simulated as constant-temperature (20 and 60°C), no-flow boundaries and the two horizontal edges are treated as adiabatic, no-flow boundaries. The simulated fracture is vertically located approximately half-way between the two vertical edges.

VI. Simulation Exercise Results

The experiment was simulated using the TOUGH code for a period of about 35 days, similar to the duration of the laboratory experiment. Included in this report are liquid and gas saturation levels computed for the last time step of the simulation (Figures 5 and 6). As illustrated in the figures, the simulated movement of water and water vapor responded to the effect of the heated boundaries in a manner similar to what was observed in the lab. A notable exception to this was the moisture movement in the elements modeled as the fracture. Closer inspection of the fracture elements revealed that the simulated fracture had liquid saturation levels greater than adjoining matrix elements in contrast to what would be expected with respect to capillary forces and the relatively larger pore size of the fracture. The possible source for this discrepancy may in the selection of the van Genuchten parameters of the fracture relative to those selected for the matrix. Further refinements in the model are being attempted in an effort to more accurately simulate the above mentioned non-isothermal physical processes, in general, and those processes affected by the fracture, in particular.

VII. References

Pruess, K, TOUGH Users Guide, NUREG/CR-4645, 1987.

Runchal, A.K., B. Sagar, R.G. Baca and N.W. Kline, PORFLO-A Continuum Model for Fluid Flow, Heat Transfer, and Mass Transport in Porous Media: Model Theory, Numerical Methods and Computational Tests., Rockwell International, DE-AC06-77RL01030.

van Genuchten, R., Calculating the Unsaturated Hydraulic Conductivity with a New, Closed-form Analytical Model Research Report 78-WR-08, Water Resources Program, Princeton, 1978.

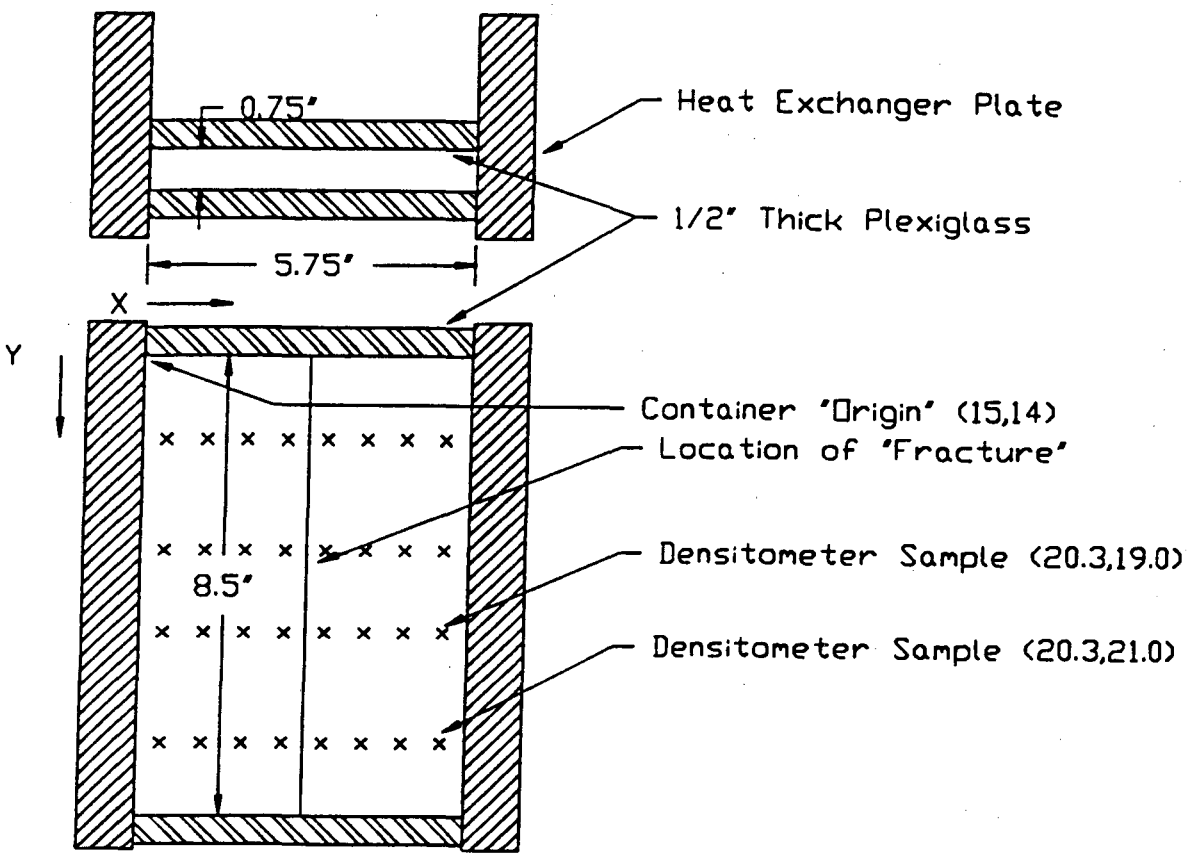

Figure 1 Container used for Test 5.

Figure 2. Photograph of test chamber at day 7 of Test 5.

Figure 3. Photograph of test chamber at day 14 of Test 5.

Figure 4. Photograph of test chamber at day 23 of Test 5.

Liquid Fraction

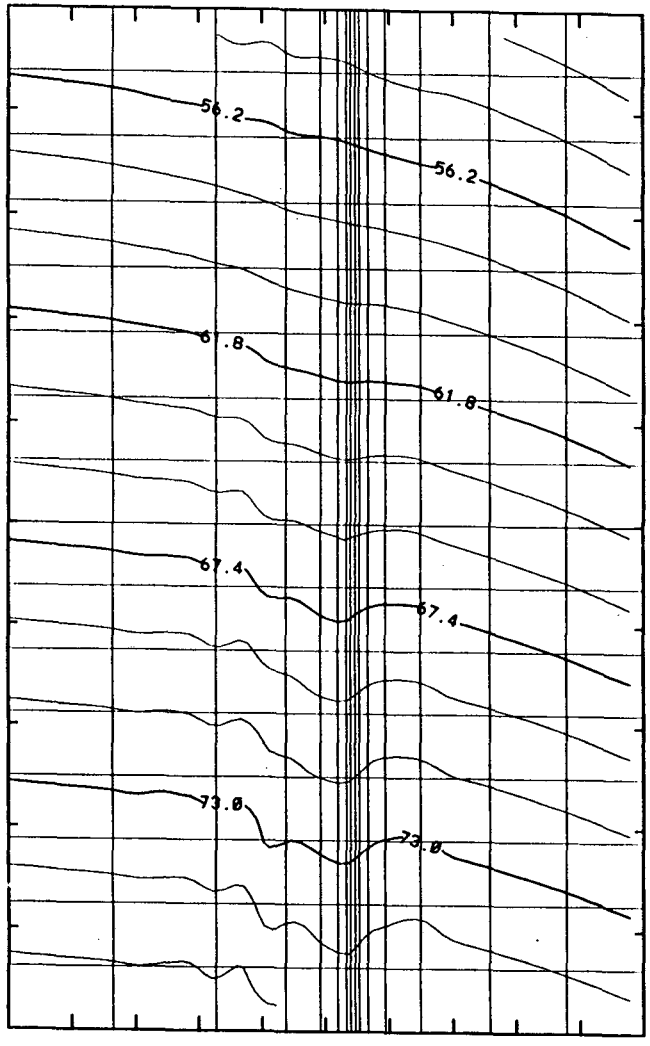

Figure 5 Liquid fraction for Test 5 at 3,000,000 seconds.

Gas Fraction

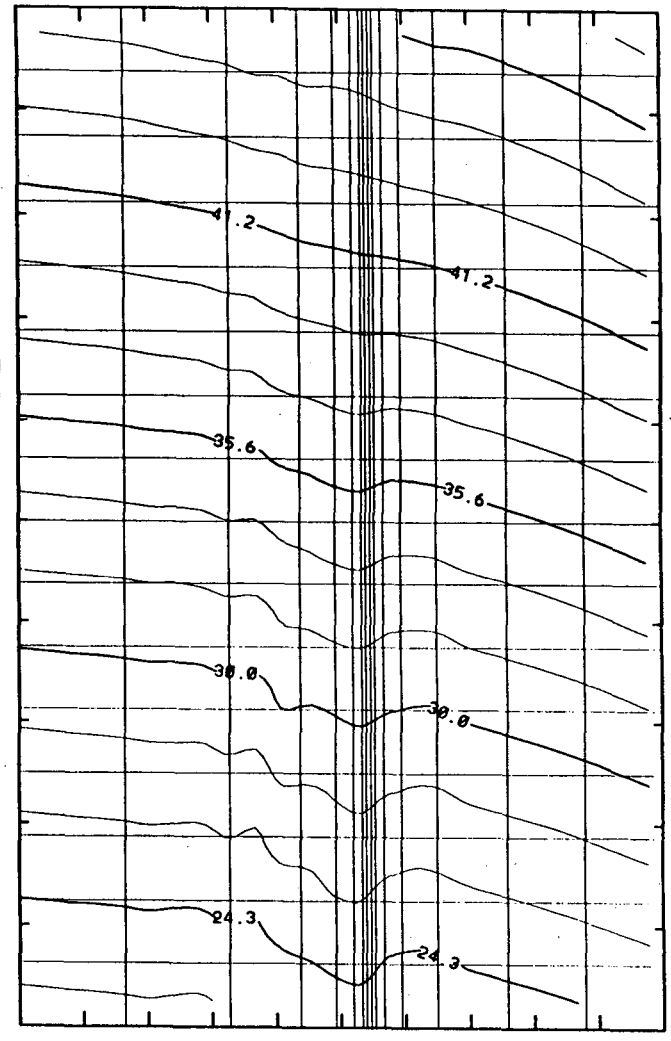

Figure 6 Gas fraction for Test 5 at 3,000,000 seconds.

Two-Phase Flow and Solute Transport Simulations in a Tuff Drillcore

Tim McCartin, Richard Codell, Tom Nicholson US NRC
Todd Rasmussen University of Arizona

INTRODUCTION

The Department of Energy is considering disposing high-level radioactive waste (HLW) in unsaturated, fractured tuff. It is uncertain how heat output from the waste will affect the thermal-hydrologic environment surrounding the waste package and the flow field in vicinity of the repository. The University of Arizona (UAZ) under contract to the Nuclear Regulatory Commission (NRC), has conducted investigative experiments in partially-saturated tuff drillcores to better understand the phenomena that control non-isothermal fluid flow and solute transport.

In addition to the experimental efforts, numerical simulations using the UAZ experimental database are being performed by NRC staff as part of its work under INTRAVAL which is an international project for examining the validity of geosphere transport models in the context of nuclear waste disposal. The UAZ laboratory and field experiments in unsaturated, fractured tuff are one test case in INTRAVAL. NRC staff have simulated a drillcore experiment using the TOUGH program for two-phase flow and an NRC-developed particle tracking routine for solute transport. The results of the simulation analyses are used to assess completeness and consistency in the experimental database and to assist further experimental design.

EXPERIMENTAL DESIGN

The UAZ experiment was designed to examine moisture redistribution and solute movement in response to a thermal gradient along the length of a partially-saturated tuff drillcore (Davies, 1987). The drillcore (diameter of 6.4 cm and length of 12.99 cm), sealed along its length to preclude moisture, vapor, and heat from escaping, was initially wetted to a saturation of 48% by volume with a 875 ppm solution of potassium iodide. The drillcore was orientated horizontally and subjected to a thermal gradient for 32 days. Throughout the experiment a constant temperature of 5 °C was maintained at one end of the drillcore while a constant temperature of 70 °C was maintained at the other end.

During the course of the experiment, measurements of temperature and saturation were made using gamma-ray attenuation at 1 cm intervals along the length of the drillcore. At the end of the 32 day period the drillcore was cut into eight sections of approximately equal length. Solute concentrations were determined in each section using high performance liquid chromatography.

The experimental results are presented in Figures 1 and 2. Following the initial 12 hours of the experiment, the temperature gradient along the drillcore was steady. The final moisture content was higher at the cold end than at the warm end, while the solute distribution showed an opposite relationship.

SIMULATION ANALYSIS OF FLOW

The experiment was performed to investigate a phenomenon rather than to validate a conceptual model, therefore, specific parametric values describing hydrologic and thermal properties of the subject drillcore were not collected. Due to the absence of parametric values specific to the drillcore, parametric values obtained from analysing numerous similar drillcores from the same tuff unit were used (Chuang, 1990). The use of these representative "average" values (see Table 1) served as a starting point with which to examine model sensitivity.

The TOUGH program (Pruess, 1987) was used to analyse model sensitivity to parameters employed to characterize the hydrologic and thermal properties of the drillcore. Local sensitivity (i.e., variation of a single parameter over its perceived range of uncertainty while all other parameters remain at their base case value) was examined for: permeability, binary diffusion coefficient, thermal conductivity, heat capacity, and the shape of the characteristic curves.

The findings of the sensitivity analysis were: 1) saturation in the drillcore was sensitive to the permeability, diffusion coefficient, and the shape of the characteristic curves; 2) saturation in the drillcore was insensitive to the thermal properties (thermal conductivity and heat capacity); 3) temperature in the drillcore was insensitive to all parametric variations attempted; and 4) regardless of which parameter was varied, the simulations were generally characterized by a sharp spatial transition from dry (<1% saturation) to wet (>60% saturation) conditions within the drillcore in contrast to the gradual transition observed in the experiment (see Figure 3). The most interesting aspect of the simulation results was the sharp spatial transition from dry to wet conditions. The reason for this sharp spatial transition is not well understood and is being studied further. It is worth noting that the effects of heterogeneity and micro-fractures within the drillcore and osmotic forces were not considered. These effects could drastically alter the characteristic curves and thereby significantly affect the simulation results.

SIMULATION ANALYSIS OF TRANSPORT

Results of the two-phase flow simulations described above were used in this analysis to calculate the transport and redistribution of the dissolved tracer which was initially uniformly-distributed throughout the drillcore. A random-walk particle-tracking algorithm (RWPTA) was developed to simulate the movement of solute based on the liquid flux calculated by the TOUGH program. Briefly, the RWPTA model consists of an advective component and a dispersive component (i.e., the result of mechanical mixing and temperature dependent molecular diffusion). It was assumed that all particle movement occured in the liquid phase and that 5,000 particles were sufficient to represent the solute mass.

Due to uncertainty in the parameters characterizing dispersion, three simulations were conducted which included the following combinations of transport phenomena: 1) advection, dispersion, and molecular diffusion, 2) advection and molecular diffusion, and 3) advection. The results (see Figure 4) of the three different simulations were quite similar. Differences between the simulations occur at the ends of the drillcore where the purely-advective model predicts a larger number of particles as compared to the other two

models. The effect of molecular diffusion significantly contributes to solute motion at ends of the drillcore where there exist low velocity zones for liquid water.

A comparison between experimental and simulation results was made of solute concentration for the eight sections measured in the drillcore. Figure 5 shows a comparison of solute amounts predicted with the "advective-dispersive" model averaged over each section and the experimental results. Agreement is qualitatively good, with modeled and measured peaks occurring in approximately the same place. Quantitatively, the experimental values of solute amounts have more pronounced changes than were predicted by the model. It is most interesting to note that the largest quantity of solute occurs in the section adjacent to rather than in the section nearest the high temperature end. This relationship could imply a drying out near the hot end of the drillcore and thus no further movement of solute into the dry section. A drying of the hot end of the drillcore was predicted in the TOUGH simulation but was not observed in the experiment (i.e., a 10 percent saturation was the lowest saturation observed).

CONCLUSIONS AND RECOMMENDATIONS

The TOUGH simulation did not predict the somewhat-linear variation in saturation along the drillcore (see Figure 3). The variation in solute along the length of the drillcore was qualitatively represented using the TOUGH-predicted fluid fluxes with a particle tracking algorithm. The reason for this apparent discrepancy is unclear, although, the behavior at the hot end of the drillcore may be linked to heterogeneity and micro-fractures in the drillcore or osmotic forces. Further simulation based on representative "average" parametric values is not considered useful. However, other experiments being conducted at UAZ are designed to obtain parametric values for the drillcore used in the experiment. Further experiments are also designed to more frequently, in time, measure the saturation and attempt to non-destructively measure solute movement during the experiment. These new experiments should provide further information to reduce the uncertainty in the current simulations and allow for a better understanding of flow and transport phenomena during the thermal period of a high-level waste repository.

REFERENCES

Chuang, Y., Haldeman, W.R., Rasmussen, T.C. and Evans, D.D., 1990, Laboratory Analysis of Fluid Flow and Solute Transport Through a Variably Saturated Fracture Embedded in Porous Tuff, U.S. Nuclear Regulatory Commission, Washington, D.C, NUREG/CR-5482.

Davies, B.E., 1987, Water Movement in Nonisothermal Tuff, Master of Science Thesis, Department of Hydrology and Water Resources, University of Arizona, Tucson, Arizona.

Pruess, K., 1987, TOUGH User's Guide, U.S. Nuclear Regulatory Commission, Washington, D.C., NUREG/CR-4645.

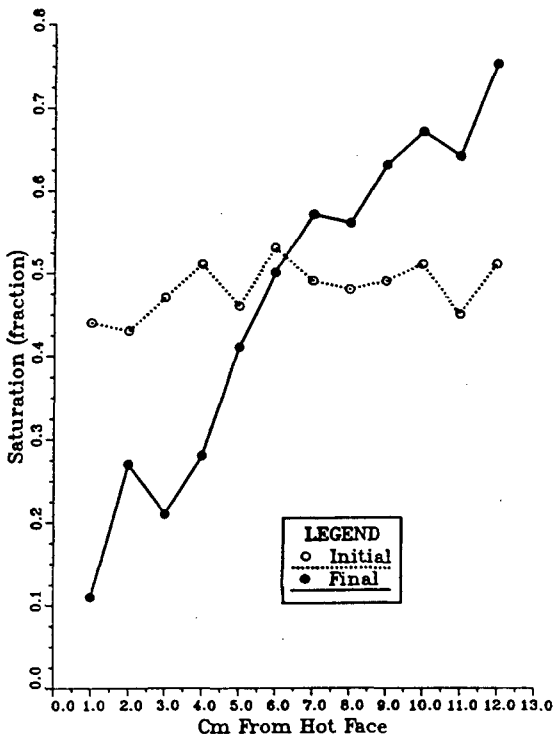

Figure 1. Initial and final saturations measured along the length of a tuff drillcore subjected to a temperature gradient for 32 days.

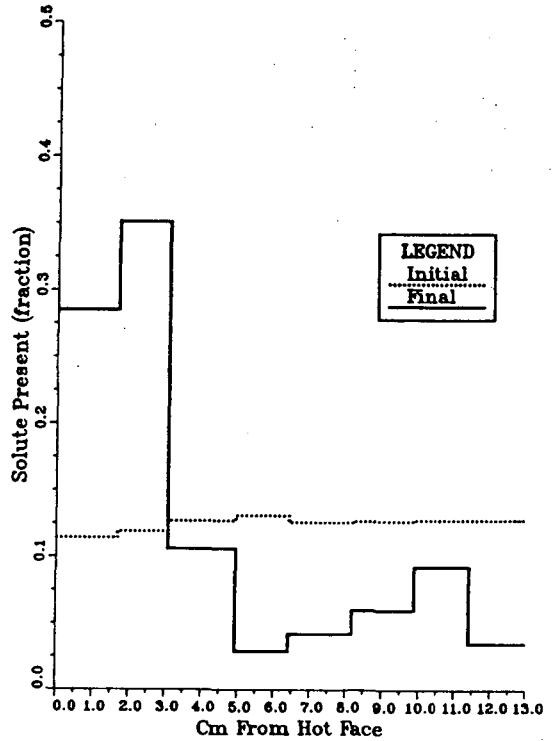

Figure 2. Initial and final solute amounts per length as determined from the laboratory analysis of a tuff drillcore subjected to temperature gradient for 32 days.

Table 1. Parametric values and their ranges used for simulating two-phase flow using the TOUGH program and solute movement using a particle tracking routine.

Parameter	Units	Base Case Value	Range
Permeability	m^2	4.0 E-16	4.0 E-14 to 4.0 E-17
van Genuchten fitting parameters;			
1) alpha	1/kPa	.046	.46 to .0046
2) n	---	1.3	1.45 to 1.15
Diffusion Coef. (air/vapor)	m^2/s	2.13 E-5	2.13 E-4 to 2.13 E-6
Specific Heat	J/kg°C	770	790 to 750
Thermal Cond.	W/m°C	2.0	2.2 to 1.8
Porosity	---	.19	------
Dispersion Length	m	.002	------
Diffusion Coef. at 25 °C (solute)	m^2/s	3.6 E-10	------

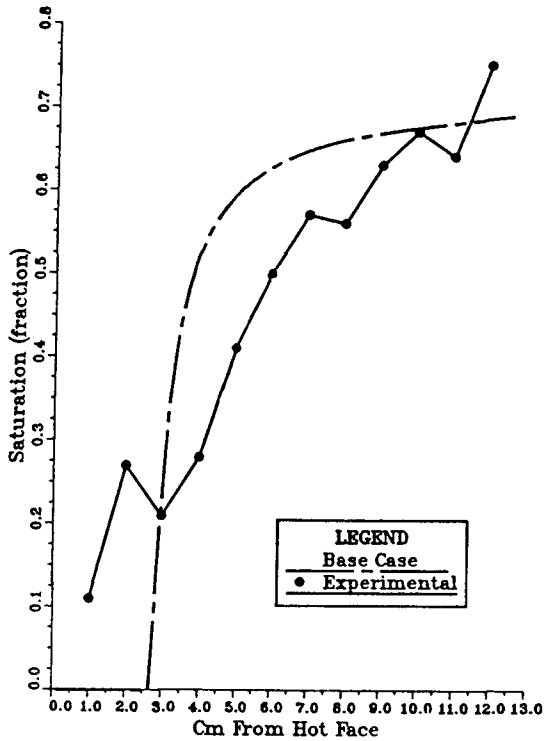

Figure 3. Comparison of measured and simulated final saturations along a tuff drillcore subjected to a temperature gradient for 32 days.

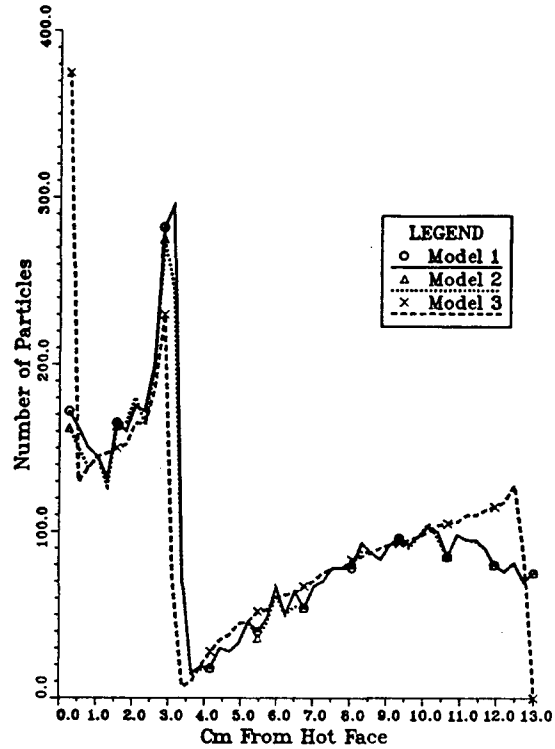

Figure 4. Comparison of final solute amounts predicted using three different models (1 - advection, dispersion and diffusion, 2 - advection and diffusion, and 3 - advection) for solute movement.

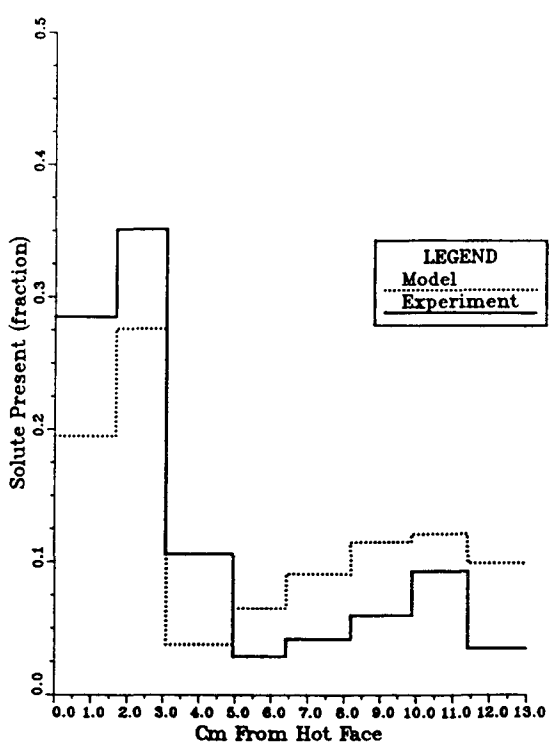

Figure 5. Comparison of experimentally determined and simulated final solute amounts per length for a tuff drillcore subjected to a temperature gradient for 32 days.

Interpretation of Hydraulic Tests in a Two-Phase Flow System Using TOUGH

S. Finsterle [1] and S. Mishra [2]

[1] Laboratory of Hydraulics, Hydrology and Glaciology (VAW),
Swiss Federal Institute of Technology (ETH), Zürich, Switzerland

[2] INTERA Inc., Austin, Texas, USA

This study presents an application of TOUGH for the interpretation of hydraulic tests conducted in a two-phase environment at a potential site for the storage of low and intermediate radioactive wastes in Central Switzerland. Both, a water and a gas injection test was analyzed taking advantage of the two-phase capabilities of the numerical simulator. The parameters obtained by model calibration are compared to standard single-phase solutions.

The TOUGH calculations indicate that single-phase evaluation methods are still applicable for determining the absolute permeability provided an appropriate test sequence is available. Concerning the gas related parameters, sensitivity studies show, that only an integrated mobility can be estimated due to the lack of parameter identifiability.

1. INTRODUCTION

The standard method for determining in-situ hydraulic properties of a permeable feature is to perform a series of hydraulic tests, e.g. constant pressure, constant flow, or pulse tests. The analytical solutions commonly used for analyzing such tests assume that the formation is fully liquid saturated. The presence of a second (gas) phase may affect the hydrogeologic measurements which may lead to errors in the estimation of the hydraulic parameters when using single-phase evaluation methods.

Nagra, the Swiss National Cooperative for the Storage of Radioactive Waste, is investigating the feasibility of various formations as potential host rocks for a repository. At the Oberbauen-stock site which is known to have the potential to contain natural gas (mainly methane), a first phase of field investigations was conducted in 1987 involving a detailed hydraulic testing program [*NTB 88-03*]. In the context of hydrogeologic site characterization, TOUGH is being used for the interpretation of these tests. Three aims are envisaged for the test interpretation:

- Comparison of the absolute permeabilities estimated by using either single-phase or two-phase evaluation methods
- Determination of a set of gas related formation parameters, (e.g. the initial gas saturation, relative permeability and capillary pressure functions), typical for the host rock
- Recommendations on future testing and analysis

In this study we describe the process of parameter estimation using TOUGH as a wellbore simulator. Two tests are analyzed:

- Water injection test: constant pressure water injection followed by pressure recovery
- Gas injection test: sequence of constant rate gas injections followed by pressure recoveries

2. WATER INJECTION TEST INTERPRETATION

Problem specification

A constant pressure water injection test has been selected for analysis because the calculated formation head indicated an abnormal value, potentially resulting from the presence of a free gas phase [*NIB 88-48*] . A change in the mobility might be detected after having created a phase boundary by water injection.

Two packers isolated an interval of 19.1 m. The flow regime was considered to be radially symmetric and horizontal. The formation was represented by 50 grid blocks with exponentially increasing radial distances up to an external radius of 100 m. The well was treated as a single grid block with a radius of 0.48 m and a volume of 0.110 m^3.

Wellbore storage does not affect the response of a constant-pressure test, but does influence the nature of the subsequent pressure recovery response. The wellbore storage coefficient was calculated from the Δp vs. Δt relationship to be 2.5 10^{-9} m^3 Pa^{-1}. From an extrapolation of the late-time pressure falloff data to infinite shut-in time on a Horner graph, the initial pressure was estimated to be 2.8 bars.

We assumed that the activities preceding the test sequence of interest have created a composite system (Figure 1). The formation gas around the borehole has been displaced to residual saturation by drilling fluid invasion. The permeability in this zone may have been altered due to clogging by mud particles. The system is thus conceptualized as consisting of several radially symmetric concentric cylindrical zones, which include (a) the borehole, (b) a skin zone with reduced permeability and at residual gas saturation, (c) an inner zone at residual gas saturation, and (d) an outer zone at initial gas saturation, separated from the inner zone by a phase boundary. In this case, we assumed the inner zone to be coincident with the skin.

Fluid parameters (density, viscosity, and internal energy of liquid water and vapor-air mixtures) are calculated internally by TOUGH [*Pruess*, 1987; *International Formulation Committee*, 1967]. Interval temperature is equal 19°C.

Calibration

Although the first sequence of the test shows some variability of the injection pressure with time, it was modeled as a period of water injection at a constant pressure of 60.0 bars. Borehole history effects were not included in the analysis, as it was believed that the large pressure differential of approximately 55 bars imposed at the borehole have dominated the effects of any background transient events. Instantaneous injection rate was not continuously measured, but was reported as a twice-an-hour estimation obtained from fluid level changes in the surface tank. It was therefore decided to use the total cumulative injected volume as the time-dependent variable of interest to be matched. Pressure data were matched during the recovery period. The following parameters were varied in order to get a visual fit:

- absolute permeability of the skin zone, absolute permeability of the formation
- residual gas saturation in the inner zone, initial gas saturation in the outer zone
- relative permeability functions

After numerous calibration runs, the fit presented in Figures 2a and 2b was regarded as acceptable. In Table 1, the parameters of the TOUGH model are compared to the results of the single-phase interpretation presented in [*NIB 88-48*].

Parameter			NIB 88-48	TOUGH
absolute permeability	k	$[10^{-16}\ m^2]$		
skin zone			2.8	1.3
formation			100.0	5.0
radius of phase boundary	r	[m]	5.0	4.0
porosity	ϕ	[%]	-	3.0
initial pressure	p_i	[bar]	4.1	2.8
initial gas saturation	S_{gi}	[%]	(0.0)	20.0
relative permeability function			-	Grant
residual gas saturation	S_{rg}	[%]	-	5.0
residual liquid saturation	S_{rl}	[%]	-	50.0
capillary pressure function			-	-
wellbore storage coefficient	C_w	$[m^3/Pa]$	-	2.5E-9

Table 1: Best fit parameter sets for water injection test

It is interesting to note that the values obtained for the absolute permeability of the inner zone are quite similar, regardless of the approach used (i.e. single-phase vs. two-phase). However, the agreement between the two estimates can be attributed to the fact that the inner zone is essentially liquid saturated with perhaps some gas at residual saturation. As far as the outer zone permeability is concerned, there is substantial difference by a factor of 20 between the estimates obtained via single-phase and two-phase analysis. Theoretical considerations suggest that the apparent permeability estimated using single-phase conditions can easily be an order of magnitude higher than the actual absolute permeability, if the system is two-phase. The simultaneous flow of liquid and gas can be described by a generalized radial diffusivity equation:

$$\frac{1}{r}\frac{r}{\partial r}\left(r\frac{\partial p}{\partial r}\right)=\frac{\phi c_t}{(k/\mu)_t}\frac{\partial p}{\partial t} \qquad (1)$$

where c_t is the 'total system compressibility' approximated by:

$$c_t \cong c_l \cdot S_l + c_g \cdot S_g \qquad (2)$$

and $(k/\mu)_t$ is the total mobility, equal to the sum of the individual phase mobilities:

$$\left(\frac{k}{\mu}\right)_t = k\left(\frac{k_{rl}}{\mu_l}+\frac{k_{rg}}{\mu_g}\right) \qquad (3)$$

The ratio between the apparent 'single-phase liquid' permeability of the outer zone and the absolute permeability may then be estimated as:

$$\frac{k_{app}}{k}=\left(\frac{k}{\mu}\right)_t\frac{\mu_l}{k}=k_{rl}+k_{rg}\frac{\mu_l}{\mu_g} \qquad (4)$$

The simulator input $S_g = 20\%$, $S_l = 80\%$, $k_{rg} = 19{,}75\%$, $k_{rl} = 80.25\%$, $\mu_g = 1.813\ 10^{-5}$ Pa·s, $\mu_l = 1.026\ 10^{-3}$ Pa·s yields

$$\left(\frac{k_{app}}{k}\right)_{calc}=k_{rl}+k_{rg}\frac{\mu_l}{\mu_g}\cong 12 \qquad (5)$$

Although the actual permeabilities estimated using single-phase or two-phase flow concepts are quite different, they can be easily related via two-phase flow parameters (e.g. relative permeability, viscosity ratio), as shown above.

Thus, the apparent permeability from single-phase analysis, when reinterpreted in terms of two-phase flow properties, is consistent with the absolute permeability obtained from a two-phase analysis. Furthermore, use of a two-phase analysis approach (with TOUGH as a wellbore simulator) allows the estimation of some gas related formation parameters.

As an example of a sensitivity study, Figure 3 shows the impact of an order-of-magnitude change in the formation permeability on the pressure recovery. As a result, the absolute permeability as a very sensitive parameter can be confined within relatively narrow bounds.

Based on our concept, a change of the irreducible gas saturation is combined with a change of the initial gas saturation in the inner zone. No significant differences occur for the injection period, since the upstream weighted mobility of the injecting fluid determines the systems behavior. On the other hand, the recovery period is more sensitive to the presence of residual gas (Figure 4). The lower the gas content in the inner zone and thus the lower the system's compressibility, the faster the pressure recovers due to the higher diffusivity.

3 GAS INJECTION TEST INTERPRETATION

During the Oberbauenstock testing program, a series of constant flow gas (nitrogen) injection tests was performed in a isolated interval of 6.6 m , consisting of the following events:

0.	Borehole history		
1.	Constant rate gas injection 1	Qcr1	(q ≈ 10 g/min)
2.	Pressure recovery 1	Pr1	
3.	Constant rate gas injection 2	Qcr2	(q ≈ 15 g/min)
4.	Pressure recovery 2	Pr2	
5.	Constant rate gas injection 3	Qcr3	(q ≈ 15 g/min)
6.	Constant rate gas injection 4	Qcr4	(q ≈ 30 g/min)
7.	Pressure recovery 3	Pr3	

It is the aim of the calibration process to match the responses of all seven events using a single set of formation and fluid parameters.

Problem specification

The flow regime was considered to be radially symmetric and horizontal. The formation was represented by 50 grid blocks with exponentially increasing radial distances up to an external radius of 50 m. The well was treated as a single grid block with a radius of 0.48 m and a volume of 0.160 m^3 during injection, and 0.040 m^3 during recovery of which 80 % are gas filled.

In general, the diagnostic plots (see [*NIB 88-03L*]) indicate that wellbore storage effects last for a long time. The appropriate wellbore storage coefficient turns out to be very large and - based on the ideal gas law - is most likely indicative of a gas volume in the test interval of at least 128 liters during injection and 32 liters during shut-in recovery. In a log-log plot, a relatively short infinite acting radial flow period is followed by boundary effects. The borehole activities prior to the gas test (including drilling, screening tests and detailed tests) were not modeled explicitly. Hence, the definition of the initial conditions for the gas test is based on the concept, that the preceding test activities might have created a water saturated zone around the borehole leading to a composite model behavior of the gas test responses (see Figure 1). The actual radius of the water saturated zone as well as the gas saturation in the inner and the outer zones are unknown and have to be determined during the calibration process.

Figure 5 presents the best fit between measured and calculated pressures that could be achieved by the variation of the following parameters:

- Absolute permeability of skin zone, absolute permeability of formation
- Relative permeability functions
- Initial gas saturation in the inner zone, initial gas saturation in the outer zone
- Radius of skin zone, radius of phase boundary

Calibration

The maximum pressure during the injection period is controlled by the absolute permeability and the location of the phase boundary. The transition from the wellbore storage dominated to the boundary dominated part of the curve turned out to be difficult to reproduce. While it is relatively easy to obtain a good match for the first injection - falloff period, the modeling of the entire test sequence using one single parameter set turns out to be difficult. This is a consequence of the fact that the gas saturation in the inner zone - which is a very sensitive parameter - is being modified for each injection period by the preceding one. The ratio of the gas saturations across the phase boundary - another sensitive characteristic - is complicated by the smearing of the phase boundary due to the preceding test events. The simplifying moving boundary assumption is not valid. However, it is possible to simulate the significant mechanisms taking place when injecting gas into a composite system.

In Table 2, the parameters of the TOUGH model are compared to the results of a single-phase gas interpretation presented in [*NIB 88-03L*].

Parameter			NIB 88-03	TOUGH
absolute permeability	k	$[10^{-16}\ m^2]$		
skin zone			included	0.2
formation			1.9	2.0
radius of phase boundary	r	[m]	-	1.0
porosity	ϕ	[%]	-	5.0
initial pressure	p_i	[bar]	2.3	2.2
initial gas saturation	S_{gi}	[%]	(100.0)	20.0
relative permeability function			-	Grant
residual gas saturation	S_{rg}	[%]	-	1.0
residual liquid saturation	S_{rl}	[%]	-	50.0
capillary pressure function			-	-
wellbore storage coefficient	C_w	$[m^3/Pa]$	-	≈1.3E-6

Table 2: Best fit parameter sets for gas injection test

The pressure response during the first injection period is very sensitive to the ratio of the initial gas saturation in the inner zone and the irreducible gas saturation (Figure 6). At the beginning of the injection period, gas has to displace the less mobile liquid phase. Due to the lower viscosity of gas, the displacement process is unstable (simulated by using Grant's relative permeability functions) so that portions of the liquid phase is bypassed; the simplifying moving boundary assumption is not valid (Figure 7). Because of the non-linearity of the relative permeability function, even a small increase of the gas saturation in the inner zone establishes a high conductive flow path to the outer zone and the system starts to respond to the formation characteristics of the outer zone with its higher total mobility and lower diffusivity, leading to a pressure stabilization or even pressure decline.

4 DISCUSSION AND RESULTS

Interpretation of a water injection test using TOUGH indicated that the absolute permeability could have been determined assuming single-phase liquid conditions provided an appropriate test sequence is available (e.g. water injection followed by shut-in recovery). Injecting water allows the estimation of the absolute permeability of the inner zone which is mainly liquid saturated. For the outer region, an estimation of the total mobility can be obtained. While it has been possible to reproduce the observed cumulative injected volume and pressure recovery data, gas related formation parameters are poorly identified.

Interpretation of a gas injection test using TOUGH indicated that injecting gas into a composite system is not very appropriate for determining gas related formation parameters because too many sensitive parameters are unknown. Injection of a fluid of low viscosity (gas) into a high viscous fluid (water) leads to smeared saturation profiles. In addition, various feedback mechanisms are a complicating feature for the interpretation of such a test. However, the parameters of interest can be estimated within reasonable bounds.

The numerical simulation suggests an absolute permeability between 10^{-16} and 10^{-15} m^2 and an initial gas saturation between 10 and 40% for the host rock at the Oberbauenstock site.

5 ACKNOWLEDGEMENT

This study was supported by the Swiss National Cooperative for the Storage of Radioactive Waste, Nagra. The authors wish to thank J.-M. Lavanchy for his contribution to this paper, and K.Pruess for his introduction to multiphase flow problems and the use of TOUGH.

6 REFERENCES

International Formulation Committee (1967):
A Formulation of the Thermodynamic Properties of Ordinary Water Substance.
IFC Secretariat, Düsseldorf, Germany

NIB 88-03L, Gartner Lee AG (March 1988):
OBS-1: Hydraulic Testing, Interval Report HGB/55.5D-Gas. Nagra, Baden, Switzerland

NIB 88-48, Andrews, R.W. (May 1988):
Preliminary interpretation of OBS hydraulic tests, and possible conceptual models for groundwater flow regime at OBS considering the effects of gas. Nagra, Baden, Switzerland

NTB 88-03, Kennedy, K.G., Davidson, L.M. (February 1989):
Oberbauenstock (OBS) 1987: Results of the Hydrogeological Testing Program OBS-1. Nagra, Baden, Switzerland

Pruess, K. (June 1987):
TOUGH User's Guide. Nuclear Regulatory Commission, Report NUREG/CR-4645

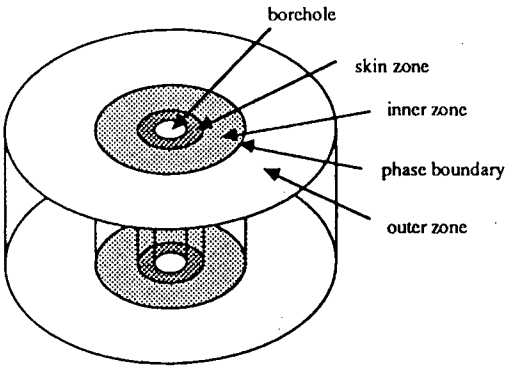

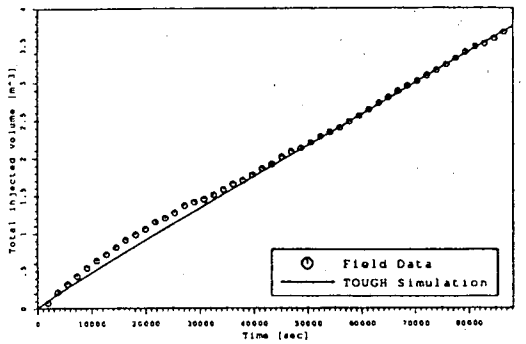

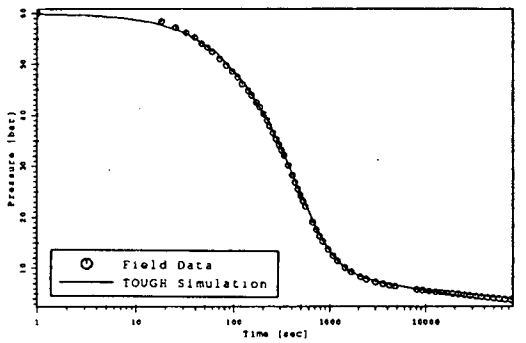

↑ Fig. 1: Schematic of composite system

↗ Fig. 2a: Calculated and observed injected volumes

→ Fig. 2b: Calculated and observed pressures

↓ Fig. 3: Sensitivity to absolute permeability

↘ Fig. 4: Sensitivity to residual gas saturation

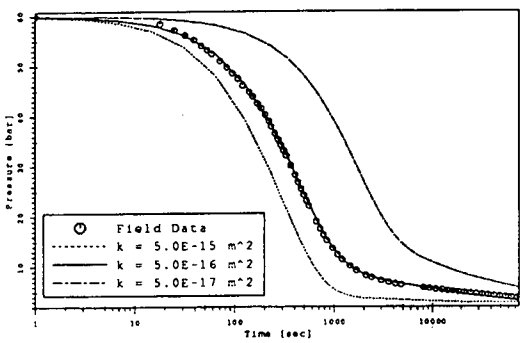

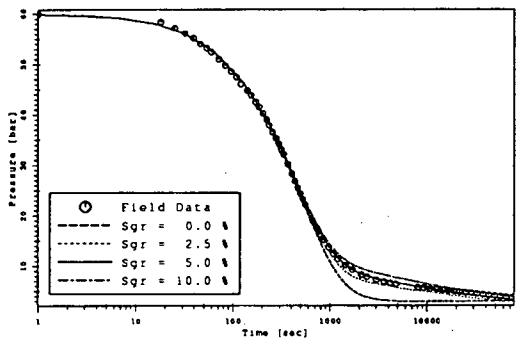

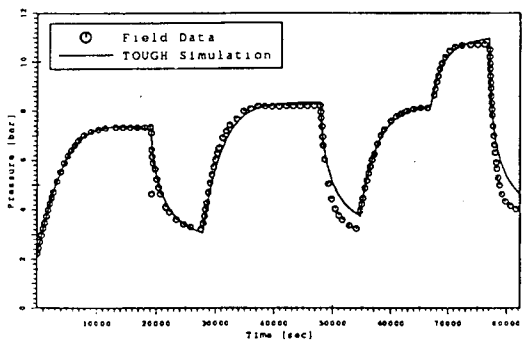

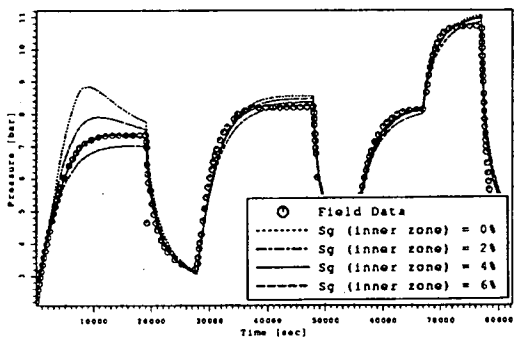

↑ Fig. 5: Calculated and observed pressures

↗ Fig. 6: Sensitivity to gas saturation in the inner zone

→ Fig. 7: Gas saturation profiles

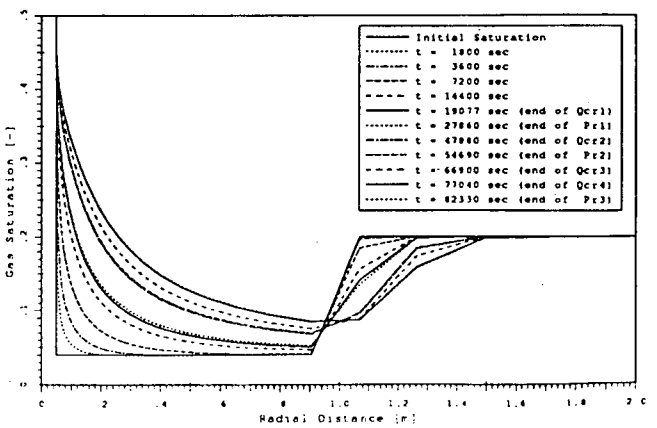

Making MULKOM/TOUGH faster and easier to use

David Bullivant
Department of Engineering Science, University of Auckland, New Zealand.

1 Introduction

MULKOM has been used at the University of Auckland for more than ten years to model geothermal reservoirs. Two areas in which improvements to MULKOM have been made are execution speed and input/output. These changes and additions, that will be detailed in this talk, have recently been transferred to TOUGH.

For large problems, the original linear equation solvers, MA28, take a long time to execute and use large amounts of memory. MA28 has been replaced by SOLVE, a conjugate gradient solver developed by George Zyvoloski (Los Alamos National Laboratory). SOLVE is good because it remains fast for large problems, uses less memory than MA28 and uses a known amount of memory.

For the input file, it is hard to make sure that everything is in the correct column. Even after MULKOM/TOUGH accepts the input file, it is still difficult to check that the numbers (volumes, lengths and areas) are correct. For the output file, it is hard to interpret the huge quantity of numbers produced. Our graphical input/output program uses a geometry file which describes the blocks and the connections. This eases the preparation of the input file by allowing the grid to be checked visually and then creating the input file automatically. The graphical interface does the work of locating information in the output file and displaying it.

In this talk, the improvements to TOUGH will be illustrated using an example. The next section describes the example problem used. Details of the geometry file and creation of the input file are given in the third section. Execution speeds for TOUGH with MA28 and TOUGH with SOLVE are compared in the fourth section. The ways in which output can be displayed are listed in section five. The last section contains ideas for further improvements.

2 Example problem

This example does not model any real situation. The aim in developing it was to create a computationally intensive and numerically difficult problem in which interesting things, such as the movement of boiling and condensation fronts, occur.

The reservoir is a cube, with side length 200 m, of uniform rock (properties given in Table I). Gravity is included. The top of the cube is maintained at atmospheric pressure and temperature (20 °C and 101.3 kPa). There is no flow of heat or mass through the sides of the cube. The heat flux entering the bottom of

the cube is 2.8125 W/m^2 and there is no mass flow through the bottom of the cube.

Table I. Rock properties

density	2700 kg/m^3
porosity	0.1
permeability	10^{-14} m^2
thermal conductivity	3 W/(m°C)
heat capacity	1000 J/(kg°C)
Corey relative permeability curves	0.3 residual liquid saturation
	0.05 residual steam saturation
no capillary pressure	

Initially the reservoir is at steady state and fully saturated. In this state all the fluid is liquid with the fluid at the bottom of the reservoir at just below boiling temperature. Pressure dependent production (wellbore pressure 1 MPa, productivity index 10^{-9} m^3) begins from a bottom corner of the reservoir (coordinates x=0, y=0, z=-200 m). Boiling starts near the production well and spreads across the bottom of the reservoir. As cooler fluid is pulled down to the production well a condensing front spreads across the bottom of the reservoir. After a year and a half the water table begins to drawdown with the largest drawdown being above the production well.

After two years, injection of cold water (rate 1 kg/s, enthalpy 0.85 MJ/kg) begins halfway down the reservoir on an edge that is on the same side as the production well (coordinates x=0, y=200 m, z=-100 m). This slows the drawdown of the water table and produces mounding above the injection well. The simulation is run for 20 years.

3 Input

A model of a geothermal reservoir is created by deciding on the horizontal structure of the model (often with a mixture of block shapes) and then repeating this in layers to achieve the necessary vertical discretization. This process is mimicked for the geometry file. For the top layer, the following are specified - the (x,y) coordinates of block corners, the verticies making up a block and the connections between blocks. Then the number of layers and the layer thicknesses are specified. As well as this general form of the geometry file there are two simplified forms. The first is for radial grids and uses cylindrical coordinates. The second, used for the example problem, is a rectangular grid. Geometry files for three discretizations - 5x5x5 (125 equal sized cubes, 5 in each direction), 7x7x7 and 9x9x9 - were created.

The grid described by the geometry file can be displayed and checked. The input file can then be created. The block volumes, connection areas, connection lengths and gravity cosines are calculated automatically and the program prompts the user for the rest of the information required for the input file (putting the information into the correct columns).

To model the constant pressure and temperature conditions at the surface, a large atmosphere block was used. The heat flow through the base was modelled using a HEAT well in each of the blocks in the bottom layer. The production was represented by a DELV well and the injection by a MASS well with a table of generation rate versus time. The initial time step was 8640 seconds.

4 Execution

SOLVE, developed by George Zyvoloski (Los Alamos National Laboratory), uses pre-conditioned conjugate gradients with GMRES (on Ax=b). Conjugate gradients was first developed for positive definite symmetric matricies. GMRES (Saad and Schultz,1986) extends conjugate gradients to non-symmetric indefinite matricies. Using exact arithmetic, conjugate gradients converges in a finite number of steps, but with computer round-off it becomes an iterative method. Pre-conditioning improves the convergence rate. The pre-conditioner is a matrix M chosen so that $M^{-1}A$ is easy to calculate and $M^{-1}A$ is closer to the identity than A. SOLVE uses an incomplete LU factorization as the pre-conditioner. A complete LU factorization would be better, but this produces a full matrix from a sparse one and takes a long time. An incomplete LU factorization restricts the amount of matrix fill-in.

In Table II, TOUGH with MA28 and TOUGH with SOLVE are compared on the basis of total execution time and solver execution time for the three discretizations of the example problem.

Table II : CPU times for the example problem

	MA28		SOLVE	
	total	solver	total	solver
5x5x5	11062.53	8800.37	1603.05	589.33
7x7x7	-	-	6408.26	2898.95
9x9x9	-	-	17943.15	10316.53

NB. CPU times are in seconds and were measured on a VAXstation 3100.

For the 5x5x5 problem, about 15 times longer was spent in MA28 than in SOLVE. The results for the two versions were similar, but the time steps they took to get to twenty years differed. For the 7x7x7 problem MA28 was still on the sixteenth time step (SOLVE took 93 time steps for the complete simulation) after over twelve hours of CPU time. MA28 was also paging to disk because there was insufficient memory (MA28 needed LICN=300000 and LIRN=150000 for the 7x7x7 grid). The time spent in SOLVE increases more than linearly with problem size, but the increase is less than quadratic.

5 Output

This section describes the ways in which the output can be displayed. There are two basic types of display.

The first type is a slice through the block layout. On this reservoir properties such as temperature or pressure or flow through the upper surface of a layer can be displayed as a number at the centre of the block or by shading the blocks according to the value of the reservoir property. Reservoir properties such as mass flow, can be displayed as arrows of differing lengths drawn at the appropriate connections.

The second type of display is a graph of how a scalar reservoir property, such as pressure, varies in a block with time or depth.

6 Future work

The linear equations can be solved faster by taking advantage of their structure. In particular, the fact that there are three equations for each block - conservation of heat, conservation of mass and conservation of air. Zyvoloski (1989) shows how two processes can be decoupled, the dominant system (half the number of equations and unknowns) solved and a solution to the original system found by back substitution and successive over-relaxation. This method can be applied to geothermal systems, where mass flow dominates.

Displaying arrows to show flows on slices through the reservoir is not entirely satisfactory because there are usually flows into and out of the plane of the slice that do not show up. A long term aim is to "draw" the 3-D grid and superimpose a stream surface to show the 3-D structure of the flows.

References

Saad, Y. and M.H. Schultz, GMRES: A generalized minimal residual algorithm for solving nonsymmetric linear systems, SIAM J. Sci. Stat. Comput., 7(3), 856-869, July 1986.

Zyvoloski, G., Efficient matrix procedures for the simulation of coupled processes, Eastern Multiconference, Computer Society of America, Tampa, Florida, March 1989.

Increasing the Efficiency of the TOUGH Code for Running Large-Scale Problems in Nuclear Waste Isolation

J.J. Nitao
Earth Sciences Department
Lawrence Livermore National Laboratory

Work performed under the auspices of the U.S. Department of Energy by the Lawrence Livermore National Laboratory under contract number W-7405-ENG-48

Abstract

The TOUGH code developed at Lawrence Berkeley Laboratory (LBL) is being extensively used to numerically simulate the thermal and hydrologic environment around nuclear waste packages in the unsaturated zone for the Yucca Mountain Project. At the Lawrence Livermore National Laboratory (LLNL) we have rewritten approximately 80 percent of the TOUGH code to increase its speed and incorporate new options. The geometry of many problems requires large numbers of computational elements in order to realistically model detailed physical phenomena, and, as a result, large amounts of computer time are needed. In order to increase the speed of the code we have incorporated fast linear equation solvers, vectorization of substantial portions of code, improved automatic time stepping, and implementation of table look-up for the steam table properties. These enhancements have increased the speed of the code for typical problems by a factor of 20 on the Cray 2 computer. In addition to the increase in computational efficiency we have added several options: vapor pressure lowering; equivalent continuum treatment of fractures; energy and material volumetric, mass and flux accounting; and Stefan-Boltzmann radiative heat transfer.

1 Introduction

Yucca Mountain, Nevada, is currently being investigated by the Department of Energy to determine its suitability for the disposal of high-level nuclear waste. Investigations at Lawrence Livermore National Laboratory include the numerical modelling of the thermal and fluid environment around the waste package in conjunction with laboratory and field experiments. The TOUGH code, which was originally developed at Lawrence Berkeley Laboratory [Preuss,1987], is one of the codes being used to simulate the thermal and hydrologic environment around the nuclear waste packages. These simulations involve the transport of water, air, and heat in the porous fractured rock found at the site. The reader is referred to a previous report [Nitao, 1988] for references related to the work in this area. In this report we wish to describe the extensive modificaions that have made to the code. Overall, about 80 percent of the code has been rewritten, enough, we feel, to justify calling it V-TOUGH, which stands for Vectorized TOUGH.

The original LBL TOUGH code is very modular and "cleanly" coded which is unusual for a large simulation code. We have attempted to continue this practice in our enhanced version. The new version runs about 20 times faster than the original version for the near-field nuclear waste simulation problem described previously in [Nitao,1988].

2 Vectorization

Most supercomputers, such as the Cray, Convex, and Alliant computers, have special hardware that enables the very fast execution of arithmetic operations between arrays, or vectors, of numbers. In order to take advantage of this capability the code must be vectorized: written such that, as much as possible, the longest do loops are inner and no data dependencies occur from one pass of the loop to the other passes. Optimizing the code in such a manner may require the use of more physical memory since in vectorization there is an advantage to storing quantities in arrays. Thus, there is some trade-off between memory usage and speed, which may be one of the reasons why the original code was not highly vectorized. The vectorization that we have performed may not have been feasible several years ago when the added memory was not available

In this section we do not consider the vectorization involved in the linear equation solver; this aspect will be covered in a later subsection devoted to that topic. The primary areas where vectorization was performed is in the subroutine MULTI which generates the Jacobian matrix, EOS which calls the PVT subroutines, and in the various PVT subroutines themselves. These routines were all completely rewritten in order to vectorize as many loops as possible. Vectorization often requires, as alluded to before, more physical memory usage because of the need for temporary arrays. In order to reduce the amount of memory we took advantage of the fact that most modern compilers re-use the memory of local variables (unless the variable is declared to be static by the FORTRAN SAVE command) by placing it back onto to a "heap" after return from the subroutine. Thus, as much as possible, arrays were not placed in COMMON but kept as local variables. Although much of the PVT and constitutive type computations were highly vectorized, with regards to the characteristic curves, only the equivalent continuum characteristic curves are vectorized; but, with the new code structure it would not be difficult to vectorize the other characteristic curves as well.

3 Steam Table Look-up

The steam table properties include the mass density and specific internal energy of subcooled and superheated water as well as the saturation pressure. In the formulation used by the code, the density and internal energy are expressed as functions of pressure and temperature while the saturation pressure is computed as a function of temperature. The original code used complex functional fits to compute the steam table values. The number of arithmetic operations required by these formulae are very large and can, therefore, use a significant amount of computer time. We have, therefore, replaced them by an efficient table look-up scheme. Table look-up applied to steam tables is somewhat complicated by the fact that range of interest for the pressure varies with temperature and the fact that the properties of water vary at different rates above and below the saturation line so that it is difficult to maintain a constant pressure interval without generating an excessively large table. (The advantage of using tables for the dependent variable having constant intervals will be seen later.) In the method that we used, we first generate the table for the saturation pressure function at every 2° C intervals from 5° to 501° C (these limits as well as others can easily

be changed). The tables for the density and internal energy of subcooled water are then generated for different pressures at these same temperature points. The pressure intervals are constant and start from the saturation pressure at the temperature point and increase to a maximum pressure which we took to be 24.7 MPa. It was found that only three pressure intervals (four pressure points) were sufficient to give good accuracy due to the fact that the properties of subcooled water are almost linear in temperature and pressure. A similar procedure is used to generate the superheated steam properties with the pressure points beginning at the saturation pressure and decreasing at constant intervals to a minimum pressure of 100 Pa. (In the look-up stage, the ideal gas law is used for pressures below this minimum.) Thirty pressure intervals are used for the superheated water properties.

The table look-up algorithm is now described. Suppose we are interested in the determining the internal energy u of superheated water at some temperature and pressure (T_0, P_0). We first show how to find the saturation pressure $P_{sat}(T_0)$ at T_0. If ΔT is the temperature interval the table index i is defined by

$$i = T_0/\Delta T \tag{1}$$

and is used to linearly interpolated between the table values $Ptab_{sat}(i)$ and $Ptab_{sat}(i+1)$. We now must find the table position j for the pressure given by

$$j = (P_0 - P_{sat}(T_0))/\Delta P_i \tag{2}$$

where ΔP_i is the constant pressure interval for the i-th temperature position. The value of u is now determined by a two dimensional interpolation between the table values of u at (i, j), $(i+1, j)$, $(i, j+1)$, and $(i+1, j+1)$. Linear interpolation is performed first with respect to the j index, first at i and then at $i+1$. The two values that result are then linearly interpolated. This procedure can be performed very efficiently since the use of constant intervals eliminates the need to search through the table and is very easily vectorized.

The arrays holding the tables must be initialized at the beginning of each run either by computing the values from subroutines that were in the original code or, if it exists, the table is read in from an unformatted file called TABLE that was created from a previous run.

4 Linear Equation Solvers

At each time step the model needs to solve a set of non-linear equations for the primary variables. The Newton-Raphson algorithm which is used to solve the equations is an iterative procedure requiring the solution of a system of linear equations at each iteration. There can be several thousand computational elements and each element has associated with it three equations. Therefore, the linear equation solution can consume a significant amount of time.

The enhanced model has three separate user options for the linear equation solver to be used: Option (0), block-banded gaussian elimination with no pivoting; Option (1), standard banded gaussian elimination with partial pivoting from the Linpack library; and Option (2), a Cray 2 highly optimized banded gaussian elimination with partial pivoting [White,1988].

Note that the MA28 solver used in the original code is not available. Option (0) was the solver used to run the problem described in [Nitao,1988]. The other two options were added to the code later. On the Cray 2, option (1) with the Linpack routines optimized for the Cray 2 is about twice as fast as option (0) while option (2) is about 5 times faster. Thus, option (2) is the preferred method on the Cray 2. Option (1) is included because optimized versions of the Linpack routines are available on many machines including the Alliant computer. Option (0) seems to be faster than option (1) when non-optimized Linpack routines are used on such machines as the Sun Workstation. Note that portable FORTRAN source code is available for option (0) and for the non-machine optimized version of option (1), but portions of option (2) is not portable since they are in Cray 2 assembly language.

5 Automatic Time Stepping

The automatic time step option in the original version of TOUGH was based on cutting back the time step when the Newton-Raphson iterations failed to converge. We found that a better algorithm is to control the maximum change in the solution vector from one time step to the next. This control can be accomplished by estimating the time step for the solution to change by a specified amount based on the solution change that ocurred in the previous two time steps. During an iteration, if the change in solution from the previous time step is too large, a re-estimation is performed and the time step started over. This method also controls to some extent the time discretization error.

We now describe the method in more detail. Let u_i be the i-th component of the solution vector at the current iteration of the Newton-Raphson method, and δu_i be equal to u_i minus the i-th component of the solution vector at the end of the previous time step. Now, let $(\delta u_i)_{max}$ be the maximum allowed change in the solution. We define the new reference time step δt by

$$\delta t = \frac{(1+w)(\delta u_i)_{max}}{w(\delta u_i)_{max} + \delta u_i} \tag{3}$$

Here, w is a "damping" factor [Grabowski et al., 1979] that is chosen between 0 to 1 in order to prevent the time step from changing too rapidly. We used a value of 0.8. The value of δt is adjusted to stay within 0.5 to 4.0 times the time step size taken in the previous time step. If the reference time step is less than the current time step because the solution changed too much, then the current time step is replaced by 0.8 times the reference, and the Newton-Raphson is restarted. The factor 0.8 is there to allow for some margin to prevent too many restarts.

6 Other Enhancements

6.1 Equivalent Continuum

Description of and references to the equivalent continuum method for modelling fracture-matrix flow are given in [Nitao,1988], and we assume that the reader is familiar with the theory. Suppose that the the suction pressures for the matrix and fracture are known

functions of the liquid saturation, $p_{cm}(s_m)$ and $p_{cm}(s_f)$, respectively. Since the model computes the bulk saturation s_b of the equivalent medium instead of the matrix and fracture saturation, s_m and s_f, these quantities must be solved in terms of the the bulk saturation if we are to compute the characteristic curves of the matrix and fracture. The bulk saturation is defined in terms of s_m and s_f through the relation

$$s_b = \frac{s_f\phi_f + s_m(1-\phi_f)\phi_m}{\phi_f + (1-\phi_f)\phi_m} \tag{4}$$

where ϕ_m is the matrix porosity and ϕ_f is the fracture porosity defined in [Nitao,1988]. The equivalent continuum assumes that the suction pressures are equal

$$p_{cm}(s_m) = p_{cf}(s_f) \tag{5}$$

In our implementation we generate a table of suction head versus bulk saturation. The entry for the suction head is tabulated at exponentially spaced intervals. For each value of suction head we equate both the suction pressure of the matrix and fracture to the given value as assumed by (5). By inverting the saturation vs. suction head relation we may find s_m and s_f in terms of the current head value. Using (4) we compute the bulk saturation s_b. The resulting table is then used during the model run to compute suction pressure as a function of bulk saturation. The composite relative permeability of the equivalent continuum is a linear combination of the relative permeabilities for the matrix and fractures. This quantity is also tabulated for each entry of suction head since the relative permeabilities can be computed using matrix and fracture saturations expressed as known function of suction head. Since the bulk saturation is known at the same point, the result is a table for equivalent continuum relative permeability versus bulk saturation.

6.2 Vapor Pressure Lowering

Vapor pressure lowering is implemented by lowering the saturated vapor pressure through the Kelvin type law [Marshall and Holmes, 1979]

$$p_v = p_{sat}(T)\exp\frac{-|p_c|}{\rho_l T R} \tag{6}$$

where

$p_{sat}(T)$	saturation pressure of bulk water as function of temperature T
ρ_l	liquid molar density
T	temperature in Kelvin
R	the gas constant

6.3 Radiative Heat Transfer

It is useful in some situations to be able to model radiative heat transfer between computational elements. An example is the heat transfer across the air gap between the waste

package and the wall of the borehole. The Stefan-Boltzmann law is used to compute the flux q_R between elements 1 and 2 by the equation

$$q_R = C({T_2}^4 - {T_1}^4) \tag{7}$$

where T_1 and T_2 are absolute temperatures and C is some user supplied and geometry dependent constant.

7 Discussion

With the new enhancements to the TOUGH code we are able to extend the size and complexity of models describing the near-field thermal and hydrological impact of nuclear waste packages. Large 2D problems with 2000 nodes, such as the one described in [Nitao,1988] can be run in less than one hour on the Cray 2; whereas, it would have required 20 hours before. Small 3D problems are also possible. Further work, will, however, be required to increase the efficiency of the code to handle larger 3D problems. Such problems spend a significant portion of their time solving the system of linear equations in the Newton-Raphson scheme. Therefore, the focus of future work will be on more efficient linear equation solvers.

References

Grabowski, J.W., P.K. Vinsome, R.C. Lin, A. Behie, and B. Rubin, A Fully Implicit General Purpose Finite-Difference Thermal Model for In Situ Combustion and Steam, Society of Petroleum Engineers paper, SPE 8396 (1979).

Marshall, T.J. and J.W. Holmes, *Soil Physics*, Cambridge University Press (1979).

Nitao, J.J., Numerical Modeling of the Thermal and Hydrological Environment around a Nuclear Waste Package using the Equivalent Continuum Approximation: Horizontal Emplacement, Lawrence Livermore National Laboratory Report, UCID-21444 (1988).

Preuss, K., TOUGH User's Guide, Lawrence Berkeley Laboratory Report, LBL-20700, (1987).

White, S., A More Robust Gaussian Elimination/Backsolve Package for the Cray 2, National Magnetic Fusion Energy Computer Center *Buffer*, vol. 12, no. 11 (Nov. 1988).

Speeding up TOUGH

Stephen White

1 Introduction

In this paper I describe some modifications made to TOUGH that increase the size of problems that can be solved on computers available to us. Much of this work was carried out under contract to G.E.R.D and they have presented a case study on the use of TOUGH with these modifications. There are two factors that limit the size of problem that can realistically be solved using TOUGH.

- Computer time taken for a run.
- Memory required for a problem.

We have developed new routines for TOUGH that significantly reduce requirements in both these areas for a large class of problems.

2 Profiling

As a first step we ran TOUGH under a profiler. This pinpointed the areas of the program that would most benefit from modification. Profiling was done for a number of different problems, mainly the test problems supplied with TOUGH and a few others of interest to us. There are two 'expensive' areas that account for at least 80 % of computer time between them in all problems. In problems with only a few connections between elements (e.g SAM1 from the distribution tape) almost 70% of the run time is spent calculating thermodynamic properties of water and steam. In problems with a larger number of connections between elements (e.g. 2D flow to a geothermal well) 80% of the total time is spent in routines associated with matrix inversion. The proportion of time spent on matrix inversion becomes even more extreme for 3D problems where matrix inversion may take over 90% of the total time.

Talking of 1D 2D and 3D problems is not really in the spirit of TOUGH which is not concerned with the dimensionality or geometry of a problem. However the geometry of the domain being modeled does have a significant effect on the time taken to solve a problem. The important parameters are really the average number of connections per element and the distance (in terms of TOUGH element numbers) between connected elements. As an example of how geometry influences run time we ran 3 problems with approximately the same number of elements but different geometries.

Dimension	Time/step (secs)	$(Time/step)^{1/D}$
1 D	4	4
2 D	56	7.4
3 D	150	5

Roughly speaking execution time depends on the number of elements to the power of the dimension of the problem.

3 Numerical Equations Solved by TOUGH

This section summarises the equations solved by TOUGH. This is presented in more detail in the TOUGH manual and all terms are defined there. For an arbitrary flow domain V_n the mass and energy balance equations in integral form are

$$\frac{d}{dt}\int_{V_n} M^{\kappa} dV = \int_{\Gamma_n} F^k.n d\Gamma + \int_{V_n} q^k dV \qquad (\kappa = water, air, heat) \tag{1}$$

Time derivatives are approximated using a fully implicit first order method.

$$f^{t+\Delta t} = f^t + \Delta t \left(\frac{df}{dt}|_{t+\Delta t}\right) \tag{2}$$

Equation 1 is discretized in space using the integral finite difference method. These two approximations reduce equation 1 to a set of nonlinear algebraic equations

$$0 = R_n{}^{k+1} = M_n{}^{(\kappa)k+1} - M_n{}^{(\kappa)k} - \frac{\Delta t}{V_n}\left(\sum_m A_{nm} F_{nm}^{(\kappa)k+1} + V_n q_n^{(\kappa)k+1}\right) \tag{3}$$

k labels the time step and $\Delta t = t^{k+1} - t^k$.

For a system that has N grid blocks this is a set of 3N nonlinear equations in the 3N primary variables. This system of equations is solved for the primary variables using a Newton Raphson iteration.

Denoting the primary variables at time $k+1$ as $x_1 \ldots x_{3N}$ the Newton Raphson iteration is

$$x^{i+1} = x^i - J^{-1} R^{k+1}(x^i) \tag{4}$$

or

$$x^{i+1} = x^i - \Delta x^i \qquad J\Delta x^i = R^{k+1}(x^i) \tag{5}$$

$$\tag{6}$$

J is the Jacobian matrix of the system $J_{ij} = \frac{\partial R_i^{k+1}}{\partial x_j}$. The Newton Raphson iteration defined in 4 involves the inversion of a $3N \times 3N$ sparse Jacobian matrix. It is this matrix

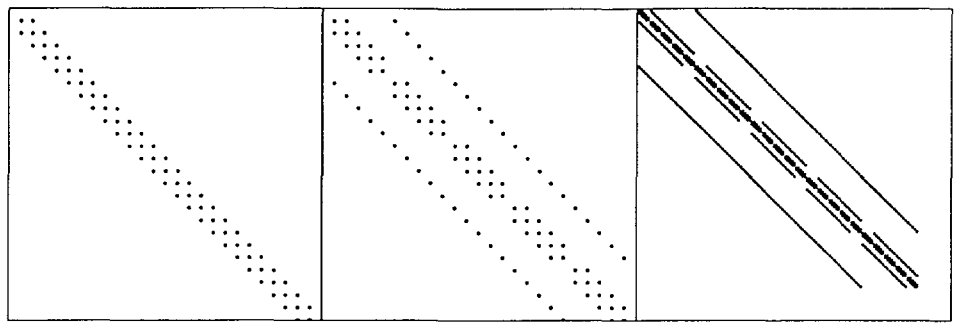

Figure 1: Some different matrix structures

inversion that dominates the computer time for most problems. This matrix inversion is normally done using the MA28 suite of the Harwell subroutine library. These are a set of routines for the inversion of general sparse matrices. By exploiting properties of the matrices occurring in TOUGH we can often solve the problem more quickly than is possible using the MA28 routines.

4 Alternative Inversion Methods

It simplifies what follows to consider J as an $N \times N$ matrix of 3×3 matrices. An examination of equation 3 shows J has a 3×3 matrix on the diagonal for each element and an additional matrix is generated for each connection to that element. Some examples of the structure of Jacobian matrices for 1,2 and 3 dimensional problems are given in figure 1. The actual structure of these matrices depends on the order in which elements are specified, there are many equivalent structures for a particular problem. We have developed two alternatives to the MA28 routines. The first of these, a generalisation of the Thomas algorithm for tri-diagonal matrices, is only applicable to 1D problems where each element is connected to its' two neighbours. The second uses an iterative method to solve 4.

4.1 Iterative Solution

Rather than solve 4 directly we can generate an approximate solution using a modified Successive Over Relaxation (SOR) iteration.

We write

$$J = D - U - L \tag{7}$$

where D is a diagonal, U a strictly upper triangular and L strictly lower triangular matrices. The conventional SOR iteration to solve the problem $Jx = R$ is defined as

$$(D - \omega L)x^{m+1} = ((1-\omega)D + \omega U)x^m + R) \tag{8}$$

or

$$x_k^{m+1} = \frac{1}{d_{kk}}(\omega \sum_{i=1}^{k-1} l_{ki} x_i^{m+1} + (1-\omega) d_{kk} x_k^m + \omega \sum_{i=k+1}^{3N} u_{ki} x_i^m + r_k)$$

As it stands equation 8 is not suitable for the Jacobian matrices generated by TOUGH as there is no guarantee that at all the diagonal elements are non zero. There are two (equivalent) ways of overcoming this problem. Either D, U and L are regarded as $N \times N$ matrices of 3×3 matrices and the three primary variables at each mesh point are solved for at once (block SOR method). Or the iteration defined in 8 can be modified. Premultiplying 8 by the inverse of the block diagonal matrix formed from the 3×3 matrices on the diagonal of J results in

$$(I - \omega L')X^{m+1} = ((1-\omega)I + \omega U')x^m + R') \tag{9}$$

. The matrix

$$\mathcal{L}_\omega = (I - \omega L')^{-1}((1-\omega)I + \omega U') \tag{10}$$

is called the point successive over relaxation matrix.

4.2 Choice of ω

Choosing an appropriate value for ω is crucial to the success of the SOR method. An optimum value of ω can reduce the number of iterations by an order of magnitude in some problems. Extensive theoretical work exists on calculating an optimum value of ω, Young is an excellent reference. Much of this work requires that the matrix have what Young refers to as property A. A matrix with this property can be transformed by a permutation matrix P into the form

$$P\mathcal{L}_\omega \mathcal{P}^{-\infty} = \begin{pmatrix} D_1 & U \\ L & D_2 \end{pmatrix} \tag{11}$$

where the matrices D_1 and D_2 are diagonal. Making this transformation also speeds up the convergence of the SOR method. This transformation is equivalent to relabeling the the mesh blocks and thus changing the order in which the SOR iteration updates variables. As an example of this figure 2 shows the matrix from a 2D rectangular mesh the transformed matrix and the relabeling of the grid. With the general nature of connections between elements allowed by TOUGH it may not be possible to transform problems in this way. For example, grids that have an element with a connection to two or more elements that are connected to each other cannot be transformed in this way. Often boundary elements may be connected to a single large element to model the effect of a constant pressure boundary. It is worth while modifying this type of grid to have one constant pressure element for each boundary element. The improved convergence of the SOR iteration more than makes up for the larger number of grid blocks.

Assuming $\mathcal{L}_\omega$ has property A then the optimum value for ω is given by

$$\omega = \frac{2}{1 + \sqrt{1 - \mu^2}} \tag{12}$$

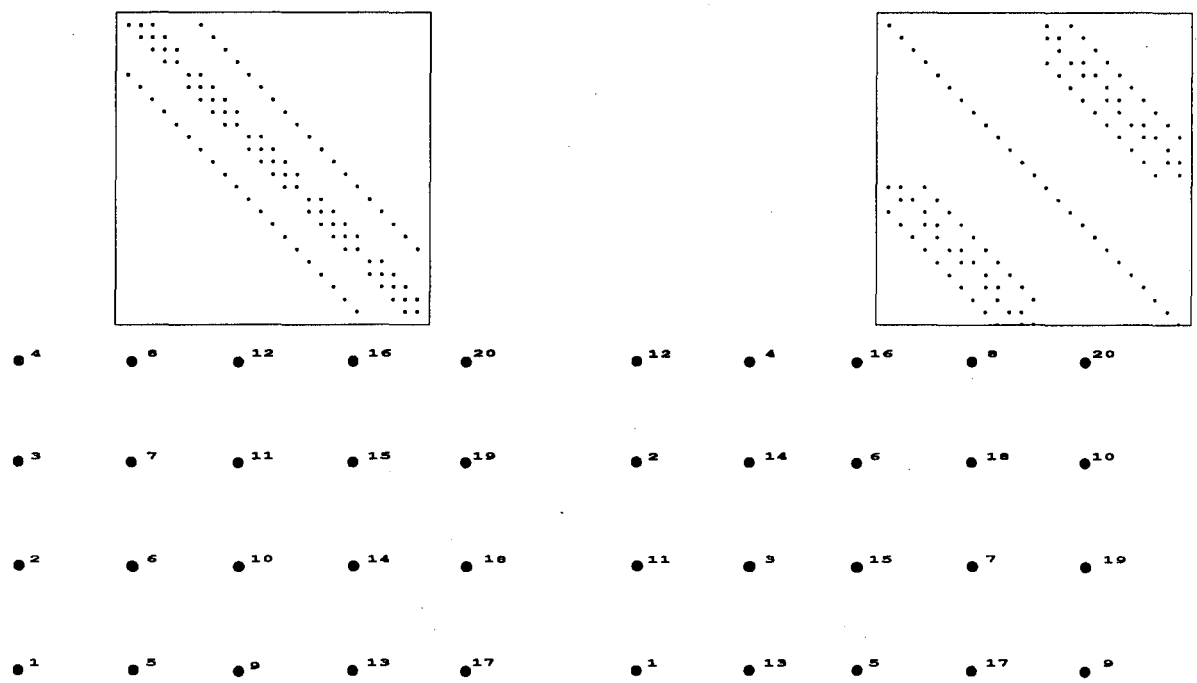

Figure 2: Permutations of the Jacobian Matrix

μ is the largest eigenvalue of $L' + U'$. μ can be determined by examining the convergence of an iteration using $\mathcal{L}_1$. If we set $\phi^0 = 1$ and then iterate with

$$\phi^{m+1} = \mathcal{L}_1 \phi^m \tag{13}$$

We form

$$\begin{aligned} \underline{\lambda}_m &= \min \frac{\phi_i^{m+1}}{\phi_i^m} \\ \overline{\lambda}_m &= \max \frac{\phi_i^{m+1}}{\phi_i^m} \end{aligned} \tag{14}$$

then

$$\lim_{m\to\infty} \underline{\lambda}_m = \overline{\lambda}_m = \mu^2 \tag{15}$$

This iteration may take some time to converge. In fact the effort required to determine an optimum acceleration parameter is of the same order as to solve the whole problem. For this reason we do not determine a value for ω at each time step but only recalculate ω when the time step changes. Adopting this strategy means we have a close to optimum value for ω at minimum cost.

time step	λ_∞	ω_{opt}
1	.16868	1.0072
10	.473188	1.1588
10^2	.7481	1.3310
10^3	.90659	1.4064
10^4	.95572	1.5453
10^5	.97199	1.6194
10^6	.9826	1.6869

Figure 3: Variation of ω_{opt} with timestep

5 Memory requirements

Using the direct method for matrix inversion requires a workspace of 2-4 times the number of nonzeros in the Jacobian matrix. For large problems this can amount to several megabytes. In contrast the SOR method requires none of this workspace. It does require some integer work arrays but these require no more space than the integer work arrays used by the direct method.

6 Thermodynamic Routines

TOUGH uses a number of subroutines to compute the thermodynamic and physical properties of water/steam/gas mixtures. For some problems up to 75 % of the total CPU time was spent executing these routines. Most of this time was spent in just two routines SUPST COWAT, which compute the density and internal energy of steam and water.

The fortran codes for SUPST and COWAT were both rewritten to remove all unnecessary array references and many of the large exponentiations. with these changes, SUPST and COWAT run approximately 70% and 40% more quickly respectively.

7 Problems and Restrictions

Almost all the testing applied has been of geothermal type problems. The techniques described here may not apply as well to other types of TOUGH problem. The eigenvalues (and thus the rate of convergence of the SOR method) of $\mathcal{L}_\omega$ depend on the timestep. Very large timesteps may cause the method to fail to converge. This is particularly a problem when the matrix does not have 'property A'. In our testing for other than 1D problems the SOR method has almost always proved to be faster than the direct method, even when the time step must be limited.

Problem	Direct inversion	SOR	Thomas Algorithim
SAM1	2.4	1.6	1.9
SAM2	28.5	24.9	
SAM3	44.1	52.4	47.8
SAM4	37.6	57.5	20
DOE test problem	72	49.6	
2D flow to geothermal well	399	66.2	
3D flow to geothermal well	900	36	

Figure 4: Timing for some test problems (Dec 5400 CPU seconds)

8 Conclusions

The SOR method described in this paper provides an alternative method for matrix inversion that extends the range of problems that can be solved by TOUGH. In particular we can now solve 3D problems, this was not previously possible on computers available to us. Use of the Thomas Algorithim and rewritten thermodynamic routines has reduced the CPU requirement for 1D problems. Some sample timings are given in figure 4.

Appendix

TOUGH Questions*

1. What do you use TOUGH for?

2. What do you like most about TOUGH?

3. What do you like least about TOUGH?

4. What enhancements to TOUGH would you like to see? (list three)

5. What enhancements to TOUGH have you produced?

6. How often would you like to have a TOUGH workshop?

7. How would you like to have information about TOUGH and TOUGH modifications distributed?

   (i) Newsletter and software distributed from TOUGH central (LBL?)
   (ii) Software distributed around informally
   (iii) Commercial deals
   (iv) Other—add comments

8. What name would you like for TOUGH?

9. Any other comments?

---

*Formulated by M. J. O'Sullivan; distributed at TOUGH Workshop, September 13–14, 1990, to solicit input for the open discussion session.

LAWRENCE BERKELEY LABORATORY
UNIVERSITY OF CALIFORNIA
INFORMATION RESOURCES DEPARTMENT
BERKELEY, CALIFORNIA 94720

AAF227
LBL Libraries